Future ElectroWeak Physics at the Fermilab Tevatron Report of the *tev_2000* Study Group

FERMILAB–PUB–96/082

DØ Note 2589 & CDF Note 3177

Editors:

D. Amidei

Department of Physics, University of Michigan

and

R. Brock

Department of Physics and Astronomy, Michigan State University

April 1, 1996

Authors of the tev_2000 Study

Top Physics [D. Amidei[um]]
P. Baringer,[uk] N. Eddy,[um] A. P. Heinson,[ucr] U. Heintz,[fnal] S. B. Kim,[um] T. LeCompte,[ui] T. Liss,[ui] M. Narain,[fnal] K. Tollefson,[ur] S. Vejcik,[um] B. Winer,[cu] D. Winn [um]

Intermediate Vector Boson Physics [U. Baur,[sunyb] M. Demarteau,[fnal] and S. Errede[ui]]
H. Aihara,[lbl] C. Balazs,[msu] W. Carithers,[lbl] T. Diehl,[fnal] J. Ellison,[ucr] D. Errede,[ui] T.A. Fuess,[anl] T. Han,[ucd] Y.K. Kim,[lbl] G. Landsberg,[fnal] L. Nodulman,[anl] J. Ohnemus,[lbl] T. Spadafora,[lbl] R. Sobey,[ucd] G. Valencia,[isu] R. Wagner,[anl] C. Wendt,[uw] D. Wood,[fnal] C.P. Yuan,[msu] D. Zeppenfeld[uw]

Light Higgs Physics [U. Heintz,[fnal] S. Kuhlmann,[anl] and S. Willenbrock[ui]]
P. Agrawal,[msu] D. Bowser–Chao,[msu] J. Cochran,[ucr] S. Mrenna,[anl] E. Shabalina,[msur] T. Stelzer,[uw] J. Womersley[fnal]

Supersymmetric Physics [K. De,[uta] and T. Kamon[tam]]
R. Arnowitt,[tam] H. Baer,[fsu] C. Chen,[fsu] D. Claes,[sb] M. Gold,[unm] G.L. Kane,[um] C. Kao,[ur] F. Keyvan,[ucla] G. Kribs,[um] J.L. Lopez,[ru] S. Mrenna,[anl] D. Norman,[tam] L. Sawyer,[uta] J. Sender,[uh] T.L. Thomas,[unm] J. Wells,[slac] J.T. White,[tam] J. Wolinski[tam]

Exotic Physics [R. Harris[fnal]]
J. Huston,[msu] K. Maeshima,[fnal] D. Norman,[tam] S. Kopp,[uc] M. Gold,[unm] A. Laasanen[pu]

Physics with a Polarized Proton Beam [R. Brock,[msu] G. Ladinsky,[msu] and H. Weerts[msu]]
D. Stump,[msu] M. Wiest[msu]

Detector Requirements [J. Womersley[fnal]]
T. Kamon,[tam] D. Norman,[tam] J.T. White,[tam] J. Wolinski[tam]

[anl] *Argonne National Laboratory,* [ucd] *University of California at Davis,* [ucla] *University of California at Los Angeles,* [ucr] *University of California, Riverside,* [uc] *University of Chicago,* [cu] *Columbia University,* [fnal] *Fermi National Laboratory,* [fsu] *Florida State University,* [uh] *University of Hawaii,* [isu] *Iowa State University,* [ui] *University of Illinois,* [uk] *University of Kansas,* [lbl] *Lawrence Berkeley Laboratory,* [um] *University of Michigan,* [msu] *Michigan State University,* [msur] *Moscow State University,* [sunyb] *State University of New York, Buffalo,* [sb] *State University of New York, Stony Brook,* [unm] *University of New Mexico,* [nu] *Northeastern University,* [pu] *Purdue University,* [ru] *Rice University,* [ur] *University of Rochester,* [snu] *Seoul National University,* [slac] *Stanford Linear Accelerator Center,* [tam] *Texas A& M University,* [uta] *University of Texas, Arlington,* [uw] *University of Wisconsin*

Contents

Chapter 1

Foreword

In particle physics, the "High Energy Frontier" defines, at any time, a set of problems of great theoretical interest and a set of future facilities of grand reach and scope. Meanwhile, the hands–on reality of High Energy Physics proceeds in the facilities of the present, with all of the unexpected twists and turns of scientific progress. The recent observation of the massive top quark at the Fermilab Tevatron reminds us that discovery and opportunity don't mark time, and that a vital experimental program should be prepared to respond to matters arising. Although there are, as always, new facilities in our future, that future is not so immediate, and we now have the opportunity to evaluate an unexpectedly rich new physics program at the Fermilab Tevatron, an existing facility with proven capability...

This document is the report of a working group established to evaluate the potential of an extended high p_T physics program at the Tevatron Collider. We have found that, in addition to a complete program of top quark physics, there is an rich catalog of topical measurements and important discovery potential in many areas. Much of this Tevatron physics potential, such as the top quark program, and significant sensitivity to light Higgs and low energy SUSY, has not been carefully evaluated until now.

The report is organized as follows. This **Foreword** describes the process which led to our organization and guided our work. A second chapter titled **Physics Conclusions and Recommendations** contains an "Executive Summary" of results from each of the physics working groups plus more general recommendations on the pursuit of an extended Tevatron program. There follow seven chapters which catalog the results in each of the physics subtopics. Finally, an **Afterword** contains some views of where this work figures into the broader scheme of things at Fermilab and more generally in High Energy Physics. To those interested in the detailed physics studies, the individual chapters should be important and stimulating. To those with general interests, the Foreword, Conclusions, and Afterword were written to stand alone as a readable document.

1.1 The Potential for Tevatron Evolution

Ideas for upgrades to the Fermilab Tevatron began to surface almost immediately after the SSC cancellation. The most fully developed ideas at this point include improvements to luminosity, and the physics thrust of this study is directed toward this prospect. Since the options and their parameters have been in flux, we briefly review them here. We note that in the running period just completed (the "1B" run) the peak luminosity was approximately $2 \times 10^{31} \mathrm{cm}^{-2}\mathrm{s}^{-1}$ with an integrated luminosity in this 18 month running period of more than 100 pb^{-1}.

1. **Luminosity Upgrade of up to** $10^{32}\mathrm{cm}^{-2}\mathrm{s}^{-1}$. This is the classic Main Injector scenario with 36 proton and antiproton bunches, 395 ns between crossings, and 3 interactions per crossing at two collision points. Further study has led to two variations on this theme:

   (a) The classic scenario, but with $\mathcal{L} = 10^{32}$ $\mathrm{cm}^{-2}\mathrm{s}^{-1}$ and 99 proton and antiproton bunches, leading to 132 ns between crossings and 1 interaction per crossing with two interaction regions. Detector upgrades have been designed to be compatible with this future variation.

   (b) An expansion of the antiproton capability which should provide even higher luminosity. The recent name for a Run II which would equal or surpass 2×10^{32} $\mathrm{cm}^{-2}\mathrm{s}^{-1}$ is "TeV$\star$". In order to reach luminosities which exceed 10^{32} $\mathrm{cm}^{-2}\mathrm{s}^{-1}$ a separate, permanent magnet storage ring of 8 GeV would be built inside the Main Injector tunnel to serve as a "Recycler" for unspent antiprotons. In this variation, the number of overlapping interactions would rise to 6/2 per crossing at 396/132 ns.

   The current plan for the beginning of the Main Injector collider run, Run II, is the "classic" scenario. It should be noted that there are now upgrade plans for CDF and DØ which very recently have been directed toward 2×10^{32} $\mathrm{cm}^{-2}\mathrm{s}^{-1}$.

2. **Luminosity Upgrade to** 10^{33} $\mathrm{cm}^{-2}\mathrm{s}^{-1}$**.** Going beyond 10^{32} $\mathrm{cm}^{-2}\mathrm{s}^{-1}$ has become a subject of considerable interest. The Main Injector and Recycler add significant capacity to the Collider Complex, and it seems that with additional low cost accelerator improvements the 10^{33} $\mathrm{cm}^{-2}\mathrm{s}^{-1}$ level is conceivable. As with the Main Injector scenarios, there are variations.

   (a) Bunch crossing time of 132 ns, at 10^{33} $\mathrm{cm}^{-2}\mathrm{s}^{-1}$ which gives rise to 9 interactions per crossing with two interaction regions.

   (b) Bunch crossing time of 19 ns, at 10^{33} $\mathrm{cm}^{-2}\mathrm{s}^{-1}$ which gives rise to 1.3 interactions per crossing with two interaction regions.

   This "superluminous" Tevatron upgrade has been dubbed "TeV33".

In addition to luminosity upgrades, other ideas being discussed for the Fermilab site include center of mass energy upgrades to 4 TeV (the "DiTevatron"), for $p\bar{p}$ or pp; an ultra–high energy pp or $p\bar{p}$ collider; a high energy e^+e^- linear collider, polarized p-unpolarized $\bar{p}$ collider; and a muon collider.

1.2 The *tev_2000* Effort

The *tev_2000* "workshop" was a grass–roots effort motivated by the richness of the physics at the Tevatron, the lack of an organized study of the Tevatron long range potential, and the notion that facilities planning for U.S. HEP in these times would do well to include a study of "what we could do with what we've got". It started with a two day meeting at the University of Michigan on October 21$^{\rm st}$ and 22$^{\rm nd}$ of 1994 to form an *ad hoc* partnership between CDF, D$\emptyset$, and the theoretical community. More than 100 physicists attended and divided into seven working groups to begin the exploration of the physics. This "extended workshop" continued throughout the winter, spring, and summer of 1995 on many U.S. campuses and at Fermilab. During this period, work within the Fermilab Accelerator Division reached the point of designing a $\bar{p}$ Recycler ring for the Main Injector project, and the high luminosity Tevatron was poised to move from a concept to an engineering design phase. We believe the physics case is now at a similar level of maturity.

The goals of the *tev_2000* effort were:

- To quantify the scientific case for high $p_{\rm T}$ and electroweak physics accessible with high luminosity at the Tevatron.
- To document this case as a foundation for further literature.

We have accomplished both goals with the completion of this report. The physics program that we have found is broad and has compelling programmatic components as well as significant discovery potential.

The subsequent chapters in this report describe in detail the first results in the following general areas:

Chapter 3: Top Physics

Chapter 4: Intermediate Vector Bosons, W's, Z's, and γ's

Chapter 5: Light Higgs Bosons

Chapter 6: Supersymmetry

Chapter 7: Exotics and Searches

Chapter 8: Physics Potential of a Polarized p–Unpolarized $\overline{p}$ Tevatron

Chapter 9: Detector Challenges

The physics studies all use a common set of assumptions regarding luminosity performance at the Tevatron. It was decided that we would first revisit the physics accessible in the classic Main Injector scenario, and then extrapolate to both modest and extreme improvements in the luminosity. The extrapolated scenarios would presumably come in different calendar periods, but the workshop chose to ignore the vagaries of calendar and to concentrate on the physics. The parameters of the strawman scenarios are:

- **Run II**
  - $p\overline{p}$ with 1TeV $\times$ 1TeV.
  - $\mathcal{L} \leq 10^{32}$ cm^{-2}s^{-1} with either 395 ns bunch spacing and 3 interactions/crossing or 132 ns bunch spacing and 1 interaction/crossing.
  - $\int \mathcal{L}\,dt = 2$ fb^{-1}.
  - Proposed CDF and DØ Run II upgrades.
- **Run II–"stretch"**
  - $p\overline{p}$ with 1TeV $\times$ 1TeV.
  - $\mathcal{L}$ increasing **beyond** 10^{32} cm^{-2}s^{-1} with either 395 ns or 132 ns bunch spacing. Interactions/crossing scale from values above.
  - $\int \mathcal{L}\,dt \sim 10$ fb^{-1}.
  - Multiple years of running, possibly overlapping with LHC.
  - Incremental CDF and DØ Run II upgrades, as required.
- **High Luminosity Running**
  - $p\overline{p}$ with 1TeV $\times$ 1TeV.
  - $\mathcal{L} = 10^{33}$ cm^{-2}s^{-1} with 9 interactions/crossing and 132 ns bunch spacing.
  - $\int \mathcal{L}\,dt = 100$ fb^{-1}. We consider this upper limit to establish the asymptotic level of statistical precision in each physics study.
  - "Reasonable" CDF and DØ Run II detector extrapolations.

We assume that it will be possible to maintain detector performance levels of the CDF and DØ Upgrades by appropriate evolution of technologies. This allows us to use standing simulations for the physics studies. Since these simulations have been tuned to existing detectors in a well studied environment, we believe that our results have a degree of credibility beyond what is usually found in proposals of this type. We have considered detector issues in a general way in Chapter 9, and we find no "show stoppers". In a few critical cases we have also explicitly evaluated the effect of high luminosity conditions, for instance the impact of 9 overlapping interactions on the SUSY sensitivity, and on mass resolution in the Higgs search, and we have found the effects in these cases to be small. But we readily acknowledge that such issues require more work, and we hope that this report will stimulate further inquiry.

Our results on the physics potential of an extended Tevatron program are summarized in Chapter 2, and described in detail in Chapters 3 through 9. Where possible, we have compared with LEPII, NLC, and the LHC. We emphasize that this is the *first* look at a post–SSC Tevatron and that these results should be considered preliminary. Experience with the Collider suggests that the ultimate physics menu which would develop with tens of fb^{-1} will be richer than what is indicated by this initial study.

Chapter 2

Physics Conclusions and General Recommendations

This chapter summarizes the results from each of the working groups and draws general conclusions. The results of the workshop indicate a rich and competitive physics program for a superluminous Tevatron.

2.1 Conclusions of the Physics Groups

2.1.1 Top Physics

A detector with high–rate capability comparable to that of the CDF or DØ upgrades will identify approximately 500 b tagged (i.e. identified) top quark events per fb^{-1} in the ℓ+ jets mode. This is 2 to 5 times the yield in this mode for equivalent luminosity at an NLC. With integrated luminosities in excess of 10 fb^{-1} it will be possible to:

- Measure a top quark mass to a precision of 2 GeV/c^2 per experiment.
- Measure the $t\bar{t}$ production cross section to 6%.
- Measure the top quark branching fraction to b quarks in association with W with precision exceeding 2%.
- Measure the ratio of dilepton to single lepton decay rates to better than 5%, yielding the partial width to non-W final states with a precision of 6%.
- Probe for $t\bar{t}$ resonances out to masses of roughly 1 TeV/c^2.
- Probe the Wtb couplings by measuring branching fractions to W helicity states with statistical precisions of a few percent.
- Isolate electroweak single top production via t-channel W-gluon fusion $qg \to t\bar{b}q'$ and s-channel W^* production $q'\bar{q} \to t\bar{b}$, and use these production modes to:

  - Measure the cross sections to $\sim 10\%$.
  - Measure the partial width , $(t \to Wb)$ to $\sim 12\%$.
  - Measure the CKM matrix element V_{tb} with a precision of 6%.
  - Search for anomalous couplings and CP violation effects.

- Probe for the rare decay $t \to c + \gamma$ with sensitivity of 10^{-4}.
- Probe for the rare decay $t \to Z + c$ with sensitivity of 10^{-3}.

The program of accessible top quark physics at the Tevatron is certainly larger than this list and it is not inconceivable that a 180 GeV/c^2 fermion may have surprises in store. This is therefore *not* the menu of all measurements, but instead a survey of *sensitivity levels* for the ultimate broad program of top physics at the Tevatron.

2.1.2 Intermediate Vector Boson Physics

With very large integrated luminosities at the Tevatron, the electroweak sector of the SM can be probed in great detail. Our preliminary studies arrive at the following conclusions:

- With 10 fb^{-1} it should be possible to measure the mass of the W boson with a precision of at least 30 MeV/c^2, and 20 MeV/c^2 may well be within reach. This is about a factor of 2 better than what one expects for LEP II. With a precision of 20 MeV/c^2 (30 MeV/c^2) for the W mass, and 2 GeV/c^2 for the top quark mass, the Higgs boson mass can be predicted with an uncertainty of about 40% (50%) of itself. This prediction may be very useful for direct Higgs searches at the Tevatron, LHC, or NLC, and comparison with the results of a direct search will constitute an essential set of tests of the SM.

- The W width can be measured with an uncertainty of about 15 MeV. This is an improvement of almost one order of magnitude of the current uncertainty. At LEP II , $_W$ can only be measured with a precision of a few hundred MeV.

- The W charge asymmetry will be a very powerful tool in constraining the parton distribution functions. In many processes the error in the parton distribution functions currently constitutes a major source of uncertainty. The forward backward asymmetry, A_{FB} in Z boson decays provides a useful cross check on the Higgs boson mass extracted from the W mass measurement.

- With 10 fb^{-1}, the WWV and $Z\gamma V$, $V = \gamma, Z$, vertices can be determined with a precision of $\mathcal{O}(10^{-1})$ and $\mathcal{O}(10^{-2} - 10^{-3})$, respectively, at the Tevatron. The expected accuracy for the WWV couplings is comparable or better than that of LEP II. However, since the methods used to extract limits on anomalous couplings at the two colliders are different, data from the Tevatron and LEP II yield complementary information. Tevatron experiments will be able to place limits on the $Z\gamma V$ couplings which are up to a factor 100 better than those which can be achieved at LEP II. At the LHC, with

100 fb^{-1}, it will be possible to place limits on anomalous WWV and $Z\gamma V$ couplings which are a factor 3 to 100 better than those one can expect for the Tevatron with 10 fb^{-1}.

- The Tevatron offers a unique chance to search for the SM "radiation zero" in $W\gamma$ production, which provides an additional test of the gauge theory nature of the SM. At the LHC, due to the large qg luminosity, QCD corrections obscure the dip in the photon lepton rapidity difference distribution which is caused by the radiation zero. This is not the case at Tevatron energies. Currently, the experimental results are statistically limited. With integrated luminosities of 2 fb^{-1} or more, it should be possible to conclusively establish the existence of the radiation zero.

- With an integrated luminosity of 10 fb^{-1}, limits on the branching ratios of rare W decays of $\mathcal{O}(10^{-5})$ to $\mathcal{O}(10^{-7})$ can be obtained. W decays into two pseudoscalar mesons offer an opportunity to probe meson decay form factors at a very high momentum transfer where these form factors have not been tested so far.

- The Tevatron offers a unique opportunity to search for CP violation in W boson production and decay since it collides protons and antiprotons, i.e. the initial state is a CP eigenstate. The extremely large number of W boson events expected at a superluminous Tevatron will make it possible to search for small CP-violating contributions to W boson production, at the level of $\mathcal{O}(10^{-3} - 10^{-4})$.

- An integrated luminosity of 10 fb^{-1}, will produce a sufficient number of $W\gamma\gamma$, $Z\gamma\gamma$ and $WW\gamma$ events to extract direct information on the quartic gauge boson couplings.

2.1.3 Light Higgs Physics

A light intermediate-mass scalar in the mass region 80 GeV/c^2 $< m_H <$ 130 GeV/c^2 is predicted by minimal supersymmetric models, and current precision electroweak data also show a slight preference for a low mass Higgs. This study confirms recent theoretical speculation that there is a **luminosity threshold for the detection of a light Standard Model Higgs boson at the Tevatron**, and suggests that this threshold varies from 5 to 25 fb^{-1} as m_H varies from 60 to 120 GeV/c^2.

- The process $q'\bar{q} \to WH$, with $H \to b\bar{b}$, is the best single mode for the detection of a light Higgs boson at the Tevatron, and leads to the luminosity thresholds stated above. The analysis relies heavily on the understanding of b tagging, the "W + flavor" backgrounds, and mass fitting with jets, and is therefore a natural complement and extension of the top physics program.

- The process $\bar{p}p \to (W,Z)H$, with $H \to \tau^+\tau^-$ and $(W,Z) \to jj$, is difficult at the Tevatron due to the large $(Z \to \tau^+\tau^-)jj$ background, but may add to the overall significance of the observation. Other channels, such as ZH with $Z \to \nu\bar{\nu}$ and $H \to b\bar{b}$, have not been investigated, and should be. A set of combined channels may have better significance than our single studied channel of WH with $H \to b\bar{b}$, and this should also be investigated.

- We have studied the potential of the $W + H \rightarrow b\bar{b}$ measurement at the LHC, assuming equivalent detection efficiencies, etc and find that it is difficult there because of large top backgrounds. It may be that the intermediate mass region is accessible at the LHC only via the rare decay mode $H \rightarrow \gamma\gamma$. Since the branching fraction to $\gamma\gamma$ varies with the choice of SUSY parameters, the LHC cannot prove that the light Higgs boson of SUSY does not exist if it is not found there.

- The process $q'\bar{q} \rightarrow WH$ is complementary to the LEP II/NLC process $e^+e^- \rightarrow ZH$, since it involves the coupling of the Higgs boson to different weak bosons. The ratio of these couplings can vary in multi-Higgs models with multiplets other than doublets (e. g., Higgs triplets).

Although further study is needed, the opportunity to detect a light Higgs boson at the Fermilab Tevatron appears to be real.

2.1.4 Supersymmetric Physics

For the next decade, the Tevatron will continue to be the highest energy accelerator in the world. We must exploit this opportunity to not only study the top quark, but to search for the signature of one of the most tantalizing new physics theories proposed beyond the Standard Model - supersymmetry (SUSY).

There are many arguments why SUSY provides an elegant extension to the Standard Model. SUSY solves the gauge hierarchy problem, unifies the SM coupling constants, provides a candidate for cold dark matter, solves the Higgs mass fine tuning problem and is naturally decoupled from Standard Model particles. The experimental consequence of these arguments for the existence of supersymmetry at the weak scale is the presence of 32 new particles in the mass range $\sim$100 to 1000 GeV/c^2. It is not surprising that none of these particles have been discovered yet, since most current limits from supersymmetric particle searches are below this range.

With a detector similar to the upgraded DØ/CDF detectors and an integrated luminosity of order 20-25 fb^{-1}, the Tevatron will be able to significantly probe a large fraction of the expected SUSY mass range for the first time. It should be noted that the light Higgs (h) search is also an important concomitant search, since SUSY predicts it to be lighter than about 130 GeV/c^2.

Using the SUSY model based on the particle spectrum of the MSSM (a SUSY partner for each SM particle with two Higgs doublets) combined with grand unification (based on supergravity) and R parity, our preliminary conclusions are:

- We will be able to search for charginos with masses up to 250 GeV/c^2. The mass reach depends on the choice of the unknown SUSY parameters. Therefore, even though the Tevatron can find a chargino with a 250 GeV/c^2 mass, it cannot completely rule out all charginos below this mass.

- We will be sensitive to gluinos with masses up to about 400 GeV/c^2, depending on the SUSY parameters. Note, that the Tevatron can find gluinos with masses below about 300 GeV/c^2 for any choice of parameter.

- The Tevatron can search for light supersymmetric top quarks in various decay modes up to about 180 GeV/c^2 mass.
- The SUSY searches at TeV33 are complementary to those at LEP-II and NLC. For example, if LEP-II found a 90-GeV chargino, we expect the gluino mass to be in the range 270-360 GeV/c^2, which will be accesible at TeV33 (but not LEP-II). A preliminary study on the determination of the gluino mass at TeV33 shows that a 300-GeV/c^2 gluino mass could be measured with a resolution of about 20 GeV/c^2. TeV33 is also competitive to NLC in the gluino/squark searches.

The Tevatron enjoys an unique window of opportunity to discover the first evidence for a highly motivated theory beyond the Standard Model. The increased luminosity available at TeV33 is necessary to exploit this opportunity during the next decade.

2.1.5 Exotic Physics

An integrated luminosity approaching 100 fb^{-1} at the Tevatron greatly extends the present mass reach for exotic objects. Specifically, a data set of 100 fb^{-1} is sensitive to:

- W' and Z' up to 1.3 TeV/c^2
- axigluons in dijet mode up to 1.3 TeV/c^2
- E_6 color triplet scalar diquarks in dijet mode up to 800 GeV/c^2
- first generation leptoquarks up to 360 GeV/c^2
- compositeness in $qqqq$ mode up to 2.8 TeV/c^2
- compositeness in $qqll$ mode up to 7.4 TeV/c^2
- excited quarks up to 1.2 TeV/c^2
- color octet ρ_t in dijet mode up to 1.0 TeV/c^2
- massive stable particles
  - color triplets up to 540 GeV/c^2
  - color sextets and octets up to 600 GeV/c^2
  - color decuplets up to 660 GeV/c^2

Without any theoretical prejudice of the mass of new particles, a superluminous Tevatron effectively *doubles* the current discovery potential.

2.1.6 Physics with Polarized Protons

The electroweak physics benefits of polarizing the proton beam have received only a zeroth–order look.

- It may be feasible to polarize the proton beam, transversely and longitudinally in the Tevatron at high luminosity. The cost is not unreasonable, but the effect on relative performance is an issue.
- Polarizing the proton beam may result in a non–negligible improvement of the signal to noise background ratio for certain measurements, in particular where there are competing QCD and electroweak processes.
- Until a solution to the anticipated reduction in luminosity is found, the arguments in favor of polarizing one beam are not compelling enough to warrant a decision to proceed at this time. This intensity loss may not be the final story, and so it is recommended that continued accelerator R&D be done to address this question. Likewise, the physics opportunities in this one polarized beam scenario should continue to be explored.
- If it were possible to polarize both the proton and the antiproton beams, then the above background arguments signficantly improve and distinct physics opportunities might arise.

2.1.7 Detector Challenges

The high luminosity environment at the Tevatron will present a challenge to detectors, and more detailed work is required. Our initial impressions are as follows:

- Tracking and vertex-tagging seem to be feasible in a high–rate environment, based on current CDF experience and simulations of both the DØ and CDF upgrade designs. Efficiencies $> 50\%$ and mistag probability of $< 1\%$ are sufficient for the most interesting physics. Maintaining this performance in the presence of many interactions per crossing remains an issue for further study.
- Calorimeter energy resolution and coverage similar to the upgraded CDF and DØ detectors should be adequate. The effects of pileup on the calorimetric performance, and especially electron identification and $\not\!\!E_{\rm T}$ have been studied in a preliminary way using real minimum bias data in simple simulations. This work suggests that electron isolation efficiencies are only slightly degraded. On the matter of $\not\!\!E_{\rm T}$, we see that the degradation of primary vertex resolution may be a significant effect, but overall, for situations in which the $\not\!\!E_{\rm T}$ distribution is flat, there seems to be only a marginal effect. There are no results as yet for steeply falling distributions.
- Muon detection performance similar to the upgraded CDF and DØ detectors should be adequate. The muon momentum measurement will continue to be dominated by the central magnetic tracking. Backgrounds will likely become a more serious problem for muon triggering and analysis.

- Given reasonable assumptions regarding future bandwidths, a first pass at a trigger list suggests that the high $p_{\rm T}$ processes of interest can be accommodated. However, the assumptions of 50 kHz/5 – 10 kHz/100 – 200 Hz for L1/L2/L3 outputs are aggressive goals relative to current CDF and DØ capabilities. The question of how the trigger rejection degrades in a high luminosity environment also needs study.

- Offline processing is always a surprise in what can be accomplished. Assuming 500 MIPS-sec per event reconstruction capability, similar to the current time, a near real–time farm would need 200 workstations of 500 MIPS each. This is not inconceivable on the timescale required.

2.2 Recommendations

As previously noted, we believe that this work is not complete. We have shown that a future path of increasing luminosity at the Tevatron will lead to a full program of measurements in Top, IVB, Higgs, SUSY, and Exotic physics. Our general conclusions, as of December 1995, are these:

2.2.1 Recommendations to Fermilab

1. Fermilab will be the top quark factory for many years. As with other heavy quarks, the top quark may be entering the first of many decades of serious scrutiny. Those planning the physics program should recognize this major scientific opportunity.

2. Our study confirms recent theoretical speculation that there is a luminosity threshold for the detection of a light Higgs boson at the Tevatron, and suggests that this threshold may be at the 5-25 fb^{-1} level. The most promising single detection technique relies on detailed understanding of b tagging and the "W + flavor" backgrounds, and is therefore a natural complement and extension of the top physics program. We recommend that:

   (a) the presence of the detection threshold and its value be confirmed in more detailed simulation, including b tagging in the presence of multiple interactions.

   (b) a Tevatron strategy for crossing the luminosity threshold be developed and implemented.

3. The Tevatron program can either discover SUSY or significantly constrain a large fraction of current theoretical prejudice. The actual sensitivity and discovery potential for supersymmetric states at the Tevatron deserves significantly more study.

4. High instantaneous luminosity conditions need to be understood better with perhaps both simulation and actual detector research and development. This is especially true for the top and Higgs studies. Will it handicap the current detectors? If so, how? We urge the Laboratory to initiate an active program to investigate these questions and to engage the high energy physics community in the effort. We believe the effort will benefit from computing, R&D, and possibly test beam resources.

5. There may be significant luminosity capability beyond the "classic" Main Injector scenario during Run II. If such incremental increases in peak luminosity cannot be handled by the detectors, could this capability be channeled into a significant increase in the useful longevity of $> 10^{32}$ stores? After all, *integrated* luminosity is the key.

6. The physics overall is tantalizing, and we believe that simply waiting for the LHC is unwise. The Laboratory and the experimental collaborations should make every effort to maximize the physics return of the Tevatron. This implies the need for **an overall plan for the long term Tevatron Program** including the accelerator, the detectors, and physics simulation.

2.2.2 Recommendations beyond Fermilab

Compared to the reach of the SSC or the LHC, the high $p_{\rm T}$ physics program at the Tevatron has sometimes been casually judged to be at an end. During the SSC era, this judgement devalued all future planning for the FNAL complex, and as the LHC era looms, this sentiment might be heard again. Meanwhile, the Tevatron has uncovered a new fermion with a mass at the weak scale, and new ideas about the Tevatron luminosity enable a compelling menu of top quark and discovery–level high $p_{\rm T}$ physics — a complete Physics Program. This research was not even contemplated a year ago as applicable to Fermilab.

A productive Fermilab facing a planned LHC is an interesting example of the tension between present and future in the age of Big Science, and the importance for balance between long range commitments and data driven progress. This issue is addressed in Chapter 10.

Chapter 3

Top Physics

3.1 Introduction

The top quark is a state which the Standard Model tells us to expect, and for which the agreement between recent direct observation at the Tevatron [1, 2] and indirect expectation [3] is already impressive. At the same time, the top quark has a mass approximately twice that of the weak bosons, making it the only fermion which decays to a real W, and the only quark without a spectroscopy of hadrons. Is this an accident or is this a clue? Experiment is the way to know, and in this case we find another curiosity: although the physics is at the limits of sensitivity at the present Tevatron, it becomes accessible with relatively modest enhancements to the accelerator and detectors.

In this chapter we describe results from several preliminary studies of the potential for top physics at a high luminosity Tevatron. We do not suppose a particular operating point or detector configuration, but simply specify the physics reach as a function of integrated luminosity, assuming maintenance of detector performance comparable to the planned CDF and DØ upgrades for Tevatron Run 2. We discuss the expectations for three luminosity goals as described in Section 1.2 of this report: the present Run 2 plan of 1-2 fb^{-1}, an aggressive "stretch" of Run 2 to 10 fb^{-1}, and finally, a more ambitious program with asymptotic statistical precision represented by 100 fb^{-1}.

We first concentrate on $t\bar{t}$ production for $m_t \approx 170$ GeV/c^2. After describing detected event yields, we discuss measurement of the $t\bar{t}$ production cross section, the top mass, some features of the Wtb vertex, decay branching ratios, rare decays, and exotic production mechanisms. We then discuss electroweak single top production, the prospect for isolation of the composite and component signals in this process and derivative measurements. Comparison is made with prospects at other facilities, and we conclude with a tabular summary of Tevatron measurements and their precision.

In all this, we believe we are only beginning to specify the catalog of interesting measurements in the top sector, and that this report is best interpreted as a survey of representative *sensitivities* in the broad program of top physics accessible at the Tevatron.

3.2 Event Samples in $t\bar{t}$

Future $t\bar{t}$ event yields at the Tevatron can be inferred with reliable precision by extrapolating from the situation presently understood at CDF and DØ . The standard $t\bar{t}$ selection is based on the expected decay chain $t\bar{t} \to (W^+b)(W^-\bar{b})$ and the subsequent decays of the W's into fermion pairs. At least one W is tagged in the mode $W \to l\,\nu$ by requiring an isolated high E_T lepton (e or μ) and large $\not\!\!E_T$. In the "dilepton" analysis the leptonic decay of the other W is identified with a loose lepton selection; this mode has small backgrounds but small branching fraction of just 4/81. In the "lepton+jets" mode, the second W decays to quark pairs, giving a larger branching fraction of $24/81 \approx 30\%$ (lepton = e or μ). The final state of (lνb)(jjb) is separated from the primary background, W+jets, by requiring a large multiplicity of high E_T jets and also evidence of a B decay, using either secondary vertex identification (SVX) or a tag of the "soft lepton" from $b \to c l \nu_l X$ (SLT).

3.2.1 Top Event Selection

We discuss the situation as understood with the CDF detector configuration, which we believe applies generically to a hadron collider detector with charged particle tracking in a magnetic field, good lepton identification, and a silicon microstrip detector for identification of secondary vertices.

In this study, dilepton selection starts with a well identified, isolated, 20 GeV lepton and $\not\!\!E_T \geq 20$ GeV, and then demands an additional lepton passing relaxed cuts and two jets with $E_T \geq 10$ GeV. The efficiency of this selection, ϵ_{dil} is approximately 16% for $M_{top} = 170$ GeV/c^2.

The present l+jets selection selection starts from a single well identified lepton and $\not\!\!E_T$ requirement as above, plus the requirement of at least 3 jets with $E_T \geq 15$ GeV and $|\eta| \leq 2.0$. The combined efficiency of this selection in the e and μ modes, ϵ_{l+3j}, is approximately 29% for $M_{top} = 170$ GeV/c^2.

The b-tagging algorithms are then applied to see which jets in these events are candidates for the 2 b jets expected from $t\bar{t}$ decay. The secondary vertex b-tagging efficiency is a function of the intrinsic efficiency of the silicon detector and the tagging algorithm for a well contained b jet, which combine to give $\epsilon_{SVX} = 44\%$. Including also the limited acceptance of the silicon system, the total probability to tag at least one b jet in any top event is 42% [1]. The soft lepton tag has an efficiency of 13% per b jet and 20% per event. Subtracting the small overlap between algorithms gives a total combined b-tagging efficiency of $\epsilon_{t\bar{t}\to b+X} = 53\%$ per event. The total efficiency for the l+3jets+btag selection is then $\epsilon_{l+3j*b} = \epsilon_{l+3j} \times \epsilon_{t\bar{t}\to b+X} = 15\%$.

The constrained fit technique presently used in the top mass measurement requires a "completely reconstructable" event, that is, all 4 final state jets consistent with the $t\bar{t}$ decay hypothesis. The present selection requires a fourth jet with $E_T \geq 8.0$ GeV and $|\eta| \leq 2.4$, and is found to have an efficiency before b-tagging of $\epsilon_{l+4j} = 25\%$.

The signal to background ratio is measured to be approximately 5:1 in the dilepton mode. In the secondary vertex analysis, requiring at least one b-tag, this ratio is 3:1 in the

3 jet selection, and 12:1 in the 4 jet selection.

When	b_{jet}^{SVX}	b_{jet}^{SLT}	$\epsilon_{t\bar{t}\to b+X}$	$\epsilon_{t\bar{t}\to 2b+X}$
Run 1b	44%	13%	53%	13%
Run 2	60%	13%	85%	42%

Table 3.1: b-tagging efficiencies at CDF. The probability to tag b in the geometrical acceptance is b_{jet}. Including detector acceptance, the probability for the combined SVX+SLT techniques to tag either or both b's in a 170 GeV/c^2 top event is given in the last 2 columns.

When	ϵ_{dil}	ϵ_{l+3j}	ϵ_{l+4j}	ϵ_{l+3j*b}	ϵ_{l+4j*b}	$\epsilon_{l+4j*2b}$
Run 1b	16%	29%	25%	15%	13%	3.2%
Run 2	23%	35%	30%	29%	25%	13%

Table 3.2: Efficiencies for kinematic and b-tag selection at CDF. The last column is for tagging both b's, the 2 columns before are for tagging *at least* one b.

3.2.2 Future Top Selection

The top event yields described above will be improved in Run II by upgrades to the CDF and DØ detectors. The impact of these upgrades has been analyzed in detail. For the case of CDF the yield of identified top events will be improved as follows:

- **High P_T Charged Lepton Identification.** The ability to find and match tracks to the shower information in the forward regions will extend good charged lepton identification into the region $1.0 \leq |\eta| \leq 2.0$. Monte Carlo studies indicate that this will increase the acceptance for a 20 GeV lepton from 170 GeV/c^2 top by 22% for each $W \to e\nu$ and 16% for each $W \to \mu\nu$ [6]. We assume here that lepton identification in the forward region will be made to work with signal to background ratios comparable to those in the present top analysis. The improvement in efficiency then scales with acceptance, up to 23% for dileptons, 35% for l + 3 jets, and 30% for l + 4 jets. Complete muon coverage in the region $1.0 \leq |\eta| \leq 2.0$, such as that at DØ will improve the yield by another 10%.

- **Secondary Vertex b-Tagging.** The improvement here is significant. The addition of the third view (along the beamline) will eliminate a large fraction of mistags, allowing more efficient selection at constant background. The standalone pattern recognition in the silicon + fibers will improve the acceptance for low P_T tracks and dense jets. The efficiency to tag a fiducial B jet from decay of a 170 GeV/c^2 top is expected to approach 60%. The new silicon system will cover the full length of the luminous region, so that all events are taggable, increasing the acceptance by $\approx 50\%$. The standalone

tracking capability of the inner tracker also extends the fiducial acceptance into the region $1.0 \leq |\eta| \leq 2.0$, where 27% of top events have at least 1 b jet. In the end, 97% of all B tracks in all top events are contained in this system [5]. The efficiency to tag at least 1 b jet in a 170 GeV/c^2 top event with a secondary vertex will be $\sim 81\%$.

- **Soft Lepton and Total b-Tag Efficiency** The soft lepton b-tag is a less powerful, but still useful complement to the secondary vertex tag. The extension of lepton identification to the region $1.0 \leq |\eta| \leq 2.0$ will improve the acceptance of the soft lepton tag by $\sim 15\%$ for each B. We assume, as before, that an acceptable signal to background ratio is achievable, and that the efficiency improvement scales with the acceptance gain. As discussed above, the electron coverage will be slightly better than the muon coverage, giving an overall net improvement of $\sim 12\%$ for each b. After subtracting the overlap fraction the combined b-tagging efficiency of the SVX + SLT algorithms is found to be $\sim 65\%$ per b jet from 170 GeV/c^2 top decay. The probability to tag at least 1 b jet in such a top event will be $\sim 85\%$. If the soft lepton tagging is limited to the central region, this probability will be only slightly reduced to $\sim 83\%$.

- **Double b-Tag** The ability to tag *both* b's in a top event will be useful in the mass measurement and other kinematic studies where it is important to suppress combinatoric confusion. With a tagging efficiency of 65% per b jet as above, we expect a double b-tag efficiency of 42%. This is probably an underestimate, since the presence of a single tag has already reduced the backgrounds considerably, and looser criteria can be applied to either identify the second B or "anti-tag" the non-b jets from W decay. We will take $\epsilon_{t\bar{t}\to 2b+X} \sim 42\%$ as the *lower limit* on the double tag efficiency.

Taking the product of the kinematic and b-tag efficiencies yields the Run II top selection efficiencies shown in Table 3.2. The products of branching ratio times efficiencies are shown in Table 3.3. We see that in the case of CDF, the effect of the upgrade will be to double the efficiency for single b-tagged events, and quadruple the efficiency for double b-tags.

These efficiencies are a function of the coverage and effectiveness of lepton identification, silicon tracking, and jet calorimetry, and can be considered typical for a generic collider detector operating with these systems in the region $|\eta| \leq 2.0$. A similar analysis of the DØ upgrade [8] has verified this by producing comparable results. We will assume in what follows that the efficiencies listed above can be maintained at high luminosities by appropriate evolution of detector technologies.

3.2.3 Yields

The calculation of absolute yields requires a cross section for top production at the Run II operating point of $\sqrt{s} = 2.0$ TeV. We use the central value from the resummed next-to-leading-order calculation of Laenen *et al.*, $\sigma_{t\bar{t}} = 6.8$ pb for $m_t = 175$ GeV/c^2 [9]. For comparison, note that the Standard Model value for the same mass at $\sqrt{s} = 1.8$ TeV is $4.95^{+0.7}_{-0.4}$ pb [10], and that the present measurement is consistent, with $\sigma_{t\bar{t}} = 6.8^{+3.6}_{-2.4}$ pb at CDF [1], and $\sigma_{t\bar{t}} = 5.2 \pm 1.8$ pb at DØ [12]. The future yields are shown for benchmark data

sets in Table 3.4. At $m_t = 175$ GeV/c^2 each inverse femtobarn at the Tevatron will produce approximately 600 b-tagged events and approximately 250 double b-tagged, completely reconstructable events.

When	dilepton	l+3j	l+4j	$l + 3j * b$	$l + 4j * b$	$l + 4j * 2b$
Run 1b	0.8%	8.7%	7.5%	4.5%	3.9%	1.0%
Run 2	1.1%	10%	8.9%	8.6%	7.6%	3.8%

Table 3.3: Total efficiency ($B \cdot \epsilon$) for top selection at CDF. The last column is for tagging both b's, the 2 columns before are for tagging *at least* one b.

Mode	1 fb^{-1}	10 fb^{-1}	100 fb^{-1}
produced	6.8K	68K	680K
dilepton	82	820	8.2K
W + 3j	680	6.8K	68.0K
W + 3j * b	584	5.8K	58.4K
W + 4j	605	6.0K	60.5K
W + 4j * b	517	5.2K	51.7K
W + 4j * bb	258	2.6K	25.8K

Table 3.4: Top yields

3.3 Measurement of the Top Quark Mass

The mass of the top quark is a fundamental Standard Model parameter and should be measured as accurately as possible. In addition, the value of m_t appears significantly in radiative corrections which connect the Standard Model parameters, and a global fit combining m_t and other experimental information tests for consistency and predicts unknowns, notably the unknown mass of the Higgs scalar, m_H. If we assume that LEPII and future Tevatron running will yield $\delta m_W = 20$ MeV/c^2, Section 4.2.4 of this report shows that measurement of m_t with a precision of 2 GeV/c^2 will constrain m_H to within 50% of itself. This is interesting in its own right, and also very useful for sharpening direct Higgs searches at future facilities.

We describe below two complementary techniques for measurement of m_t at the Tevatron using the lepton + jets mode and the dilepton mode. Since the control of systematic effects in these measurements benchmarks the precision for much of the top physics program, the discussion is detailed. We estimate the probable precision of each method as a function of luminosity. We conclude with a projection on the ultimate m_t precision at the Tevatron.

3.3.1 Mass Reconstruction in Lepton+Jets Using a Constrained Fit

The most accurate technique at present for top mass measurement at the Tevatron is complete reconstruction in $t\bar{t} \rightarrow$ W + 4 jets [1, 2, 13]. Events are selected according to the prescription described in Sec. 2.1, and the lepton and the four highest E_T jets in the event are fit to the hypothesis $t\bar{t} \rightarrow (Wb)(Wb) \rightarrow (l\nu b)(jjb)$. Each jet is extrapolated back to a parton energy by correcting on average for instrumental effects (e.g. calorimeter nonlinearity) and physics complications (e.g. out of cone radiation, semileptonic B decays). The fit tries all jet-parton assignments, allowing jet energies to vary within the expected resolution, constraining $M(l\nu) = M(jj) = m_W$ and $m_t = M_{\bar{t}}$. The 2-C fit has multiple solutions in each top event due to incorrect assignment of jets to primary partons and the quadratic ambiguity in the longitudinal momentum of the neutrino from $W \rightarrow l\nu$. Solutions are chosen according to low or lowest χ^2 and consistency with b-tagging. The shape of the mass spectra for various values of m_t, as well as that expected for the W+4 jets and other backgrounds, are derived from Monte Carlo samples, and a maximum likelihood fit to the data yields the best estimate of the top mass. The outcome of this procedure in the present analysis is $m_t = 176 \pm 8 \pm 10$ GeV/c^2 at CDF and $m_t = 170 \pm 15 \pm 10$ GeV/c^2 at DØ [1, 14].

3.3.2 Experimental Issues in the Constrained Fit

Almost all of the individual systematic uncertainties in the top mass measurement are coupled to the reliability of the Monte Carlo models for the distribution of fit masses in background and signal. This issue has both theoretical and experimental components. We describe here the experimental issues as presently understood, and return to the theoretical issues later.

The expected mass distribution in top events has been studied with the HERWIG Monte Carlo [15] and the CDF detector simulation. The calorimeter response in this simulation has been tuned to the data in a variety of ways, from single track response to jet balancing in large inclusive samples, and the simulated jet energies are extrapolated back to parton energies using the same prescription employed for real data. The shaded histogram in Fig. 3.1 shows the mass distribution at $m_t = 170$ GeV/c^2 when the MC level information is used to pick the correct final state assignments. The distribution is approximately Gaussian, with mean of 170.0 GeV/c^2 and $\sigma = 11.0$ GeV/c^2.

The instrumental contributions to the jet energy resolution include calorimeter nonlinearity, losses in cracks and dead zones, and absolute energy scale. However, the dominant part of the jet energy uncertainty is related to the reliability of the extrapolation to parton energies, and it is the understanding of QCD, not the detector, which presently limits the mass resolution. Both issues can be addressed by *in situ* calibration procedures which use energy balance in e.g. γ+ jet and (Z $\rightarrow$ ee) + 1 jet events. For the instrumental calibration one constructs an energy and position dependent map of the hadronic response in terms of the well measured electromagnetic one. For the QCD issues one studies energy flow in the jet cone and its comparison to Monte Carlo simulations. The latter has many subtleties: Is the hadronic environment in the control samples applicable to top events? How much does

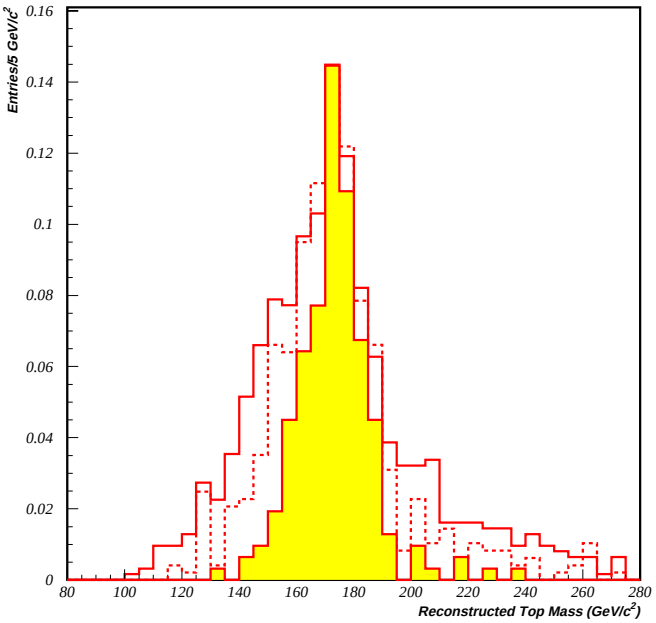

Figure 3.1: The distribution of constrained fit masses for HERWIG $t\bar{t}$ events with $m_t = 170$ GeV/c^2. Shaded curve is correct jet-parton assignment, solid curve is the lowest χ^2 solution with 1 b tagged, dashed curve is with 2 b's tagged.

jet energy tuning depend on parton flavor?

In addition to the jet energy uncertainties, the mass resolution is broadened by combinatoric confusion in the identification of the right parton-jet assignment. The HERWIG model of the procedure suggests that the four jet selection employed here is contaminated by an ISR or FSR initiated jet approximately 50% of the time, and that the minimum χ^2 solution contains an incorrect assignment (above and beyond an ISR/FSR substitution) approximately 40% of the time. All told, the correct 4 jet assignment is ~30% probable. In Fig. 3.1 the mass distribution of the solution with lowest $\chi^2 \leq 10$ and one b-tag is shown as the solid curve. The mean shifts only slightly but the width broadens by 40% to $\sigma = 15$ GeV/c^2. Since the level of combinatoric confusion depends strongly on the population of extra jets and the population of kinematic configurations which give "multiple" solutions, it is again clear that the reliability of the QCD models is the greatest source of systematic uncertainty.

Although the single b-tag requirement reduces the number of possible combinations from 24 to 12, it has little effect on the overall width compared to the case of no b-tagging. The impact of single b-tag is on background control. However the effect of double b-tagging on the combinatoric width is significant. The mass distribution in events with both b's identified is shown as the dashed curve in Fig. 3.1. The double tag restores the width of the

Effect	.07 fb^{-1}	1 fb^{-1}	10 fb^{-1}	comment
Jet scale QCD	7.7	2.0	0.6	$1\sqrt{N}$ scaling
Jet scale calorimetry	3.1	0.8	0.3	$1\sqrt{N}$ scaling
Jet scale total	8.3	2.1	0.7	sum in quad of above
Jet scale total		3.3	1.0	realistic (see 3.4.B)
b-Tagging Bias	2.4	0.6	0.2	control studies
Background Shape	1.6	1.6	0.6	control studies
Fitting Technique	3.1	0	0	
Monte Carlo Stats	3.1	0	0	
Total	10	3.7	1.2	

Table 3.5: Systematic uncertainties in top mass determination. All errors are in GeV/c^2. The first column is based on a preliminary CDF Run 1 result. The extrapolation to higher luminosities is discussed in text

central peak to $\sigma = 12$ GeV/c^2, leaving most of the effect of the combinatoric confusion in modest non-Gaussian tails.

The quantitative relation between the individual uncertainties (i.e. δE^{jet}_{scale}) and the final fit top mass is presently the object of serious study. The size of each uncertainty is estimated from a control sample study, and physics models like HERWIG and VECBOS [16] are used with detector models to propagate the effect through the full simulation including combinatoric confusion. A rule that seems to be emerging is that there is an approximately linear relation between jet energy uncertainties of all kinds and the top mass precision, given by

$$\delta m_t(\mathrm{Gev/c^2}) \approx (1.0) \times \delta E^{jet}_{scale}(\%)$$

The presently understood uncertainties from jet scale ambiguities due to both calorimetry and QCD are shown in the left-most column in Table 3.5, which represents conclusions from an analysis using 67 pb^{-1}at CDF.

Several other sources of uncertainty as understood at present are also listed in the leftmost column of Table 3.5. The size of any potential bias from the b-tagging requirements is studied with B control samples and top Monte Carlo. The reliability of the W+4 jet background model (VECBOS) is verified in the data at low jet multiplicity and a mass uncertainty is derived by studying the fit mass for reasonable variations of the model input parameters. In the present analysis there are small but significant uncertainties due to limited Monte Carlo samples and changes seen with variation of statistical techniques. The sum of all effects at present is estimated to be 10 GeV/c^2.

3.3.3 Future Precision of the Constrained Fit

Early studies have verified that the statistical uncertainty in the constrained fit does scale like $1/\sqrt{N}$ [17]. The HERWIG model studies above can then be normalized to the present

Mode	δm_t	.07 fb^{-1}	1 fb^{-1}	10 fb^{-1}
stat. W+4j	$38/\sqrt{N}$	12	1.6	0.5
stat. W+4j+b	$35/\sqrt{N}$	8	1.5	0.5
stat. W+4j+bb	$27/\sqrt{N}$	25	1.7	0.5
sys. W+4j+b	$43/\sqrt{N}$	10	2.5	0.8
sys. W+4j+b	Table 5	10	3.7	1.2
total W+4j+b	$\delta^2_{stat} + \delta^2_{sys}$	13	4.0	1.3

Table 3.6: Expected precision on the top mass, all entries in GeV/c^2. The statistical errors use the yields from Table 4. The total error is computed using the systematic uncertainties from Table 5.

yields in order to predict future precision. The statistical errors for the three event classes W+4j, W+4j+b, and W+4j+bb are shown in Table 3.6 for the present measurement and the first two luminosity scenarios, where the latter cases assume the event yields outlined in Sec. 2.3. We see that in any of the possible b-tagging modes, the statistical error is well below 1 GeV/c^2 by 10 fb^{-1}.

If the systematic error is linearly related to its component uncertainties, and these uncertainties are measured by mean values in data driven control studies, we expect the systematic uncertainty to also scale as $\approx 1/\sqrt{N}$. This scaling has been observed in CDF W mass results over the Tevatron history, and the measurement of the W mass, like the top mass, is dominated by calorimetric and energy scale uncertainties. If the systematic precision in m_t scales like statistics, the present studies imply the evolution given in the 4th row of Table 3.6.

A slightly more careful accounting of probable evolution of the systematic error is tabulated under the single horizontal line in Table 3.5. The dominant uncertainties due to jet energy scales are discussed in detail below. The b-tag bias can be addressed in control sample studies, and should scale as $1/\sqrt{N}$. Limitations due to the size of Monte Carlo samples and statistical techniques are clearly artifacts of the present immaturity, and we assume that these will go to zero with time. The small but significant uncertainty due to background modelling is a Monte Carlo derived quantity; we assume that progress will become possible when a control sample does, this is discussed below. The net effect of this somewhat more careful consideration of the systematic error is listed at the bottom of Table 3.5 and in the fifth row of Table 3.6, and is seen to be only slightly degraded from simple $1/\sqrt{N}$ scaling.

Adding in quadrature the more conservative of the systematic errors with the statistical error leads to the top mass precision listed at the bottom of Table 3.6. With 10 fb^{-1} at the Tevatron, the experimental contributions to the top mass uncertainty will be limited to the order of 1.3 GeV/c^2 per experiment.

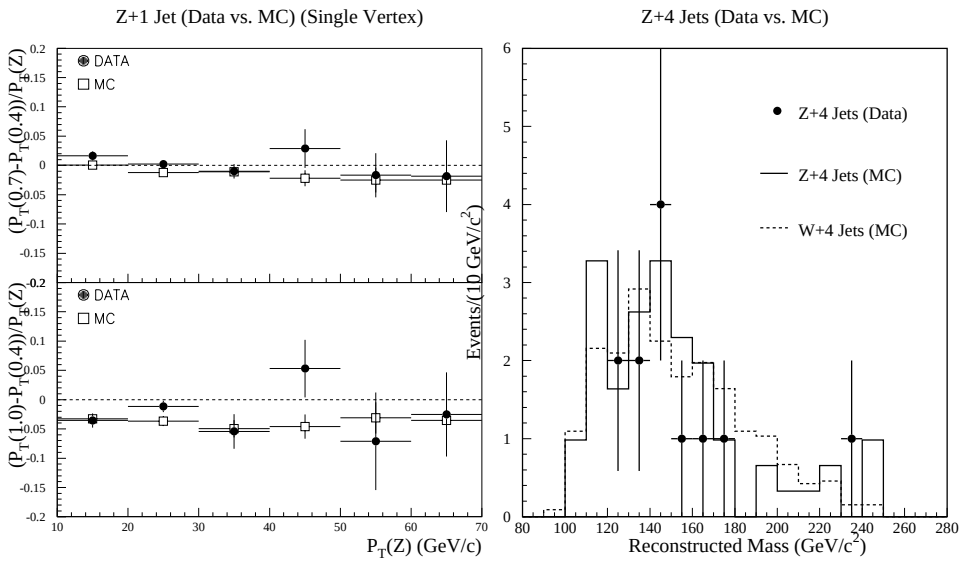

Figure 3.2: The left plot shows calibration of QCD jets in Z + 1 jet events. The right-hand plot shows calibration of background models with Z+4 jets in the Run 1B CDF data.

3.3.4 Elaborations on Future Precision of the Constrained Fit

The systematic uncertainty on m_t will scale as $1/\sqrt{N}$ until the precision is good enough to resolve problems that are *not* amenable to calibration in the data set. We have considered a number of issues and approaches, which, although not exhaustive, suggest that large data sets will provide ample opportunities for the control of systematic effects.

A. Calibration of Jet Scale Using ($Z \to e^+e^-$) + 1 Jet Events

Jet balance studies using γ+jet events are compounded by photon backgrounds and fragmentation complications; as large statistics become available, Z+1 jet events will be sample of choice for this technique. The Z P_T is assumed to measure the P_T of the recoil jet, which can then be compared to simulation to study instrumental scales, soft final state radiation, etc. A model study of the latter [18] is summarized in Fig. 3.2. The energy flow around the jet or parton is quantified in terms of energy in the annulus of, e.g. $\Delta R = 1.0-0.4$, and a comparison is made between data and Monte Carlo as a function of jet P_T. It is of interest to note that the effect of multiple interactions on the measured jet energies is included in this study.

The present CDF analysis has used 10% for the uncertainty represented here, leading to the 7.7 GeV uncertainty for the Run 1B "Jet scale QCD" in Table 3.5. Fig. 3.2 suggests that this is an overestimate. In addition, we may imagine that a study of this kind can be used to *tune* the Monte Carlo response model, in which case there would be a bin-by-bin correction to the Monte Carlo jet energies, with precision then limited by the statistical error on the data points in Fig. 3.2. If such a tuning works, then, assuming a conservative value of 3% for the statistical error in Fig. 3.2, and a transfer function $\delta m_t(\mathrm{GeV/c^2}) = 1.0 \times \delta E^{jet}_{scale}(\%)$, the jet scale error would decrease to $\approx$ 1 GeV/c^2 at 1 fb^{-1}and 0.3 GeV/c^2 at 10 fb^{-1}. A similar treatment of the absolute energy scale reaches the same precision.

With very good resolution it may become clear that there are differences in the details of jets in Z+jets and top events, and scaling the precision from this technique will break down. For instance B jets may require a different calibration, or the cleanliness of the events

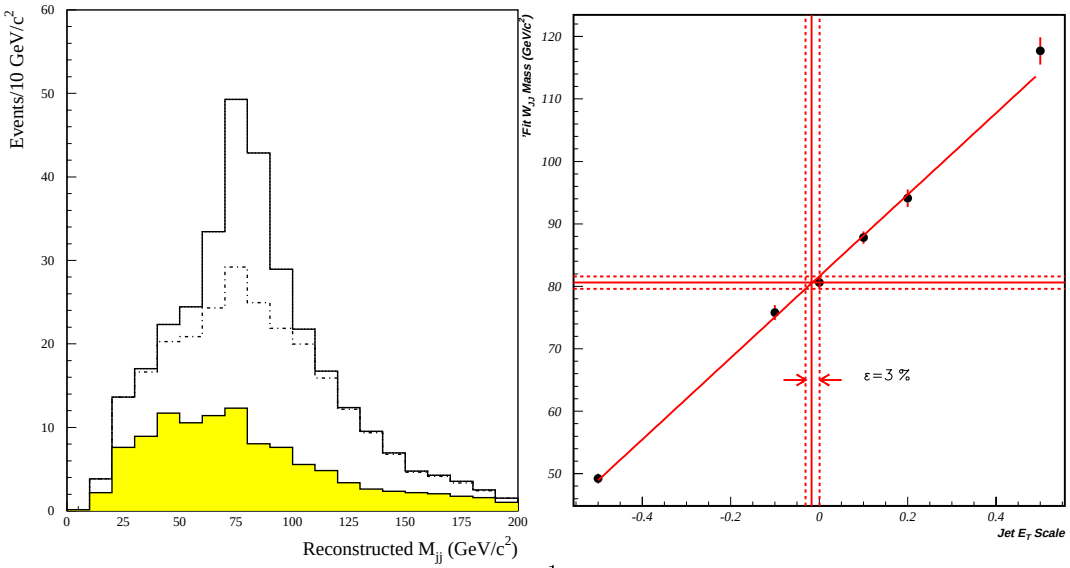

Figure 3.3: The W → jj signal in 1 fb^{-1} is the unshaded histogram in the left plot. The shaded curve is the QCD background. The dashed histogram is the QCD background plus the combinatoric background in top events. The excess in the W mass region is 103 events. The right hand plot shows the precision $\delta E^{jet}_{scale}(\%)$ vs $\delta M(jj)$ expected for 1 fb^{-1}.

may have a discernable effect. In this case, *in situ* calibrations, such as the study of light quark jets from W → jj as described below will be crucial; however, the statistics and ease of interpretation in the Z+jets sample will continue to make it an essential part of the jet calibration program.

B. Calibration of Total Jet Scale Using W → jj in Top Events

This mode is an *in situ* calibration of the instrumental response to and the QCD modeling of light quark jets. We have studied this technique by using the constrained fitting algorithm with the M(jj) = m_W constraint removed. We use the full CDF calorimeter simulation, and the HERWIG and VECBOS models of signal and background, with the ratio normalized to that presently seen in the CDF data. Fig. 3.3 shows the situation expected with 1 fb^{-1}. The shaded histogram is the misidentified W → jj in the W+jet background events which fit to the top hypothesis, the dotted histogram is the sum of this and the combinatoric background in top events, and the solid curve represents the correctly identified excess of 103 W → jj decays. The excess can be fit to a Gaussian of width 12 GeV/c^2, and implies an accuracy on the mean W mass, in this sample, of ∼ 1.3 GeV/c^2.

The transfer function between E^{jet}_{scale} and a Gaussian fit to the W mass is studied with HERWIG and the CDF simulation, and found to be well fit by the linear relation displayed on the right in Fig. 3.3. The energy scale precision derived from the W → jj signal in 1 fb^{-1} is found to be $\delta E^{jet}_{scale} \approx 3.0\%$. This calibration procedure will certainly improve as $1/\sqrt{N}$. If it is correct, and there were only light quarks in top decay, the E^{jet}_{scale} contribution to m_t in 1 and 10 fb^{-1} runs would be as given in the 4th row of Table 3.5, slightly worse than $1/\sqrt{N}$ scaling from the first column, but still rather respectable. Of course, the jets are not all light quarks, there are B jets as well, and this issue is discussed in Section C below.

Another interesting feature of this measurement is the distinguishable combinatoric background to W → jj from top events. In events with double b-tag we know, in principle,

which jets should be coming from the W. With sufficient statistics the sidebands on the $W \to jj$ peak will therefore be an indirect calibration of the Monte Carlo model dependence for extra jets in top events and final state kinematics.

C. Calibration of B jet energy scale

There is a significant difference between the calorimeter measurement for B jets and light quark jets: some B jets contain muons and neutrinos from cascade decays, and the measured energies have a low side tail not present in light quark jets. At present the effect on the top mass measurement is modelled using Monte Carlo, but several avenues for systematic studies in control samples have been identified. A preliminary study done at CDF suggests that it is possible to improve the B jet energy scale using double b-tagged dijet events [19], however, the improved statistics of Run 2 will be required for real progress. Good b-tagging and implementation of a secondary vertex trigger may allow isolation of the $Z \to b\bar{b}$ peak, providing a b jet calibration tool similar to the $W \to jj$ method described above. Finally, we note that a great deal of information on the energy flow in b jets already exists in LEP data, and this may be a fruitful topic for a LEP-Fermilab collaboration.

D. Calibration of Backgrounds Using ($Z \to e^+e^-$) + 4 Jet Events

The top mass determination involves subtraction of the W+4 jet background, whose shape is modelled with the VECBOS Monte Carlo, and whose uncertainty is presently estimated by varying the VECBOS inputs. As shown in Fig. 3.2 the mass spectrum of the W+4 jet model is very similar to that found with the Z+4 jet model, which can be tested unambiguously in the data [20]. As an example, note that with the present sample of 12 events in 67 pb^{-1}, the mean mass of the Z+4 jet data distribution is known to a precision of 8 GeV/c^2. With 10 fb^{-1}, the corresponding precision is 0.6 GeV/c^2, and will be a stringent test of the VECBOS model of Z+4 jets and W+4 jets as well.

E. Double b-Tagged Events

Table 3.6 shows that with a large sample the statistical error in the *double tagged* sample becomes comparable to that in the single tagged sample. This is obviously because of the reduced combinatoric confusion and therefore improved resolution, as seen in Fig 3.1. It is probable that this sample will also have a smaller systematic error: the backgrounds will be miniscule, and, as mentioned above, the identifiable $W \to jj$ from top decays will be a laboratory for the study of jet and Monte Carlo modelling. The double tag sample may be the sample of choice for the ultimate top mass analysis, with better control of systematic effects than present studies can anticipate.

3.3.5 Top Mass Measurement in the Dilepton Mode

Dilepton events can provide a measurement of the top quark mass complementary to that obtained from l+jets decays. Any differences derived from the two complementary data samples will provide insight into systematic effects or non-standard physics. The signature of a dilepton event consists of two isolated high-p_T leptons, missing p_T due to the neutrinos,

and two jets from the fragmentation of the b quarks. The measurement of the top quark mass from dilepton decays is particularly challenging due to the presence of the two neutrinos in the final state. In this case, in contrast to l+jets events, the measured particle momenta do not contain sufficient information to uniquely constrain the final state. For a given event, in the absence of sufficient constraints for kinematic fitting, an estimator for the top quark mass is defined using a likelihood method.

We describe here a study of top mass finding in dilepton events using the DØ detector model. Monte Carlo samples have been generated using ISAJET and processed through GEANT to simulate the DØ detector response.

3.3.6 Methodology in the Dilepton Mode

We classify dilepton events into three separate categories depending on the flavor of the charged leptons, ee, $e\mu$, and $\mu\mu$. The current DØ event selection criteria are summarized in Table 3.7 [2].

channel	$p_T(e)[Gev/c]$	$p_T(\mu)[Gev/c]$	$p_T(jet)$[Gev/c]	$\not\!\!p_T$[Gev/c]	H_T[Gev]
ee	> 20	—	> 15	> 25	> 120
$e\mu$	> 15	> 12	> 15	> 20	> 120
$\mu\mu$	—	> 15	> 15	—	> 100

Table 3.7: Selection criteria for dilepton events.

There are 18 unknowns (6 momentum vectors) that specify completely a dilepton final state. We measure 14 observables; 3 each from $\vec{p}(\ell)$, $\vec{p}(\overline{\ell})$, $\vec{p}(b)$, $\vec{p}(\overline{b})$ and the two components of $\not\!\!\vec{p}_T = \vec{p}_T(\nu) + \vec{p}_T(\overline{\nu})$.

In addition, there are four constraints on the mass of the W boson and top quarks: $m(\ell\overline{\nu}) = m(\overline{\ell}\nu) = m_W$ and $m(\ell\overline{\nu}\overline{b}) = m(\overline{\ell}\nu b) = m_t$. For each assumed value of the top quark mass, m_t, we can therefore solve for the 18 unknowns. In general there are 0, 2 or 4 possible solutions for the top quark momentum vectors. In the analysis, the two highest p_T jets in the events are assumed to be the b jets. Initial and final state gluon radiation can produce additional jets in the event leading to only 53% correct assignments of b jets for top mass of 140 GeV/c^2. Furthermore, since one does not distinguish between b and $\overline{b}$ jets, there is an additional two-fold ambiguity, doubling the possible number of solutions.

For the purpose of constructing an event likelihood for a particular top quark mass hypothesis, a weight w is assigned to each of these possible solutions. The weight w consists of two factors a) parton distribution functions for the initial partons and b) the energy distribution of the charged leptons produced by the decaying top quark in its rest frame [21, 22]. We sum over the weights w for all solutions. Next, in order to account for the detector resolution effects, we generate a pseudo-event-sample by fluctuating the observed lepton p_T, missing p_T, and jet p_T's within the known resolution functions of the DØ detector.

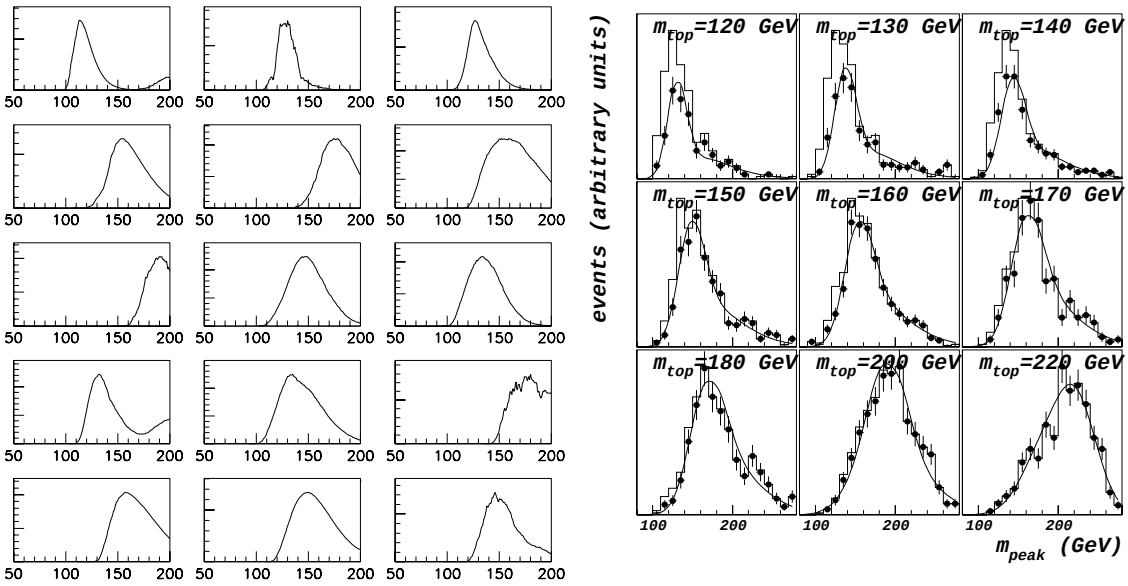

Figure 3.4: Left: Likelihood distributions for fifteen Monte Carlo $t\bar{t} \rightarrow e\mu X$ events with $m_t = 140$ GeV/c^2. Right: Distributions of m_{peak} for Monte Carlo ee events with m_t between 120 and 220 GeV/c^2. The histograms(points) are before(after) the H_T cut and the smooth curves are parametrizations.

The average weight of this pseudo-event-sample is defined as the event likelihood value. This procedure is then repeated for a range of top quark mass hypotheses between 80 GeV/c^2 and 280 GeV/c^2 to get the likelihood curve as a function of top mass for the event [23, 24].

The event likelihood curves for 15 events from a MC sample generated with m_t=140 GeV/c^2 are shown on the left in Fig. 3.4. For each event, we use the peak of this distribution as an estimator of the top quark mass. On the right in Fig. 3.4 we show the distributions of the peak masses for $t\bar{t} \rightarrow ee$ MC samples generated between 120 and 220 GeV/c^2.

3.3.7 Dilepton Mass measurement

To measure the top mass from a sample of events we perform a maximum likelihood fit of the shapes in Fig. 3.4 to the observed peak masses. Figure 3.5 shows the peak masses for five dilepton events in the DØ data sample, the best fit signal shape and the expected background shape. In a preliminary analysis of the DØ dilepton data sample [25], we determine the top quark mass to be

$$m_{top} \;=\; 145 \pm 25 \pm 20 \text{ GeV/c}^2,$$

where the first error is statistical and the second systematic.

3.3.8 Future prospects in the Dilepton Mode

We first consider the statistical error. We generate many pseudo-experiments by selecting samples of MC events. Each of these experiments contain $e\mu$, ee, $\mu\mu$ events distributed in the proportion 2 : 1 : 1, as expected in the SM. We then treat these samples as if they were data and subject them to the same fitting procedure to measure the top quark mass. The rms of the fitted top quark mass per event obtained from 4-event ensembles ranges between

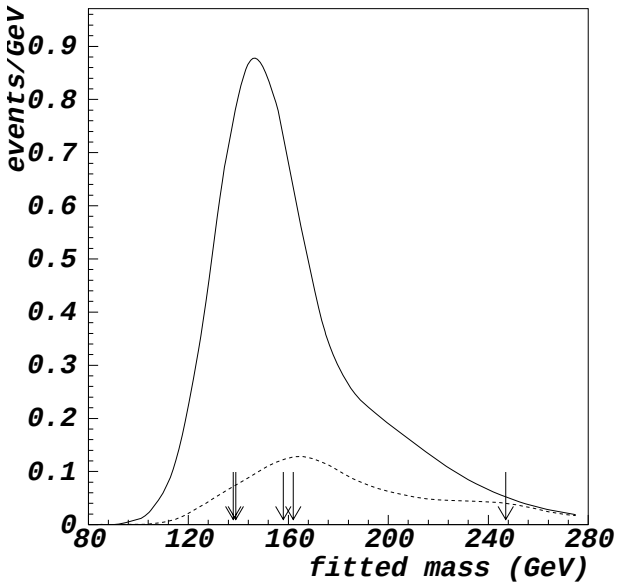

Figure 3.5: Distribution of peak masses for DØ dilepton candidates are shown as arrows. The two curves are the fits for the signal (solid) and the expected background (dashed).

42–56 GeV/c^2 for top masses between 140 and 200 GeV/c^2. Studies for 16-event ensembles show that the statistical precision scales as $\sqrt{\frac{1}{N}}$, and one can easily extrapolate to larger event samples expected with the upgraded Tevatron. The dilepton yields from Table 3.4 are used to calculate the statistical precision of this measurement for various running scenarios. These estimates are shown in the first row in Table 3.8.

At present the major systematic limitations arise from uncertainty about the jet energy scale and the modeling of the gluon radiation in the Monte Carlo generators. The issue of jet energy scale error is an experimental one. The current estimate of this error is 10% which leads to a 7% error in the mass determination. The size of this error depends on the number of Z+jet and W+jet events available to calibrate the jet scale and will therefore decrease as $1/\sqrt{N}$.

Our present understanding of QCD is a limiting factor in the modeling of gluon radiation effects. Uncertainty in the modeling is a large contribution to the systematic error. An estimate of this error is obtained by analyzing samples generated with Monte Carlo event generators which have different underlying models for parton showering and gluon radiation. Using samples of 160 GeV/c^2 $t\bar{t} \rightarrow \ell\ell'$ events generated with three different Monte Carlo models, ISAJET, HERWIG and PYTHIA, we find this error to be 9 GeV/c^2. We also expect this understanding to improve with increased data samples.

Other sources of systematic uncertainty in this measurement have been considered in detail. The estimates of the uncertainties and possible biases due to parametrization of the

likelihood functions, from the finite Monte Carlo statistics available, and our understanding of the signal to background ratio are listed in Table 3.8. The first column lists the errors as understood in the current DØ analysis. These estimates are obtained by reanalyzing a $t\bar{t}$ 160 GeV/c^2 Monte Carlo with changed parameters. The error due to uncertainties in the background normalization will decrease with increasing data samples since the amount of background will be measured more precisely.

Larger dilepton event samples will enable us to utilize the requirement of b-jet tagging for event selection. The double b-jet tagging efficiency of the upgraded detectors is expected to be about 42% (see section 2.2). Even though we lose half the statistics by using this requirement, it reduces the combinatoric confusion in the events. Lower combinatorics will reduce the tails in the peak mass distributions in Fig. 3.4 and lead to lower statistical and systematic errors. Quantitative studies are in progress.

Source	70 pb^{-1}	1 fb^{-1}	10 fb^{-1}
Statistical	25	6.2	2
Jet energy scale	11	2.7	0.9
Event Generator	9	—	—
Background Normalization	4	1	0.3
Monte Carlo Statistics	5	—	—

Table 3.8: Estimates of systematic uncertainties on the top mass measurement from the dilepton mass analysis. All entries are in GeV/c^2.

3.3.9 Conclusions on Dilepton Mass Measurement

With a large top data sample expected from an upgraded Tevatron, the top quark mass measurement in the dilepton channel has good sensitivity as well being a very interesting measurement. While the statistical precision is somewhat less than for the l+jets measurement, it provides an independent measurement of the top quark mass with a data sample that has much less background than the l+jets sample. Moreover, both measurements are likely to be systematically limited with a 10 fb^{-1} data set, so that a second measurement with somewhat different systematics will be valuable.

3.3.10 Ultimate Top Quark Mass Precision at the Tevatron

We have presented two techniques for the measurement of the top mass with precision approaching the order of 1 GeV/c^2 with 10 fb^{-1}. These two initial approaches will certainly be augmented by new ideas and additional techniques. Preliminary studies already suggest the possibility of isolating a signal and making a competitive mass measurement in the 6 jet final state at CDF [26]. In another interesting example, Ref. [27] studies the relation between m_t and the mean b decay length, and suggests that with large statistics the decay

length in the tagged b's, accurately measured in the silicon vertex detectors, could yield an asymptotic statistical precision $\delta m_t \approx 1$ GeV/c^2 . This would give *four* techniques: l+jet, dilepton, all-jet, and decay-length, which are all statistically independent, and for which precise mass values could be combined. Meanwhile, large data sets will provide additional avenues for the study of systematic effects in all cases. We believe that it is reasonable to expect that an integrated data set of 10 fb^{-1} will allow a combined measurement of the top mass with control of the experimental uncertainties at the level of 1 GeV/c^2.

There are additional theoretical complications. For instance, the distribution of fit masses used as input templates to the likelihood fit are ultimately derived from a theoretical calculation, and several studies raise questions concerning the modelling of hard gluon radiation and other subtleties in the final state [28] . Examination of these issues is only beginning, and the final answers will require much more statistical precision than presently available, but we believe it is reasonable to expect that these theoretical uncertainties will ultimately be controlled at the level of the experimental precision, of order 1 GeV/c^2.

Taking all of the above into account, we believe that 10 fb^{-1} at the Tevatron will allow a **measurement of the top mass with a precision of 2 GeV/c^2 per experiment**. This level of precision will challenge the program of precision electroweak measurements. What new measurements should be planned in order to derive maximum benefit from δm_t ~2 GeV/c^2 ? As the electroweak program enters its next decade this will be an interesting question for further study.

3.4 Top Quark Production

The main top production process at the Tevatron is the creation of $t\bar{t}$ pairs through strong $q\bar{q}$ annihilation and gluon fusion. Many models exist for new physics which could modify the rate and final state kinematics of pair production. In addition, electroweak processes can produce a single top quark in association with a b quark, at about 35% of the pair production rate. We discuss below the prospects for measurements and tests with top pair production. Single top physics is discussed in Sec. 6.

3.4.1 Measurement of the $t\bar{t}$ Production Cross Section

An accurate measurement of the $t\bar{t}$ production cross section is a precision test of QCD. A cross section significantly higher than the theoretical expectation would be a sign of non-Standard Model production mechanisms, for example the decay of a heavy resonant state into $t\bar{t}$ pairs [29], or anomalous couplings in QCD [30].

The current measurement of the top production cross section at $\sqrt{s} = 1.8$ TeV, for m_t = 175 GeV/c^2, is $\sigma_{t\bar{t}} = 6.8^{+3.6}_{-2.4}$ pb at CDF and $\sigma_{t\bar{t}} = 5.2 \pm 1.8$ pb at DØ compared to the theoretical value at this mass of $4.95^{+0.7}_{-0.4}$ pb [1, 12, 10].

The uncertainty on the current measurement is dominated by the statistics of the event sample. In the future, systematic uncertainties will be the limiting factor. For the l+jets mode, which dominates the statistics of the measurement, the largest systematic uncertainties are now those on the total acceptance (about 30%), and on the background (about 35%).

The uncertainty on the integrated luminosity is currently about 10%, but will eventually fall to 3.5%, the accuracy of the effective cross section for the luminosity monitor. In Run 2 and beyond, the luminosity will be measured differently, either through the $W \to l\nu$ rate, or the mean number of interactions per crossing. The former is presently understood to 5%, and we will assume this value for the future precision of the luminosity normalization.

	1 fb^{-1}	10 fb^{-1}	100 fb^{-1}
Acceptance	8.4%	2.7%	0.9%
Backgrounds	10%	3.3%	1.0%
Integrated Luminosity	5.0%	5.0%	5.0%

Table 3.9: Assumed systematic uncertainties for the $t\bar{t}$ cross section measurement

Lum	# b-tagged $t\bar{t}$ events	# Background events	Cross section precision
1 fb^{-1}	580	165	11%
10 fb^{-1}	5.8K	1.6K	5.9%
100 fb^{-1}	58K	16K	5.1%

Table 3.10: Precision of $t\bar{t}$ cross section measurement

The systematic uncertainty on the total acceptance is due primarily to three factors: Initial state radiation, jet energy scale, and b-tagging efficiency. Initial state radiation can be studied using a sample of Z+jets, while the jet energy scale uncertainty can be addressed as in the top mass discussion. Both of these techniques are limited in their accuracy by the size of the event sample and so the uncertainties should be substantially reduced in Run II and beyond. The b-tagging efficiency in top events is now measured using a combination of inclusive lepton events and Monte Carlo. The uncertainty is due in part to the comparison between data and Monte Carlo and in part to the size of the inclusive lepton sample. With more than 1 fb^{-1} of data, however, it will be possible to measure the b-tagging efficiency *in top events*, using dilepton events (selected without a b-tag) and the ratio of single to double tags in lepton plus jets events. Thus we expect a significant reduction of the uncertainty on the tagging efficiency in Run II and beyond as well.

The systematic uncertainty on the background estimate for the lepton plus jets mode is dominated by the uncertainty on the heavy flavor content in W+jet events, which is based on Monte Carlo. With sufficient data one can measure the bottom and charm content as a function of jet multiplicity in W + jet events using the $c\tau$ distribution of the tagged jets and use this to tune the Monte Carlo for W + 3 or more jet events, thus significantly reducing the uncertainty.

Lum	Cross section ratio precision
1 fb^{-1}	14%
10 fb^{-1}	4.8%
100 fb^{-1}	1.5%

Table 3.11: Precision of $t\bar{t}$ cross section ratio measurement

It is clear that there are many handles for reducing the systematic uncertainties in the top cross section measurement. In what follows we make the assumption that the systematic uncertainties will decrease according to $1/\sqrt{N}$. Although somewhat arbitrary, this scaling is already observed between the CDF Run 1A vs. Run 1B analyses. We assume that the luminosity uncertainty will increase to 5% . In Table 3.9 we list the expected systematic uncertainties for integrated luminosities of 1, 10 and 100 fb^{-1}.

The background from mis-tags is assumed to drop to zero with three dimensional silicon tracking, and the remainder of the background is assumed to scale both with top acceptance and integrated luminosity. We note that, within reasonable bounds, the cross section uncertainty is rather insensitive to the amount of background for integrated luminosities of 1 fb^{-1} and above. In Table 3.10 we list the expected precision of the $t\bar{t}$ cross section measurement in the l+jets mode for integrated luminosities of 1, 10 and 100 fb^{-1}. With 10 fb^{-1} at the Tevatron it will be possible to measure the total $t\bar{t}$ production rate with a precision of approximately 6%.

3.4.2 The ratio of dilepton to l+jets production rates

The ratio of the $t\bar{t}$ cross section measured using dilepton events to that measured using single lepton plus jets events is also of interest. A value of this ratio significantly different than 1.0 is a signature for non-Standard Model decay modes of the top quark because the acceptances for the two modes are predicated on the assumption of the decay sequence t$\rightarrow W \rightarrow$ leptons. Whereas the measurement of $BF(t \rightarrow b)$ discussed in Section 5.2 is a way to test for top decays without b quarks in the final state, the cross section ratio is primarily aimed at decays without W bosons in the final state, such as charged Higgs t $\rightarrow$ H$^+$b and light stops t $\rightarrow \tilde{t} + \tilde{\chi}^0$.

To estimate the future precision of the cross section ratio, we again assume the event yields from Table 4. We assume that the luminosity and all acceptance uncertainties, except that due to b-tagging which is not used in the dilepton selection, cancel in the ratio. We assume that the background uncertainties *do not* cancel in the ratio but, as above, that they decrease as $1/\sqrt{N}$ for both channels. For large data sets the uncertainty is simply dominated by the dilepton statistics. In Table 3.11 we list the precision of the measured ratio as a function of integrated luminosity. In section 5.3 we show that with a sample of 10 fb^{-1}, the ratio of the dilepton to l+jets production rates will be sufficient to measure the branching fraction to W in association with b with precision of 3.5%.

3.4.3 Search for $t\bar{t}$ Resonances

Several models have been proposed for extensions of the Standard Model which could produce enhancements or resonances in the $t\bar{t}$ invariant mass ($M_{t\bar{t}}$) spectrum [29, 31]. A color-octet vector meson associated with a top condensate [32] and multiscale technicolor[33] are two examples of phenomena that can enhance $t\bar{t}$ production. In certain theoretical models, the branching fraction of $X \to t\bar{t}$ is large. For example, a topcolor Z′ has a branching fraction to $t\bar{t}$ of 50-80% depending on the Z′ width [34]. It is important to search for heavy objects decaying to $t\bar{t}$ pairs since it may be difficult to observe the resonance in other decay channels. Although alternative techniques have been proposed [31], for this study we directly search for a resonance (a peak) in the $M_{t\bar{t}}$ distribution.

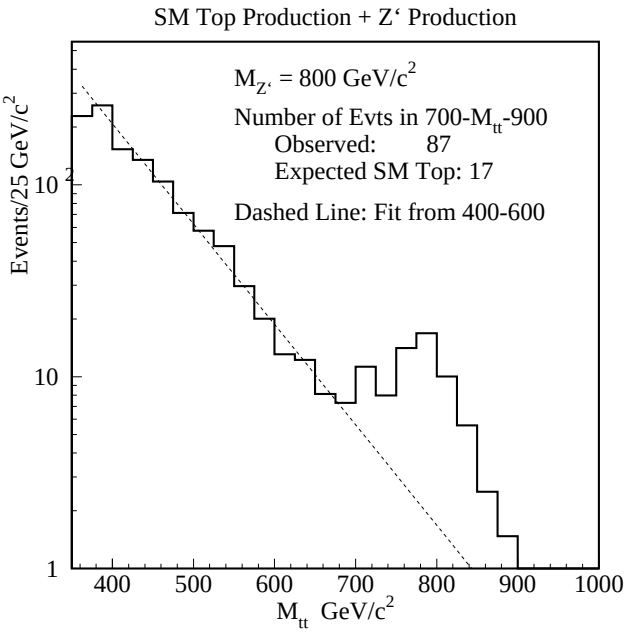

Figure 3.6: A hypothetical $M_{t\bar{t}}$ spectrum with an 800 GeV/c^2 Z′ topcolor boson. The rate is based on the theoretical predicted cross section for $t\bar{t}$ production and Z′ production [34] with 2 fb^{-1}. The standard model prediction (17) in the region 700-900 GeV/c^2 is estimated from the fit. The Z′ results in an addition 70 events in the high mass region.

We reconstruct $M_{t\bar{t}}$ on an event-by-event basis using the same event sample and constrained fitting techniques used in the top mass measurement (see Section 3). We want the best $M_{t\bar{t}}$ resolution possible and therefore we use an additional constraint that the t and $\bar{t}$ decay products have a mass equal to the measured M_{top}. This improves the resolution on $M_{t\bar{t}}$ by a factor of two [35]. Systematic studies show that constraining to an incorrect M_{top} shifts the peak position of the resonance but does not greatly affect the mass resolution. The shift in $M_{t\bar{t}}$, $\Delta M_{t\bar{t}}$, is about twice the shift in M_{top}, $(M_{top}^{true} - M_{top}^{constrained})$. Since M_{top} will be precisely measured, the effect on a resonance peak position will be very small.

For definiteness, we use the example of a topcolor Z′ decaying to a $t\bar{t}$ pair. The cross section, $\sigma \cdot B(X \to t\bar{t})$, is determined by theory. We use the PYTHIA Monte Carlo to provide the decay $X \to t\bar{t}$ and calculate the acceptance. The acceptance is 6.5% and approximately

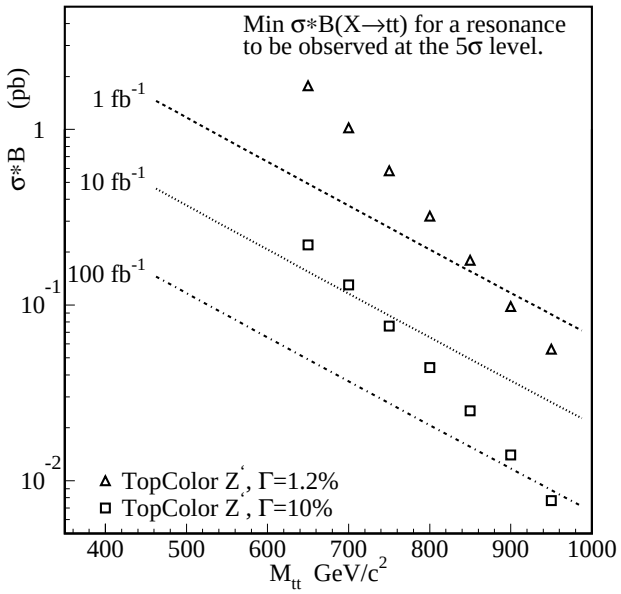

Figure 3.7: $\sigma \cdot B(X \to t\bar{t})$ vs $M_{t\bar{t}}$, where the lines represent the minimum $\sigma \cdot B$ to observe a 5σ excess of events in a sample with 1, 10, and 100 fb^{-1} of integrated luminosity. The triangles (squares) show the $\sigma \cdot B$ for a topcolor Z' with width , $= 1.2\%$ (10%)[34, 36].

flat versus $M_{t\bar{t}}$. This acceptance includes the branching fractions ($W \to \ell\nu$, $W \to jj$), lepton and jet selection, at least one b-tagged jet, and the reconstruction efficiency of the constrained fitting technique. As a simple example, we add the $M_{t\bar{t}}$ distribution for a Z$'$ ($M_{Z'}$ = 800 GeV/c^2, , $_{Z'} = 1.2\%$) to the $M_{t\bar{t}}$ distribution from standard model $t\bar{t}$ production. The result is shown in Figure 3.6. A clear resonance can be seen near 800 GeV/c^2. A simple quantification of the excess can be determined by fitting the $M_{t\bar{t}}$ distribution below the resonance to estimate the background in the region 700-900 GeV/c^2. The estimate yields 17 events. With the Z$'$, a total of 87 events are expected in the same region. This excess is well above the 5σ level. More sophisticated methods, involving fitting to standard model and $X \to t\bar{t}$ $M_{t\bar{t}}$ distributions, are being developed to extract an excess of events due to a resonance [35].

We generalize this procedure to determine the minimum $\sigma \cdot B(X \to t\bar{t})$ for a process $X \to t\bar{t}$ to yield a $\geq 5\sigma$ excess of events. For this study we assume the natural width of the object is less than the detector resolution on $M_{t\bar{t}}$ ($\approx 6\%$ at $M_{t\bar{t}} = 800$ GeV/c^2). If the resonance is wider it can still be observed; however, it simply requires a larger data sample. Figure 3.7 shows the minimum $\sigma \cdot B(X \to t\bar{t})$ for the production of $X \to t\bar{t}$ in order to observe a $\geq$5 sigma excess. The three lines show the results for 1, 10, and 100 fb^{-1} of data. If a theoretical model has a $\sigma \cdot B$ above a line, that object could be observed at a $\geq 5\sigma$ level for the given luminosity. For comparison, the theoretical expectation for a topcolor Z$'$ and , $=$ 1.2% (10%) is show by the triangles (squares) [36]. The comparison of the 5σ lines with the , $_{Z'} = 10\%$ values (squares) is slightly optimistic since , $_{Z'}$ is larger than the experimental resolution. However, it does represent the approximate reach for these wide resonances. With 10 fb^{-1}, we will be able to observe a narrow Z' resonance out to approximately 800 GeV. A 100 fb^{-1} sample of $t\bar{t}$ events will provide an excellent mass reach for the search for

new phenomena and will test a wide variety of theoretical models.

3.5 Top Quark Decays

In the Standard Model with three generations, existing experimental constraints and the unitarity of the CKM matrix require $| V_{tb}| \simeq 1$, predicting that the weak decay of the top will proceed almost exclusively through W + b. The $t \to Wb$ decay vertex is completely fixed by the universal V – A coupling to the SU(2) bosons. The decay width is given by [37]

$$, (t \to bW^+) \;=\; \frac{G_F m_t^3}{8\sqrt{2}\pi}|V_{tb}|^2[1 - \frac{m_W^2}{m_t^2}]^2[1 + 2\frac{m_W^2}{m_t^2}]$$

For m_t = 175 GeV/c^2, this partial (almost total!) decay width is $\sim$ 1.8 GeV, corresponding to a lifetime of $\sim 0.4 \times 10^{-24}$ seconds. This rapid decay cuts off the long distance part of the strong interaction; there is no hadronization, and all strong interaction issues for the top quark should be well described by perturbative QCD. The top quark provides the first opportunity to study the decays of a naked quark, with experimental techniques and advantages familiar from muon decay.

We describe measurements of the decay couplings, branching fractions, rare decays, and a limit on $|V_{tb}|$. The measurement of the decay width, which involves all of these things, is possible through the electroweak production of $t\bar{b}$ pairs, and is discussed in Section 6.

3.5.1 The Structure of the Wtb Vertex

Because the top is heavy, it is possible that the physics of an underlying theory at a high mass scale may manifest itself via new non-universal top interactions. [38]. Very few constraints exist on these parameters from low energy data. A recent analysis of the CLEO $b \to s\gamma$ result [40] suggests that V+A couplings should be small. A recent analysis of LEP results [42] succeeds in limiting only neutral current couplings of the top.

In the case of direct measurements at the top, nature provides a tool which does not exist for the light quarks: a two body weak decay which precedes hadronization and therefore carries helicity information related to the fundamental couplings. In the Standard Model, there are three important conclusions [39]:

- A top decays only to left-handed or longitudinal W's. The longitudinal component of the W is an item of some interest in the Standard Model.

- The ratio of longitudinal to left-handed W's in top decay is given in the Standard Model as

$$\frac{W_{long}}{W_{left}} \;=\; \frac{1}{2}(\frac{m_t}{m_W})^2$$

  which is 2.23 for m_t = 170 GeV/c^2. Alternatively, we may say that in the Standard Model the branching fraction of the top to longitudinal bosons is an exact prediction

depending only on the top mass, and for e.g. $m_t = 170$ GeV/c^2 we expect to find

$$B(t \to bW_{long}) = \frac{\frac{m_t^2}{2m_W^2}}{1 + \frac{m_t^2}{2m_W^2}} = 69.2\%$$

- Non-universal top couplings will, in many cases, appear as a departure of $B(t \to bW_{long})$ from the value expected for the measured m_t.

The polarization state of the decay W is experimentally accessible through the charged lepton helicity angle, $\cos\theta_e^*$, which is conveniently measured in the lab frame [39] as

$$\cos\theta_e^* \approx \frac{2m_{eb}^2}{m_{eb\nu}^2 - m_W^2} - 1.$$

The resulting $\cos\theta_e^*$ distribution can then be fit to the superposition of W helicity amplitudes to measure $B(t \to bW_{long})$ or, more generally, to measure any possible contribution of non-universal weak couplings in top decay. A method employing the neutrino from W decay to analyse the top couplings is discussed in Ref. [41]

We study the expected sensitivities at the Tevatron using the charged lepton helicity angle technique. We use a four vector level Monte Carlo employing a general chiral Lagrangian treatment of the Wtb vertex and maintaining full helicity information in top decay [42]. For the Standard Model couplings, the unbiased distribution of $\cos\theta_e^*$, constructed as above, using 129K generated events at $m_t = 170$ GeV/c^2, is shown in Fig. 3.8. Superposed on the expected distribution are the two anticipated individual contributions for $m_t = 170$ GeV/c^2

$$\begin{aligned} \frac{dN}{d(\cos\theta_e^*)} &= 0.31 \mid M(W_{left}) \mid^2 + 0.69 \mid M(W_{long}) \mid^2 \\ &= 0.31 \times \frac{1}{4}(1 - \cos\theta_e^*)^2 + 0.69 \times \frac{1}{2}(\sin\theta_e^*)^2 \end{aligned}$$

as well as the sum, which is seen to provide a good fit to the simulation result.

We now consider a CDF/DØ style analysis for $m_t = 170$ GeV/c^2. We assume, to start, that the constrained mass fit will allow us to measure the $\not\!\!E_T$, the longitudinal component of the neutrino momentum, and all jet energies perfectly, and that we always know which b jet belongs to the semi-leptonic top decay. The effects of smearing all these will be considered below. We impose an event selection similar to the CDF lepton + jets analysis, and use the Monte Carlo to understand how to correct the $\cos\theta_e^*$ distribution for the bias imposed by these cuts. This acceptance corrected distribution for 1000 events is shown as the points on the right in Fig. 3.8. The uncertainties are computed bin by bin and include the uncertainty in the bias correction. We fit the distribution in Fig. 3.8 to the Standard Model hypothesis and get a good fit with $B(t \to bW_{long}) = 0.708 \pm 0.030$, as shown.

We conclude that in the case given here, a sample of 1000 tagged top events will allow the measurement of $B(t \to bW_{long})$ with a statistical precision of roughly 3%. With some confidence in our Monte Carlo tools, we then perform this analysis on a variety of sample sizes, to determine the statistical error as a function of the number of events. The result is

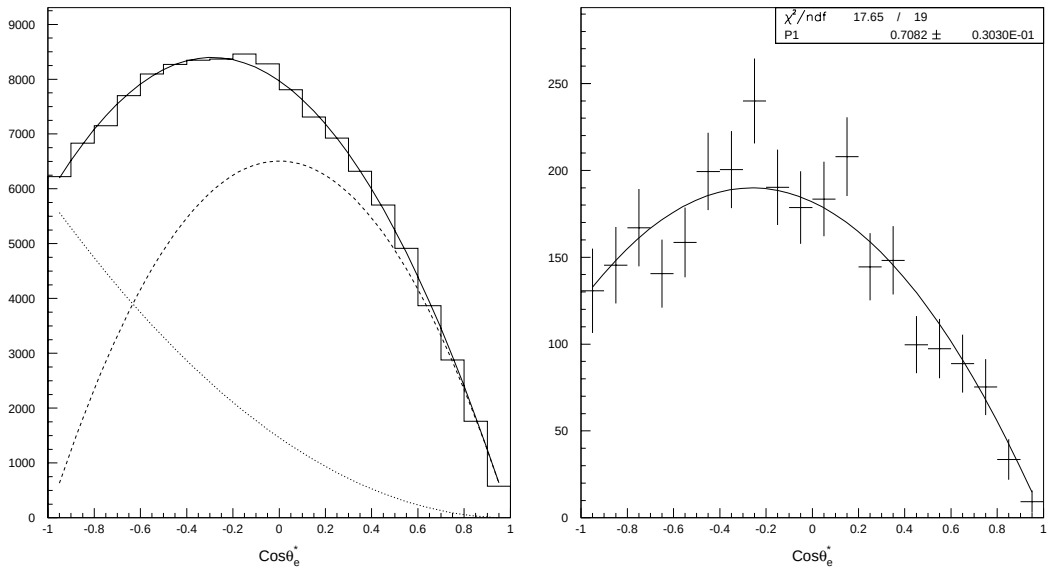

Figure 3.8: Left: The $\cos\theta_e^*$ distribution with perfect reconstruction fitted to the sum (solid) expected contributions from W_{left} (dot) and W_{long} (dash) in the Standard Model. Right: The $\cos\theta_e^*$ distribution for 1000 events (points with errors) and fit to the Standard Model hypothesis.

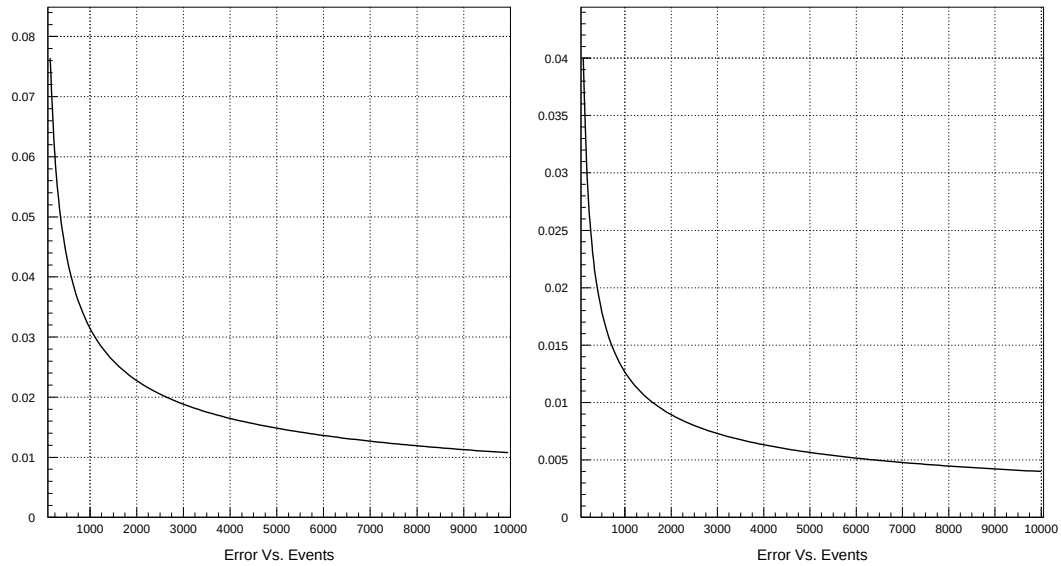

Figure 3.9: Left: The statistical error in $B(t \to bW_{long})$ as a function of sample size. Right: The statistical error in $B(t \to bW_{right})$ as a function of sample size.

Effect	1 fb^{-1}	10 fb^{-1}	100 fb^{-1}
$\delta B(t \to bW_{long})\%$	6.5	2.1	0.7
$\delta B(t \to bW_{right})\%$	2.6	0.8	0.3

Table 3.12: Total precision on top branching fractions to W helicity states

shown in Fig. 3.9. As expected, the statistical error falls as $1/\sqrt{N}$. We see that for sample sizes expected to be available at a high luminosity Tevatron, of order 10K and above, the top quark decay branching fraction to longitudinal W bosons may be measured with a statistical precision approaching 1%, and is systematically limited.

Beyond the benchmark measurement $B(t \to bW_{long})$, full understanding of any non-standard couplings requires a general angular analysis. For instance, the addition of a right-handed decay will not change the branching fraction to longitudinal W, it will only decrease the branching fraction to left-handed W's. We consider a small V+A contribution as a model for potential sensitivity to nonstandard contributions. The right handed W decay distribution is proportional to $(1 + \cos\theta_e^*)^2$ and top decays with a right handed helicity will most likely have $\cos\theta_e^*$ near one. The Standard Model predicts there should be nothing at this $\cos\theta_e^*$, and this analysis is therefore fairly sensitive to right handed decays. To quantify, we add a right-handed term and fit to Monte Carlo experiments of various sizes. The resulting statistical errors are plotted in Fig. 3.9, and indicate that with a sample of order 10K top events a right handed top decay that occurred 5% of the time would appear as a 5σ effect.

The most important sources of systematic uncertainty in these measurements are jet energy and $\not\!\!E_T$ resolution, combinatoric confusion in top decay product assignment, and backgrounds. The resolutions should be well controlled by use of the constrained mass fit algorithm in reconstruction of the final state kinematics. As in the case of the top mass analysis, the contributions of incorrect combinations and backgrounds to the $\cos\theta_e^*$ distribution can be modelled with Monte Carlo and subtracted. Systematic uncertainties from these effects may therefore be considered as equivalent to a reduction of a factor of approximately 2 in statistics and therefore a degradation of order $\sqrt{2}$ in the overall predicted precision. The expected precision, including systematic errors, are shown for the standard sample sizes in Table 3.12.

In conclusion, we have studied the way in which angular correlations in the top final state probe the Wtb vertex. We find that for sample sizes of 10 fb^{-1} the Standard Model prediction for $B(t \to bW_{long})$ and the presence of a V+A term may be probed with precision of a few percent, and that with such a sample these measurements are already systematically limited.

3.5.2 Measurement of a $t \to b$ Branching Fraction and Limit on V_{tb}

In the Standard Model, a 170 GeV/c^2 top quark decays almost exclusively via the $t \to Wb$ mode, because $V_{tb} \simeq 1$, and because there is no kinematic suppression of this decay. The statement $V_{tb} \simeq 1$ *assumes* the unitarity of the CKM matrix, a hypothesis that we would like to test.

Nonstandard model physics can change this value, as well as the interpretation of other phenomena. Suppose there were a fourth generation $(t', b', \sigma, \nu_\sigma)$. This would remove the 3-generation unitarity constraint on V_{tb}, allowing it to be smaller, and thus reduce the $t \to Wb$ branching fraction in favor of $t \to Ws$ or $t \to Wd$. This new generation also influences mixing: there is an additional contribution to K^0, D^0 and B^0 mixing from a box diagram with an t' or b' quark in the loop. Because of the electroweak radiative corrections to the W mass, the t' and b' quarks must be nearly degenerate in mass, which implies that the large difference in the rate of mixing between the slow $D^0 - \overline{D}^0$ and fast $K^0 - \overline{K}^0$ and $B^0 - \overline{B}^0$ systems is a consequence of the relative magnitude of CKM elements, rather than the large t to b mass ratio as in the Standard Model.

In principle, measuring $|V_{tb}|$ is simple. One looks at top events containing W's, and measures the branching fraction into b's:

$$B_b = B(t \to W(b)) = \frac{t \to Wb}{t \to Wq} = \frac{|V_{tb}|^2}{|V_{td}|^2 + |V_{ts}|^2 + |V_{tb}|^2}$$

The notation above is meant to indicate that a W has been required in the final state, and this is not the decay fraction to W+b, but the fraction of decays with W's which *also* contain b's. Since the standard analysis identifies $t\bar{t}$ events by requiring at least 1 W and 1 b, $B(t \to W(b))$ is measured from the number and distribution of tagged b-jets in top events. There are three basic techniques which can be used to measure this ratio:

• The ratio of double b-tagged to single b-tagged events in the b-tagged lepton plus jets sample: Requiring one b jet to be tagged leaves the second jet unbiased, and from a known tagging efficiency, one can extract the branching ratio from the ratio of tagged to untagged "second jets".

• The number of b tagged jets in the dilepton sample: Since b-tagging is not required to identify tops decaying to dileptons, the whole b-tag multiplicity distribution in these events contains information on $B(t \to W(b))$. Despite the smaller branching fraction to dileptons, the statistical power of the dilepton and l+jets samples are comparable.

• The distribution of double tags: If there are two tagging algorithms (soft leptons and secondary vertex), one can compare the number of times that events tagged by both algorithms have both tags in the same jet vs. the number of times the tags are in different jets. Small values of $B(t \to Wb)/B(t \to Wq)$ result in large values of the same to different jet ratio.

These techniques are not exclusive, and can be combined. CDF has used a maximum likelihood estimator to do this combination in Run 1 data. With 67 pb^{-1}, CDF has a $\pm 30\%$ statistical uncertainty on the branching fraction, but only an $\pm 11\%$ systematic uncertainty.

	Run 1	Run 2	Run 3	
Luminosity (fb^{-1})	0.12	1.0	10	100
Event Tag Probability	54%	85%	85%	85%
Tagged l+jets events	40	580	5800	58000
Double-tagged l+jets events	15	300	3000	30000
Same jet double tags	4	90	900	9000
Other jet double tags	12	240	2400	24000
Dilepton events	12	80	800	8000
Tagged dilepton events	7	65	670	6700

Table 3.13: Counting single and double tags

The systematic uncertainty is dominated by the uncertainty on the tagging efficiency, which is measured in the data using b rich inclusive lepton samples. This uncertainty should fall as $1/\sqrt{N}$. The small non-$t\bar{t}$ backgrounds will be measured to high accuracy by Run 2.

We calculate the expected sensitivity for three hypothetical runs with the usual luminosity assumptions: a Run 1 of 120 pb^{-1}, a Run 2 of 1.0 fb^{-1}, and a Run 3 of 10-100 fb^{-1}. The number of expected top events in the various categories is shown in Table 3.13, and the branching fraction uncertainty is shown in Table 3.14. Combining all three methods, we see that 10 fb^{-1} allows the measurement of the branching fraction $B(t \to W(b))$ with a precision of 1%.

	Run 1	Run 2	Run 3	
Luminosity [fb^{-1}]	0.12	1.0	10	100
Single/Double Tag Ratio	1.6 ± 0.5	$0.94 \pm .07$	0.895 ± 0.022	0.895 ± 0.007
$B(t \to Wb)$ Uncertainty	20%	4%	1.8%	0.56%
Different/Same Jet Tag Ratio	2.4 ± 1.0	$2.3 \pm .4$	2.19 ± 0.08	2.189 ± 0.025
$B(t \to Wb)$ Uncertainty	60%	14%	2.6%	0.81%
Dilepton Tag/No Tag Ratio	1.2 ± 0.2	4.9 ± 1.4	5.1 ± 0.5	5.10 ± 0.15
$B(t \to Wb)$ Uncertainty	20%	4.5%	1.4%	0.45%
Overall $B(t \to Wb)$ Uncertainty	15%	3.3%	1.0%	0.33%
Limits on $\|V_{tb}\|$ (95% CL)	> 0.1	> 0.22	> 0.40	> 0.71

Table 3.14: Expected precision on $B(t \to Wb)$ and $|V_{tb}|$

The branching fraction $B(t \to W(b))$ can be used to compute V_{tb} via the following relation:

$$|V_{tb}|^2 = \frac{B_b}{1 - B_b}\left[|V_{td}|^2 + |V_{ts}|^2\right]$$

The branching fraction limits are converted to $|V_{tb}|$ limits under the assumption that $|V_{td}| = 0.009$ and $|V_{ts}| = 0.039$, the midpoints of the 90% CL ranges in the Particle Data Book. Since these values are determined partially by unitarity, this is an assumption (although the correct one to test the Standard Model), and different assumptions of the values of $|V_{td}|$ and $|V_{ts}|$ will produce different relationships between the $|V_{tb}|$ and $B(t \to W(b))$.

Statistical uncertainties for $|V_{tb}| \approx 1$ are shown in Table 3.14. The 95% CL limits on $|V_{tb}|$ from this measurement are > 0.22 with 1 fb^{-1}, > 0.71 in a 100 pb^{-1} Run 3 with one experiment, and > 0.85 with two. It is ironic that the relation between the branching fraction and V_{tb} turns excellent precision on B_b into only modest limits on V_{tb}. An alternative and complementary measurement of $|V_{tb}|^2$ is available in the rate of electroweak $t\bar{b}$ production, and this is discussed in detail in Section 6.

3.5.3 Measurement of a $t \to W$ Branching Fraction

If all top decays proceed through W emission, the ratio of dilepton to single lepton events is $R_l = 1/6$. If some fraction of top decays are through a non-W state with a different branching rate to leptons, the change in the ratio R_l indirectly measures the departure of $B(t \to W)$ from 1.0. In the case where t decays include a non-W state with no leptonic decays, the branching fraction to W's is given in terms of the ratio R_l as

$$B(t \to b(W)) = \frac{9R_l}{1 + 3R_l}$$

The notation above mirrors that used in Sec. 5.2, and indicates that this is the fraction of decays with b's which *also* contain W's. This analysis is obviously model dependent, but consistent with the popular non-standard model that $t \to Wb$ may be augmented with $t \to H^+b$ where in this case $B(H^+ \to c\bar{s}) = 100\%$. Different models for non-standard top decays will obviously require different treatments; the discussion here is meant to be illustrative, and to provide a benchmark for the measurement precision.

The uncertainty on R_l *vs.* luminosity has been estimated in Section 4.2. Propagating this through the above, we find the precision of $B(t \to b(W))$ *vs.* luminosity as given in Table 3.15. With 10 fb^{-1} the ratio of dilepton to single lepton rates in top events will allow determination of the top branching fraction to W's in association with b to a precision of 3.5%. The conversion of this information to a limit on the amount of non-W decay is discussed in the next section.

Effect	1 fb^{-1}	10 fb^{-1}	100 fb^{-1}
$\delta B(t \to b(W))$	10%	3.5%	1.0%

Table 3.15: Statistical error on top branching fractions to W

Luminosity	95% CL limit on $B(t \to Hb)$
1 fb^{-1}	15%
10 fb^{-1}	6%
100 fb^{-1}	1.7%

Table 3.16: Limits on charged Higgs decay

3.5.4 $t \to H^{\pm} b$

A charged Higgs occurs naturally in SUSY models, and for a light charged Higgs, the process $t \to H^+ b$ is of interest. The CLEO $b \to s\gamma$ branching fraction [43] appears to place a limit on the Higgs mass ($m_{H^+} > 260$ GeV/c^2), but this limit assumes that there is no destructive interference from a chargino contribution. The decay $t \to H^+ b$ could still occur (and in fact, dominate) for large values of $\tan\beta$.

The best direct search strategies are to look for a τ excess from $H^+ \to \tau\nu$ or to find a dijet mass bump from the mode $H^+ \to c\overline{s}$, where the favored mode depends on $\tan\beta$. A study of prospects in the τ mode is underway [45].

There is, in addition, an indirect search technique for this or any other top decay to non-W states. As discussed in Sections 4 and 5.3 (above), the ratio of the top cross section as measured in the dilepton and lepton plus jets channels is sensitive to a missing W component, which manifests itself as a deficit of leptons. Recasting the discussion in 5.3 to measure the *non-W* fraction, we find

$$\frac{\sigma(t\overline{t})_{L+J}}{\sigma(t\overline{t})_{DIL}} \approx 1 + \frac{3}{2} B(t \to H^+ b)$$

where the numerator is the $t\overline{t}$ cross section as measured in the lepton plus jets channel and the denominator is the $t\overline{t}$ cross section as measured in the dilepton channel, assuming SM decays. This assumes a 100% branching fraction of the Higgs to $c\overline{s}$, and also assumes an 80 GeV/c^2 Higgs, so that the dijet masses give no separation between $t \to H^+ b$ and $t \to W^+ b$. In this somewhat pessimistic case, we expect to be able to set limits on this decay to the accuracy given in Table 3.16. For the even more pessimistic case of decays dominated by $H^+ \to \tau\nu$, the limits are approximately a factor of 2 worse.

For a Higgs mass substantially different from the W mass, there is the additional handle of the dijet mass distribution in top events: the Higgs will produce a peak in this distribution, in addition to changing the ratio of cross sections. This will improve the branching fraction limits by an amount dependent on m_{H^+}.

The limits attainable by 10-20 fb^{-1} of $p\overline{p}$ data, in conjunction with the CLEO $B(b \to s\gamma)$ measurement will be enough to exclude (or discover!) $m_{H^+} \leq m_t$ for *any* value of $\tan\beta$.

3.5.5 Rare Top Decays to W, Z, and γ

The presence or absence of certain particle decays can herald the arrival of new physics. For example, the absence of the flavor changing neutral current decay $K_L^0 \to \mu^+\mu^-$ was early evidence for charm, even though the charm quark's mass is three times the mass of the kaon. More recently, observation of the decay $b \to s\gamma$ by CLEO[43] can be used to exclude charged Higgs particles with masses less than 260 GeV/c^2 in some models; a 5 GeV/c^2 particle's decays can be used to probe physics at a mass scale 50 times larger.

As an illustrative example of the reach of rare top decays, we consider the flavor changing neutral current decay $t \to c\gamma$. Standard Model predictions for the branching fractions of FCNC decays are around 10^{-10} [44], so any observation will signal new physics, possibly at very high mass. Here we make estimates of the sensitivity of an upgraded Tevatron collider program to this sort of physics.

There are two signatures for this decay, depending on the decay of the W for the second top in the event. If it decays leptonically, the signature is a lepton, missing E_T, a high E_T photon (usually above 50 GeV), and two jets, one of which is b-taggable. If the W instead decays hadronically, the signature is a high E_T photon, no missing energy, four jets, one of which is b-taggable.

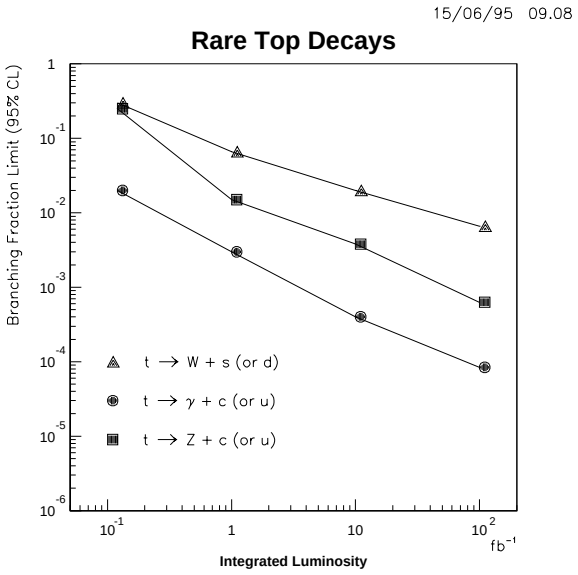

Figure 3.10: Limits on rare top decays

As it turns out, the acceptance of the $c + \gamma$ decay with the second top in the leptonic channel is almost the same as the standard model lepton plus jets mode. The background from $W + \gamma$ (plus two jets) is about 1 fb. Although it is unlikely that this background will be kinematically consistent with $t\bar{t}$ (for example, that $m_{\gamma+j} = m_t$), we take the very conservative assumption that this background is irreducible. It is then straightforward to scale from the number of observed events in the lepton plus jets mode to the 95% limit on

this branching fraction.

A 120 pb^{-1} Run 1 will yield about 40 tagged tops at CDF, and with a tagging efficiency of about 55% per event, this corresponds to a limit of approximately 4%. By a 1 fb^{-1} Run 2, assuming one background event is seen, the limit from each experiment would be approximately 5.7×10^{-3}.

Things are somewhat different by a 10 (or 100) fb^{-1} Run 3. At this point there will be 10 (100) background events; to set a limit, we would need to apply an additional selection, such as b-tagging. This will reduce the efficiency (and thus the limit) by about 60% (there is only one b to tag) but with 6K (60K) top events, a limit of 6.2×10^{-4} (1.3×10^{-4}) per experiment can be achieved, assuming zero (two) background events survive the b tagging. We emphasize that this is entirely without kinematic requirements.

The case where the second top decays hadronically is somewhat harder to estimate. There are certainly many high p_T photons with 4 jets from QCD processes, and a small fraction of them have real $b\overline{b}$ in them. It appears that both b tagging and kinematic cuts will have to be applied. We assume that the kinematic cuts will be 100% efficient in Run 1, 50% efficient in Run 2, and 30% efficient in Run 3, although it must be stressed that these are estimates: we haven't integrated enough luminosity to date to measure the background to this decay reliably. The expected limits, assuming one remaining background event in Runs 2, zero in a 10 fb^{-1} Run 3, and two by a 100 fb^{-1} Run 3, are shown in Table 3.17.

	Run 1	Run 2	Run 3	
Luminosity	120 pb^{-1}	1 fb^{-1}	10 fb^{-1}	100 fb^{-1}
$l + \gamma$+2 jets limit	4%	5.7×10^{-3}	6.2×10^{-4}	1.3×10^{-4}
γ+4 jets limit	4%	6.5×10^{-3}	1.1×10^{-3}	2.4×10^{-4}
Overall limit	2%	3.0×10^{-3}	4.0×10^{-4}	8.4×10^{-5}

Table 3.17: Sensitivity for $t \to c\gamma$.

	Run 1	Run 2	Run 3	
Luminosity	120 pb^{-1}	1 fb^{-1}	10 fb^{-1}	100 fb^{-1}
$3l$+2 jets limit	50%	4.3%	7.4×10^{-3}	1.0×10^{-3}
$2l$+4 jets limit	50%	2.6%	7.9×10^{-3}	1.7×10^{-3}
Overall limit	25%	1.5%	3.8×10^{-3}	6.3×10^{-4}

Table 3.18: Sensitivity for $t \to Zc$.

Note that the two search modes are roughly comparable. (It is also of interest that the CLEO $b \to s\gamma$ branching fraction is $(1.87 \pm 0.67) \times 10^{-4}$ [43]. With two comparable experiments at the Tevatron, the equivalent level of sensitivity for $t \to c\gamma$ is reached at about 11 fb^{-1}.)

Sensitivity to other rare decays can be scaled from this estimate. For example, one can consider $t \to Zc$, where the Z decays to leptons. The acceptances are similar, but one needs to consider the Z branching fraction to leptons of 6.7%, compared to the photon reconstruction efficiency of about 80%. To first order, the limits will be a factor of 12 worse. However, the trilepton backgrounds are substantially smaller than the $W\gamma$ backgrounds: about a quarter of an event in Run 2 (without a b-tag) and a third of an event in a 100 fb^{-1} Run 3 (with a b-tag). Here we assume zero observed background events until 100 fb^{-1}, where we assume one. For the hadronic decays of the W, the backgrounds are again lower. We are assuming that only b-tagging is necessary in Runs 1 and 2 (where 0.06 and 0.5 background events are expected) and kinematic cuts that are 50% efficient (with a remaining background of .02 events/fb^{-1}) are necessary in Run 3. Expectations for this search are summarized in Table 3.18 and Fig. 3.10.

There are other rare decays, such as $t \to WZb$. This mode is interesting because it is close to threshold and might provide an accurate measure of the top mass and also because it directly probes the $t - t - Z$ vertex. As long as the backgrounds are small, as they often are for these rare modes, the sensitivity scales as $1/N$, rather than $1/\sqrt{N}$. Modest increases in running time, luminosity, acceptance and efficiency can contribute to substantial improvements in physics reach.

Although this section has been written in terms of limit estimates, we wish to emphasize that there is a more exciting prospect ahead of us, *discovery* of these rare decays, which would cause us to rethink our understanding of high mass physics.

3.6 The Physics of Single Top Quark Production

The preceding discussion has focussed on physics capabilities with the dominant top production mode, strong production of $t\bar{t}$ pairs. However, top quarks can also be produced singly via the electroweak interaction [46, 47, 48], and this process offers an interesting and complementary program of measurements. The principal processes leading to single top production are shown in Fig. 3.11, along with their higher order corrections. The first process $q'\bar{q} \to t\bar{b}$, proceeds via an s-channel W^* and the second, $qb \to q't$, involves a t-channel W. We will refer to the first process and its corrections as "W^*", and the second process, together with its corrections ($qg \to q't\bar{b}$), as "W-gluon fusion". Other processes, such as $gb \to tW$, are important at higher energies, but contribute only a few percent to the rate at 2.0 TeV.

The cross sections for all top production mechanisms in $p\bar{p}$ collisions at $\sqrt{s}$=2.0 TeV are shown in Fig. 3.12 [9, 49]. For $m_t = 170$ GeV/c^2, W-gluon fusion, at 1.6 pb, is twice as large as W^* at 0.8 pb, and the combined rate for single top production by these two processes, ~ 2.4 pb, is over a third of the $t\bar{t}$ rate at this energy. Single top studies at the Tevatron will have good statistical power.

The production of a $t\bar{b}$ pair from a W is closely related to the decay of a t quark through a Wb, and the the single top cross section turns out to be directly proportional to the partial width , $(t \to Wb)$. As shown at the beginning of Section 5, , $(t \to Wb)$ is a function of both the decay couplings and $|V_{tb}|^2$. The single top sample will provide a very accurate measurement of the decay width, and in the absence of anomalous couplings this is

Figure 3.11: Representative Feynman diagrams for single top quark production at the Tevatron: (a) W^* boson s-channel $p\bar{p} \to t\bar{b}$ + X; (b) W boson t-channel $p\bar{p} \to tq$ + X; (c) $p\bar{p} \to tW$ + X.

an accurate measure of $|V_{tb}|$. This sample is also an independent top laboratory with some unique physics opportunities described later.

We present here a study of single top quark yields using Monte Carlo parton level events combined with simple parametrizations of detector effects. We then estimate the potential accuracy of a number of possible measurements as a function of the data sample size.

3.6.1 Single Top Quark Simulation

Simulations of electroweak single top production and the principal backgrounds have been performed using the ONETOP Monte Carlo [42, 48]. Two different values of the mass of the top quark are used, 170 and 200 GeV/c^2, and the center of mass energy of the $p\bar{p}$ collisions is set to 2.0 TeV.

The ONETOP program makes a tree level calculation of the two main signal processes. The $qb \to q't$ cross section was scaled to the total tree level W-gluon fusion cross section, which properly accounts for the higher order process $qg \to q't\bar{b}$ [50], and this rate was then added to the $q\bar{q}' \to t\bar{b}$ cross section. We use the ONETOP default scale factors and parton distribution functions. $Q^2 = M_Z^2$ for all processes except $t\bar{t}$ where the average value of the transverse mass is taken as the scale. The CTEQ2L leading order fit [51] is used for the parton distribution function.

The ONETOP simulation decays the top quark into bW^+ with $W^+ \to e^+\nu_e$. In calcu-

Figure 3.12: Electroweak single top production cross section from $p\bar{p}$ interactions (LO), with the top quark pair cross section (resummed NLO) shown for comparison.

lating our yields for these processes we double the number obtained from the Monte Carlo once to account for $W^+ \to \mu^+\nu_\mu$, and again to account for the $\bar{t}$ antiquark charge conjugate processes. In the background processes, ONETOP also decays the W^+ into $e^+\nu_e$ and the muonic decays are again accounted for by simply doubling the yields.

In our simulations and yield calculations we take the b-tagging efficiency (per jet) to be 50% [52]. This figure includes geometrical acceptance within the fiducial volume of the detector, and intrinsic silicon microstrip detector efficiency, as well as the efficiency for the secondary vertex finding algorithms. The probability of incorrectly tagging a gluon or light quark jet as a b jet, known as the mistag probability, is taken as 0.4%, based on the current CDF silicon vertex detector experience. The lepton identification efficiency is taken to be 70% [53], which includes factors for the efficiencies of the triggers as well as the reconstruction.

Parton and lepton momenta are smeared according to the resolution functions of the current DØ detector [54]. The charged lepton energy resolution is parametrized using $15\%/\sqrt{E} \oplus 3\%$. The final state quarks are treated as jets and so their energy is smeared using $82\%/\sqrt{E} \oplus 18\%$. The missing transverse energy is recalculated after smearing the jet energies. Note that the constant term in the energy resolution will be greatly reduced in Run 2, and that the mass resolution may be considerably better than what we find below.

3.6.2 Single Top Analysis

We perform an example analysis using the following data selection criteria:

- Exactly two jets with $E_T > 20$ GeV, $|\eta|_{\text{jets}} < 2.5$

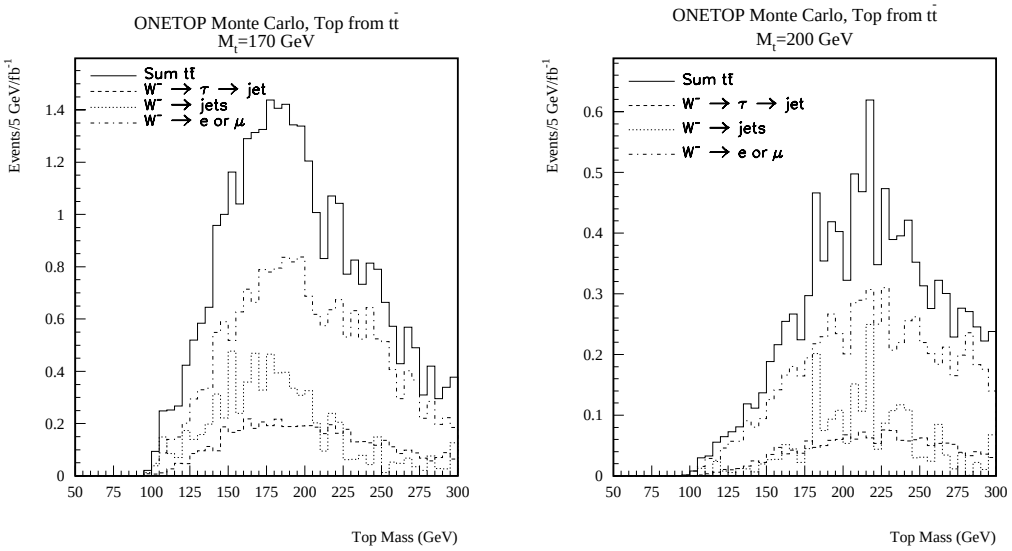

Figure 3.13: Wb mass distribution for $t\bar{t}$ background processes in single top analysis, with (a) a 170 GeV/c^2top quark and (b) a 200 GeV/c^2top quark.

- $\Delta R = \sqrt{(\Delta\phi)^2 + (\Delta\eta)^2} > 0.5$ between all jet pairs and jet-electron pairs
- $E_T(\text{electron}) > 20$ GeV
- $|\eta|_{\text{electron}} < 2.5$
- Missing $E_T > 20$ GeV
- No second isolated electron present with $E_T > 20$ GeV
- At least one jet tagged as a b jet.

The signal for single top production is a peak in the Wb invariant mass plot. The x and y components of the neutrino momentum are taken from the vector missing E_T. The z component is then calculated by requiring that the invariant mass of the electron and neutrino equal the W mass. There are generally two solutions which satisfy this constraint. The solution with the smaller $|p_z|$ is selected.

In the real data one does not know *a priori* which jet is the b jet arising from the top quark decay. Even with detached vertex b-tagging, some of our signal processes have a $\bar{b}$ jet produced together with the top quark, giving some ambiguity. In our analysis, if both b jets are tagged, the jet with the largest (most positive) η is selected. The charge of the W distinguishes between top quark and $\bar{t}$ antiquark candidates. For antitop one would choose the more backward jet (most negative η). We have compared the signal shape obtained with this technique to the shape obtained using the known b jet from the Monte Carlo. The shapes are quite similar, with a small broadening in the channels where confusion with the $\bar{b}$ quark is possible.

The principal background sources for single top production are $q'\bar{q} \to Wb\bar{b}$ and $q\bar{q}, gg \to t\bar{t}$. Most other backgrounds, such as WW and WZ, will be very small after suitable cuts. Imperfect b jet identification will lead to other backgrounds, as discussed below.

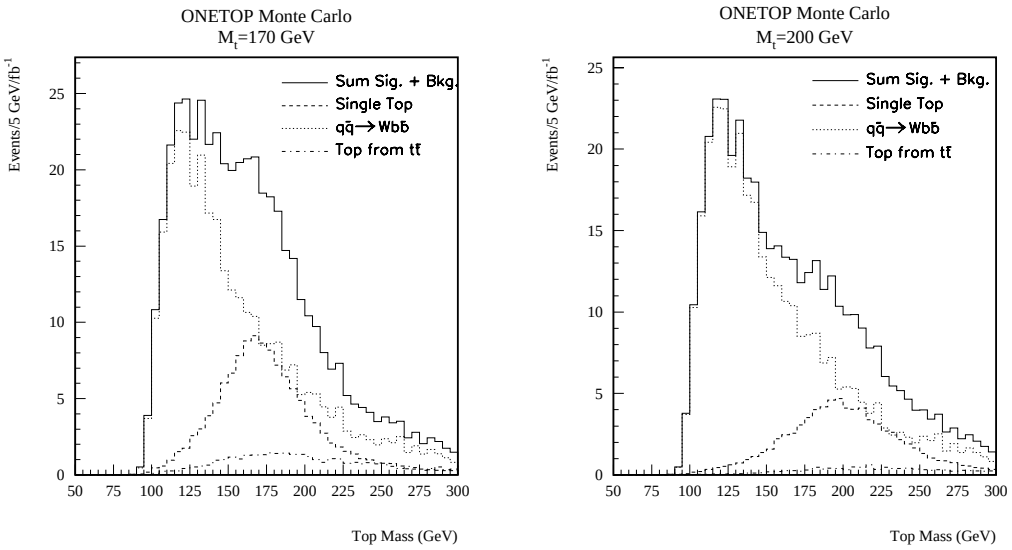

Figure 3.14: Wb mass distribution for single top signal and background processes, with (a) a 170 GeV/c^2top quark and (b) a 200 GeV/c^2top quark.

The $Wb\bar{b}$ background has been scaled to agree with current CDF $t\bar{t}$ analysis [11]. The ONETOP Monte Carlo was run at $\sqrt{s} = 1.8$ TeV with current CDF $t\bar{t}$ selection cuts, and the program's $Wb\bar{b}$ yield was compared to the CDF b-tagged yield of $Wb\bar{b}, Wc\bar{c}$ and Wc events (with mistags excluded). The Monte Carlo was found to overestimate the actual yield, and a correction factor of 0.6 has therefore been employed. The "$Wb\bar{b}$" yields in Table 3.19 therefore also account for backgrounds from $Wc\bar{c}$ and Wc events. (The lifetime of the c quark and the larger $Wc\bar{c}$ cross section cause about a third of the single tagged "$Wb\bar{b}$" sample to actually come from c quarks.)

Light quark and gluon jets can also contribute to the background. The mistag rate with the current CDF silicon vertex detector is 0.5% per jet and a smaller mistag rate is expected for Run II detectors. If we take this rate to be 0.4%, then because the $Wb\bar{b}$ cross section is roughly 0.01 of the total Wjj cross section, the background from Wjj will be the same size as the background from $Wb\bar{b}$ with 50% b-tagging efficiency. We therefore account for the Wjj background by simply doubling the size of the $Wb\bar{b}$ background. We also assume here that the shape in the mass plot for Wjj events is the same as that for $Wb\bar{b}$; studies show this to be a reasonable assumption. The "Wjj" line in Table 3.19 reflects this doubling, and the "$Wb\bar{b}$" mass distribution in Fig. 3.14 is just the calculated $Wb\bar{b}$ distribution doubled to include the effect of Wjj. All three backgrounds ($Wb\bar{b}$, Wjj and $t\bar{t}$) are included when calculating the uncertainties in Table 3.20.

We note here that one can reduce the $Wb\bar{b}$ background by about a factor of two by increasing the cut on E_T(jet 1) from 20 to 40 GeV. This is not entirely advantageous, however, because this causes the background to peak in the signal region. The optimal value of this cut for single top signal extraction will depend strongly on the top quark mass.

No scaling was applied to the $t\bar{t}$ background as the Monte Carlo cross sections from ONETOP (7.2 pb at $m_t = 170$ GeV/c^2, 3.0 pb at $m_t = 200$ GeV/c^2, $\sqrt{s} = 2.0$ TeV) agree with expectations from the measured values at $\sqrt{s} = 1.8$ TeV. In Figs. 3.13(a) and (b), the composition of the $t\bar{t}$ background is shown in more detail. In our Monte Carlo the W^+ from top always decays to a positron and a neutrino (and we double the yields to include the

	$m_t = 170$ GeV/c^2		$m_t = 200$ GeV/c^2	
	Yield/fb^{-1}	Peak Region/fb^{-1}	Yield/fb^{-1}	Peak Region/fb^{-1}
single top signal	123	107	76	63
Wbb background	163	109	163	63
Wjj background	163	109	163	63
$t\bar{t}$ background	32	21	11	7

Table 3.19: Yields for single top analysis. The "peak region" is within 50 GeV/c^2 of the generated top quark mass. The jets in the Wjj background are gluons and light quarks where one jet is mistagged as a b quark.

contribution from W^+ to muon and neutrino). The W^- from $\bar{t}$ decay is then treated for the three separate cases of decay to electron or muon, decay to tau (followed by tau decay to hadrons), and decay to jets. With these cuts, the jets contribution is negligible (due to the requirement of only two jets in the final state) and the $t\bar{t}$ background comes primarily from the dilepton channel (where the second lepton is either not isolated, is outside the fiducial region, or has a $E_T < 20$ GeV).

We have considered the background contribution from QCD multijet events, where one jet is misidentified as a lepton and there is a mismeasurement of the jet energies leading to large missing E_T which fakes a neutrino. In the current CDF W+jets event sample, it is estimated that ~10% is actually QCD multijet events, which means the misidentified QCD multijet events will add an additional 11% (one fake W for every nine real W's) to the $Wb\bar{b}$ and Wjj backgrounds included in the calculation.

The single top signal is presented in Fig. 3.14 and Table 3.19, together with the contributions from the $Wb\bar{b}$, Wjj, and $t\bar{t}$ backgrounds, for two different top masses. The vertical scales in Fig. 3.14 have been normalized to give the expected numbers of events in 1 fb^{-1} of Run II data. In each plot the summed signal and background curve is easily distinguished from the background shape alone. The cross section is lower for the 200 GeV/c^2 top quark, but the peak is out in a region of smaller background, so the signal to noise is similar to the case of the 170 GeV/c^2 top mass. At the time of Run II, the top mass should be well enough known and the signal shape well enough understood that the peak will be easily picked out above a smooth background in fits to the data. Event yields can then be extracted from the area of the signal shape in these fits.

3.6.3 The Single Top Quark Cross Section

The single top cross section may be obtained from the mass plots in a straightforward manner. We calculate the fractional statistical uncertainty in the cross section as $\sqrt{S+B}/S$, where the size of signal (S) and background (B) are the numbers of each kind of event in the mass peak window of 50 GeV/c^2 around the generated top quark mass. The results are summarized in Table 3.20 for our two input top masses of 170 and 200 GeV/c^2. For the case $m_t = 170$ GeV/c^2 we find that 10 fb^{-1} will allow measurement of the single top cross

	$m_{top} = 170\text{GeV}/c^2$	$m_{top} = 200\text{GeV}/c^2$
S/B	0.45	0.47
% error with 2 fb^{-1}	12.3	15.7
% error with 10 fb^{-1}	5.5	7.0
% error with 100 fb^{-1}	1.7	2.2

Table 3.20: Signal to background ratio and estimated statistical error for 2, 10, and 100 fb^{-1}.

Effect	1 fb^{-1}	10 fb^{-1}	100 fb^{-1}
$\delta\sigma_{t\bar{b}X+b\bar{t}X}$	26%	10%	7%
δ, $(t \to Wb)$	28%	12%	10%
$\delta\|V_{tb}\|$	14%	6%	5%

Table 3.21: Measurement precisions in the single top program.

section with a statistical precision of 5.5%.

Many of the sources of systematic uncertainty in the single top cross section are common to the $t\bar{t}$ cross section measurement discussed in Section 4. We assume that systematic uncertainties related to selection efficiencies and backgrounds will shrink as $1/\sqrt{N}$ and find that for large samples the dominant uncertainty is that of the luminosity normalization. The cross section precisions for our standard luminosity benchmarks are shown in Table 3.21 for $m_t = 170$ GeV/c^2. For the case of 10 fb^{-1} we find that the measurement of the single top cross section will have a total uncertainty of approximately 10% [56].

3.6.4 Top Quark Decay Width and $|V_{tb}|$ from Single Top

At a hadron collider, the top quark decay width , $(t \to X)$ cannot be directly measured in the $t\bar{t}$ sample, but its main component can be accessed through single top processes. The single top cross section is directly proportional to the partial width , $(t \to Wb)$ and, assuming there are no anomalous couplings, this is a direct measure of $|V_{tb}|^2$.

We have made a detailed study of the extraction of , $(t \to Wb)$, and $|V_{tb}|^2$ from the combined single top cross section [55, 56]. The constant of proportionality between the cross section and the width has theoretical uncertainties originating in α_s, the parton distribution functions, and the choice of scale Q^2. These are estimated to total roughly 10% at present [57], and we assume that better measurements of parton distributions and $\sigma_{t\bar{t}}$ will improve this to 7%. Combining all uncertainties yields anticipated precisions on , $(t \to Wb)$ and $|V_{tb}|^2$ as displayed in Table 3.21. We find that a measurement of the inclusive single top cross section with 10 fb^{-1} will yield the partial width , $(t \to Wb)$ with precision of 12%, and therefore V_{tb} with a precision of 6%.

3.6.5 Isolation of the W^* Process and a Separate Measurement of $|V_{tb}|$

If large data sets are available, it may be that the width is best found by measuring the single top rate from the W^* s-channel process separately from the W-gluon fusion process. The theoretical determination of the $q'\bar{q} \to W^* \to t\bar{b}$ rate is less prone to the uncertainties involved in the W-gluon fusion calculation since initial state effects can be measured in the similar Drell-Yan process $q'\bar{q} \to l\nu$. Reference [58] discusses prospects for isolating the W^* piece of the single top signal at the next Tevatron run. Their strategy is to require that both jets be tagged as b jets. In addition, they require no more than two final state jets, which substantially reduces the W-gluon fusion background, leaving only some small fraction of $qg \to q't\bar{b}$, where the light quark jet has escaped detection.

We now modify our earlier analysis to require that both jets be tagged as b jets. We also adopt two additional cuts from Ref. [58]: $\Delta R_{b\bar{b}} > 0.7$ and $M_{b\bar{b}} > 110$ GeV/c^2. These cuts serve to provide needed additional reduction of the $Wb\bar{b}$ background. For $m_{top} = 170$ GeV/c^2, we obtain yields per fb^{-1} in the peak region (as defined in Table 3.19) of 8.1 events from the W^* process, 2.1 events from W-gluon fusion, 6.7 events from $Wb\bar{b}$, and 3.0 events from $t\bar{t}$. This gives a total number of background events per fb^{-1} of $B = 11.8$ compared to a signal of $S = 8.1$. We ignore the Wjj background here due to the double b jet tag. The fractional statistical error, $\sqrt{S+B}/S$, would thus be 39% with 2 fb^{-1} of data, 17% with 10 fb^{-1}, and 5.5% with 100 fb^{-1}.

The authors of Ref. [58] use a different Monte Carlo program, make different cuts and different detector assumptions, use a slightly different top quark mass (175 GeV/c^2), and include additional backgrounds, but their conclusions are similar. They find that, assuming $|V_{tb}|$ is close to unity, 12 fb^{-1} of integrated luminosity yields a 10% measurement of the partial width , $(t \to Wb)$ and hence a 5% measurement of $|V_{tb}|$. Our more pessimistic detector parameters account for much of the difference between the analyses. In either case, the balance between systematics and statistics in the W^* measurement yields a final precision on $|V_{tb}|$ which is comparable to the result of using the full single top sample. It will be interesting to see how these differences play out in the real measurement.

Ref. [58] also suggests that the W^* signal could be difficult to extract at the LHC. The $t\bar{t}$ and W-gluon fusion backgrounds are relatively larger than at the Tevatron because they are initiated by gluons, while the signal is a quark-antiquark annihilation process and is thus heavily suppressed. At the LHC these backgrounds are each about twice as large as the signal, and have the same shape in the invariant mass m_{Wb} spectrum.

3.6.6 Other Physics Measurements with Single Top

In Standard Model single top production, the top quark is produced from a left-handed W boson resulting in a significant polarization of the top spin in the direction of the b in the $W*$ process and in the direction of the light quark in the W-gluon fusion process [59]. Since the top spin information is preserved in the final state (because the top decays before it can hadronize) this polarization may provide additional handles on the single top signal. In addition, if there are non-standard sources of CP violation in top decay, this polarization

will make their detection much simpler.

One can also look for CP violation in the production of the top quark. Since the initial $p\bar{p}$ state is a CP eigenstate, any difference between the cross sections for $p\bar{p} \to tX$ and $p\bar{p} \to \bar{t}X$ is a signal for CP violation. From our calculated event yields, and assuming $\sigma(p\bar{p} \to tX) \approx \sigma(p\bar{p} \to \bar{t}X)$, we can estimate the precision to which we can measure any asymmetry using:

$$A = \frac{\sigma(p\bar{p} \to tX) - \sigma(p\bar{p} \to \bar{t}X)}{\sigma(p\bar{p} \to tX) + \sigma(p\bar{p} \to \bar{t}X)}.$$

Taking the mass peak region yields for the 200 GeV/c^2 top quark, we see that the absolute statistical uncertainty in A is 0.16 with 2 fb^{-1} of data, 0.07 with 10 fb^{-1} and 0.02 with 100 fb^{-1}.

Finally, we note that the top quark mass will be determined from single top events with different systematic errors than those found in the $t\bar{t}$ analysis. The jet-parton combinatorics are less severe, since there are fewer jets and the correct b jet to combine with the W can be identified more often. Our model simulation does not include the detailed effects of gluon radiation, multiple interactions, or the underlying event, so no conclusions can be reached here about the possible accuracy of the mass determination, but we believe it will be an interesting and useful independent measurement.

3.6.7 Conclusions for Single Top

We have demonstrated the capability of isolating the "electroweak" production of single top. The production rate for this process is proportional to the partial top width , ($t \to Wb$) which measures the product of $|V_{tb}|^2$ and the top decay couplings. In the absence of anomalous couplings, 10 fb^{-1} at the Tevatron will allow determination of $|V_{tb}|$ to an accuracy of approximately 6%. With larger samples it will be possible to isolate the W^* component of single top production, allowing determination of $|V_{tb}|$ with somewhat larger statistical error than above, but better control of theoretical uncertainties. Finally, since our simulations show that it is reasonably straightforward to extract a signal from data gathered at a high luminosity Tevatron, we are optimistic that other interesting areas of the single top physics program will also be realized.

3.7 Top Physics at Other Facilities

3.7.1 NLC

An extensive literature exists on the potential for top physics at a high energy e^+e^- collider (see [60, 63] and other papers in these collections). We review here a few illustrative issues.

Since the massive top decays before hadronizing, there is no toponium resonance. For $m_t = 175$ GeV/c^2, the cross section rises smoothly from 0.6 pb at threshold to 1.4 pb at $E_{cm} = 500$ GeV. There are backgrounds from W pair production with $\sigma \sim 10$ pb, and $q\bar{q}$ + ISR + gluons with $\sigma \sim 30$ pb. Most studies use kinematic discrimination to isolate the top

signal, and suggest selection efficiencies of $\sim 50\%$ for all decay modes [60]. At threshold, the yield is 600 events per fb^{-1} in all modes. If at least one $W \to l\,\nu$ decay is needed to suppress combinatoric background in final state fits [63], the yield will be $\sim$ 100 events per fb^{-1}.

The yield is low, but control of the initial state offers some interesting possibilities. The structure of the production cross section at threshold is a function of m_t and α_s, and somewhat more weakly of , $_t$ and λ_{tH}, the Higgs Yukawa coupling. The analysis of Ref. [64] supposes a scan of 9 points in the threshold region, with 1 fb^{-1} per point, assuming that the center of mass energy can be known with precision better than 10^{-3}. In this case, the expected precisions for $m_t = 180$ GeV/c^2 are $\delta m_t = 500$ MeV/c^2 and $\delta\alpha_s = 0.009$. Ref [61] suggests that if m_t and α_s are known with infinite precision, a second scan with comparable luminosity could yield a 50% measurement of , $_t$ and λ_{tH}, although the width measurement is difficult for $m_t \geq 150$ GeV/c^2.

The crux of these measurements is control over E_{cm} in a linear collider. The intrinsic energy spread is typically 0.1-1.0% [65], and this is further degraded by "beamstrahlung" and initial state radiation, but the discussion in Ref. [64] suggests that the resulting "luminosity spectrum" can be reconstructed by monitoring the spent beams and small angle Bhaba scattering. The very precise control of operating conditions, not to mention extended running off the peak energy, suggest that threshold measurements in the top system will occur somewhat later in the full program of measurements at a linear collider.

Besides the top threshold behavior, a number of other measurements are possible in the top sample which can be accumulated at a linear collider. The study of couplings at the production vertex is unique to e^+e^-, and there is a natural top polarization correlated with a forward-backward asymmetry which may have utility in this regard [62]. A simulation study suggests that 50 fb^{-1}would allow the measurement of the static form factors at production and decay with a precision of a few percent [66]. In the case of measurements which depend on the final state only, such as rare decays, we would expect comparable sensitivities between similar sized samples at any facility.

3.7.2 LHC

Top physics at the LHC will be done primarily during the early running at relatively low luminosities of $10^{32} - 10^{33}$cm^{-2}s^{-1}. At the full luminosity of the machine it is expected that multiple interactions will render b-tagging ineffective and thereby make top physics much more difficult. In pp collisions at the final LHC energy of $\sqrt{s}$=14 TeV the $t\bar{t}$ production cross section is about 100 times larger than that at the Tevatron. If the low luminosity running at the LHC turns out to be equivalent to a typical calendar year at 10^{33}cm^{-2}s^{-1}, or 10 fb^{-1}, and detection efficiencies are roughly similar, the LHC experiments will have a statistical advantage of approximately two orders of magnitude over a 10 fb^{-1} Tevatron run. In comparing top measurements at the Tevatron with similar measurements at LHC it is clear that in most cases the statistical advantage will be significant. Below, we briefly review the LHC version of each of the Tevatron measurements discussed in the preceding pages.

A. Mass Measurement

Statistical uncertainties in the top mass measurement with 2 fb^{-1} are already quite

small at the Tevatron, when compared to the systematic uncertainties. At the LHC, the statistical uncertainty will be negligible. As discussed in Section 3, systematic effects on the measurement are studied, in large part, using control samples in the data, and uncertainties due to many systematic effects are therefore likely to scale with $1/\sqrt{N}$. Systematics due to b-tagging bias are already small with 2 fb^{-1} at the Tevatron and should remain negligible at LHC. Another major systematic uncertainty is that due to the shape of the background. As discussed in Section 3, this can be controlled with a sufficiently large sample of Z+4 jet events, which will certainly be accumulated at LHC. The major systematic top mass uncertainty at LHC is likely to be, as it is at the Tevatron, related to the jet energy scale. With a sufficiently large sample of $t\bar{t}$ events, much of the energy scale uncertainty can be calibrated away *in situ* using the $W \to q\bar{q}$ mass peak in $t\bar{t}$ events (see Sec. 3.4B). This will certainly be an effective technique at LHC and the light quark jet energy scale uncertainty should be quite small. Uncertainties in the b jet energy scale can, in principle, be controlled using $Z \to b\bar{b}$ events or possibly $WZ \to \ell\nu b\bar{b}$, if such samples can be isolated. As mentioned in Section 3, there is significant resolution broadening which results from hard gluon radiation, and here the situation at LHC will be worse than that at the Tevatron as a result of the higher energy. We have found no detailed studies of these effects at LHC energies, so it is difficult for us to quantify the effect on the mass resolution, but it is the one feature of the mass measurement in which the Tevatron is at an advantage over LHC. It should be mentioned that the 'extra jet' effect can be somewhat ameliorated by careful event selection, such as requiring four and only four jets, which becomes effective only when there are sufficient statistics.

The ultimate precision of the LHC mass measurement is somewhat difficult to gauge. Many of the systematic uncertainties will scale down statistically from the values cited in Section 3 for the Tevatron. Uncertainties which *do* scale this way are likely to be negligible in the overall scheme of things at LHC. It is therefore those effects which *don't* scale as $1/\sqrt{N}$ that will determine the ultimate sensitivity. It is likely that the gluon radiation effects mentioned above will be in this category, but it is nearly impossible to predict where the "brick wall" will be reached in controlling these effects. The LHC literature [67] quotes an ultimate mass uncertainty of $\pm$ 2 GeV/c^2. Given the recent Tevatron experience, this seems quite conservative and it is likely that the final result will be better than this, perhaps as small as $\pm$ 1 GeV/c^2.

It is perhaps worth noting that the obvious application of an accurate top mass is in the precision electroweak program, and, even assuming the best measurements possible by the year 2005, this program is limited by other factors (δm_W, $\alpha_{em}(Z)$, etc) for top mass precision better than 2 GeV/c^2. See Chapter 4, Section 2.4, for further details.

B. Production Cross Section

This is a measurement which at LHC is quite complementary to the measurement at the Tevatron. The ultimate uncertainty at the LHC is likely to be limited, as it is at the Tevatron, by the knowledge of the integrated luminosity. As a test of QCD, one clearly wants both the Tevatron and LHC measurements. In terms of searching for non-Standard Model production mechanisms such as resonance production, the LHC presumably has more reach as a result of the higher energy. However, this conclusion depends somewhat on exactly what the presumed resonance is. Since $t\bar{t}$ production at the LHC is primarily via gluon fusion, it

is insensitive to a spin-one color singlet, whereas at the Tevatron where $t\bar{t}$ production is a $q\bar{q}$ process, there is no such restriction.

C. Wtb Couplings

The statistical uncertainties in the measurement of the fraction of longitudinal and right-handed W bosons at LHC drop by a factor of 10-30 compared to the Tevatron numbers quoted in Table 12 of Section 5.1. Therefore the LHC measurement uncertainty is likely to be dominated by systematic effects. These systematic effects are the same as those mentioned in 5.1 and are similar to the systematic effects seen in the mass measurement. As with the LHC mass analysis discussed above, it is difficult to quantify where the uncertainties will plateau, but a factor of at least 2-3 improvement over the Tevatron uncertainties seems a reasonably conservative expectation.

D. Rare Decays

The Standard Model rates for FCNC are unobservable even at the LHC. With a factor of 100 improvement in statistics, the LHC clearly has more reach for detection of non-Standard Model branching fractions. For $t \to Ws$ the Standard Model prediction is of order 10^{-3}. In principle this might be observable at the LHC, but without detailed studies of efficiencies and backgrounds it is far from certain.

E. Single Top Production

Single top production via the W-gluon fusion process discussed in Section 6 can be detected at LHC with comparable or slightly better S/B as at the Tevatron. The extraction of $|V_{tb}|$ from the measured cross section will suffer from the same uncertainty from the gluon distribution as at the Tevatron.

For single top produced by the s-channel W* process, however, one expects approximately a 6% uncertainty on the measurement of V_{tb} (see Section 6.4), and this measurement is likely to be better at the Tevatron than at LHC. The reason is that at the Tevatron one can effectively separate the W* from the W-gluon fusion events by vetoing on the presence of an additional jet [58]. The growth in cross section for single top production via W-gluon fusion and $t\bar{t}$ production (via glue-glue) between $\sqrt{s} = 2$ TeV and $\sqrt{s} = 14$ TeV is much greater than that for single top production via W*, which is a valence $q\bar{q}$ process. As a result, the W* signal is swamped by W-gluon fusion and $t\bar{t}$ events at LHC, even after the additional cuts are applied.

3.8 Conclusions

We have reviewed the prospects for a top physics program at the Fermilab Tevatron in the Main Injector Era. The conclusions are preliminary, but have the strength of being extrapolations from real measurements in the well understood environments of the present day Collider experiments.

The results are summarized in Table 3.22. The CDF and DØ experiments will each record over 500 identified $t\bar{t}$ events per fb^{-1}. With an integrated luminosity in excess of 10 fb^{-1}: the top mass will be measured with an accuracy of 2 GeV/c^2; the total cross section measurement will be limited only by the luminosity normalization precision, presently 5%, and non-standard production mechanisms will be resolvable down to total cross sections of $\sim$ 25 fb; the branching fraction to b quarks and branching ratio to the various W helicity states will be measured with with precisions of order 1-2%; the branching fraction to non-W states may be explored at the level of 5%; and the magnitude of a FCNC decay will be probed down to branching fractions of 0.1%. We have demonstrated the capability to isolate the electroweak production of single top, where the production rate is proportional to the partial width , $(t \to Wb)$. A data set in excess of 10 fb^{-1}will allow determination of , $(t \to Wb)$ to 12%, and inference of $|V_{tb}|$ with a precision of 6%.

We believe that this is only the beginning of the catalog of top physics measurements at the Tevatron, and that this report is best interpreted as a survey of *sensitivities* in each of the categories of mass reconstruction, cross sections, branching ratios, decay dynamics, and rare decays. In the event that this very massive fermion harbors surprises, this study benchmarks the capability to explore the new physics at the Tevatron facility.

Measurement	1 fb^{-1}	10 fb^{-1}	100 fb^{-1}	Comment
Yields				
N_{3jet*b}	580	5.8K	58K	*identified* events
$N_{4jet*2b}$	260	2.6K	26K	best m_t sample
δm_t	3.5	2.0	??	total precision GeV/c^2
Production				
$\delta\sigma_{t\bar{t}}$	11%	6%	5%	test top QCD couplings
$\delta\sigma_{ll}/\sigma_{l+j}$	14%	4.8%	1.5%	test non W decay
$\delta\sigma_{t\bar{b}X+b\bar{t}X}$	26%	10%	7%	isolate "single top"
$\delta\sigma \cdot B(Z' \to t\bar{t})$	100 fb	25 fb	10 fb	"topcolor" $M_{Z'} = 1$ TeV/c^2
Decay				
$\delta B(t \to W(b))$	3%	1.0%	0.3%	from N(bb)/N(bX)
$\delta B(t \to b(W))$	10%	3.5%	1.0%	from N(ll)/N(lX)
$\delta B(W_{V+A})$	3%	0.8%	0.3%	$W \to l\nu$ helicity
$\delta B(W_{long})$	6%	2.1%	0.7%	$\frac{W_{long}}{W_{left}} = \frac{1}{2}(\frac{m_t}{m_W})^2$
δ, $(t \to Wb)$	28%	12%	10%	using single top
δV_{tb}	14%	6%	5%	from above
Rare Decays				
B(c γ)	$\leq 3.0 \times 10^{-3}$	$\leq 4.0 \times 10^{-4}$	$\leq 8.4 \times 10^{-5}$	(95% CL)
B(cZ)	$\leq 1.5 \times 10^{-2}$	$\leq 3.8 \times 10^{-3}$	$\leq 6.3 \times 10^{-4}$	(95% CL)
B(Hb)	$\leq 15\%$	$\leq 6\%$	$\leq 2\%$	from σ_{ll}/σ_{l+j}

Table 3.22: A Top Physics Program: Summary of expected precision vs integrated luminosity at the Tevatron

Acknowledgements

Many people have helped in the organization and discussion leading up to this document. We gratefully acknowledge the assistance of A. Belyaev, A. Beretvas, E. Boos, J. Butler, D. Carlson, W. Cobau, D. Gerdes, J. Hylen, J. Incandela, J. Konigsberg, M. Kruse, S. Parke, T. Stelzer, P. Tipton, J. Wells, S. Willenbrock, W.M. Yao, and C.-P. Yuan.

P.B. would like to thank the Physics Department of U. Michigan for kind hospitality during his sabbatical leave from U. Kansas.

Bibliography

[1] F. Abe *et al.*(The CDF Collaboration), Phys. Rev. Lett. **74**, 2626 (1995).

[2] S. Abachi *et al.* (The DØ Collaboration), Phys. Rev. Lett. **74**, 2632 (1995).

[3] LEP Electroweak Working Group, LEPEWWG/95-02 (August 1995); P. H. Chankowski and S. Pokorski, Phys. Lett. **B356**, 307-312 (1995); J. Ellis, G.L. Fogli, and E. Lisi, hep-ph/9507424.

[4] T. LeCompte et al., "Extension of Central Muon Coverage for Run 2", CDF Note 3116 (April 1995).

[5] The CDF Collaboration, "Proposal for Run II Tracking System Upgrades for CDF", CDF Note 3079 (March 1995).

[6] We thank Mark Kruse for discussion of this point.

[7] The CDF B Tag Group, "A Generator Study of b Jets from TOP Decay", CDF Internal Note 2568 (May 1994).

[8] W. Cobau, private communication.

[9] E. Laenen, private communication.

[10] E. Laenen, J. Smith, and W.L. van Neerven, Phys. Lett. **B321**, 254 (1994).

[11] F. Abe et al., Phys. Rev. D. **50**, 2966 (1994).

[12] Qi Zhong Li-Demarteau, for the DØ Collaboration, at the Aspen Winter Conference (January 1996).

[13] M. Stronvink, in the Proceedings of the 10th Topical Workshop on Proton-Antiproton Collider Physics, Fermilab, DØ note 2611 (May 1995).

[14] S. Gruenendahl, for the DØ Collaboration, at the NLC Workshop, Stanford Linear Accelerator Center (February 1996).

[15] G. Marchesini and B.R.Weber, Nucl. Phys. **B310**, 461 (1988).

[16] F.A.Berends, W.T.Giele, H. Kuijf and B. Tausk, Nucl. Phys **B357**, 32 (1991).

[17] S. Vejcik, S.B. Kim, "Statistical Uncertainties for the Top Mass in Run 1B", CDF Note 2833 (September 1994).

[18] S.B. Kim and S. Vejcik, "Study of Gluon Radiation and Jet Energy Scale Using Z+jets and Photon + jets", CDF Note 3006 (February 1995).

[19] W. Yao, L. Galtieri, M. Garcia-Scrivers, and J. Lys, "Studies of Gluon Radiation Systematic Error with b-bbar Events and a Proposal of Multiple Underlying Events Correction on the Jet Energy", CDF Note 3257 (July 1995).

[20] S.B.Kim, S. Vejcik, and B. Harral, "Background Shapes of the Reconstructed Top Mass", CDF Internal Note 3007 (February 1995).

[21] R.H. Dalitz and G.R. Goldstein, Phys. Rev. D**45**, 1531 (1992).

[22] K. Kondo, Journal of the Physical Society of Japan, **57** 4126 (1988) and **60**, 836 (1991).

[23] U. Heintz, "Top Mass Analysis of Dilepton Events," DØ Note 2658 (July 1995).

[24] J. Cochran and U. Heintz, "A Measurement of Top quark Mass with Dilepton Events" DØ Note 2659 (August 1995).

[25] S. Snyder, to appear in the Proceedings of the European Physical Society Meeting, DØ Note 2836, (July 1995).

[26] P. Azzi *et al.*, "Evidence for $t\bar{t}$ Production in the All Hadronic Channel", CDF Note 3187 (June 1995).

[27] J. Incandela, "Using the B Decay Length Distribution in Top Events to Measure m_t", CDF Note 1921 (December 1992).

[28] L. Orr, T. Stelzer, and W.J. Stirling, Phys. Rev. D **52**, 124-132 (1995); Phys. Lett. **B354**, 442-446 (1995); L. Orr and W.J. Stirling, Phys. Rev. D **51**, 1077-1085 (1995); S. Mrenna and C.-P. Yuan, Phys. Rev. D. **46**, 1007-1021 (1992); Yu. L. Dokshitzer, V.A. Khoze and S.I. Troyan, Proceedings of the 6th International Conference on Physics in Collision, Singapore (1987); G. Marchesini and B.R. Webber, Nucl.Phys. **B330**, 261-283.

[29] C.T. Hill, Phys. Lett. **B345**, 483-489 (1995).

[30] P. Cho and E.H. Simmons, Phys. Rev. D **51**, 2360 (1995); D. Atwood, A. Kagan and T. Rizzo, Phys. Rev. D **52**, 6264-6270 (1995).

[31] K. Lane, Phys. Rev. D **52**, 1546-1555 (1995).

[32] C. T. Hill, Physics Lett. **B266**, 419 (1991).

[33] K. Lane and E. Eichten, Phys. Lett. **B222**, 274 (1989); K. Lane and M.V. Ramana, Phys. Rev. D **44**, 2678 (1991).

[34] C. Hill, R. Harris, private communication

[35] K. Tollefson, R. Hughes, P. Tipton, B. Winer, "Search for Resonances Decaying to $t\bar{t}$", CDF Note 3105 (1995).

[36] For any given theoretical model, there may be angular correlations that either increase or decrease the acceptance and therefore the 5σ lines will move up or down slightly.

[37] I. Bigi *et al.*, Phys Lett. **B181**, 157 (1986).

[38] For example, see G. Kane, C.-P. Yuan, and G. Ladinsky, Phys. Rev. D. **45**, 124 (1992); D. Atwood, A. Aeppli, and A. Soni, Phys. Rev. Lett. **69**, 2754 (1992); R.S. Chivukula, S.B. Selipsky, E.H. Simmons, Phys. Rev. Lett. **69**, 575 (1992); M. Peskin, talk presented at the Second International Workshop on Physics and Experiments at a Linear e+e- Collider, Waikoloa, HI (April 1993); M.Peskin and P. Zerwas, talks presented at the First International Workshop on Physics and Experiments at a Linear e+e- Collider, Saariselka, Finland (September 1991); D. Carlson, E. Malkawi, C.-P. Yuan, Phys. Lett. **B337**, 145 (1994).

[39] G. Kane, C.-P. Yuan, and G. Ladinsky, Phys. Rev. D. **45**, 124 (1992).

[40] K. Fujikawa and A. Yamada, Phys. Rev. Lett. **49**, 5890 (1994).

[41] M. Jezabek and J.H. Kuhn, Phys. Lett. **B329**, 317 (1994).

[42] E. Malkawi, C.-P. Yuan, Phys. Rev. D. **50**, 4462 (1994).

[43] E. Thorndike, "Rare B Decays from CLEO, with emphasis on $b \to s\gamma$", Proceedings of the XXVII International Conference on High Energy Physics, Glasgow, UK (July 1994).

[44] S. Parke, "Summary of Top Quark Physics", FERMILAB -Conf-94/322-T, and Proceedings of DPF'94, University of New Mexico, Albuquerque, NM (August 1994).

[45] C. Couyoumtzelis, J. Conway, and A. Clark, private communication.

[46] S. Dawson, Nucl. Phys. **B249**, 42 (1985); S.S.D. Willenbrock and D.A. Dicus, Phys. Rev. D **34**, 155 (1986); S. Dawson and S.S.D. Willenbrock, Nucl. Phys. **B284**, 449 (1987); C.-P. Yuan, Phys. Rev. D **41**, 42 (1990); S. Cortese and R. Petronzio, Phys. Lett. **B253**, 494 (1991); G.V. Jikia and S.R. Slabospitsky, Phys. Lett. **B295**, 136 (1992), R.K. Ellis and S. Parke, Phys. Rev. D **46**, 3785 (1992); G. Bordes and B. van Eijk, Z. Phys. **C57**, 81 (1993); G. Bordes and B. van Eijk, Nucl. Phys. **B435**, 23 (1995).

[47] T. Moers, R. Priem, D. Rein and H. Reitler, in the Proceedings of the Large Hadron Collider Workshop, Aachen, 418 (1990).

[48] D.O. Carlson and C.-P. Yuan, Phys. Lett. **B306**, 386 (1993).

[49] A.P. Heinson, A.S. Belyaev and E.E. Boos, "Electroweak top quark production at the Fermilab Tevatron", in the proceedings of the Workshop on Physics of the Top Quark, Iowa State University, Ames, Iowa (May 1995), hep-ph/9509274.

[50] F.I. Olness and W.-K. Tung, Nucl. Phys. **B308**, 813 (1988).

[51] J. Botts, J.G. Morfin, J.F. Owens, J. Qiu, W.-K. Tung and H. Weerts, (CTEQ Collaboration) Phys. Lett. **B304**, 159 (1993).

[52] "The DØ Upgrade" by the DØ Collaboration, presented to the Fermilab PAC (April 1995).

[53] The electron efficiency in the DØ central calorimeter is 79.2%, and in the end calorimeters it is 63.1% [RECO V11.19, P. Grudberg, DØ Note 2316 (1994)].

[54] S. Chopra and R. Raja, DØ Note 2098 (April 1994).

[55] A.P. Heinson, A.S. Belyaev and E.E. Boos, "Single top quarks at the Fermilab Tevatron", in preparation.

[56] A.P. Heinson, DØ Note 2777 (1995).

[57] H. Weerts, private communication.

[58] T. Stelzer and S. Willenbrock, Phys. Lett. **B357**, 125-130 (1995).

[59] We thank S. Parke for discussion on this point.

[60] K. Fuji, "Top Physics at Future e^+e^- Colliders, Experimental Aspects", First International Workshop on Physics and Experiments at a Linear e+e- Collider, Saariselka, Finland (September 1991).

[61] G. Bagliesi *et al.*, *ibid.*

[62] M. Peskin *et al.*, *ibid.*

[63] P. Igo-Kemenes, M. Martinez, R. Miquel, and S. Orteau in Second International Workshop on Physics and Experiments at a Linear e+e- Collider, Waikoloa, HI (April 1993).

[64] P. Igo-Kemenes, *ibid.*

[65] D. Treille, *ibid.*

[66] G.A. Ladinsky and C.-P. Yuan, *ibid.*

[67] See for example D. Froidevaux, Top Quark Physics at LHC/SSC CERN/PPE/93-148 and Proceedings of Moriond 1993: Electroweak: 509-526 (March 1993).

Chapter 4

Intermediate Vector Boson Physics

4.1 Introduction

Because of its success in describing low energy phenomenology and its relative economy in the number of fundamental fields, the $SU(3)_C \times SU(2)_L \times U(1)_Y$ theory of strong and electroweak interactions, based on the principle of non-abelian gauge invariance, has become the Standard Model (SM). $SU(3)_C$ embodies the current theory of the strong interactions, Quantum Chromodynamics (QCD), and is deemed to be an unbroken symmetry of nature. The $SU(2)_L \times U(1)_Y$ sector is the basis of the Standard Electroweak Model and is spontaneously broken at a mass scale $v = (\sqrt{2}G_\mu)^{-1/2} = 246$ GeV into $U(1)_Q$, the Abelian gauge group of electromagnetism.

The SM has been very successful phenomenologically. It has provided the theoretical framework for the description of a very rich phenomenology spanning a wide range of energies, from the atomic scale up to the Z boson mass, M_Z. It is being tested at the level of a few tenths of a percent, both at very low energies and at high energies [1, 2]. However, the SM has a number of shortcomings. In particular, it does not explain the origin of mass and the observed hierarchical pattern of fermion masses, and why there are three generations of quarks and leptons. It is therefore widely believed that at high energies, or in very high precision measurements, deviations from the SM will appear, signaling the presence of new physics.

In this chapter we discuss the potential of probing the electroweak sector of the SM at the Tevatron ($\sqrt{s} = 1.8$ TeV to 2 TeV) using very large integrated luminosities ($\int \mathcal{L} dt = 1, \ldots 10$ fb^{-1}). With recent advances in accelerator technology, Tevatron collider luminosities of $\mathcal{L} = 10^{33}$ cm^{-2} s^{-1} may become reality within the next few years [3], resulting in integrated luminosities of up to 10 fb^{-1}/year. The electroweak physics potential with such large integrated luminosities is best illustrated by the expected event yields for W/Z and di-boson production which are listed in Table 4.1. The approximately 10 million $W \to e\nu$ and the 700,000 $Z \to e^+e^-$ events (a similar number is expected in the muon channel) can be employed to measure the W mass and width, M_W and $, _W$, with very high precision (Section 2), and to extract information on parton distributions from the W boson decay lepton charge asymmetry. The Z boson decay lepton forward backward asymmetry, A_{FB},

Table 4.1: Expected W, Z and di-boson event yields at the Tevatron for an integrated luminosity of 10 fb^{-1}. Standard CDF/DØ lepton trigger and identification cuts are imposed. In addition, a cluster transverse mass larger than 90 GeV/c^2 is required for $W\gamma$ production, and $m(ee\gamma) > 100$ GeV/c^2 for $p\bar{p} \to Z\gamma$, $Z \to e^+e^-$. In both processes a $\Delta R(e,\gamma) > 0.7$ cut is imposed. In WW production, a jet veto is imposed to reduce the $t\bar{t}$ background, and both charged leptons are required to have $|\eta(\ell)| < 1$.

channel	number of events
$W + X$, $W \to e\nu$, $\|\eta(e)\| < 1.2$	$6.4 \cdot 10^6$
$Z + X$, $Z \to e^+e^-$	$7.4 \cdot 10^5$
$W\gamma$, $W \to e\nu$, $E_T(\gamma) > 10$ GeV, $\|\eta(\gamma)\| < 2.4$	$4.8 \cdot 10^3$
$Z\gamma$, $Z \to e^+e^-$, $E_T(\gamma) > 10$ GeV, $\|\eta(\gamma)\| < 2.4$	$1.5 \cdot 10^3$
$Z\gamma$, $Z \to \bar{\nu}\nu$, $E_T(\gamma) > 40$ GeV, $\|\eta(\gamma)\| < 1$	$1.1 \cdot 10^3$
W^+W^-, $W \to \ell\nu$, $\ell = e, \mu$	500
WZ, $W \to \ell\nu$, $Z \to \ell^+\ell^-$, $\ell = e, \mu$	200
ZZ, $Z \to \ell^+\ell^-$, $\ell = e, \mu$	30

can be used to determine $\sin^2\theta^{lept}_{eff}$ with high precision. Both the W mass and $\sin^2\theta^{lept}_{eff}$ can be utilized to extract the Higgs boson mass, M_H, from electroweak one-loop corrections. The W and Z asymmetries are discussed in detail in Section 3 of this chapter. The transverse momentum distribution of the Z boson can be used to measure the strong coupling constant α_s (Section 4) while the very large sample of W boson events can also be employed to search for rare W decays (Section 5) and novel CP violating interactions [4] (Section 6).

One of the most direct consequences of the $SU(2)_L \times U(1)_Y$ gauge symmetry are the self-couplings of the W, Z and photon. A direct measurement of these vector boson couplings is possible through the study of pair and triple gauge boson production processes like $p\bar{p} \to W^+W^-$, $W\gamma$, $Z\gamma$, WZ and $p\bar{p} \to W\gamma\gamma$, $Z\gamma\gamma$, $W^+W^-\gamma$, *etc.*. For an integrated luminosity of 10 fb^{-1} one expects, *e.g.*, about 5,000 $W\gamma$, $W \to e\nu$, and approximately 1,500 $Z\gamma$, $Z \to e^+e^-$, events with a photon of $E_T(\gamma) > 10$ GeV (see Table 4.1). The large number of expected di-boson events will make it feasible to study the three boson self-interactions in detail. In $W\gamma$ production, Tevatron experiments can also search for the SM "radiation zero", which provides an additional powerful test of the gauge theory nature of the SM. Measuring the transverse momentum distribution of the $W\gamma$ system provides a test of QCD. Quantum Chromodynamics predicts a p_T distribution of the $W\gamma$ system which is considerably harder than that observed in W production. For integrated luminosities of 10 fb^{-1} or more, Tevatron experiments might also offer a first glimpse at triple electroweak boson production [5]. Triple gauge boson production provides a chance to measure the quartic gauge boson couplings

directly.

The first and major goal of measuring the self-couplings of W and Z bosons will be a confirmation of the SM predictions. A precise and direct measurement of the trilinear and quartic couplings of the electroweak vector bosons and the demonstration that they agree with the SM would beautifully corroborate spontaneously broken, non-abelian gauge theories as the basic theoretical structure describing the fundamental interactions of nature. At the same time, such measurements may be used to probe for new physics. Since it is possible to build extensions of the SM where the quartic couplings are modified but not the three vector boson couplings [6], it is necessary to measure both the trilinear and the quartic couplings separately in order to completely determine the self-interactions of the electroweak vector bosons. Di-boson production is considered in Section 7. In Section 8 we present a brief survey of triple vector boson production and the relevant background processes.

Finally, our conclusions are presented in Section 9.

4.2 W Mass and Width Measurement

4.2.1 Preliminaries

The mass of the W boson, M_W, is a fundamental parameter of the SM. Direct, precision measurements of M_W, and of the top quark mass, M_{top}, provide an indirect constraint on the Higgs boson mass, M_H, via top quark and Higgs boson electroweak radiative corrections to M_W. The ultimate test of the SM may lie in the comparison of these indirect determinations of M_H with its direct observation at the Tevatron (for $M_H < 130$ GeV; see Chapter 6), or the LHC.

At the Tevatron, the W mass is extracted from a fit to the W transverse mass, M_T^W, distribution which sharply peaks in the vicinity of M_W. From the data collected in Run 1a (19 pb^{-1}), CDF finds [7]

$$M_W = 80.41 \pm 0.18 \text{ GeV/c}^2. \tag{4.1}$$

The DØ Collaboration has not published a final result of their W mass analysis yet. The current world average [1],

$$M_W^{\text{World}} = 80.26 \pm 0.16 \text{ GeV/c}^2 \tag{4.2}$$

is dominated by the CDF measurement from Run 1a.

4.2.2 W Mass Measurement at a Superluminous Tevatron

In estimating the precision of M_W which one may expect at high integrated luminosities, it is important to note that, besides the theoretical errors from electroweak one loop corrections and higher order corrections which each contribute about 20 MeV/c^2 to the current uncertainty in M_W, the dominant systematic errors are determined from control datasets

(Z boson events, J/ψ events). One therefore expects that the uncertainties on the W mass originating from those sources will approximately scale as $1/\sqrt{N}$, where N is the number of events, the same scaling law which applies to statistical errors.

In order to reduce the theoretical errors, improved calculations of radiative corrections are essential. Recently, a complete calculation of radiative W and Z boson production and decay, including initial and final state bremsstrahlung, finite W/Z decay lepton masses, and finite W/Z width effects [8] has been carried out. This will make it possible to reduce the error associated with radiative corrections substantially in the future, although certain non-factorizable QED final state interaction effects in $qg \to W(\to \ell\nu)q'$ and higher order QED corrections which have not been calculated yet could conceivably induce an additional error in M_W of $\mathcal{O}(10\ \mathrm{MeV/c^2})$ [9].

Some systematic errors, such as those originating from the W p_T distribution, or from uncertainties in the structure functions, are quasi-theoretical in nature and are associated with the details of the production process. These errors do not necessarily scale like $1/\sqrt{N}$. Structure function effects are controlled in part through the measurement of the W asymmetry which will be discussed in Section 3 of this chapter. In the case of the W p_T spectrum, the Z^0 transverse momentum distribution and a new theoretical calculation of W and Z production which includes soft gluon resummation effects and W/Z decays in a Monte Carlo approach (RESBOS) [10] are expected to provide appropriate checks and improved theoretical guidance, and will make it possible to substantially reduce the current uncertainty of 45 MeV/c^2 in M_W associated with the $p_T(W)$ distribution. Since the uncertainty in the ratio of the W and Z transverse momentum distributions is, independent of the details of the nonperturbative parameterization, only a few per cent [11], the error originating from the W p_T distribution is controlled by how well the Z boson transverse momentum distribution is measured.

Theoretical predictions of the W transverse mass distribution including soft gluon resummation (solid line) and at NLO in QCD (dashed line) are shown in Fig. 4.1. In contrast to the resummed W transverse mass spectrum, the M_T^W distribution is ill defined in the peak region at NLO in QCD, due to the singularity in the W transverse momentum distribution at $p_T(W) = 0$. To obtain the NLO result shown in Fig. 4.1, the transverse mass distribution for $p_T(W) > p_T^{sep}$ and the M_T^W distribution integrating from zero p_T to p_T^{sep} were added. The NLO transverse mass distribution resulting from this procedure then depends explicitly on the value of p_T^{sep} chosen. Fixing p_T^{sep} by requiring that the total cross section at NLO and including resummation effects is the same, one obtains the dashed line in Fig. 4.1.

With increasing luminosity, the average number of interactions per bunch crossing, I_C, may become considerably larger than one. For a luminosity of $\mathcal{L} = 10^{32}$ cm^{-2} s^{-1} ($\mathcal{L} = 10^{33}$ cm^{-2} s^{-1}) and a bunch spacing of 395 ns (132 ns) at the Tevatron, one expects $I_C \approx 3$ ($I_C \approx 9$) [3]. Multiple interactions degrade the resolution of the missing transverse energy (see Chapter 9) and thus of the M_T^W distribution. This is demonstrated in Fig. 4.2 where we show the W transverse mass distribution for various values of I_C. Multiple interactions are seen to considerably broaden the M_T^W distribution and to shift the peak position by several GeV/c^2. From our simulations we find that the resolution of the M_T^W distribution degrades approximately like $\sqrt{I_C}$. The impact of multiple interactions on the projected uncertainty in the W mass, ΔM_W, as a function of the integrated luminosity is illustrated

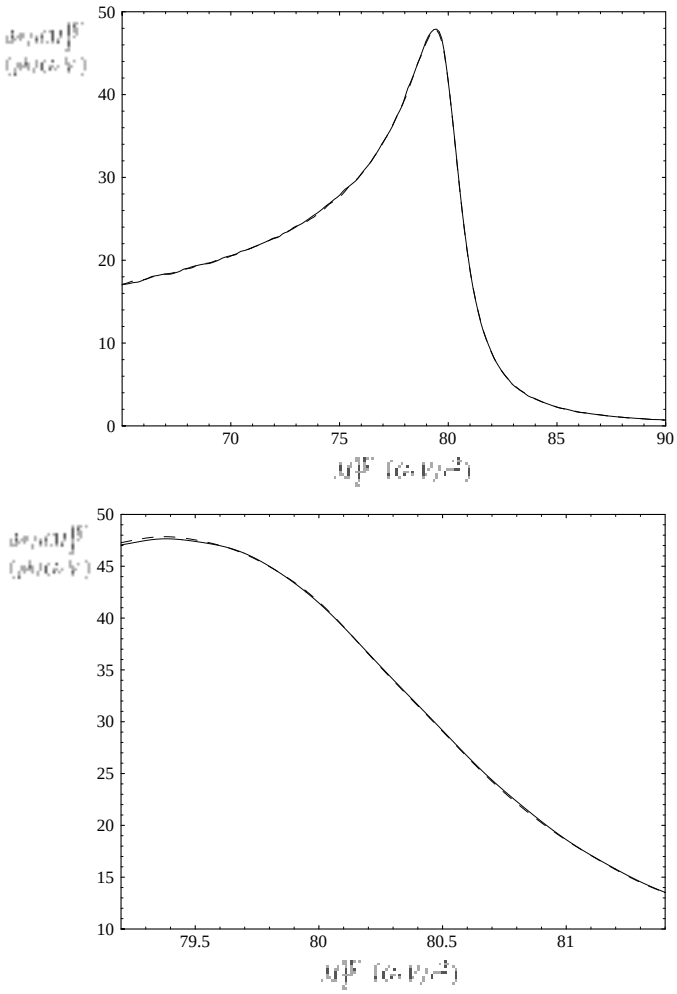

Figure 4.1: Distribution of the W transverse mass, at NLO (dashed line) and including soft gluon resummation effects (solid line) for $p_T(\ell) > 25$ GeV/c, $\not\!\!E_T > 25$ GeV, and $p_T(W) < 20$ GeV/c [7].

for the case $I_C = 3$ in Fig. 4.3. To present graphically how 3 interactions per crossing affect the resolution of the transverse mass distribution, the scaling of the error on the mass reach is varied gradually such that it approaches the resolution for 3 interactions per crossing for 1 fb^{-1}. For $\int \mathcal{L} dt > 1$ fb^{-1}, a fixed average number of $I_C = 3$ interactions per crossing is assumed in this figure.

If one assumes that the theoretical uncertainties, due to calculational improvements such as those mentioned above, virtually also scale like $\sqrt{I_C/N}$, the total systematic error in M_W can be parameterized by

$$\Delta M_W|_{\rm sys} = (17.9 \text{ GeV/c}^2) \sqrt{\frac{I_C}{N}} \ , \tag{4.3}$$

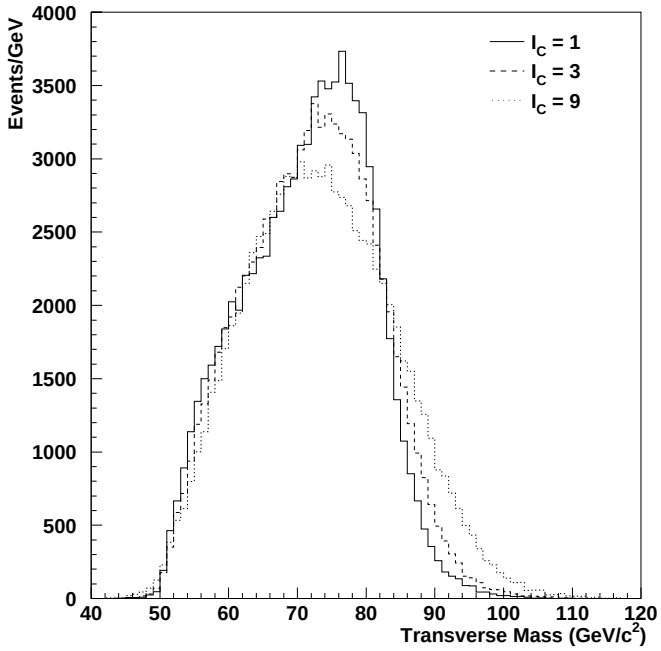

Figure 4.2: The effect of multiple interactions on the W transverse mass distribution. Standard kinematic cuts of $p_T(e) > 25$ GeV/c, $|\eta(e)| < 1.2$, $\not\!\!p_T > 25$ GeV/c and $p_T(W) < 30$ GeV/c are imposed. The effect of multiple interactions is simulated by adding additional minimum bias events to the event containing the W boson.

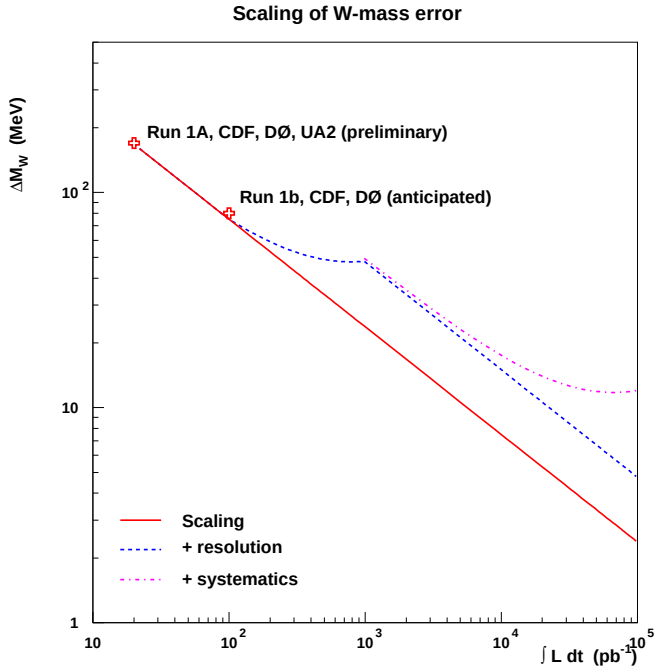

Figure 4.3: The effect of multiple interactions on the W mass uncertainty as a function of the integrated luminosity.

Table 4.2: Projected statistical and systematic errors (per experiment) on the W mass at the Tevatron, combining the $W \to e\nu$ and $W \to \mu\nu$ channel. Beneficial effects of the CDF and DØ upgrades for Run 2 are not included in the estimate.

ΔM_W	$\int \mathcal{L} dt = 1$ fb^{-1}, $I_C = 3$	$\int \mathcal{L} dt = 10$ fb^{-1}, $I_C = 9$
statistical	29 MeV/c^2	17 MeV/c^2
systematic	42 MeV/c^2	23 MeV/c^2
total	51 MeV/c^2	29 MeV/c^2

where N is the number of events. Similarly, the statistical uncertainty can be expressed as

$$\Delta M_W|_{\rm stat} = (12.1 \text{ GeV/c}^2) \sqrt{\frac{I_C}{N}} \; . \tag{4.4}$$

The projected statistical and systematic errors per experiment, derived from Eqs. (4.3) and (4.4), for integrated luminosities of 1 fb^{-1} and 10 fb^{-1} are listed in Table 4.2. In order to obtain the normalization of Eqs. (4.3) and (4.4), we have combined the uncertainties of the $W \to e\nu$ and $W \to \mu\nu$ channels, using for definiteness the current efficiencies of CDF. This means that several beneficial effects of the CDF and DØ upgrades for Run 2 are not included in our estimate. The uncertainties in M_W listed in Table 4.2 will improve slightly by combining the results of CDF and DØ. Details, however, depend largely on which portion of the systematic errors will be common to both experiments in the future. This has not been studied yet and, therefore, we have not attempted to estimate the combined uncertainty.

For $\mathcal{L} = 10^{33}$ cm^{-2} s^{-1}, multiple interactions are the dominating source of uncertainties in the W mass measurement. If one divides the total W sample into subsamples corresponding to a fixed number of interactions per crossing, it may be possible to reduce the negative effect of multiple interactions on ΔM_W. Performing a separate fit to the W mass in each of the subsamples, one can study in detail how multiple interactions affect the resolution of the transverse mass distribution. This may then help to develop techniques to correct for the effect [12], and thus to achieve an ultimate uncertainty ΔM_W considerably smaller than 29 MeV/c^2. However, we have not explored this approach in detail yet.

Presently contemplated upgrades of the CDF and DØ detectors will allow for operation with a bunch spacing of 132 ns. As described in Ref. [3], bunch separations of as low as 19 ns are possible for $\mathcal{L} = 10^{33}$ cm^{-2} s^{-1}. For a bunch spacing of 19 ns, $I_C \approx 1$, with a corresponding improvement in the uncertainty of M_W which one can hope to achieve. However, for such very short bunch separations, further detector upgrades, beyond those planned for Run 2, are necessary.

In summary, the values for ΔM_W listed in Table 4.2 are expected to be realistic. As a benchmark, we assume in the following that the W boson mass can be determined with an uncertainty of $\Delta M_W = 30$ MeV/c^2 for $\int \mathcal{L} dt = 10$ fb^{-1}. In view of the possibilities to improve the precision of the W mass measurement discussed above, however, a precision of

$\Delta M_W = 20$ MeV/c^2 may well be within reach.

In our discussion we have concentrated on the transverse mass distribution to extract M_W. As is clear from our discussion, the $\not\!\!E_T$ resolution will be the main effect in limiting the precision of future W mass measurements using the transverse mass distribution. M_W can also be determined from other quantities, such as the energy distribution [13] or the p_T spectrum of the charged W decay lepton. Both methods only require a measurement of the charged lepton four-momentum and are therefore independent of the missing transverse energy resolution. However, in contrast to the M_T^W spectrum, the lepton p_T and energy distributions are very sensitive to higher order QCD corrections, in particular resummation effects [10]. We have not studied the potential of measuring the W mass using the charged lepton energy and transverse momentum distributions in detail. However, using the results of Ref. [13] and assuming that the systematic errors scale as $1/\sqrt{N}$, we estimate that M_W could be measured with a precision of ~ 20 MeV using the lepton energy distribution.

4.2.3 Comparison with LEP II and LHC

The uncertainties listed in Table 4.2 should be compared with the errors on M_W expected from other collider experiments. At LEP II, M_W is expected to be measured with an accuracy of 60 MeV/c^2 to 80 MeV/c^2 per experiment [14] from either direct reconstruction of WW events, or a threshold scan. Taking common errors into account, this results in a projected overall precision of $\Delta M_W = 40$ MeV/c^2 at LEP II [15]. No detailed study on the prospects of measuring the W mass at the LHC exists at this time. In principle, M_W can be extracted from the transverse mass distribution at the LHC. However, the large average number of interactions per crossing ($I_C \approx 20$ at design luminosity) severely degrades the resolution of the M_T^W distribution. In addition, due to the high trigger threshold of $E_T > 40$ GeV for electrons [2, 1, 18], most $W \to e\nu$ events have a large recoil energy, which increases the background from heavy flavor decays and jets faking electrons. Without performing a detailed study, it thus not clear how well the W mass can be measured at the LHC.

4.2.4 Physics Significance of the W Mass Measurement at an Upgraded Tevatron

As we have mentioned before, the results of a precise measurement of the W and the top quark mass can be used to extract information on the Higgs boson mass which can then be confronted with the results of a direct search at the Tevatron or the LHC. This is illustrated in Fig. 4.4 which displays the results of the direct M_W and M_{top} measurements at the Tevatron with 10 fb^{-1} in the (M_{top}, M_W) plane [20], assuming that the W mass (top quark mass) can be measured with a precision of 30 MeV/c^2 (2 GeV/c^2 [see Chapter 3]) and that the current central values of M_W and M_{top} will not change. The cross hatched bands show the SM prediction for the indicated Higgs boson masses. The width of the bands is due primarily to the uncertainty in the electromagnetic coupling constant at the Z mass scale, $\alpha(M_Z)$, which has been assumed to be $\delta\alpha(M_Z) = 0.0004$. Recent estimates of the uncertainty in $\alpha(M_Z)$ give $\delta\alpha(M_Z) \approx 0.0004 - 0.0007$ [21]. Future measurements at Novosibirsk, Daphne and Beijing, combined with theoretical progress, may well lead to a

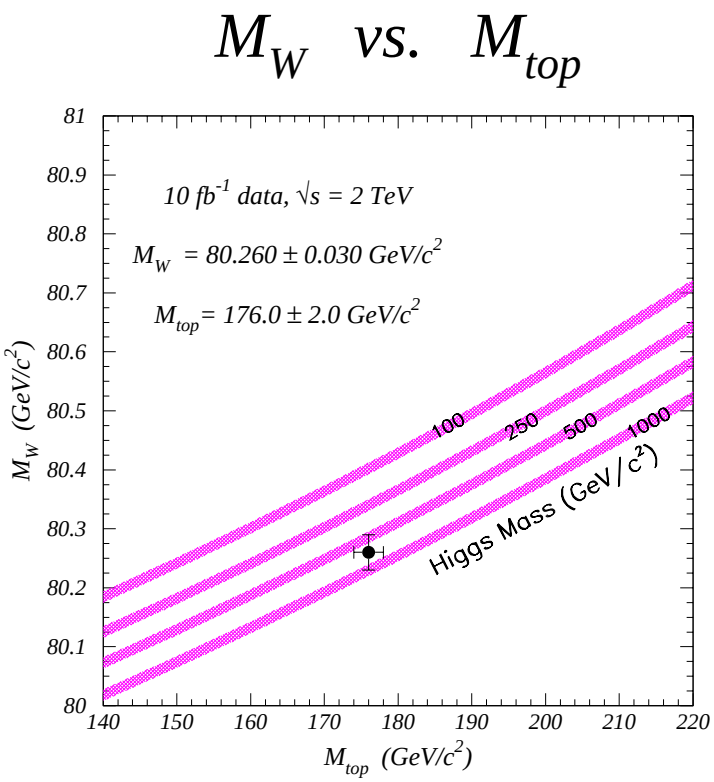

Figure 4.4: Expected results of a direct W and top quark mass measurement at the Tevatron with 10 fb^{-1} versus SM predictions for various Higgs boson masses in the (M_{top}, M_W) plane, assuming that the current central values of M_W and M_{top} will not change. For the W mass, the current World average, and for M_{top} the present CDF central value are taken for definiteness. The theoretical predictions are based on the results of Ref. [19] and incorporate the effects of higher order electroweak and QCD corrections to $\Delta\rho$ and Δr.

reduction in the error of $\alpha(M_Z)$ of up to a factor 2. For the anticipated precision in $\delta\alpha(M_Z)$, M_W and M_{top}, the Higgs boson mass can be predicted with an accuracy of approximately

$$M_H \; {}^{+(f-1)M_H}_{-(1-f^{-1})M_H} \tag{4.5}$$

with $f \approx 1.5$ [20]. This is illustrated in Fig. 4.5 which shows the theoretical expectations for the W mass versus the Higgs boson mass for $M_{top} = 176.0 \pm 2.0$ GeV/c^2. A W mass measurement of $M_W = 80.260 \pm 0.030$ GeV/c^2 would constrain the Higgs boson mass to $M_H = 685^{+355}_{-230}$ GeV/c^2. The corresponding log-likelihood function of the electroweak one-loop corrections to M_W is shown in Fig. 4.6. If the W mass can be determined with a precision of 20 MeV/c^2, a somewhat smaller error on the Higgs boson mass is obtained: $M_H = 685^{+245}_{-180}$ GeV/c^2. From Fig. 4.5 it is obvious that the Higgs boson mass obtained from a fit of the data to the SM electroweak radiative corrections depends very sensitively on the W boson mass. For example, from a measurement of $M_W = 80.330 \pm 0.020$ GeV/c^2, one would obtain $M_H = 285^{+105}_{-80}$ GeV/c^2.

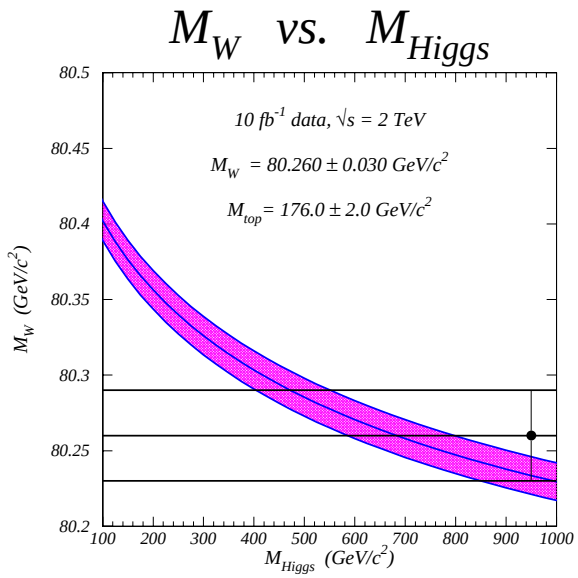

Figure 4.5: Predicted W versus Higgs boson mass for $M_{top} = 176.0 \pm 2.0$ GeV/c^2. The theoretical predictions are based on the results of Ref. [19] and incorporate the effects of higher order electroweak and QCD corrections to $\Delta\rho$ and Δr.

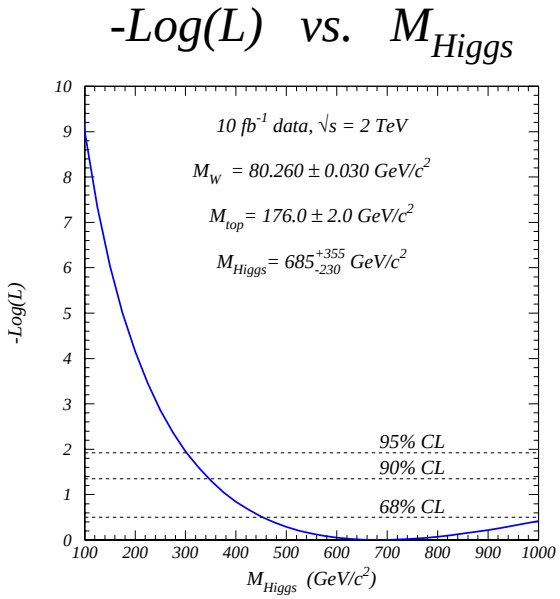

Figure 4.6: The negative log-likelihood function for $M_W = 80.260 \pm 0.030$ GeV/c^2 and $M_{top} = 176.0 \pm 2.0$ GeV/c^2. The theoretical predictions are based on the results of Ref. [19] and incorporate the effects of higher order electroweak and QCD corrections to $\Delta\rho$ and Δr.

Table 4.3: Expected experimental uncertainties (per experiment) on , $_W$ from a fit to the W transverse mass distribution in the electron channel at the Tevatron.

Δ, $_W$	$\int \mathcal{L}dt = 1$ fb^{-1}, $I_C = 3$	$\int \mathcal{L}dt = 10$ fb^{-1}, $I_C = 9$
statistical	40 MeV	13 MeV
background	8 MeV	5 MeV
$p_T(W)$	17 MeV	8 MeV
energy scale	6 MeV	3 MeV
electron energy resolution	10 MeV	8 MeV
$\not\!\!E_T$ resolution	14 MeV	8 MeV
total	48 MeV	20 MeV

4.2.5 W Width and Branching Fraction Measurements

An important cross-check of our understanding of electroweak radiative corrections is provided by a measurement of the W leptonic branching ratio $B(W \to \ell\nu)$, $\ell = e, \mu$, and the total W width, , $_W$. Deviations from the SM predictions would signal the presence of new decay modes of the W boson. If the new states involved couple predominantly to quarks with a coupling constant much smaller than α_s, such particles are difficult to detect in other measured quantities such as the di-jet invariant mass distribution.

The total width of the W boson can be measured directly from the tail of the M_T^W distribution [22]. $B(W \to \ell\nu)$ can be extracted from the cross section ratio

$$R_{W/Z} = \frac{\sigma_W \cdot B(W \to \ell\nu)}{\sigma_Z \cdot B(Z \to \ell^+\ell^-)} \ , \tag{4.6}$$

using the theoretical production cross section ratio $\sigma(p\bar{p} \to W)/\sigma(p\bar{p} \to Z)$ and the LEP measurement of the branching ratio $B(Z \to \ell^+\ell^-)$. Assuming that the partial decay width , $(W \to \ell\nu)$ is given by the SM, the measured cross section ratio $R_{W/Z}$ can then be turned into a second, independent, determination of , $_W$ [23]. Presently, the uncertainty on the W width is about 85 MeV per experiment from the measurement of the cross section ratio [23], and 324 MeV from the direct determination using the transverse mass distribution [22].

The projected experimental uncertainties (per experiment) for , $_W$ from a fit to the W transverse mass distribution in the electron channel, are summarized in Table 4.3 for integrated luminosities of 1 fb^{-1} and 10 fb^{-1}. A similar precision is expected to be achieved in the muon channel. For 10 fb^{-1}, the overall accuracy of 10 MeV which one hopes to reach combining the electron and muon channels, and measurements from CDF and DØ, approaches the level of the electroweak radiative corrections to , $_W$ [24].

With $\int \mathcal{L}dt = 10$ fb^{-1}, the expected precision for the cross section ratio $R_{W/Z}$ measured

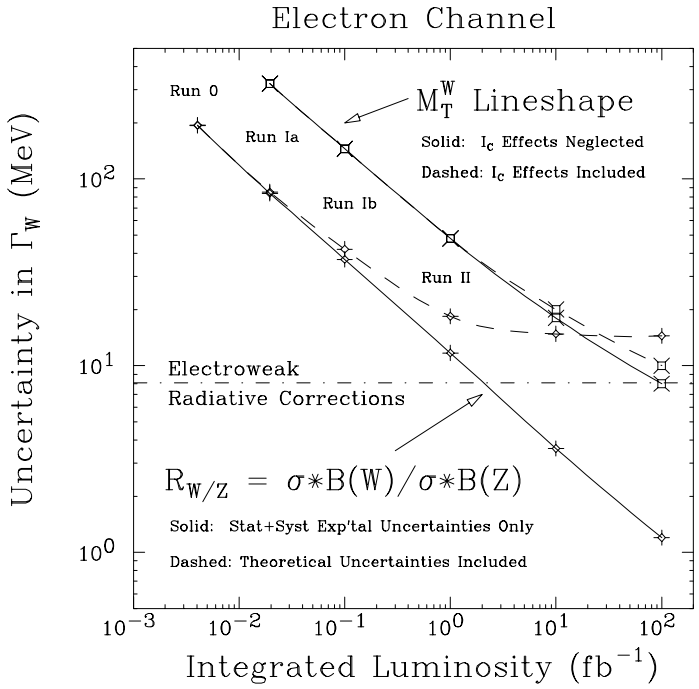

Figure 4.7: Projected uncertainty in , $_W$ versus the integrated luminosity. The dot dashed line gives the absolute magnitude of the electroweak radiative corrections in the SM [24].

in the electron channel is,

$$\Delta R_{W/Z} = \pm 0.013 \text{ (stat.)} \pm 0.012 \text{ (exp. syst.)} \tag{4.7}$$

which corresponds to an error in $B(W \to e\nu)$ of $\pm 1.8 \cdot 10^{-4}$. This translates into a direct experimental uncertainty of Δ, $_W = \pm 3.4$ MeV, which is substantially better than what is expected from the direct measurement from the M_T^W spectrum. Unfortunately, the current theoretical error on the W/Z production cross section ratio,

$$\frac{\sigma(p\bar{p} \to W)}{\sigma(p\bar{p} \to Z)} = 3.358 \pm 0.020 \tag{4.8}$$

adds a systematic error of $\Delta B(W \to e\nu) \approx 7.5 \cdot 10^{-4}$, or Δ, $_W|_{\text{syst.}} \approx 12$ MeV (the uncertainties from , $(W \to \ell\nu)$ [theoretical] and $B(Z \to \ell^+\ell^-)$ [LEP] are negligible compared to the error from $\sigma(p\bar{p} \to W)/\sigma(p\bar{p} \to Z)$). The error on the production cross section ratio in Eq. (4.8) arises from uncertainties in the parton distributions, the value of α_s, and higher order QCD corrections.

The expected precision for , $_W$ in the electron channel (per experiment) versus the integrated luminosity is shown in Fig. 4.7. Effects from multiple interactions are seen to only marginally influence the W width measurement. For the current theoretical error from the production cross section ratio, the W width measurement from $R_{W/Z}$ rapidly loses its power for integrated luminosities above 1 fb^{-1}, and for $\int \mathcal{L} dt > 20$ fb^{-1} the direct measurement

from the M_T^W lineshape yields better results. Thus, in order to realize the full potential of the W width measurement from $R_{W/Z}$, the theoretical error on the production cross section ratio has to be reduced.

At LEP II, , $_W$ can only be measured with a precision of about 400 MeV [25]. No studies for the LHC exist at this time.

Since the production cross section ratio in Eq. (4.8) is sensitive to the parton distributions, $R_{W/Z}$ can in principle be used to discriminate between sets of parton distribution functions, if one assumes SM W and Z branching ratios. However, distributions which are sensitive to structure function effects, such as the triply differential di-jet distributions [26], or the same side – opposite side two jet ratio [27] contain more information than the single number resulting from a measurement of $R_{W/Z}$ and are therefore expected to yield better constraints on the parton distributions.

4.3 Weak Boson Asymmetries

Uncertainties in the parton distribution functions (PDF's) are one of the major contributions to the error in the current W mass measurement [7]. The W charge asymmetry,

$$A(\eta_\ell) = \frac{d\sigma(W^+)/d\eta_\ell - d\sigma(W^-)/d\eta_\ell}{d\sigma(W^+)/d\eta_\ell + d\sigma(W^-)/d\eta_\ell} \ . \tag{4.9}$$

is a sensitive probe of the difference between u and d quark distributions, in particular of the slope of the d/u ratio versus x [28] at $Q^2 = M_W^2$. Here, η_ℓ is the lepton pseudorapidity. The CDF measurement of $A(\eta_\ell)$ in Run 1a [29] has demonstrated that the W charge asymmetry indeed provides a strong constraint on the PDF's. Recent fits [30] use the CDF data as an input when extracting the PDF's.

With very large integrated luminosities, $A(\eta_\ell)$ will be a very powerful discriminator between different sets of PDF's. In Fig. 4.8a, the W charge asymmetry is shown for two sets of parton distribution functions, together with the statistical uncertainties expected for 100 pb^{-1} (MRSD–'), and 2 fb^{-1} (CTEQ2M). The $\sqrt{(\chi^2)}$ for CTEQ2M versus MRSD–' distributions, which is an estimate of the discriminating power of the W charge asymmetry between different sets of structure functions, is shown in Fig. 4.8b for the two integrated luminosities as a function of the maximum lepton rapidity. In order to fully utilize the sensitivity of the W charge asymmetry to the PDF's, a lepton pseudorapidity coverage out to $|\eta^\ell|_{\rm max} = 2.0$ is necessary. With an integrated luminosity of 100 pb^{-1} (2 fb^{-1}), a measurement with a significance of about 10σ (50σ) can be made. However, this does not mean that the uncertainty in M_W originating from the PDF's can be reduced by $\sqrt{(\chi^2)}$. $A(\eta_\ell)$ does not fully determine the parton distribution functions. For a complete determination it has to be supplemented by measurements of other quantities sensitive to the PDF's.

Since the lepton rapidity is not a singular quantity in W production, one naively expects that the NLO and the resummed calculations predict the same $A(\eta_\ell)$ distributions. However, once realistic lepton and $\not\!\!E_T$ identification cuts are imposed, this is no longer true [10]. In a high precision measurement of PDF's from the W charge asymmetry it will be necessary to take these effects into account, as well as electroweak corrections.

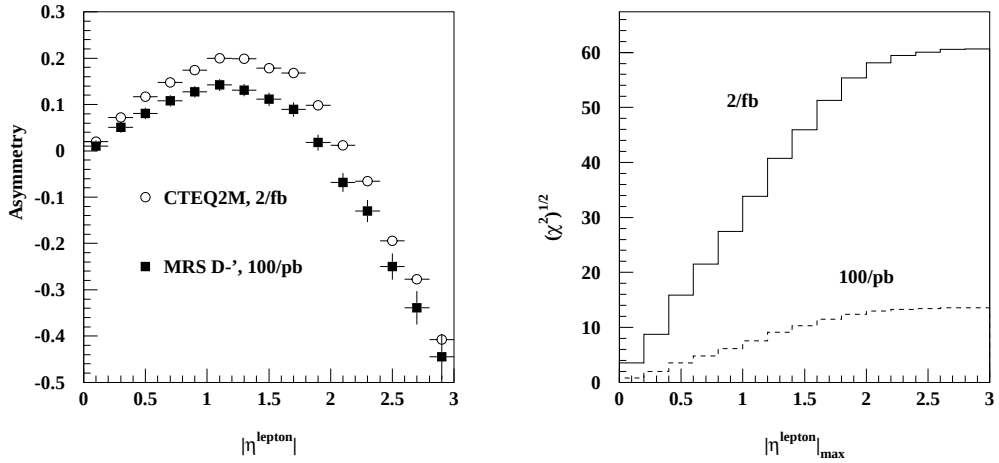

Figure 4.8: a) The predicted lepton charge asymmetry for W decays as a function of the lepton pseudorapidity. The error bars indicate the statistical uncertainty expected for 100 pb^{-1} and 2 fb^{-1}. b) The significance, $\sqrt{(\chi^2)}$, which results from a comparison of the MRSD–' and CTEQ2M sets of parton distributions, as a function of the pseudorapidity coverage of the detector.

The forward-backward asymmetry, A_{FB}, in $p\bar{p} \to \ell^+\ell^-$ events arises from the parton level process $q\bar{q} \to \ell^+\ell^-$. This asymmetry depends on the vector and axial vector couplings of the quarks and leptons to the Z and is therefore sensitive to $\sin^2\theta^{lept}_{eff}$. The current combined error on $\sin^2\theta^{lept}_{eff}$ from asymmetry measurements [1] at LEP and SLC is 0.00028.

The SM tree level prediction [31] for A_{FB} as a function of $m(e^+e^-)$ for $q\bar{q} \to \ e^+e^-$ is displayed in Fig. 4.9a for u and d quarks. The largest asymmetries occur at parton center-of-mass energies of around 70 GeV and above 110 GeV. The forward backward asymmetry as a function of the e^+e^- final state invariant mass in $p\bar{p} \to e^+e^-$ at the Tevatron is shown in Fig. 4.9b. The error bars indicate the statistical errors for 100,000 events, corresponding to an integrated luminosity of about 2 fb^{-1}. A preliminary study of the systematic errors, such as higher order electroweak corrections, indicates that most sources of error are small compared with the statistical error. The main contribution to the systematic error originates from unknown $\mathcal{O}(\alpha^3)$ corrections and the uncertainty in the parton distribution functions – since the vector and axial vector couplings of u and d quarks to the Z are different, the measured asymmetry depends on the ratio of u to d quarks in the proton. Most of the systematic errors are expected to scale with $1/\sqrt{N}$, where N is the number of events. Using the rather conservative systematic errors of the existing CDF analysis of data taken in the 1988-89 run [32], we estimate the combined statistical and systematic error from the forward-backward asymmetry in the electron channel (per experiment) on $\sin^2\theta^{lept}_{eff}$ to be

$$\pm 0.001 \text{ for } 1 \text{ fb}^{-1}, \tag{4.10}$$

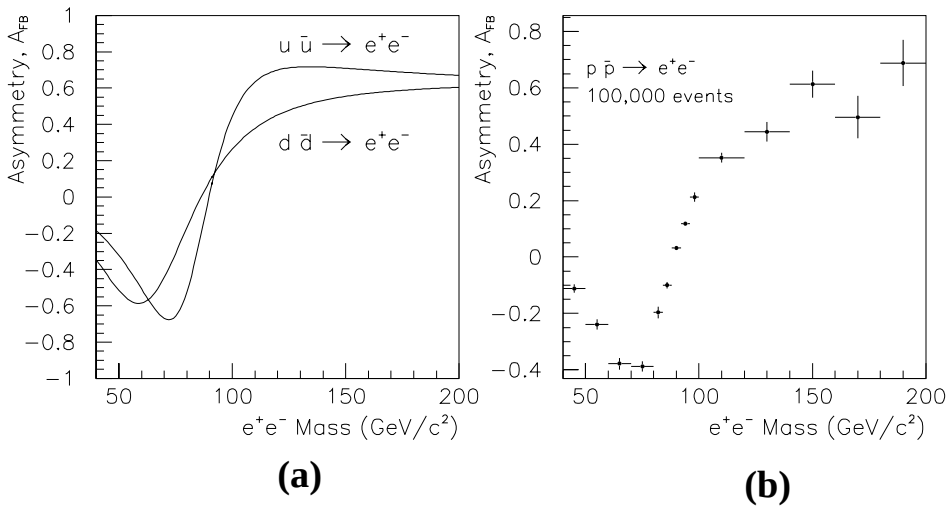

Figure 4.9: Forward-backward asymmetry as a function of e^+e^- invariant mass. (a) Standard Model tree level prediction for $u\bar{u} \rightarrow\ e^+e^-$ and $d\bar{d} \rightarrow\ e^+e^-$; (b) Simulation of $p\bar{p} \rightarrow\ e^+e^-$ showing statistical errors for approximately 2 fb^{-1}.

$$\pm 0.00032 \text{ for } 10 \text{ fb}^{-1}, \tag{4.11}$$

and

$$\pm 0.00010 \text{ for } 100 \text{ fb}^{-1}. \tag{4.12}$$

It is found that most of the sensitivity of this measurement to $\sin^2\theta^{lept}_{eff}$ is at $m(e^+e^-) \approx m_Z$ due to the strong variation of A_{FB} with $\sin^2\theta^{lept}_{eff}$ and the high statistics in this region. The expected precision of $\sin^2\theta^{lept}_{eff}$ in the electron channel (per experiment) versus the integrated luminosity is shown in Fig. 4.10, together with the combined current uncertainty from LEP and SLC experiments. A similar precision is expected in the muon channel.

Analogous to the W mass, a very high precision measurement of $\sin^2\theta^{lept}_{eff}$ can be used to extract information on the Higgs boson mass [33]. This becomes clear from Fig. 4.11 which shows the theoretical expectation for $\sin^2\theta^{lept}_{eff}$ as a function of the Higgs boson mass together with the precision expected for 10 fb^{-1} in the electron channel. Here we have assumed $M_{top} = 176 \pm 2$ GeV/c^2, an uncertainty of $\delta\alpha(M_Z) = 0.0004$ (see Section 2.4) and that the current central value of $\sin^2\theta^{lept}_{eff} = 0.23143$ [1] will not change. As we have mentioned above, the precision which can be achieved for $\sin^2\theta^{lept}_{eff}$ is expected to be dominated by the statistical uncertainty. Combining the results of the electron and the muon channel, an overall uncertainty of 0.00023 for $\sin^2\theta^{lept}_{eff}$ is expected. A measurement of $\sin^2\theta^{lept}_{eff} = 0.23143 \pm 0.00023$ would constrain the Higgs boson mass to $M_H = 415^{+225}_{-150}$ GeV/c^2.

The Higgs boson mass can thus be extracted with comparable accuracy from M_W and $\sin^2\theta^{lept}_{eff}$ for an integrated luminosity of 10 fb^{-1}. While the determination of A_{FB} is in principle straightforward, the W mass measurement involves a number of unknown effects, like

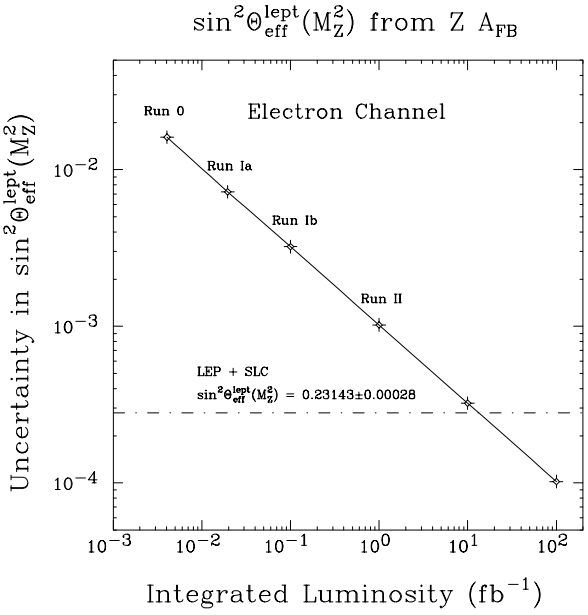

Figure 4.10: Projected uncertainty in $\sin^2\theta^{lept}_{eff}$ versus the integrated luminosity.

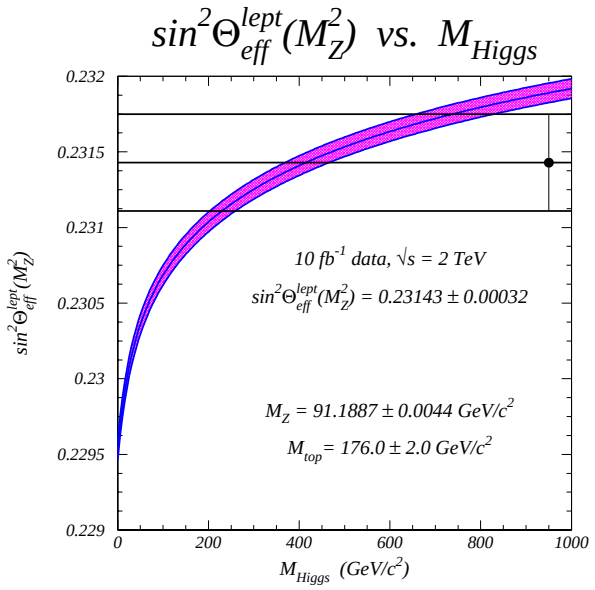

Figure 4.11: Predicted $\sin^2\theta^{lept}_{eff}$ versus the Higgs boson mass for $M_{top} = 176.0 \pm 2.0$ GeV/c^2. The theoretical predictions are based on the results of Ref. [19] and incorporate the effects of higher order electroweak and QCD corrections to $\Delta\rho$ and Δr.

pile-up effects. A measurement of $\sin^2\theta^{lept}_{eff}$, therefore, provides additional useful information on the Higgs boson mass. Since the systematic errors are very different for A_{FB} and the W mass measurement, it is straightforward to extract the expected precision on M_H from the combined measurement of the two variables. We find that $M_W = 80.260 \pm 0.030$ GeV/c^2 and $\sin^2\theta^{lept}_{eff} = 0.23143 \pm 0.00023$ yield $M_H = 540^{+185}_{-140}$ GeV/c^2, *i.e.* the Higgs boson mass can be determined with an overall precision of $\sim 30\%$.

At the LHC, with 100 fb^{-1}, a statistical error of $\delta \sin^2\theta^{lept}_{eff} = 6 \cdot 10^{-5}$ is expected [33], using the $Z \to \mu^+\mu^-$ decay channel. However, in contrast to the Tevatron, the initial state is charge symmetric (pp collisions), which makes it more difficult to determine the forward backward asymmetry.

4.4 Determination of α_s from the Z Boson p_T Distribution

Measurements of the coupling strength of the strong interaction, α_s, and of its energy dependence are key issues in probing the SM. At present, a large number of α_s measurements from e^+e^- annihilation, from deep inelastic scattering, hadron colliders and from heavy quarkonia exists [34]. The energies covered range from the τ lepton mass to the Z boson mass. While the results from low and high energy data overall are consistent with each other, the value of $\alpha_s(M_Z)$ extracted from low energy data is approximately 2σ lower than that found from data collected at high energies [34]:

$$\alpha_s(M_Z) = \quad 0.1140 \pm 0.0032 \quad \text{at low energies,} \tag{4.13}$$

$$\alpha_s(M_Z) = \quad 0.1212 \pm 0.0034 \quad \text{at high energies.} \tag{4.14}$$

Future experiments at the Tevatron offer an excellent opportunity to perform precision measurements of the strong coupling constant. In inclusive jet production, α_s can be extracted over a broad range of momentum transfers [35], whereas the Z boson transverse momentum distribution offer a possibility to measure $\alpha_s(M_Z)$ directly. The Z boson transverse momentum can be reconstructed entirely from the four momentum vectors of the Z decay leptons. Consequently, the systematic errors are significantly smaller than in jet measurements, and the $p_T(Z)$ distribution is an ideal candidate quantity for measuring $\alpha_s(M_Z)$ [36].

Determining α_s at a hadron collider differs significantly from measuring it at LEP. At a hadron collider, cross sections depend on the PDF's which themselves are associated with $\alpha_s(M_Z)$ as an input parameter. In order to extract the strong coupling constant from future Tevatron experiments, one therefore needs parton distribution functions where α_s can be varied. Fits to the PDF's with variable α_s have recently become available [37].

In the simulations carried out, modified versions of the CTEQ2 and CTEQ3 structure functions with variable α_s have been used. The Z boson p_T distribution was calculated using the results of Ref. [38] in the region $p_T(Z) > 40$ GeV, where the perturbative result accurately describes the data [39]. The factorization and normalization scale in the calculation were chosen to be equal to the Z boson mass. Using the CTEQ3M set, which corresponds to $\alpha_s(M_Z) = 0.112$, as a reference set, we show in Fig. 4.12 the relative change in the integrated

cross section above a minimum Z boson transverse momentum, $q_{T\min}$, as a function of $q_{T\min}$ for a variety of values for α_s. From Fig. 4.12a one observes that the Z boson transverse momentum distribution is primarily sensitive to values of $\alpha_s(M_Z) < 0.112$. For values of $q_{T\min}$ between 40 GeV and 60 GeV, the relative change in the cross section varies only slightly with $q_{T\min}$. The theoretical uncertainties originating from the choice of the renormalization scale are much smaller than those from varying α_s. For $\alpha_s(M_Z) < 0.112$, the Z boson cross section is falling with the strong coupling constant, as expected from the parton level cross section formula. For $\alpha_s(M_Z) > 0.112$, on the other hand, the situation is more complicated. In this region the shape change in the PDF's for the CTEQ3 parameterization partly compensates the increase from the parton level cross section. In the CTEQ3 fit, the shape parameter is one of those variables which are determined from the fit to the data.

The shape change of the PDF's with the strong coupling constant depends rather sensitively on which parameterization is used. This is illustrated in Fig. 4.12b where the relative change of the cross section is shown for CTEQ2 parton distribution functions. Varying the parton distribution functions for constant α_s produces a relative change of the cross section similar to that of varying $\alpha_s(M_Z)$ from 0.107 to 0.120.

The inclusive $Z \to e^+e^-$, $\mu^+\mu^-$ production cross section for Z boson transverse momenta larger than 50 GeV is approximately 13 pb. For integrated luminosities of 1 fb^{-1} or more, the cross section, therefore, can be measured with a statistical error smaller than 1%. The systematic errors are expected to be dominated by the luminosity uncertainty ($\sim 3.6\%$) [40], the lepton energy scale ($\sim 1\%$), the lepton energy resolution ($\sim 1\%$), and the uncertainty of the angular resolutions. The luminosity uncertainty, which currently dominates, may be reduced substantially in the future by using the $W \to e\nu$ and $Z \to e^+e^-$ cross sections to determine the integrated luminosity. Alternatively, the cross section ratio $\sigma_Z(q_T > q_{T\min})/\sigma_Z$, where σ_Z is the total Z boson cross section can be used. The luminosity uncertainty cancels in the cross section ratio. The precision which can be achieved for $\alpha_s(M_Z)$ will then crucially depend on how well the parton distribution functions can be determined in other experiments.

4.5 Rare W and Z Decays

With the copious number of leptonic W and Z decays to be collected in future Tevatron experiments, one can begin to look for rare W and Z decays. The number of $Z \to e^+e^-$, $\mu^+\mu^-$ events expected at the Tevatron with 10 fb^{-1} is similar to that collected at LEP so far. Hence, one does not expect that the current limits on rare Z decays can be significantly improved in future Tevatron experiments, and we shall concentrate on rare W decays in the following. For a survey of rare Z decays we refer the reader to Ref. [41].

4.5.1 Theoretical Overview

W decays into a pseudoscalar meson and a photon, $W \to P\gamma$, and two pseudoscalar mesons, $W \to P_1P_2$, are particularly attractive. Decays into a pseudoscalar meson and a photon are sensitive to new physics which affects the $WW\gamma$ vertex. A search for $W \to P\gamma$ decays

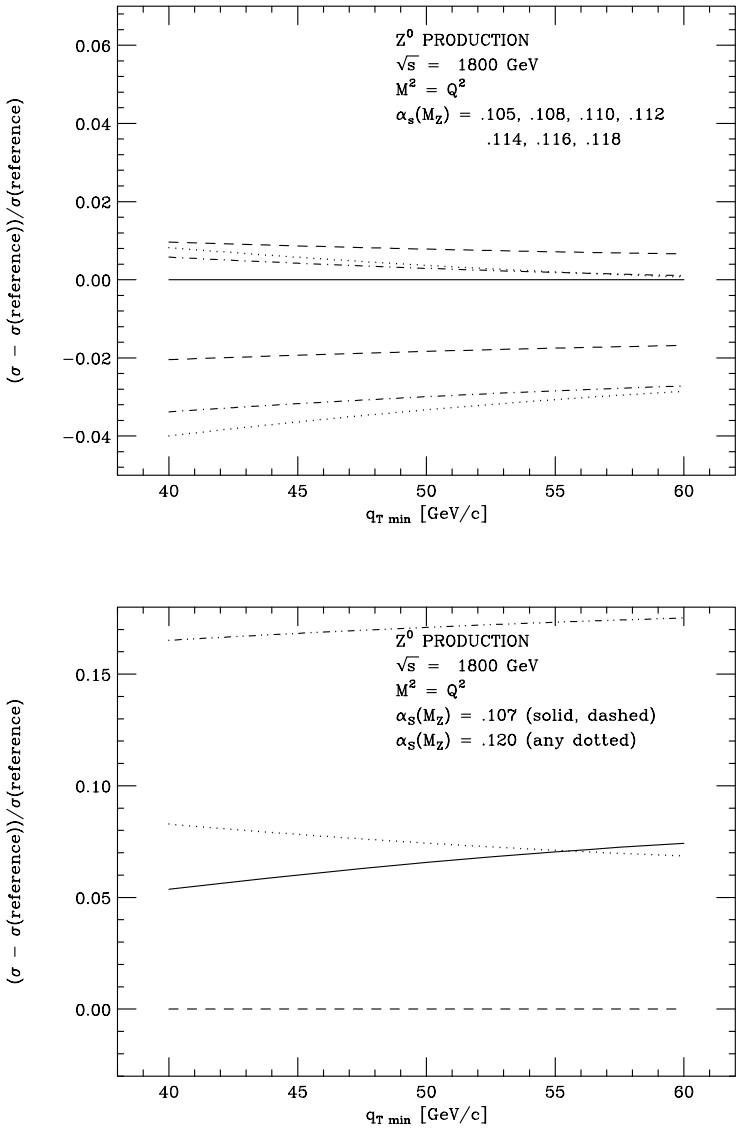

Figure 4.12: Relative change of the Z boson cross section above a minimum Z boson transverse momentum $q_{T\min}$, as a function of $q_{T\min}$. a) The solid line gives the result for the CTEQ3M set of parton distribution functions, which correspond to $\alpha_s(M_Z) = 0.112$. This set serves as a reference point. The upper (lower) dashed, dot-dashed and dotted lines correspond to $\alpha_s(M_Z) = 0.114$ (0.110), 0.116 (0.108), and 0.118 (0.105). b) The relative change of the Z boson cross section for CTEQ2 PDFs with the same shape parameters for $\alpha_s = 0.107$ (solid and dashed lines) and $\alpha_s = 0.120$ (dotted and dot-dashed lines).

thus complements the di-boson analysis described in detail in Section 7. On the other hand, $W \to P_1 P_2$ decays offer an opportunity to probe meson decay form factors at a very high momentum transfer where these form factors have not been tested so far. Currently, experimental results exist only for the decay $W \to \pi\gamma$ [42, 43].

The $W \to P\gamma$ decay rate can be expressed in terms of one vector and one axial vector form factor [44],

$$\frac{, (W \to P\gamma)}{, (W \to \ell\nu)} = \frac{1}{4}\alpha\pi|V_{ij}|^2 \left(|V_P(M_W^2)|^2 + |A_P(M_W^2)|^2\right) M_W^2 \left(1 - \frac{m_P^2}{M_W^2}\right)^3 . \tag{4.15}$$

Here, V_P and A_P are the vector and axial vector form factor, respectively, m_P is the mass of the pseudoscalar meson P, and V_{ij} is the relevant quark mixing matrix element.

In all cases of interest, the mass of the pseudoscalar meson is much smaller than the W mass. In this situation, the large momentum transfer behaviour of the vector form factor can be calculated from QCD [45]:

$$V_P(q^2) \;=\; -\frac{f_P}{q^2}\left(1 + \mathcal{O}(\alpha_s(q^2))\right) \qquad \text{for} \qquad q^2 \to \infty \tag{4.16}$$

where q^2 is the momentum transfer squared and f_P is the pseudoscalar decay constant. A detailed QCD analysis has not been carried out for the axial vector form factors so far. However, because the weak charged current is purely lefthanded, one expects that

$$\frac{A_P(q^2)}{V_P(q^2)} \to 1 \qquad \text{for} \qquad q^2 \to \infty. \tag{4.17}$$

The branching ratios for the $W \to P\gamma$ decays calculated from Eqs. (4.15) – (4.17) are listed in Table 4.4. Here we have used

$$f_\pi \;=\; 132 \text{ MeV}, \tag{4.18}$$

$$f_K \;=\; 158 \text{ MeV}, \tag{4.19}$$

$$f_D \;=\; 210 \text{ MeV}, \tag{4.20}$$

$$f_{D_s} \;=\; 230 \text{ MeV}, \tag{4.21}$$

$$f_B \;=\; 190 \text{ MeV}, \tag{4.22}$$

$$f_{B_c} \;=\; 500 \text{ MeV}. \tag{4.23}$$

The present theoretical uncertainties in the D, D_s and B decay constants are substantial, and experimental results indicate that the D_s decay constant could well be a factor 1.5 larger [46] than the value listed in Eq. (4.23). The value of f_{B_c} can rather accurately be predicted from potential models [47].

From Table 4.4 one observes that, in the SM, all $W \to P\gamma$ decays are expected to have very small branching ratios. The $W \to \pi\gamma$ and $W \to D_s\gamma$ modes are predicted to be the most prominent $W \to P\gamma$ decays. The CDF Collaboration has searched for $W \to \pi\gamma$ in the 1988-89 and 1992-93 run and established a limit of $BR(W \to \pi\gamma) < 2 \times 10^{-4}$ (95% CL) [42].

Table 4.4: Branching ratios of rare W decays in the SM. The branching ratios for decays into two pseudoscalars are obtained in the nearest pole model (see Eq. (4.24)) with $f_+^{\pi^+\pi^0}(0) = \sqrt{2}$, $f_+^{K\pi}(0) = 1.37$, and $f_+^{DK}(0) = 0.75$ (see Ref. [48]). In all other cases we use $f_+^{P_1P_2}(0) = 1$.

mode	br. ratio	mode	br. ratio
$W \to \pi\gamma$	$3.3 \cdot 10^{-9}$	$W \to \pi\pi$	$2.2 \cdot 10^{-10}$
$W \to K\gamma$	$2.4 \cdot 10^{-10}$	$W \to K\pi$	$2.0 \cdot 10^{-11}$
$W \to D\gamma$	$3.4 \cdot 10^{-10}$	$W \to D\pi$	$2.3 \cdot 10^{-10}$
$W \to D_s\gamma$	$1.0 \cdot 10^{-8}$	$W \to DK$	$4.1 \cdot 10^{-9}$
$W \to B\gamma$	$7.1 \cdot 10^{-14}$	$W \to B\pi$	$3.6 \cdot 10^{-12}$
$W \to B_c\gamma$	$7.7 \cdot 10^{-11}$	$W \to BD$	$1.2 \cdot 10^{-9}$

The rate for the decay of a W boson into two pseudoscalar mesons P_1 and P_2 can be expressed in terms of the $P_1 \to P_2\ell\nu$ decay form factor $f_+^{P_1P_2}(q^2)$, where P_1 is the heavier of the two pseudoscalar mesons. Assuming $m_{P_1},\ m_{P_2} \ll M_W$, one finds:

$$, (W \to P_1P_2) = \frac{G_F}{\sqrt{2}}\ \frac{M_W^3}{48\pi}\ |V_{ij}|^2\ \left|f_+^{P_1P_2}(M_W^2)\right|^2 . \tag{4.24}$$

In order to derive a numerical value for $, (W \to P_1P_2)$, one needs to know $f_+^{P_1P_2}(M_W^2)$. Presently, a QCD calculation of these form factors is not available and one has to rely on a simple model to make quantitative predictions. The available data from $P_1 \to P_2\ell\nu$ decays [46, 48] are consistent with a simple nearest pole model of the form

$$f_+^{P_1P_2}(q^2) = f_+^{P_1P_2}(0)\ \frac{m_V^2}{m_V^2 - q^2} \tag{4.25}$$

where m_V is the mass of the nearest vector meson with the appropriate quantum numbers (m_ρ for $f_+^{\pi^+\pi^0}$, m_{K^*} for $f_+^{K\pi}$, m_{D^*} for $f_+^{D\pi}$, $m_{D_s^*}$ for f_+^{DK}, m_{B^*} for $f_+^{B\pi}$, and $m_{B_c^*}$ for f_+^{BD}). The branching ratios obtained with this ansatz are also listed in Table 4.4.

However, in $P_1 \to P_2\ell\nu$ the form factors are only measured for small momentum transfers of a few GeV^2 at most, which results in large uncertainties when they are extrapolated to $q^2 = M_W^2$. At small momentum transfer, one expects rather large non-perturbative contributions to the weak decay form factors. The pole model may thus well overestimate the $W \to P_1P_2$ rates and in W decays, *i.e.* at high momentum transfer, these effects should be absent [49]. On the other hand, it is not excluded that the nearest pole model underestimates the $W \to P_1P_2$ decay rates.

In conclusion, the numerical results listed in Table 4.4 should only be used as guidance. Presently, no reliable calculation of weak decay form factors at high q^2 exists. A perturbative QCD calculation of these form factors similar to that of Ref. [45] is clearly warranted.

4.5.2 Experimental Aspects

Within the context of the SM, from an experimental perspective, integrated luminosities of 100 fb^{-1} (or more) will be required in order to have any hope of observing even the most promising of these rare decay modes of the W boson listed in Table 4.4. Observation of any of these decay modes in significant excess of their SM predictions would certainly be exciting, and could be interpreted as an indicator of new physics beyond the SM, or a complete inadequate understanding of meson decay form factors. As mentioned already, W decays into two pseudoscalar mesons offer an opportunity to probe meson decay form factors at very high momentum transfer where these form factors have not been probed before. Hence searches for these and other rare decay modes of both the W and the Z are important to carry out whenever the opportunity exists.

For the rare decay $W^{\pm} \to P^{\pm}\gamma$, where $P^{\pm}$ is a charged pseudoscalar meson, the dominant background at the Tevatron is due to photon + jet production, where the jet fragments to a single, leading charged particle, if $P^{\pm} = \pi^{\pm}$ or $K^{\pm}$, or fragments to a low charged multiplicity jet, if $P^{\pm} = D^{\pm}, D_s^{\pm}, B^{\pm}, B_c^{\pm}$. Although the photon + jet cross section is large, this background can be suppressed by the requirement of an isolated single high p_T charged track. Alternatively, a low multiplicity of isolated charged tracks, such that the invariant mass of photon+tracks is $\sim M_W$ can be required. In addition, the p_T distributions of both daughter particles from W decay display the characteristic shape of a Jacobian peak at $\sim M_W/2$, whereas the background is steeply falling with p_T.

The current 95% CL experimental upper limit on the branching ratio for $W^{\pm} \to \pi^{\pm}\gamma$ is $BR(W^{\pm} \to \pi^{\pm}\gamma) < 2 \times 10^{-4}$ from 16.7 pb^{-1} Run 1a CDF data [42]. The trigger for these events requires an isolated, high p_T photon in the central ($|\eta| < 1$) region of the detector. No requirement is made at the trigger level for an additional isolated high p_T track, as this is not necessary. The mass resolution for photon + single charged track, each with a transverse momentum of $\sim M_W/2 \sim 40$ GeV/c from W decay is excellent, $\Delta M_W \sim 1.7$ GeV/c^2 ($< , {}^{W}_{tot} \sim 2.1$ GeV). Hence the offline event selection required an isolated high p_T central photon and an isolated high transverse momentum central track within a ~ 4 GeV/c^2 mass window centered on M_W. This selection reduces the background from photon+jet processes dramatically. One candidate event is observed within the mass window with an estimated background of $2.6 \pm 1.0(stat) \pm 1.3(syst)$ events. The overall acceptance times efficiency for this W decay mode, for central photons and $\pi^{\pm}$ is $(6.0 \pm 0.2 \pm 0.7)\%$.

With greatly increased integrated luminosity, it will be difficult to maintain a good signal/background ratio without substantially diminishing the overall $W^{\pm} \to \pi^{\pm}\gamma$ detection efficiency by tightening up cuts used in the present analysis. Since the W boson has a natural width comparable to the size of the mass window used in the current analysis, narrowing the mass window will result only in a linear reduction in background, even if the mass resolution were substantially improved. Developing improved analysis methods for enhanced rejection of the single track background from the photon + jet "continuum" will be important if reductions in the experimental upper limit on this branching ratio are to be achieved.

An irreducible background to $W^{\pm} \to \pi^{\pm}\gamma$ originates from the weak decay $W \to q\bar{q}'$, where the q and $\bar{q}'$ jets fragment in such a way that a leading, single charged track from one jet mimics a $\pi^{\pm}$, and a leading π^0 (or η) from the other jet mimics a photon. In the present

CDF analysis, this background has been estimated to have an effective branching ratio of $BR(W \to q\bar{q}' \to \pi^{\pm} + \text{“}\gamma'') \sim 3 \times 10^{-8}$ (approximately one order of magnitude larger than the SM prediction for the $W^{\pm} \to \pi^{\pm}\gamma$ signal and about two orders of magnitude higher than the SM prediction for the true two-body $W^{\pm} \to \pi^{\pm}\pi^0$ process – *c.f.* Table 4.4).

If single track $W^{\pm} \to P^{\pm}\gamma$ decays are observed, it will be difficult to distinguish a $\pi^{\pm}$ with $p_T \sim 40$ GeV/c from a $K^{\pm}$. Good particle identification, which works well in this momentum region is required. However, from the SM prediction of the ratio of branching ratios, we expect

$$\frac{BR(W^{\pm} \to K^{\pm}\gamma)}{BR(W^{\pm} \to \pi^{\pm}\gamma)} \simeq \frac{f_K^2 \ |V_{us}|^2}{f_\pi^2 \ |V_{ud}|^2} \sim 0.07, \tag{4.26}$$

hence $W^{\pm} \to \pi^{\pm}\gamma$ is expected to dominate any observed photon + single track signal, within the context of the SM.

The rare W decays with single charged charm and/or B mesons in the final state have backgrounds from photon + charm (*e.g.* $gc \to \gamma c$; $q\bar{q} \to \gamma g,\ g \to c\bar{c}$) and photon + b (*e.g.* $gb \to \gamma b,\ b \to c + X$; $q\bar{q} \to \gamma g,\ g \to b\bar{b}$) where the charm or b-jet fragments to a leading single charged charm or B meson, respectively. At $\sqrt{\hat{s}} \sim M_W$, these cross sections are known to be substantially less than the photon + light-quark jet cross section. Note also that the SM prediction for $BR(W \to D_s\gamma)$ is the largest of this class of rare W decays.

The rare W decay modes $W \to D(B)\gamma$ are suppressed by the quark mixing matrix element relative to $W \to D_s(B_c)\gamma$. Focussing on the charmed meson rare W decay modes (since these have the most favorable SM predictions), the all-charged 3-body decay modes of the D and D_s charmed mesons have branching fractions of $BR(D^+ \to K^-\pi^+\pi^+) \sim 9.1\%$ and $BR(D_s^+ \to K^+K^-\pi^+) \sim 4.8\%$, respectively. Using these decay modes, a well-identified, isolated 3-prong secondary vertex requirement can be made using 3-D silicon microvertex information to reject light quark backgrounds, and suppress photon + charm and photon + b-jet backgrounds. An electromagnetic calorimeter isolation cut, centered on the axis of the 3 charged tracks, can be used to further suppress backgrounds with one or more π^0/η's. A hadron calorimeter isolation cut on the excess hadron energy can be used to additionally suppress backgrounds with one or more K_L^0 or neutrons present in the jet.

The mass resolution on the parent charmed particle, $\sigma_M/M \simeq 0.7\%$ is extremely good for all-charged 3-body decay modes. This is illustrated in Fig. 4.13 for the decay $D_s^+ \to K^+K^-\pi^+$. Smearing the transverse momenta of the daughter kaons and the pion according to the CDF p_T resolution, a mass resolution of $\sigma_{M_{D_s^+}} \simeq 13.5$ MeV/c^2 is found. Cuts on a mass window, *e.g.* ± 15 MeV/c^2 wide centered on M_{D^+}, $M_{D_s^+}$ can be made to further reduce backgrounds. It would be extremely useful to have the ability to distinguish $\pi^{\pm}$ from $K^{\pm}$ for these decays. However, the typical momenta of daughter particles from 3-body decays of charged charmed mesons from W decay is $p_T \sim \frac{1}{3}\frac{M_W}{2} \sim 15$ GeV/c, which is very difficult to achieve for either dE/dX or time-of-flight measurements. Candidate events can be kept if an acceptable fit is found for either (or both) decay modes. The fraction of D^+ vs. D_s^+ can be determined via detailed MC simulations using kinematic information only, but can also be cross-checked via study of the proper decay-time distribution, since $\tau_{D^+} \simeq 1.06$ ps and

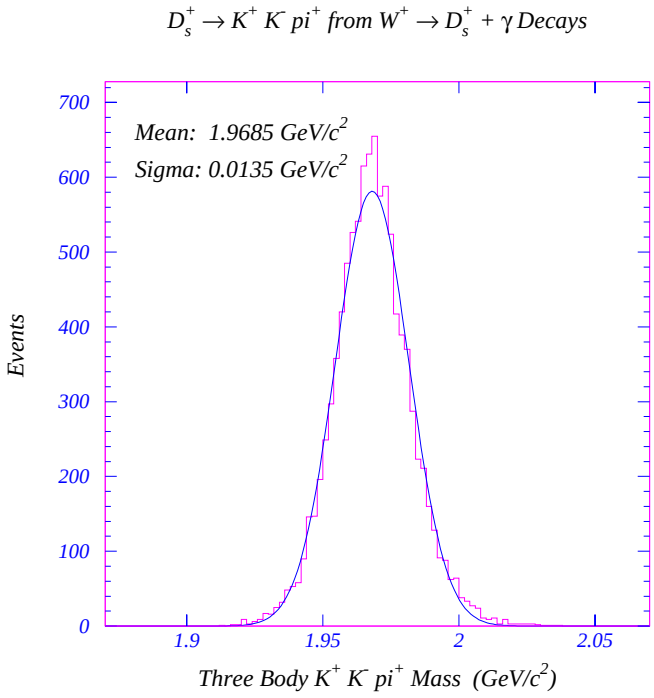

Figure 4.13: Invariant mass resolution for $D_s^+ \to K^+K^-\pi^+$ from $W^+ \to D_s^+\gamma$.

$\tau_{D_s^+} \simeq 0.47$ ps. Here again, we expect

$$\frac{BR(W^\pm \to D^\pm\gamma)}{BR(W^\pm \to D_s^\pm\gamma)} \simeq \frac{f_D^2\ |V_{cd}|^2}{f_{D_s}^2\ |V_{cs}|^2} \sim 0.034, \tag{4.27}$$

hence $W^\pm \to D_s^\pm\gamma$ is expected to dominate. Experimentally, with a 10 fb^{-1} data sample, 95% CL upper limits of $BR(W^\pm \to D^\pm\gamma) < 10^{-5}$ and $BR(W^\pm \to D_s^\pm\gamma) < 2 \times 10^{-5}$ could be achieved.

The decays $W \to K^\pm\pi^0/K^0\pi^\pm$ are Cabbibo-suppressed relative to $W \to \pi^\pm\pi^0$. As we have mentioned above, the light quark background from the weak decay $W \to q\bar{q}'$ has been estimated to be approximately two orders of magnitude higher than the $W \to \pi\pi$ rate with current analysis techniques. It is not clear whether this two-body class of true rare W decays can ever be observed over this background. There is some optimism for improving the signal to background ratio. Whether or not it can be improved by two or more orders of magnitude remains to be demonstrated, and will certainly be a challenge! If it can, then with a 10 fb^{-1} data sample, 95% CL upper limits of $BR(W^\pm \to \pi^\pm\pi^0) < 10^{-7}$ and $BR(W^\pm \to K^\pm\pi^0) < 2 \times 10^{-5}$ could be achieved.

Note however, that if the effective branching ratio $BR(W \to q\bar{q}' \to \pi^\pm + \text{“}\gamma'') \sim 3 \times 10^{-8}$ is actually this high, then this becomes an intriguing way in and of itself to potentially measure the W boson mass (and width) – *i.e.* force the jet fragmentation from $W \to q\bar{q}'$ decays into the low charged track multiplicity region for both jets, use only the track momenta

and electromagnetic calorimeter information associated with the jet (which is well-measured) to compute M_{jj} on an event-by-event basis. The trigger used for capturing such events to tape is essentially a di-tau trigger.

There is somewhat greater hope for observing the rare decays $W^+ \to D^0 K^+$ and $W^+ \to D^+ K^0_L / K^0_S$. The D^0 meson has branching fractions to all-charged decay modes of $BR(D^0 \to K^- \pi^+) \simeq 4.0\%$ and $BR(D^0 \to K^- \pi^+ \pi^+ \pi^-) \simeq 8.1\%$. Again, the dominant background here will be due to photon + charm and photon + B jet production. Event selection cuts very similar to those used for $W^+ \to D^+ (D^+_s) \gamma$ are equally useful here for D^0 selection, in terms of rejecting/suppressing background. For the $D^0 K^+$ decay mode, a requirement of an isolated high p_T track is used for the K^+. Experimentally, with a 10 fb^{-1} data sample, a 95% CL upper limit of $BR(W^+ \to D^0 K^+) < 6 \times 10^{-6}$ could be achieved.

For the $W^+ \to D^+ K^0_L$ mode, the K^0_L is so long-lived that it is only detected via its shower, nearly entirely in the hadron calorimeter. Unfortunately, the resolution of typical hadron calorimeters is significantly worse than that for electromagnetic calorimeter. Hence the resolution on the W mass for this particular decay mode is $\sigma_M / M \sim 12\%$, requiring a larger W mass window of at least ± 10 GeV/c^2 centered on M_W, which correspondingly lets in significantly more background. Experimentally, with a 10^{-1} fb data sample, a 95% CL upper limit of $BR(W^+ \to D^+ K^0_L) < 8 \times 10^{-5}$ could be achieved.

For the $W^+ \to D^+ K^0_S$ mode, the K^0_S decays $\sim 69\%$ of the time to $\pi^+ \pi^-$. The typical decay length for a K^0_S from $W^+ \to D^+ K^0_S$ decay is $L_{K^0_S} = \gamma \beta c \tau \simeq 215$ cm. Hence the $K^0_S \to \pi^+ \pi^-$ and overall $W^+ \to D^+ K^0_s$ reconstruction efficiency will be exceedingly small, due to the relatively long lifetime of the K^0_S meson.

In summary, the experimental sensitivities for rare W decays and 10 fb^{-1} are expected to be at least two orders of magnitude away from the branching ratios estimated in the SM. However, since the SM estimates are quite uncertain, a continued and extended search for $W \to P \gamma$ and $W \to P_1 P_2$ decays will yield useful information on our understanding of decay form factors in the high momentum transfer regime.

4.6 Searching for CP Violation in W Production and Decay

4.6.1 Preliminaries

The origin of CP violation remains one of the unsolved questions in particle physics. It is therefore imperative to search for signals of CP violation in all experimentally accessible processes. The Tevatron offers a unique opportunity to search for CP violation in W boson production and decay because it collides protons and antiprotons, *i.e.* the initial state is a CP eigenstate. The extremely large number of W boson events expected at a superluminous Tevatron will make it possible to look for small CP violating contributions to W boson production. CP violating effects can affect W production in various different ways. CP nonconservation in parton distribution functions, or at higher twist, is one possibility. In this case one would expect that other processes such as inclusive jet production also possess a CP violating component. Here we shall concentrate on CP violation in the Wqq' and

$W\ell\nu$ vertices. Our discussion closely follows that of Ref. [4], which complements Refs. [50] and [51].

Kaon, charm and B-decay decay experiments tell us that CP violating effects in the SM are extremely small. In addition, CP odd observables in the SM vanish in the limit of massless fermions. The SM does not produce a sufficiently large CP odd signal to be observed with the number of W boson events anticipated at the Tevatron with 10 fb^{-1} [52]. Popular extensions of the SM in the context of CP violation include multi-Higgs boson models. In these models, CP violation is also proportional to fermion masses and thus negligible in the processes we are interested in. We shall, therefore, assume that studies of CP violation in W production at hadron colliders will only be sensitive to non-SM sources. To parameterize possible CP violating operators, we shall use an effective Lagrangian approach. The operators are assumed to originate from the mechanism which breaks the electroweak symmetry.

4.6.2 $p\bar{p} \to W^{\pm}X \to \ell^{\pm}\nu X$

Under a CP transformation, the lepton rapidities and transverse momenta transform as

$$y_{\ell^-} \overset{CP}{\longleftrightarrow} -y_{\ell^+}, \quad p_{T\ell^-} \overset{CP}{\longleftrightarrow} p_{T\ell^+}. \tag{4.28}$$

In terms of these variables the simplest CP-odd observables which can be constructed are the asymmetries:

$$\begin{aligned}
\tilde{R}_1 &\equiv \frac{\sigma^+ - \sigma^-}{\sigma^+ + \sigma^-} \\
\tilde{R}_2(y_0) &\equiv \frac{\frac{d\sigma^+}{dy_\ell}\,|_{y_\ell=y_0} - \frac{d\sigma^-}{dy_\ell}\,|_{y_\ell=-y_0}}{\frac{d\sigma^+}{dy_\ell}\,|_{y_\ell=y_0} + \frac{d\sigma^-}{dy_\ell}\,|_{y_\ell=-y_0}} \\
\tilde{R}_3(p_T) &\equiv \frac{\frac{d\sigma^+}{dp_T} - \frac{d\sigma^-}{dp_T}}{\frac{d\sigma^+}{dp_T} + \frac{d\sigma^-}{dp_T}},
\end{aligned} \tag{4.29}$$

where $\sigma^{\pm}$ refers to $\sigma(p\bar{p} \to \ell^{\pm}\nu X)$.

If the p and $\bar{p}$ beams are unpolarized, and the polarization of the final state lepton is not measured, it is necessary to have an absorptive phase, ϕ, in order to generate the CP odd observables in Eq. (4.29). In the following we consider the CP violating four-fermion operator

$$\mathcal{L}_{CP} = \frac{4\pi}{\Lambda^2} e^{i\phi} \overline{c}_L \gamma_\mu s_L \overline{\ell}_L \gamma^\mu \nu_L + \text{ h. c.} \tag{4.30}$$

where Λ is the scale of new physics. We consider the operator Eq. (4.30), instead of a similar one with $\bar{u}d$ quarks for two reasons. First, for the operator with $\bar{u}d$ there is a cancellation between two contributions to $p\bar{p} \to \ell^{\pm}\nu$ as discussed in Ref. [50]. This cancellation is exact for the resonant process studied here, but it does not occur for the operator with $\overline{c}s$ of Eq. (4.30). Furthermore, while there are several indirect constraints from low energy experiments on the operator with $\bar{u}d$ [50], analogous constraints on the operator in Eq. (4.30) depend on naturalness assumptions.

In the narrow W width approximation, the operator of Eq. (4.30) results in

$$\tilde{R}_1 = \tilde{R}_2(y_0) = \tilde{R}_3(p_T) \approx -\frac{1}{3}\frac{M_W^2}{\Lambda^2}\sin\phi \tag{4.31}$$

for the CP violating asymmetries. In order to observe a signal at the one-standard deviation level, the number of W boson events, N, for integrated asymmetries is required to be greater than

$$N > \frac{1}{\tilde{R}_1^2} \approx 200,000\left(\frac{\Lambda}{1\ \text{TeV}}\right)^4 \frac{1}{\sin^2\phi}\ . \tag{4.32}$$

For the W event sample expected at the Tevatron for 10 fb^{-1}, it should in principle be possible to observe CP violation coming from new physics at the TeV scale.

4.6.3 $p\bar{p} \to W^\pm + 1$ jet $\to \ell^\pm\nu + 1$ jet

In this process there are several parton subprocesses that contribute at leading order in α_s and there are enough independent four-vectors to give rise to T-odd correlations. The interest of these correlations lies in the fact that they can generate CP odd observables without requiring additional absorptive phases and thus may test different types of CP violating physics than the asymmetries of Eq. (4.29).

For the $W + 1$ jet process there is one T-odd correlation that can be observed; in the laboratory frame it is given by the triple product $\vec{p}_\ell \cdot (\vec{p}_{\text{beam}} \times \vec{p}_{\text{jet}})$. There are several equivalent ways to use this correlation to construct a T-odd observable. The basic idea is to define the plane formed by the beam and jet momenta and count the number of events with the lepton above the plane minus the number of events with the lepton below the plane:

$$A^\pm = \sigma^\pm[(\vec{p}_{\text{beam}} \times \vec{p}_{\text{jet}}) \cdot \vec{p}_\ell > 0] - \sigma^\pm[(\vec{p}_{\text{beam}} \times \vec{p}_{\text{jet}}) \cdot \vec{p}_\ell < 0]. \tag{4.33}$$

Here, $A^\pm$ refers to the observable for $W^\pm$ events (or $\ell^\pm\nu$ events). A practical way to implement this observable in the calculation (or in the experiment) is to weigh the matrix element squared for a parton subprocess (or to weigh the observed event) by the sign of $\vec{p}_\ell \cdot (\vec{p}_{\text{beam}} \times \vec{p}_{\text{jet}})$. Invariance under a CP transformation predicts that $A^+ = A^-$.

To use jet variables it is necessary to assume that the algorithm that defines the jet is CP blind in the sense that the probability of finding that a collection of particles with certain momenta forms a jet is the same as the probability of finding that a collection of the respective anti-particles with the momenta reversed forms a jet. No simulations have been carried out so far to verify this assumption.

Analogous to the observables of Eq. (4.29), it is useful to construct not only the fully integrated asymmetry, but asymmetries for distributions as well. One obvious reason is that the simultaneous study of the different distribution asymmetries provides a handle on the possible CP odd biases of a detector. Another reason is that it is possible for the integrated asymmetry to vanish while having non-vanishing asymmetries for distributions. Some T-odd CP odd observables are then:

$$R_1 \equiv \frac{A^+ - A^-}{\sigma^+ + \sigma^-}$$

$$R_2(y_0) \equiv \frac{\frac{dA^+}{dy}\mid_{y=y_0} - \frac{dA^-}{dy}\mid_{y=-y_0}}{\frac{d\sigma^+}{dy}\mid_{y=y_0} + \frac{d\sigma^-}{dy}\mid_{y=-y_0}}$$

$$R_3(p_T) \equiv \frac{\frac{dA^+}{dp_T} - \frac{dA^-}{dp_T}}{\frac{d\sigma^+}{dp_T} + \frac{d\sigma^-}{dp_T}}, \tag{4.34}$$

where y and p_T represent the rapidity and transverse momentum of the lepton or the jet (or the W).

CP violating triple product correlations of the form (4.33) require operators which depend on the momentum carried by the fermions in the $Wf\overline{f'}$ coupling such as

$$\mathcal{L} = -\frac{\sqrt{2}}{\Lambda^2}\left[\tilde{\kappa}\overline{\Psi}_L \overleftarrow{D}_\alpha \gamma_\mu \Sigma\tau_- \Sigma^\dagger \overrightarrow{D}^\alpha \Psi_L \Sigma_+^\mu + \tilde{\kappa}^\star \overline{\Psi}_L \overleftarrow{D}_\alpha \gamma_\mu \Sigma\tau_+ \Sigma^\dagger \overrightarrow{D}^\alpha \Psi_L \Sigma_-^\mu\right]. \tag{4.35}$$

In unitary gauge $\Sigma = 1$ and $\Sigma_\pm^\mu = -\frac{g}{2}W^{\mu\pm}$. For the processes of interest there is only one W boson and no Z bosons, so the covariant derivatives refer only to QED and QCD:

$$D_\alpha \Psi_L \rightarrow (\partial_\alpha + \frac{i}{2}g_S\lambda^a G_\alpha^a + ieQA_\alpha)\begin{pmatrix} u \\ d_\theta \end{pmatrix}_L. \tag{4.36}$$

The fully integrated asymmetry R_1 vanishes for the interaction of Eq. (4.35). The asymmetry in the electron rapidity distribution, $R_2(y_e)$, is shown in Fig. 4.14 for $Im\ \tilde{\kappa} = 1$ and $\Lambda = 1$ TeV. A transverse momentum cut of $p_{Tjet} > 30$ GeV, and a rapidity cut of $|y_{jet}| < 3$ are imposed on the jet. At the one standard deviation level some 10^6 $W^\pm$ plus one jet events are needed to observe this asymmetry. For 10 fb^{-1} one expects approximately $0.5 \cdot 10^6$ $W + 1$ jet events within the cuts listed above. Lowering the p_{Tjet} cut to, say, 15 GeV would result in a larger event sample. $R_2(y_e)$ depends only marginally on the jet transverse momentum threshold. If the background can be controlled at the level required (see Section 6.4) to observe CP-violating effects for the lower p_T threshold, it should be possible to observe $R_2(y_e)$ for the values of $\tilde{\kappa}$ and Λ chosen. It should be noted, however, that measuring this asymmetry for arbitrary values of y_e is complicated by the fact that the acceptance of the detector must be the same for y_e and $-y_e$. Figure 4.14 shows that the asymmetry does not necessarily vanish at $y_e = 0$, making this a particularly interesting point to search for CP violation.

4.6.4 Detector Requirements

In order to be sensitive to CP-violating effects at the 10^{-3} level and below in W boson production and decay, it is necessary to have a detector that is intrinsically "CP-symmetric" to better than the anticipated sensitivity level of CP violation, as was the case for each of the "classic" fixed target experiments that first discovered, and then measured CP violation in the neutral K-meson system.

For example, for a sample of $W \rightarrow e\nu$ events associated with an integrated luminosity of 10 (100) fb^{-1}, obtained with standard CDF/DØ lepton trigger and identification cuts, the statistical accuracy for integrated asymmetries is approximately 4×10^{-4} (1.25×10^{-4}). For

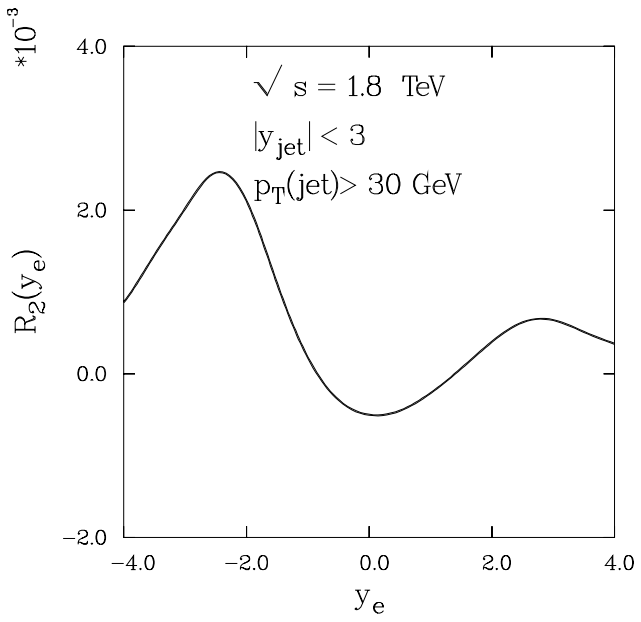

Figure 4.14: CP violating asymmetry in the lepton rapidity distributions as defined in Eq. (4.34) for $\Lambda = 1$ TeV and $Im\ \tilde{\kappa} = 1$. $R_2(y_e)$ scales as $Im\ \tilde{\kappa}/\Lambda^2$.

differential asymmetries, such as lepton rapidity binned in units of $\Delta y_e = 0.2$ the statistical accuracy per bin is $\sim 1.25 \times 10^{-3}$ (4×10^{-4}). A similar analysis for $W + 1$ jet events yields a statistical accuracy per bin of $\sim 5 \times 10^{-3}$ (1.6×10^{-3}) for $p_{Tjet} > 30$ GeV and $|y_{jet}| < 3$. This is shown in Fig. 4.15 for $\tilde{R}_2(y_e)$ in inclusive $W \to e\nu$ production with 10 fb^{-1}, and $R_2(y_e)$ for $W + 1$ jet, $W \to e\nu$, production with the p_T and rapidity cuts listed above. For $\tilde{R}_2(y_e)$ we also display the value expected from Eq. (4.31) for $\Lambda = 1$ TeV and $\sin\phi = 1$ (dashed horizontal line). Thus, all contributions from systematic effects – detector biases at the trigger level and offline analysis must be less than the above statistical uncertainties for integral and/or differential asymmetries.

There are numerous potential sources of detector bias which can in principle mimic a false CP-violating effect. Fortunately, most, if not all of these can be adequately dealt with in such types of analyses. While in principle the response of an electromagnetic calorimeter is identical to high p_T electrons and positrons at the trigger level and in offline analysis, dead, noisy or mis-calibrated calorimeter towers can introduce a CP-bias due to the intrinsic charge asymmetry in W production and decay. However, such effects are routinely monitored during data-taking, and can be properly taken into account. The relative response of the electromagnetic calorimeter is calibrated using high-statistics samples of inclusive electrons taken throughout the run. The absolute energy scale can be determined *e.g.* by fitting the lineshape of the E/p distribution from $W \to e\nu$ decay, cross-checking the E/p distribution for inclusive electrons versus positrons and W^+ versus W^- decays as a function of y_e, E_T^e, p_T^e and M_T^W, as well as e.g. studies of the E/p distribution for e^+ versus e^- from $Z \to e^+e^-$ production and decay. The absolute energy scale of the electromagnetic calorimeter can also be independently cross-checked using $Z \to e^+e^-$ data. Time-dependent effects on electromagnetic calorimeter gain calibrations can in principle be adequately accounted for via these methods.

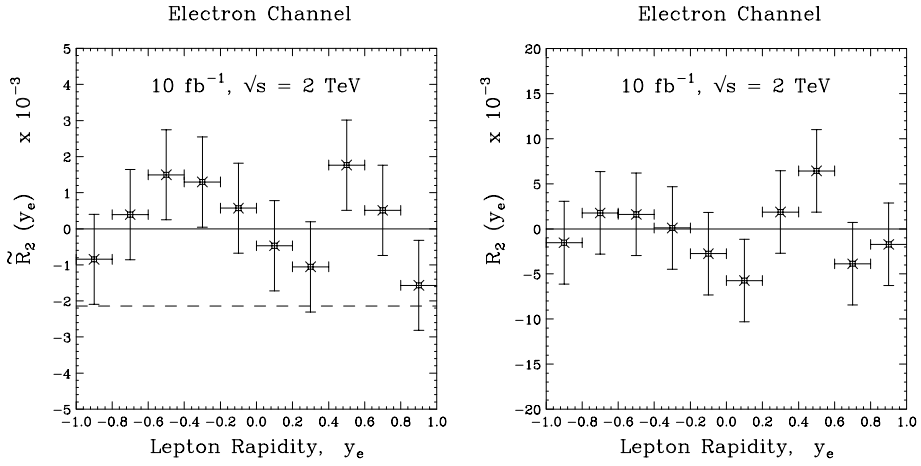

Figure 4.15: Statistical accuracy for 10 fb^{-1} of $\tilde{R}_2(y_e)$ for inclusive $W \to e\nu$ production, and $R_2(y_e)$ for $W+1$ jet, $W \to e\nu$, production with the p_T and rapidity cuts listed in the text, versus y_e . Also shown is what one expects for $\tilde{R}_2(y_e)$ from Eq. (4.31) for $\Lambda = 1$ TeV and $\sin\phi = 1$ (dashed horizontal line).

If the event vertex is not located at the symmetry point of the detector ($z = 0$), but is shifted away from this point, a CP-bias can arise. Again, the event vertex distribution is routinely monitored throughout the data-taking run and can be explicitly corrected for in the offline analysis. In principle, the best way to control this potential systematic effect is to ensure that the data being taken is properly located in z throughout the entire run.

The missing transverse energy, $\not\!\!E_T$, is calculated using the transverse energy of the electron as measured in the calorimeter and the transverse energy deposited in the calorimeter by the rest of the event excluding the electron, U. Assuming there is no manifest CP-bias associated with the E_T^e distribution, it is still possible to induce a false CP-effect if it originates with U. The transverse energy U associated with the underlying event is measured in the calorimeter, and is typically such that $U \ll E_T^e$. A CP-bias can arise in U *e.g.* from mis-calibration effects at low E_T in the two detector hemispheres, which can asymmetrically couple into W^+ versus W^- production due to the intrinsic charge asymmetry associated with W production and decay. Fortunately, it is again possible to monitor (and compensate) for such biases in U throughout the data-taking by using high-statistics samples of minimum bias data, and ensuring that the low E_T response of both the electromagnetic and hadron calorimeter towers of the detector are CP-symmetric to the required degree of accuracy. Note also that U is measured using all, or nearly all of the calorimeter rapidity coverage of the detector.

A false CP-violating U can potentially also be induced from higher-order QCD effects [53] associated with $W+$ jet production, due to a few-percent asymmetry in the jet angular distribution and mis-calibration of the calorimeters in the two detector hemispheres. Again, this potential bias can in principle be properly and fully accounted for, in a careful analysis.

For CP violation studies involving triple-product type tests using $W+$ jet data samples, *e.g.* for $p_{Tjet} > 30$ GeV, gain and efficiency variations across the hadronic calorimeter at this energy scale must also be known throughout the run, in addition to those for the electromagnetic calorimeter. High-statistics samples of minimum bias data, di-jet and/or photon+jet data can be used for accomplishing this task if one assumes that the data sample(s) used for such calibration(s) do not contain a manifestly CP-violating process, at least at a comparable level to that being searched for in the primary $W \to e\nu$ data sample.

An important and useful cross check on any observed CP-violating signal in the electron W data sample can be obtained by repeating the analysis using muon W data. The systematics associated with these two W decay channels are not identical. Electrons from W decay can be, and currently are, obtained using a calorimeter-only based trigger. They can be obtained as well as from an independent calorimeter + tracking trigger. Muons from W decay are obtained primarily using a tracking trigger. The $\not\!\!E_T$ is calculated using the transverse energy of the electron or muon track p_T^μ and the transverse energy associated with the underlying event, U. Verifying that the tracking devices in the experiment do not introduce a false CP-violating signal at the trigger and/or offline level also requires some degree of effort. Assuming no such effects to be present in J/ψ, Υ and $Z \to \ell^+\ell^-$ production and decay, these data samples, acquired simultaneously throughout the run can be used to search for, and place limits on tracking induced CP-biases. Since the number of Z boson events is approximately one order of magnitude smaller than the number of W candidates, the Z sample alone will not be able to place constraints on potential CP-biases at the level required for the W data.

Assuming that the results associated with the muon channel W data sample are compatible with those from the electron W data sample and that lepton universality holds in such CP violation searches, combining muon W data with electron W data results in an improvement by a factor of $\sqrt{2}$ in statistical sensitivity of the physics result.

Similarly, it is worthwhile to carry out searches for CP violation in W production and decay using tau W data samples. Even though tau W data samples historically have reduced statistical power, due to the reduction in $W \to \tau\nu$ trigger efficiency and offline analysis cuts relative to electron/muon W data, they still have sufficient statistical power, and quite different systematics to warrant studying them for such effects.

4.7 Di-boson Production and Anomalous Gauge Boson Couplings

4.7.1 Introduction

One of the most direct consequences of the $SU(2)_L \times U(1)_Y$ gauge symmetry are the non-abelian self-couplings of the W, Z and photon (WWV, $Z\gamma V$, $V = \gamma$, Z, $WW\gamma\gamma$ etc.). A direct measurement of the three vector boson couplings at the Tevatron is possible through the study of pair production processes like $q\bar{q} \to W^+W^-$, $W\gamma$, $Z\gamma$, WZ. Quartic couplings can be probed in multi weak boson production, such as $p\bar{p} \to W\gamma\gamma$, WWZ, etc. Here we shall concentrate on the measurement of the three gauge boson couplings.

Analogous to the introduction of arbitrary vector and axial vector couplings g_V and g_A for the coupling of gauge bosons to fermions, the measurement of the WWV couplings can be made quantitative by introducing a more general WWV vertex. For our discussion of experimental sensitivities below we shall use a parameterization in terms of the phenomenological effective Lagrangian [54]

$$\begin{aligned} i\mathcal{L}_{eff}^{WWV} &= g_{WWV}\left[g_1^V\left(W_{\mu\nu}^\dagger W^\mu - W^{\dagger\,\mu}W_{\mu\nu}\right)V^\nu + \kappa_V\, W_\mu^\dagger W_\nu V^{\mu\nu} + \right. \\ &\left. \frac{\lambda_V}{M_W^2}\, W_{\rho\mu}^\dagger W^{\mu}{}_{\nu} V^{\nu\rho} + i g_5^V \varepsilon_{\mu\nu\rho\sigma}\left((\partial^\rho W^{\dagger\,\mu})W^\nu - W^{\dagger\,\mu}(\partial^\rho W^\nu)\right)V^\sigma\right]. \end{aligned} \tag{4.37}$$

Here the overall couplings are defined as $g_{WW\gamma} = e$ and $g_{WWZ} = e\cot\theta_W$, $W_{\mu\nu} = \partial_\mu W_\nu - \partial_\nu W_\mu$, and $V_{\mu\nu} = \partial_\mu V_\nu - \partial_\nu V_\mu$. Within the SM, at tree level, the couplings are given by $g_1^Z = g_1^\gamma = \kappa_Z = \kappa_\gamma = 1$, $\lambda_Z = \lambda_\gamma = g_5^Z = g_5^\gamma = 0$. For on-shell photons, $g_1^\gamma = 1$ and $g_5^\gamma = 0$ are fixed by electromagnetic gauge invariance; g_1^Z and g_5^Z may, however, differ from their SM values. Deviations are given by the anomalous coupling parameters

$$\Delta g_1^Z \equiv (g_1^Z - 1)\ , \quad \Delta\kappa_\gamma \equiv (\kappa_\gamma - 1)\ , \quad \Delta\kappa_Z \equiv (\kappa_Z - 1)\ , \quad \lambda_\gamma\ , \quad \lambda_Z\ , \quad g_5^Z\ . \tag{4.38}$$

To simplify our discussion, we shall assume $g_5^Z = 0$ in the following. The effective Lagrangian of Eq. (4.37) parameterizes the most general Lorentz invariant and CP conserving WWV vertex which can be observed in processes where the vector bosons couple to effectively massless fermions. The C and P conserving terms in $\mathcal{L}_{eff}^{WW\gamma}$ correspond to the lowest order terms in a multipole expansion of the $W-$photon interactions, the charge Q_W, the magnetic dipole moment μ_W and the electric quadrupole moment q_W of the W^+ [55]:

$$Q_W = e g_1^\gamma\ , \tag{4.39}$$

$$\mu_W = \frac{e}{2M_W}\left(g_1^\gamma + \kappa_\gamma + \lambda_\gamma\right)\ , \tag{4.40}$$

$$q_W = -\frac{e}{M_W^2}\left(\kappa_\gamma - \lambda_\gamma\right)\ . \tag{4.41}$$

Analogous to the general WWV vertex it is possible to parameterize anomalous $Z\gamma V$, $V = \gamma, Z$ couplings. In the following, we shall be interested in constraints from $Z\gamma$ production processes, *i.e.* we may treat the photon and the Z as being on-shell. As before we are only considering CP-even couplings. Let us denote the Feynman rule for the $V_\mu(P) \to Z_\alpha(q_1)\gamma_\beta(q_2)$ vertex by $ie,{}_{Z\gamma V}^{\alpha\beta\mu}(q_1, q_2, P)$. The most general such vertex compatible with Lorentz invariance has been discussed in Ref. [54] and it can be parameterized in terms of two free parameters, h_3^V and h_4^V,

$$,{}_{Z\gamma V}^{\alpha\beta\mu}(q_1, q_2, P) = \frac{P^2 - M_V^2}{M_Z^2}\left[h_3^V\,\varepsilon^{\mu\alpha\beta\rho}q_{2\rho} + \frac{h_4^V}{M_Z^2}P^\alpha\varepsilon^{\mu\beta\rho\sigma}P_\rho q_{2\sigma}\right]. \tag{4.42}$$

Within the SM, at tree level, $h_3^V = h_4^V = 0$. The overall factor $P^2 - m_V^2$ in Eq. (4.42) is implied by Bose symmetry for on-shell V and/or by gauge invariance for $V = \gamma$.

Because of the subtle cancellations between the different processes for di-boson production in the Standard Model, any deviation of the couplings from their standard model

values will result in an increase in cross section. While the SM contributions to the di-boson production amplitudes are bounded from above for fixed scattering angles, the anomalous contributions rise without limit as the parton center of mass energy squared, $\hat{s}$, increases, eventually violating S-matrix unitarity. Anomalous couplings therefore must show a form factor behaviour at very high energies [56]. In our subsequent analysis we will assume a simple power law behaviour, *e.g.*

$$\Delta\kappa_V(\hat{s}) = \frac{\Delta\kappa_V^0}{(1+\hat{s}/\Lambda_{FF}^2)^n}\ , \tag{4.43}$$

and similarly for the other couplings. Here, Λ_{FF} is the form factor scale which is a function of the scale of new physics, Λ, which is responsible for the non-standard vector boson self-interactions. For WWV couplings we shall use the exponent $n = 2$, which will be referred to as the 'dipole form factor' below. For $Z\gamma V$ couplings we choose $n = 3$ ($n = 4$) for h_3^V (h_4^V). Due to the form factor behaviour of the anomalous couplings, the experimental limits extracted from hadron collider experiments explicitly depend on Λ_{FF}.

Information on anomalous WWV and $Z\gamma V$ couplings can be obtained by comparing the shape of measured and predicted distributions which reflect the high energy behaviour of the di-boson production amplitudes, such as the p_T distribution of the W, Z or photon.

4.7.2 Present Tevatron Limits

The CDF and DØ Collaborations have observed $W\gamma$ [57, 58, 59], $Z\gamma$ [59, 60, 61], W^+W^- [62, 63, 64], and WZ [62, 64] production in the data samples accumulated in Run 1a and 1b. Di-boson data samples are extracted from inclusive e/μ channel W/Z data. The main background for $W\gamma$ and $Z\gamma$ production is $W/Z+$ jet(s) production, where one of the jets fakes an isolated photon. In its $WW, WZ \to \ell\nu jj$ and $ZW \to \ell^+\ell^- jj$ analysis, CDF eliminates the $W/Z+$ jets background by requiring 60 GeV/c^2 $< m(jj) <$ 110 GeV/c^2 and $p_T(jj) >$ 130 (100) GeV/c [62]. This also eliminates the SM signal but retains good sensitivity for non-zero WWV anomalous couplings. DØ, in its WW, $WZ \to e\nu jj$ analysis, performs a fit to the $p_T(jj)$ distribution for $W+ \geq 2$ jet, $W \to e\nu$, events with 50 GeV/c^2 $< m(jj) <$ 110 GeV/c^2 [64]. The muon channel is not considered. In the $WW \to \ell_1\nu_1\ell_2\nu_2$, $\ell_{1,2} = e$, μ, channels, $\bar{t}t$ production constitutes the most significant background. It can be removed either through a jet veto, or a cut on the transverse energy of the hadrons in the event [63].

Direct experimental limits on $WW\gamma$ and $Z\gamma V$ anomalous couplings for the $W\gamma/Z\gamma$ processes are obtained via binned maximum likelihood fits to the $E_T(\gamma)$ distribution. Bounds from the $\ell\nu jj$ and $\ell^+\ell^- jj$ final states are extracted via comparison of observed events to the expected signal within cuts, including systematic uncertainties due to luminosity normalization, jet energy scale and resolution, structure function choice and higher order QCD corrections, *etc.* Limits on WWV anomalous couplings from the $WW \to \ell_1\nu_1\ell_2\nu_2$ mode have been derived via comparison of the 95% CL upper limit of $\sigma(WW)_{expt} < 87$ pb (DØ) with $\sigma(WW)_{pred}$ as a function of the anomalous couplings.

The limits obtained from $W^+W^- \to \ell_1\nu_1\ell_2\nu_2$ and WW, $WZ \to \ell\nu jj$ are summarized and compared to those obtained from $W\gamma$ production in Fig. 4.16a. In extracting limits on

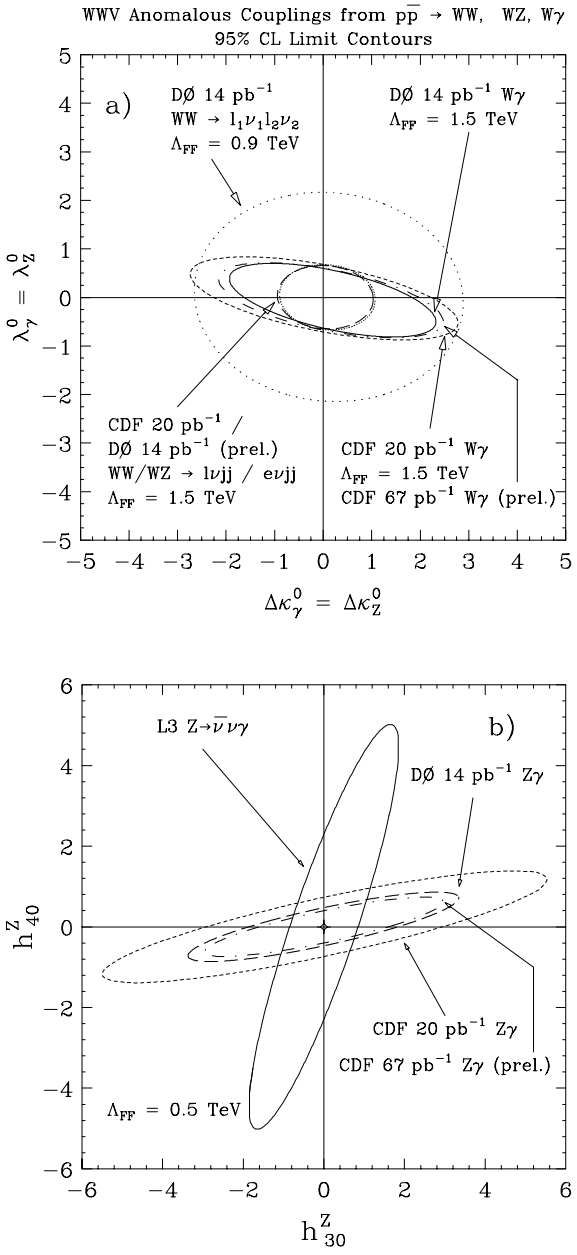

Figure 4.16: Present limits on anomalous WWV and $ZZ\gamma$ couplings from Tevatron and LEP experiments.

non-standard WWV couplings from W pair production, $\Delta\kappa_\gamma^0 = \Delta\kappa_Z^0$, $\lambda_\gamma^0 = \lambda_Z^0$, and $\Delta g_1^Z = 0$ have been assumed. The 95% CL limit contours from the current CDF $WW, WZ \to \ell\nu jj$ and DØ $WW, WZ \to e\nu jj$ searches are almost identical.

The current CDF [60] and DØ [61] 95% CL limit contours for anomalous $ZZ\gamma$ couplings are shown in Fig. 4.16b, together with the L3 constraint from $e^+e^- \to \bar{\nu}\nu\gamma$ [65]. In order to derive these limits, generalized dipole form factors with $\Lambda_{FF} = 0.5$ TeV, and powers $n = 3$ ($n = 4$) for h_3^V (h_4^V), are assumed. LEP and Tevatron experiments are seen to yield complementary information on $ZZ\gamma$ couplings. Since the anomalous contributions to the $Z\gamma$ helicity amplitudes grow faster with energy than those in $W\gamma$ production, the experimental limits on h_{30}^V and h_{40}^V depend rather sensitively on the form factor scale chosen. The maximum form factor scale which can be probed with present experimental data is $\Lambda_{FF} \approx 500$ GeV; for larger values S-matrix unitarity yields stronger bounds. The limit contours for $Z\gamma\gamma$ couplings obtained by CDF and DØ are similar to those shown in Fig. 4.16b for $ZZ\gamma$ couplings. Single photon production at LEP is very insensitive to $Z\gamma\gamma$ couplings.

Table 4.5 summarizes the current results on anomalous WWV and $Z\gamma V$ couplings from colliders. With the limited statistics of di-boson events currently available, deviations from the SM cross section have to be large at least in some regions of phase space in order to lead to an observable effect. The best direct limits on $\Delta\kappa_V^0$ are currently obtained from the $\ell\nu jj$ final state. $W\gamma$ production results in somewhat better bounds on λ_γ^0 than $p\bar{p} \to WW, WZ \to \ell\nu jj$. So far, no attempt has been made to combine the limits of CDF and DØ and/or from different channels.

4.7.3 Expectations for the Main Injector Era and Beyond

The substantial increase in integrated luminosity expected in the future will make it possible to test the WWV and $Z\gamma V$ vertices at the Tevatron with much greater precision than in current experiments. In Figs. 4.17 and 4.18 we show the 95% CL limits on anomalous $WW\gamma$ and $ZZ\gamma$ couplings expected from $W\gamma$ and $Z\gamma$ production at the Tevatron for high integrated luminosities. Here, and in all subsequent sensitivity plots, we assume that no deviation from the SM prediction is observed in future experiments. To derive bounds on non-standard WWV couplings, a dipole form factor is assumed. For the $Z\gamma V$ couplings we use form factor powers of $n = 3$ (h_3^V) and $n = 4$ (h_4^V). The limits on $Z\gamma\gamma$ couplings are very similar to those found for $ZZ\gamma$ couplings and are therefore not shown.

For $W\gamma$ production, the $W \to e\nu$ channel is analyzed. The electron is required to have $|\eta(e)| < 1.0$, and a pseudorapidity cut of $|\eta(\gamma)| < 2.4$ is imposed on the photon. The acceptances are calculated using the following transverse energy and separation cuts:

$$E_T(e) > 25 \text{ GeV}, \qquad \not\!\!E_T > 25 \text{ GeV}, \tag{4.44}$$

$$E_T(\gamma) > 10 \text{ GeV}, \qquad \Delta R(e,\gamma) > 0.7. \tag{4.45}$$

In addition, a cut on the transverse W mass of $m_T^W > 50$ GeV/c^2 and a cluster transverse mass cut of $m_T(e\gamma; \not\!\!E_T) > 90$ GeV/c^2 are imposed. The efficiencies for electron and photon identification were taken from the current CDF analysis, as well as the probability for a jet to fake a photon, $\mathcal{P}_{j\to\gamma}(E_T)$. The systematic uncertainty from the integrated luminosity,

Table 4.5: 95% CL limits on anomalous WWV, $V = \gamma$, Z, and $ZZ\gamma$ couplings from collider experiments. Only one of the independent couplings is allowed to deviate from the SM at a time. The bounds obtained by CDF and DØ for $Z\gamma\gamma$ couplings are very similar to those derived for the $ZZ\gamma$ couplings and are therefore not shown.

experiment	channel	limit
CDF (prel.) 67 pb^{-1}	$p\bar{p} \to W^{\pm}\gamma \to \ell^{\pm}\nu\gamma$ $\ell = e,\ \mu$	$-1.8 < \Delta\kappa_{\gamma}^{0} < 2.0$ $-0.7 < \lambda_{\gamma}^{0} < 0.6$
DØ 14 pb^{-1}	$p\bar{p} \to W^{\pm}\gamma \to \ell^{\pm}\nu\gamma$ $\ell = e,\ \mu$	$-1.6 < \Delta\kappa_{\gamma}^{0} < 1.8$ $-0.6 < \lambda_{\gamma}^{0} < 0.6$
CDF 20 pb^{-1}	$p\bar{p} \to W^{\pm}Z \to \ell^{+}\ell^{-}jj$ $\ell = e,\ \mu$	$-8.6 < \Delta\kappa_{Z}^{0} < 9.0$ $-1.7 < \lambda_{Z}^{0} < 1.7$
CDF 20 pb^{-1}	$p\bar{p} \to W^{+}W^{-},\ W^{\pm}Z \to \ell^{\pm}\nu jj$ $\ell = e,\ \mu,\ \kappa_{\gamma} = \kappa_{Z},\ \lambda_{\gamma} = \lambda_{Z}$	$-1.0 < \Delta\kappa_{V}^{0} < 1.0$ $-0.6 < \lambda_{V}^{0} < 0.7$
DØ (prel.) 14 pb^{-1}	$p\bar{p} \to W^{+}W^{-},\ W^{\pm}Z \to e^{\pm}\nu jj$ $\kappa_{\gamma} = \kappa_{Z},\ \lambda_{\gamma} = \lambda_{Z}$	$-0.9 < \Delta\kappa_{V}^{0} < 1.1$ $-0.7 < \lambda_{V}^{0} < 0.7$
DØ 14 pb^{-1}	$p\bar{p} \to W^{+}W^{-} \to \ell_1\nu_1\ell_2\nu_2$ $\ell_{1,2} = e,\ \mu,\ \kappa_{\gamma} = \kappa_{Z},\ \lambda_{\gamma} = \lambda_{Z}$	$-2.6 < \Delta\kappa_{V}^{0} < 2.8$ $-2.2 < \lambda_{V}^{0} < 2.2$
CDF (prel.) 67 pb^{-1}	$p\bar{p} \to Z\gamma \to \ell^{+}\ell^{-}\gamma$ $\ell = e,\ \mu,\ \Lambda_{FF} = 0.5$ TeV	$-1.6 < h_{30}^{Z} < 1.6$ $-0.4 < h_{40}^{Z} < 0.4$
DØ 14 pb^{-1}	$p\bar{p} \to Z\gamma \to \ell^{+}\ell^{-}\gamma$ $\ell = e,\ \mu,\ \Lambda_{FF} = 0.5$ TeV	$-1.9 < h_{30}^{Z} < 1.8$ $-0.5 < h_{40}^{Z} < 0.5$
L3	$e^{+}e^{-} \to Z \to \bar{\nu}\nu\gamma$ $\Lambda_{FF} = 0.5$ TeV	$-0.85 < h_{30}^{Z} < 0.85$ $-2.32 < h_{40}^{Z} < 2.32$

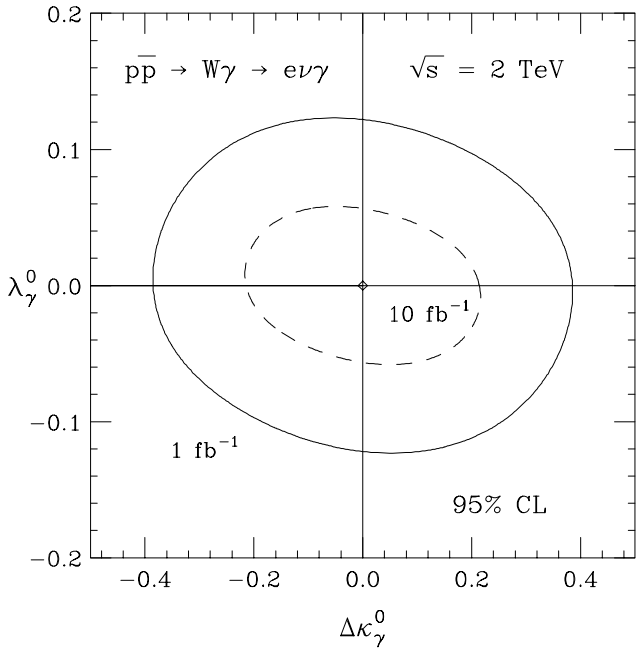

Figure 4.17: Projected 95% CL sensitivity limits for $WW\gamma$ couplings from $W\gamma$ production at the Tevatron for integrated luminosities of 1 fb^{-1} and 10 fb^{-1}.

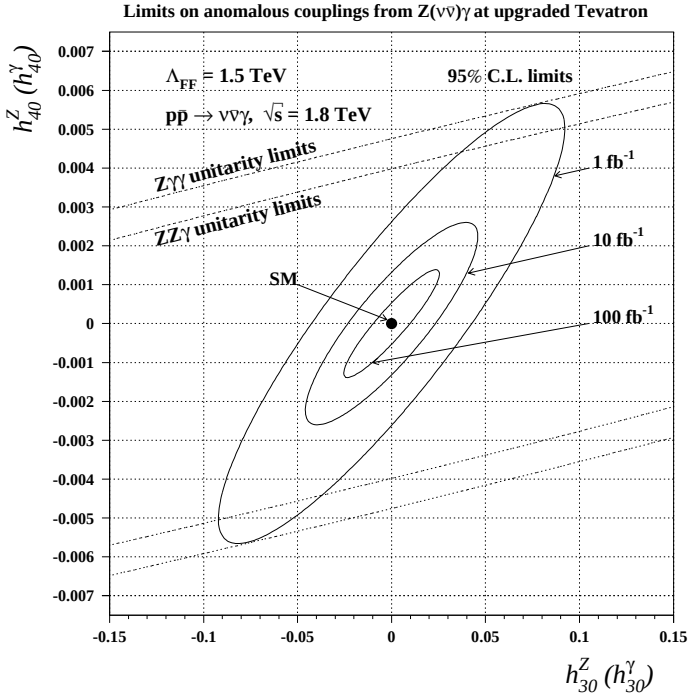

Figure 4.18: Projected 95% CL sensitivity limits for $Z\gamma V$ couplings from $Z\gamma$, $Z \to \bar{\nu}\nu$ production at the Tevatron for integrated luminosities of 1 fb^{-1}, 10 fb^{-1} and 100 fb^{-1}.

parton densities, and higher order QCD corrections was assumed to be 5%. From Fig. 4.17 one observes that the current limits on anomalous gauge boson couplings can be improved by about a factor 5 – 15 in $W\gamma$ production if an integrated luminosity of 10 fb^{-1} can be realized. Each additional factor 10 in integrated luminosity leads to roughly another factor 2 improvement in the sensitivities which can be achieved. Very similar results are obtained if DØ efficiencies and acceptances are used.

In Fig. 4.18 we show the limits on $Z\gamma V$ couplings expected from $p\bar{p} \to Z\gamma \to \bar{\nu}\nu\gamma$, together with the constraints from unitarity, for a form factor scale of 1.5 TeV. The projected experimental limits for $ZZ\gamma$ and $Z\gamma\gamma$ couplings are virtually identical. The signal consists of a single high p_T photon accompanied by a large amount of missing transverse energy. Compared to the charged lepton decay modes of the Z boson, the decay $Z \to \bar{\nu}\nu$ offers potential advantages. Due to the larger $Z \to \bar{\nu}\nu$ branching ratio, the differential cross section is about a factor 3 larger than that for $q\bar{q} \to e^+e^-\gamma$ and $q\bar{q} \to \mu^+\mu^-\gamma$ combined. Furthermore, final state bremsstrahlung and timelike virtual photon diagrams do not contribute to the $\bar{\nu}\nu\gamma$ final state. On the other hand, there are several potentially serious background processes which contribute to $p\bar{p} \to \gamma \not{p}_T$, but not to the $\ell^+\ell^-\gamma$, $\ell = e, \mu$ final state. The most important background processes are from $W \to e\nu$ where the electron fakes a photon, cosmic muons, prompt photon production, $p\bar{p} \to \gamma j$, with the jet rapidity outside the range covered by the detector and thus "faking" missing transverse momentum, and two jet production where one of the jets is misidentified as a photon while the other disappears through the beam hole. To eliminate these backgrounds [66] as well as beam halo effects, we impose an $E_T(\gamma)$, $\not{E}_T > 40$ GeV cut and require the photon to be central. From Fig. 4.18 one observes that the present limits on $Z\gamma V$ couplings from $Z\gamma$ production with $Z \to \ell^+\ell^-$ can be improved by a factor 50 – 200 (80 – 400) for an integrated luminosity of 1 fb^{-1} (10 fb^{-1}). The sensitivities expected from $Z\gamma$ production with $Z \to \ell^+\ell^-$, $\ell = e, \mu$, are about a factor 2 to 3 worse than those obtained from $\bar{\nu}\nu\gamma$ production [67] (see Table 4.6). If the center of mass energy of the Tevatron can be increased to 2 TeV, slightly better limits than those shown in Fig. 4.18 can be obtained.

To estimate the sensitivity of W^+W^-, $W^\pm Z \to \ell\nu jj$ and $WZ \to \ell^+\ell^- jj$, $\ell = e, \mu$, to non-standard WWV couplings in future Tevatron experiments, we require charged leptons to have $E_T > 20$ GeV and $|\eta(\ell)| < 2$, and impose a missing transverse energy cut of 20 GeV. The two leading jets are required to have $E_T(j) > 30$ GeV and 60 GeV/c^2 $< m(jj) <$ 110 GeV/c^2. Events containing an extra jet with $E_T > 50$ GeV are vetoed in order to suppress the top quark background and to reduce the effect of QCD corrections [68, 69]. To suppress the $W/Z+$ jets background, a cut on the transverse momentum of the jet pair is imposed, similar to the requirement in the current CDF analysis. The value of the $p_T(jj)$ cut varies with the integrated luminosity assumed:

$$p_T(jj) > 150 \text{ GeV/c} \qquad \text{for } \int \mathcal{L}dt = 100 \text{ pb}^{-1}, \tag{4.46}$$

$$p_T(jj) > 200 \text{ GeV/c} \qquad \text{for } \int \mathcal{L}dt = 1 \text{ fb}^{-1}, \tag{4.47}$$

$$p_T(jj) > 250 \text{ GeV/c} \qquad \text{for } \int \mathcal{L}dt = 10 \text{ fb}^{-1}. \tag{4.48}$$

The number of signal events expected is calculated using the event generator of Ref. [70].

The trigger and particle identification efficiencies are assumed to be the same as in the current CDF data analysis. To estimate the $t\bar{t}$ and $W/Z+$ jets background, ISAJET and VECBOS [71] are used. The top quark mass is taken to be $M_{top} = 170$ GeV/c^2.

Confidence levels are obtained by counting events above the $p_T(jj)$ cut. The resulting 95% CL contours at $\sqrt{s} = 1.8$ TeV for integrated luminosities of 100 pb^{-1}, 1 fb^{-1} and 10 fb^{-1} are shown in Fig. 4.19a. To calculate the sensitivity limits in Fig. 4.19a, we have assumed a form factor scale of $\Lambda_{FF} = 2$ TeV and the so-called "HISZ scenario" [67, 72], which reduces the number of independent WWV couplings from five to two. Choosing $\Delta\kappa_\gamma$ and λ_γ as independent parameters, the WWZ couplings are then given by:

$$\Delta g_1^Z = \frac{1}{2\cos^2\theta_W}\Delta\kappa_\gamma, \tag{4.49}$$

$$\Delta\kappa_Z = \frac{1}{2}(1-\tan^2\theta_W)\Delta\kappa_\gamma, \tag{4.50}$$

$$\lambda_Z = \lambda_\gamma. \tag{4.51}$$

The sensitivity limits depend only marginally on the value of Λ_{FF} assumed. For different relations between anomalous couplings, similar bounds are obtained. The limits shown in Fig. 4.19a can be improved by 20 – 40% if a fit to the shape of the $p_T(jj)$ distribution is performed.

With growing integrated luminosity, it is necessary to raise the $p_T(jj)$ cut to eliminate the $W/Z+$ jets background. For increasing values of $p_T(jj)$, more and more jets tend to coalesce. As a result, the two jet reconstruction efficiency drops rapidly for $p_T(jj) > 250$ GeV/c, and jet coalescing severely degrades the limits on anomalous WWV couplings which can be achieved for $\int\mathcal{L}dt \geq 10$ fb^{-1}. WW and WZ production with all leptonic decays therefore may be more potent than the semihadronic channels in constraining the WWV vertices at very high luminosities.

In contrast to the WW, $WZ \to \ell\nu jj$ and $\ell^+\ell^- jj$ channels, double leptonic WZ decays are relatively background free and thus provide an excellent testing ground for non-standard WWZ couplings. $WW \to \ell_1\nu_1\ell_2\nu_2$ final states are plagued by background from $t\bar{t}$ production, which, however, can be almost completely eliminated by either imposing a jet veto, or a cut on the hadronic transverse momentum in the event [63, 73]. Using recent calculations of $W^\pm Z$ and WW production which include NLO QCD corrections [69, 73], sensitivity limits for the $p\bar{p} \to W^\pm Z \to \ell_1^\pm\nu_1\ell_2^+\ell_2^-$, and $WW \to \ell_1^+\ell_2^-\not{p}_T$, $\ell_{1,2} = e, \mu$, channel were estimated. No full detector simulation was carried out, however, lepton identification cuts of $p_T(\ell_{1,2}) > 20$ GeV/c and $|\eta(\ell_{1,2})| < 2.5$, and a missing p_T cut of 20 GeV/c (30 GeV/c) for WZ (WW) production have been imposed to roughly simulate detector response. Particle momenta are smeared according to the resolution of the CDF detector. The 95% CL limit contours for $\sqrt{s} = 1.8$ TeV and $\Lambda_{FF} = 1$ TeV, obtained from a χ^2 fit to the $p_T(Z)$ distribution for WZ production, and the $p_T(\ell_1^+\ell_2^-)$ spectrum in the WW case, are displayed in Fig. 4.19b. Here we have again assumed the relations of Eqs. (4.49) – (4.51) for $WW\gamma$ and WWZ couplings. If the center of mass energy of the Tevatron can be increased to 2 TeV, slightly better limits can be obtained. WZ production is seen to result in somewhat better limits on $\Delta\kappa_\gamma^0$, whereas the $\ell_1^+\ell_2^-\not{p}_T$ final states are expected to yield more stringent

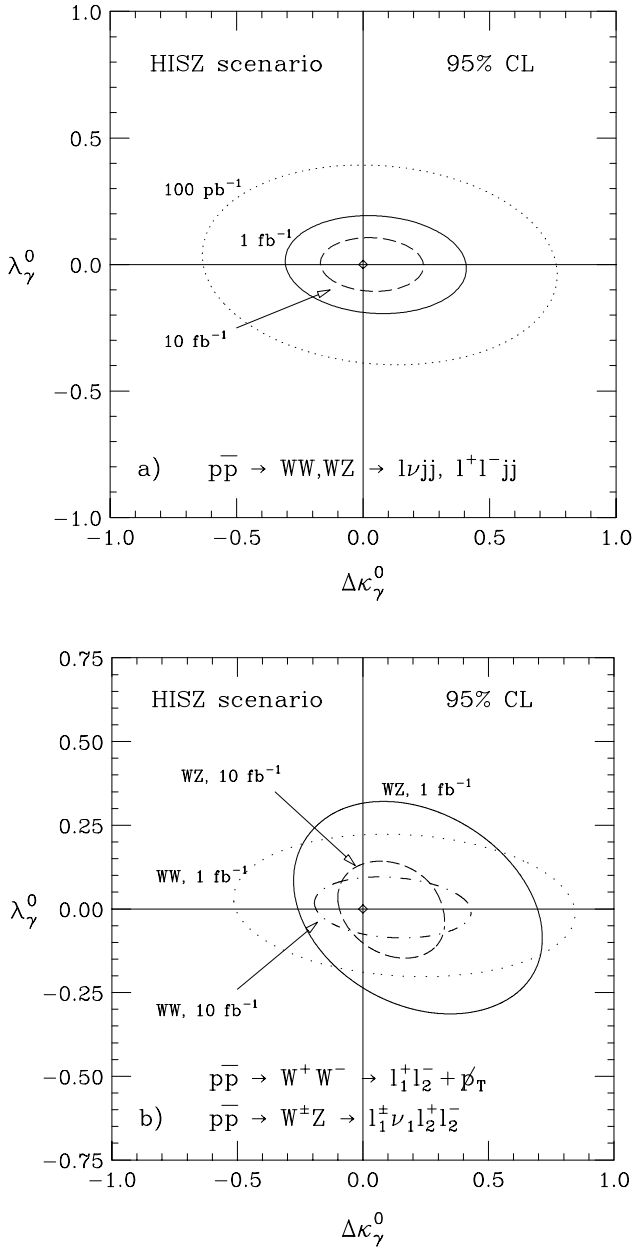

Figure 4.19: Expected 95% CL sensitivity limits for the WWV couplings in the HISZ scenario [see Eqs. (4.49) – (4.51)] a) from $p\bar{p} \to WW, WZ \to \ell\nu jj$ and $\ell^+\ell^- jj$, and b) from $p\bar{p} \to W^\pm Z \to \ell_1^\pm \nu_1 \ell_2^+ \ell_2^-$ and $p\bar{p} \to W^+W^- \to \ell_1^+ \ell_2^- \not{p}_T$ for 1 fb^{-1} and 10 fb^{-1}.

bounds on λ_γ^0. For $\int \mathcal{L} dt = 1$ fb^{-1}, the small number of all leptonic events (see Table 4.1) severely limits the sensitivity, and the limits obtained from $WW, WZ \to \ell\nu jj$ and $\ell^+\ell^- jj$ are significantly better than those from double leptonic WZ and WW decays for most of the parameter space. For 10 fb^{-1}, jet coalescing starts to negatively influence the semihadronic channels, and double leptonic and $WW, WZ \to \ell\nu jj$ and $\ell^+\ell^- jj$ final states yield comparable results. The contour limits shown in Figs. 4.17 and 4.19 depend only marginally on the form factor scale assumed; only the limits on the $Z\gamma V$ couplings are more sensitive to the value of Λ_{FF} chosen.

The expected sensitivity bounds from future Tevatron experiments, varying only one of the independent couplings at a time, are summarized in Table 4.6. In order to demonstrate that the bounds obtained in the HISZ scenario are indeed representative, we also list the limits for $W^\pm Z \to \ell_1^\pm \nu_1 \ell_2^+ \ell_2^-$ and $W^+W^- \to \ell_1^+ \nu_1 \ell_2^- \nu_2$ in the case where each of the WWZ couplings is varied separately, with all other WWV couplings assuming their SM values. Future experiments at the Tevatron can measure $\Delta\kappa_V$ and Δg_1^Z with a precision of about 0.1 – 0.2. λ_V can be determined to better than about 0.1 for $\int \mathcal{L} dt \geq 1$ fb^{-1}. The limits for $Z\gamma V$ couplings are of order $10^{-2} - 10^{-3}$. While $W\gamma$ production is seen to yield the best bounds at the Tevatron over a large fraction of the parameter space, it is clear that the limits obtained from the various processes are all of similar magnitude. Performing a global analysis of all di-boson production channels thus is expected to result in a significant improvement of the sensitivity bounds which can be achieved.

4.7.4 Comparison with LEP II and LHC

In Fig. 4.20 we compare the limits expected from $e^+e^- \to W^+W^- \to \ell\nu jj$, $p\bar{p} \to W^\pm\gamma \to e^\pm\nu\gamma$, $p\bar{p} \to W^\pm Z \to \ell_1^\pm \nu_1 \ell_2^+ \ell_2^-$ and $p\bar{p} \to WW, WZ \to \ell\nu jj$, $\ell^+\ell^- jj$ in the HISZ scenario [see Eqs. (4.49) – (4.51)] for the envisioned energies and integrated luminosities of the Tevatron and LEP II. The limits expected for $\Delta\kappa_\gamma$ are quite similar, whereas the Tevatron enjoys a clear advantage in constraining λ_γ, if correlations between the two couplings are taken into account. It should be noted, however, that the strategies to extract information on vector boson self-interactions at the two machines are very different. At the Tevatron one exploits the strong increase of the anomalous contributions to the helicity amplitudes with energy to derive limits. At LEP II, on the other hand, information is extracted from the angular distributions of the final state fermions. Data from the Tevatron and LEP II thus yield complementary information on the nature of the WWV couplings.

Because of the much higher energies accessible at the Tevatron and the steep increase of the anomalous contributions to the helicity amplitudes with energy, Tevatron experiments will be able to place significantly better limits (of $\mathcal{O}(10^{-2} - 10^{-3})$) on the $Z\gamma V$ couplings than LEP II (≈ 0.5) [67]. The Tevatron limits, however, do depend non-negligibly on the form factor scale assumed.

At the LHC, with 100 fb^{-1}, one expects to probe anomalous WWV couplings with a precision of $\mathcal{O}(10^{-1} - 10^{-3})$ if the form factor scale Λ_{FF} is larger than about 2 TeV [67]. For $\Delta\kappa_V$ (λ_V) the limits expected at the LHC are about a factor 3 (10) better than those projected for the Tevatron with 10 fb^{-1}. For $Z\gamma V$ couplings, the LHC will yield limits which are a factor 10 to 100 better than those one hopes to achieve at the Tevatron, depending on

Table 4.6: Expected 95% CL limits on anomalous WWV, $V = \gamma$, Z, and $ZZ\gamma$ couplings from future Tevatron experiments. Only one of the independent couplings is assumed to deviate from the SM at a time. The limits found for $Z\gamma\gamma$ couplings are very similar to those obtained for h_3^Z and h_4^Z.

channel	limit $\int \mathcal{L} dt = 1$ fb^{-1}	limit $\int \mathcal{L} dt = 10$ fb^{-1}
$p\bar{p} \to W^{\pm}\gamma \to e^{\pm}\nu\gamma$	$-0.38 < \Delta\kappa_\gamma^0 < 0.38$	$-0.21 < \Delta\kappa_\gamma^0 < 0.21$
$\sqrt{s} = 2$ TeV	$-0.12 < \lambda_\gamma^0 < 0.12$	$-0.057 < \lambda_\gamma^0 < 0.057$
$p\bar{p} \to W^+W^-$, $W^{\pm}Z \to \ell^{\pm}\nu jj$, $\ell^+\ell^- jj$	$-0.31 < \Delta\kappa_\gamma^0 < 0.41$	$-0.17 < \Delta\kappa_\gamma^0 < 0.24$
$\ell = e$, μ, HISZ scenario	$-0.19 < \lambda_\gamma^0 < 0.19$	$-0.10 < \lambda_\gamma^0 < 0.11$
$p\bar{p} \to W^{\pm}Z \to \ell_1^{\pm}\nu_1\ell_2^+\ell_2^-$	$-0.26 < \Delta\kappa_\gamma^0 < 0.70$	$-0.09 < \Delta\kappa_\gamma^0 < 0.32$
$\ell_{1,2} = e$, μ, HISZ scenario	$-0.24 < \lambda_\gamma^0 < 0.32$	$-0.10 < \lambda_\gamma^0 < 0.13$
$p\bar{p} \to W^{\pm}Z \to \ell_1^{\pm}\nu_1\ell_2^+\ell_2^-$	$-0.78 < \Delta\kappa_Z^0 < 1.68$	$-0.33 < \Delta\kappa_Z^0 < 0.96$
$\ell_{1,2} = e$, μ	$-0.24 < \lambda_Z^0 < 0.32$	$-0.10 < \lambda_Z^0 < 0.14$
	$-0.18 < \Delta g_1^{Z0} < 0.48$	$-0.06 < \Delta g_1^{Z0} < 0.22$
$p\bar{p} \to W^+W^- \to \ell_1^+\nu_1\ell_2^-\nu_2$	$-0.51 < \Delta\kappa_\gamma^0 < 0.84$	$-0.19 < \Delta\kappa_\gamma^0 < 0.43$
$\ell_{1,2} = e$, μ, HISZ scenario	$-0.19 < \lambda_\gamma^0 < 0.22$	$-0.075 < \lambda_\gamma^0 < 0.094$
$p\bar{p} \to W^+W^- \to \ell_1^+\nu_1\ell_2^-\nu_2$	$-0.44 < \Delta\kappa_Z^0 < 0.65$	$-0.17 < \Delta\kappa_Z^0 < 0.32$
$\ell_{1,2} = e$, μ	$-0.24 < \lambda_Z^0 < 0.28$	$-0.10 < \lambda_Z^0 < 0.13$
SM $WW\gamma$ couplings	$-1.03 < \Delta g_1^{Z0} < 1.62$	$-0.45 < \Delta g_1^{Z0} < 0.83$
$p\bar{p} \to Z\gamma \to e^+e^-\gamma$	$-0.105 < h_{30}^Z < 0.105$	$-0.044 < h_{30}^Z < 0.044$
$\sqrt{s} = 2$ TeV, $\Lambda_{FF} = 1.5$ TeV	$-0.0064 < h_{40}^Z < 0.0064$	$-0.0025 < h_{40}^Z < 0.0025$
$p\bar{p} \to Z\gamma \to \bar{\nu}\nu\gamma$	$-0.038 < h_{30}^Z < 0.038$	$-0.024 < h_{30}^Z < 0.024$
$\sqrt{s} = 1.8$ TeV, $\Lambda_{FF} = 1.5$ TeV	$-0.0027 < h_{40}^Z < 0.0027$	$-0.0013 < h_{40}^Z < 0.0013$

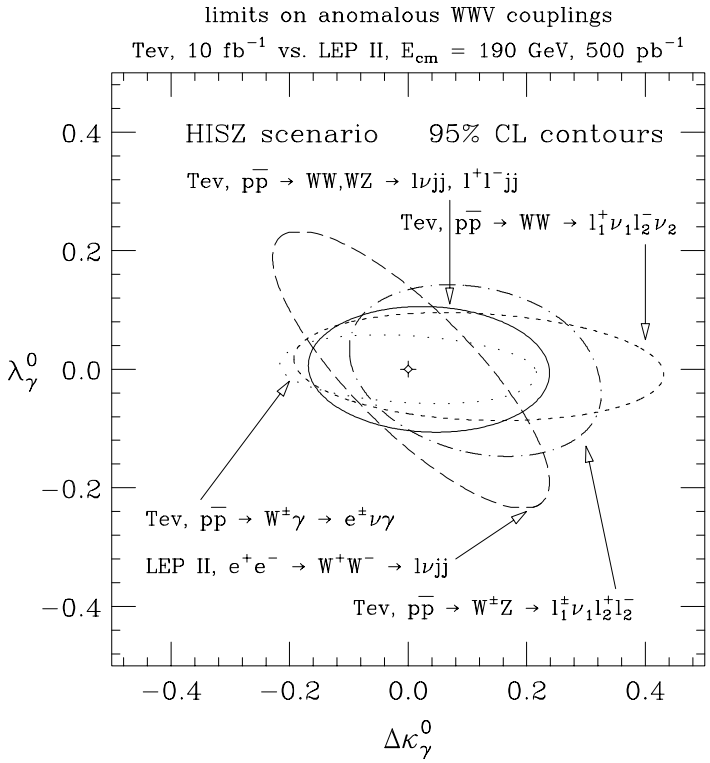

Figure 4.20: Comparison of the expected sensitivities on anomalous WWV couplings in the HISZ scenario from $e^+e^- \to W^+W^- \to \ell\nu jj$ at LEP II and various processes at the Tevatron.

the form factor scale assumed [67].

4.7.5 Radiation Zero and Rapidity Correlations in $W\gamma$ Production

$W\gamma$ production in hadronic collisions is of special interest due to the presence of a zero in the helicity amplitudes. It is well known that all SM helicity amplitudes of the parton-level subprocess $q_1\bar{q}_2 \to W^\pm\gamma$ vanish for [74]

$$\cos\theta^* = \frac{Q_1 + Q_2}{Q_1 - Q_2} = \pm\frac{1}{3}\ , \tag{4.52}$$

where θ^* is the scattering angle of the W-boson with respect to the quark (q_1) direction in the $W\gamma$ rest frame, and Q_i ($i = 1, 2$) are the quark charges in units of the proton electric charge e. This zero is a consequence of the factorizability of the amplitudes in gauge theories into one factor which contains the gauge coupling dependence and another which contains spin information. Although the factorization holds for any four-particle Born-level amplitude in which one or more of the four particles is a gauge-field quantum, the amplitudes for most processes may not necessarily develop a kinematical zero in the physical region. The

amplitude zero in the $W^{\pm}\gamma$ process has been further shown to correspond to the absence of dipole radiation by colliding particles with the same charge-to-mass ratio [75], a realization of classical radiation interference and is therefore often referred to as the "radiation zero".

Non-standard $WW\gamma$ couplings in general destroy the amplitude zero in $W\gamma$ production. Searching for the radiation zero thus provides an additional powerful test of the gauge theory nature of the SM.

Unfortunately, the amplitude zero in $q_1\bar{q}_2 \to W\gamma \to \ell\nu\gamma$ is not easy to observe in the $\cos\theta^*$ distribution in pp or $p\bar{p}$ collider experiments. Structure function effects transform the zero in the $W\gamma$ case into a dip in the $\cos\theta^*$ distribution. Higher order QCD corrections, finite W width effects, and photon radiation from the final state lepton line also tend to fill in the dip.

The main complication in the extraction of the $\cos\theta^*$ distribution, however, originates from the finite resolution of the detector and ambiguities in reconstructing the parton center of mass frame. The ambiguities are associated with the nonobservation of the neutrino arising from W decay. Identifying the missing transverse momentum with the transverse momentum of the neutrino of a given $W\gamma$ event, the unobservable longitudinal neutrino momentum, $p_L(\nu)$, and thus the parton center of mass frame, can be reconstructed by imposing the constraint that the neutrino and charged lepton four momenta combine to form the W rest mass. The resulting quadratic equation, in general, has two solutions. In the approximation of a zero W decay width, one of the two solutions coincides with the true $p_L(\nu)$. On an event by event basis, however, it is impossible to tell which of the two solutions is the correct one. This ambiguity considerably smears out the dip caused by the amplitude zero.

Instead of trying to reconstruct the parton center of mass frame and measure the $\cos\theta^*$ or the equivalent rapidity distribution in the center of mass frame, one can study rapidity correlations between the observable final state particles in the laboratory frame. Knowledge of the neutrino longitudinal momentum is not required in determining this distribution. Event mis-reconstruction problems originating from the two possible solutions for $p_L(\nu)$ are thus automatically avoided. In $2 \to 2$ reactions differences of rapidities are invariant under boosts. One therefore expects that the double differential distribution of the rapidities, $d^2\sigma/dy(\gamma)dy(W)$, where $y(W)$ and $y(\gamma)$ are the W and photon rapidity, respectively, in the laboratory frame, exhibits a "valley" located at $y(\gamma) - y(W) \approx -0.4$, signaling the SM amplitude zero [76]. In $W^{\pm}\gamma$ production, the dominant W helicity is $\lambda_W = \pm 1$ [77], implying that the charged lepton, $\ell = e,\ \mu$, from $W \to \ell\nu$ tends to be emitted in the direction of the parent W, and thus reflects most of its kinematic properties. As a result, the valley signaling the SM radiation zero should manifest itself also in the $d^2\sigma/dy(\gamma)dy(\ell)$ distribution of the photon and lepton rapidities. The theoretical prediction of the $d^2\sigma/dy(\gamma)dy(\ell)$ distribution in the Born approximation is shown in Fig. 4.21 and indeed exhibits a pronounced valley for rapidities satisfying $\Delta y(\gamma,\ell) = y(\gamma) - y(\ell) \approx -0.3$. To simulate detector response, transverse momentum cuts of $p_T(\gamma) > 5$ GeV/c, $p_T(\ell) > 20$ GeV/c and $\not{p}_T > 20$ GeV/c, rapidity cuts of $|y(\gamma)| < 3$ and $|y(\ell)| < 3.5$, a cluster transverse mass cut of $m_T(\ell\gamma;\not{p}_T) > 90$ GeV/c^2 and a lepton photon separation cut of $\Delta R(\gamma,\ell) > 0.7$ have been imposed. For 10 fb^{-1}, a sufficient number of events should be available to map out $d^2\sigma/dy(\gamma)dy(\ell)$.

For smaller data sets, the rapidity difference distribution, $d\sigma/d\Delta y(\gamma,\ell)$, is a more useful

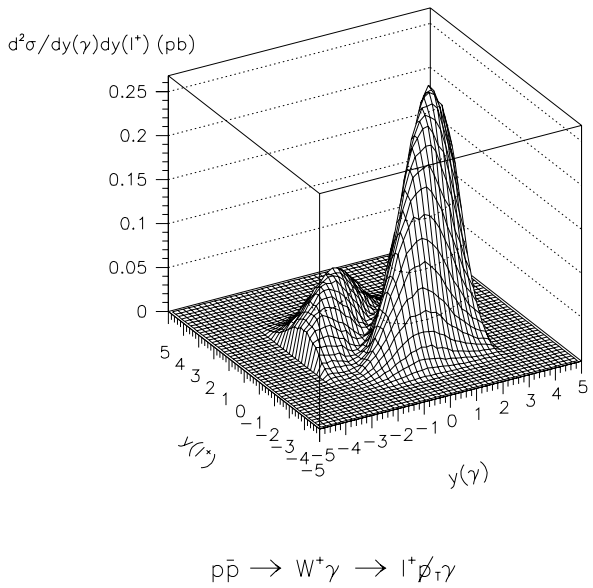

Figure 4.21: The double differential distribution $d^2\sigma/dy(\gamma)dy(\ell)$ for $p\bar{p} \to W^+\gamma \to \ell \not{p}_T \gamma$ at the Tevatron.

variable. In the photon lepton rapidity difference distribution, the SM radiation zero leads to a strong dip located at $\Delta y(\gamma, \ell) \approx -0.3$ [76]. The LO and NLO predictions of the SM $\Delta y(\gamma, \ell)$ differential cross section for $p\bar{p} \to \ell^+ \not{p}_T \gamma$ at the Tevatron are shown in Fig. 4.22a.

Next-to-leading QCD corrections do not seriously affect the significance of the dip. However, a sufficient rapidity coverage is essential to observe the radiation zero in $d^2\sigma/dy(\gamma)dy(\ell)$ and/or the $\Delta y(\gamma, \ell)$ and distribution [76]. This is demonstrated in Fig. 4.23, which displays simulations of the rapidity difference distribution for 1 fb^{-1} in the electron channel. If both central ($|y| < 1.1$) and endcap ($1.5 < |y| < 2.5$) electrons and photons can be used (Fig. 4.23a), the simulations indicate that with integrated luminosities ≥ 1 fb^{-1} it will be possible to conclusively establish the dip in the photon lepton rapidity difference distribution which signals the presence of the radiation zero in $W\gamma$ production. On the other hand, for central electrons and photons only, the dip is statistically not significant for 1 fb^{-1}. With the detector upgrades currently planned for the Main Injector Era and beyond, both experiments should have the capability to analyze the $\Delta y(\gamma, \ell)$ distribution over the full rapidity range of $|y| < 2.5$.

In pp collisions, the dip signaling the amplitude zero is shifted to $\Delta y(\gamma, \ell) = 0$. Because of the large qg luminosity, the inclusive QCD corrections are very large for $W\gamma$ production at multi-TeV hadron colliders [78]. At the LHC, they enhance the cross section by a factor $2 - 3$. The rapidity difference distribution for $W^+\gamma$ production in the SM for pp collisions at $\sqrt{s} = 14$ TeV is shown in Fig. 4.22b. Here we have imposed the following lepton and photon

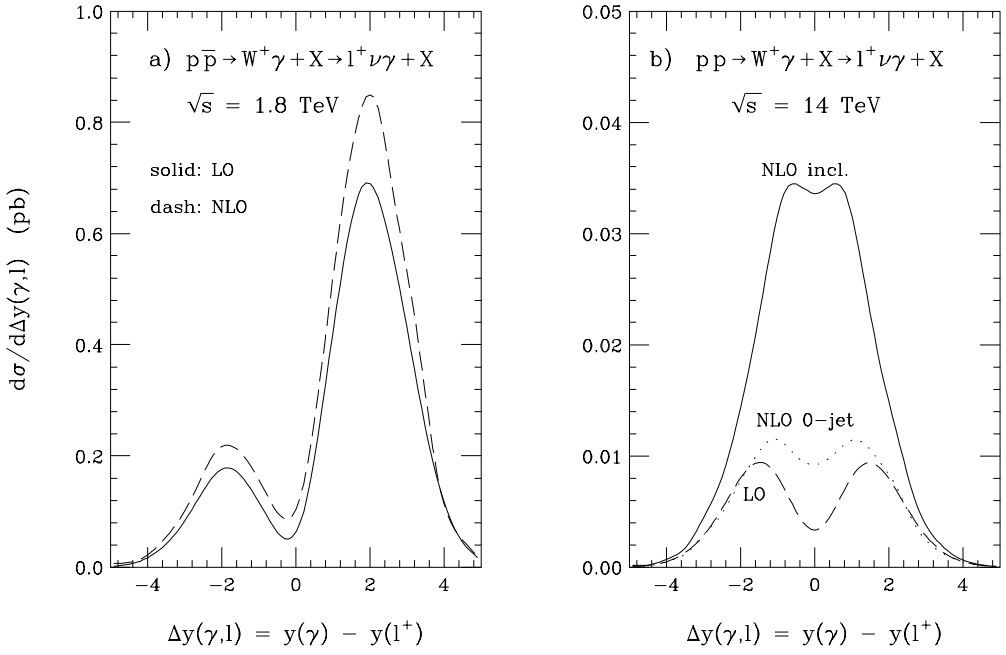

Figure 4.22: Photon lepton rapidity difference distribution for $W\gamma$ production in the SM at a) the Tevatron and b) the LHC.

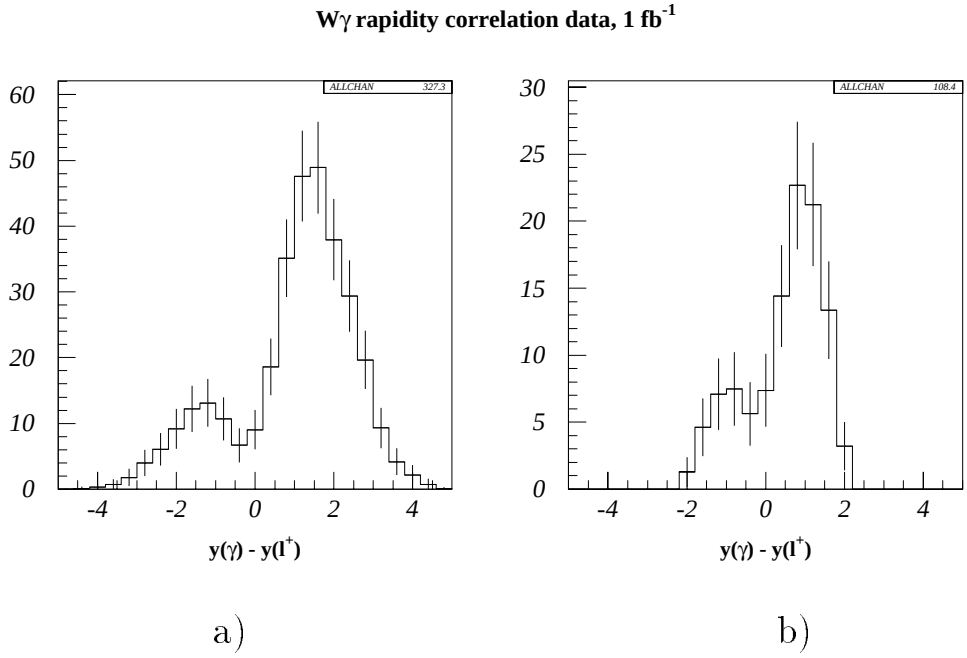

Figure 4.23: Simulation of the photon lepton rapidity difference distribution for $W\gamma$ production for 1 fb^{-1}, a) for central and endcap photons and electrons, b) for central electrons and photons only.

detection cuts:

$$p_T(\gamma) > 100 \text{ GeV/c}, \qquad |\eta(\gamma)| < 2.5, \tag{4.53}$$

$$p_T(\ell) > 25 \text{ GeV/c}, \qquad |\eta(\ell)| < 3, \tag{4.54}$$

$$\not{p}_T > 50 \text{ GeV/c}, \qquad \Delta R(\gamma, \ell) > 0.7, \tag{4.55}$$

The inclusive NLO QCD corrections are seen to considerably obscure the amplitude zero. The bulk of the corrections at LHC energies originates from quark gluon fusion and the kinematical region where the photon is produced at large p_T and recoils against a quark, which radiates a soft W boson which is almost collinear to the quark. Events which originate from this phase space region usually contain a high p_T jet. A jet veto therefore helps to reduce the QCD corrections. Nevertheless, the remaining QCD corrections still substantially reduce the visibility of the radiation zero in $W\gamma$ production at the LHC [76].

Given a sufficiently large integrated luminosity, experiments at the Tevatron studying lepton photon rapidity correlations therefore offer a *unique* chance to observe the SM radiation zero in $W\gamma$ production.

Indirectly, the radiation zero can also be observed in the $Z\gamma$ to $W\gamma$ cross section ratio [79]. Many theoretical and experimental uncertainties at least partially cancel in the cross section ratio. On the other hand, in searching for the effects of the SM radiation zero in the $Z\gamma$ to $W\gamma$ cross section ratio, one has to assume that the SM is valid for $Z\gamma$ production. Since the radiation zero occurs at a large scattering angle, the photon E_T distribution in $W\gamma$ production falls much more rapidly than that of photons in $Z\gamma$ production. As a result, the SM $W\gamma$ to $Z\gamma$ event ratio, $N_{W\gamma}/N_{Z\gamma}$, as a function of the photon transverse energy, E_T^γ, drops rapidly. As demonstrated in Fig. 4.24 for the electron channel, the event ratio can be mapped out to $E_T^\gamma \approx 200$ GeV with 10 fb^{-1}, thus making it possible to conclusively establish the rapid drop in the event ratio predicted by the SM (solid line). From a comparison of the observed cross section ratio with the SM prediction, one can in principle also extract limits on anomalous $WW\gamma$ and $Z\gamma V$ couplings.

4.7.6 Probing QCD in $W\gamma$ Production

For an integrated luminosity of 10 fb^{-1}, one expects approximately 5,000 $W^\pm\gamma$, $W \to e\nu$ events. Besides detailed tests of the $WW\gamma$ couplings the large data sample expected will make it possible to measure a number of interesting observables, such as the p_T distribution of the $W\gamma$ pair. Similar to the transverse momentum distribution of the W and Z bosons [80], a measurement of the $W\gamma$ p_T spectrum constitutes an excellent test of QCD. In the small transverse momentum region, soft gluon resummation, and non-perturbative QCD effects are probed [81]. Perturbative QCD is tested for $p_T(W\gamma) > 40$ GeV/c. Presently, only a calculation of $W\gamma$ production at NLO in QCD exits; resummation effects have not yet been included in the theoretical predictions.

At large $W\gamma$ transverse momenta, QCD predicts a collinear enhancement factor in the $qg \to W\gamma q'$ partonic cross section [78]. It arises from the kinematical region where the photon recoils against a quark jet, which radiates a soft W boson which is almost collinear to the quark. QCD corrections therefore change the shape of the photon transverse

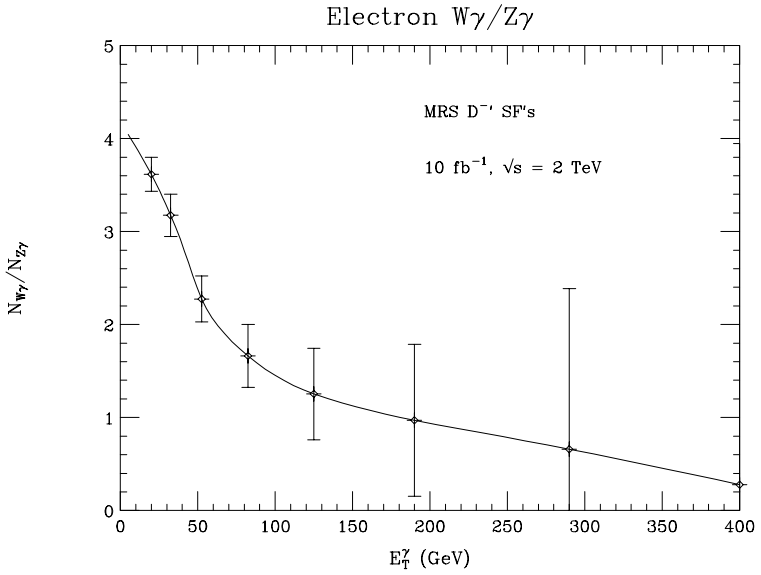

Figure 4.24: $W\gamma$ to $Z\gamma$ cross section ratio. The solid line is the SM prediction.

momentum distribution, and lead to a rather hard $p_T(W\gamma)$ distribution in the region above 40 GeV/c, where the $W\gamma$ transverse momentum spectrum is dominated by the contribution from $W\gamma + 1$ jet production.

The effect of the collinear enhancement factor on the $p_T(W\gamma)$ distribution in the perturbative region is illustrated in Fig. 4.25. The solid line displays the lowest order QCD prediction from the calculation of Ref. [78]. The dashed line, on the other hand, shows the $W\gamma$ transverse momentum distribution one would expect, *if* the shape of the $W\gamma$ p_T distribution and the W transverse momentum distribution would be identical. To obtain the dashed line, $W\gamma$ events were generated using the leading (Born) order calculation of Ref. [82], and boosting the $W\gamma$ system in the transverse plane according to the W transverse momentum distribution measured by CDF in the 1988-89 run [83]. The measured $p_T(W)$ distribution was found to agree very well with the QCD prediction [84] in the perturbative region. The normalization of the dashed line was adjusted by multiplying the LO $W\gamma$ cross section within cuts by the ratio of NLO to LO cross sections (k-factor). Identical cuts ($E_T(\gamma) > 10$ GeV, $E_T(e)$, $\not\!\!E_T > 20$ GeV, $\Delta R(e,\gamma) > 0.7$, $|\eta(\gamma)|$, $|\eta(e)| < 2.5$, $m_T(e\gamma;\not\!\!E_T) > 90$ GeV/c^2, standard photon isolation) and parameters have been used to obtain the two curves.

Figure 4.25 shows that the shape of the $W\gamma$ transverse momentum distribution predicted by QCD is significantly harder than that of the $p_T(W)$ spectrum. The error bars in Fig. 4.25 indicate the expected statistical uncertainties for an integrated luminosity of 10 fb^{-1}. The size of the error bars shows that, with 10 fb^{-1}, it should be feasible to map out the $p_T(W\gamma)$ distribution to transverse momenta in excess of 100 GeV and to discriminate between the two distributions approximately at the 7σ level.

A similar measurement can be carried out for $Z\gamma$ production, although the significantly smaller number of events limits the accessible p_T range.

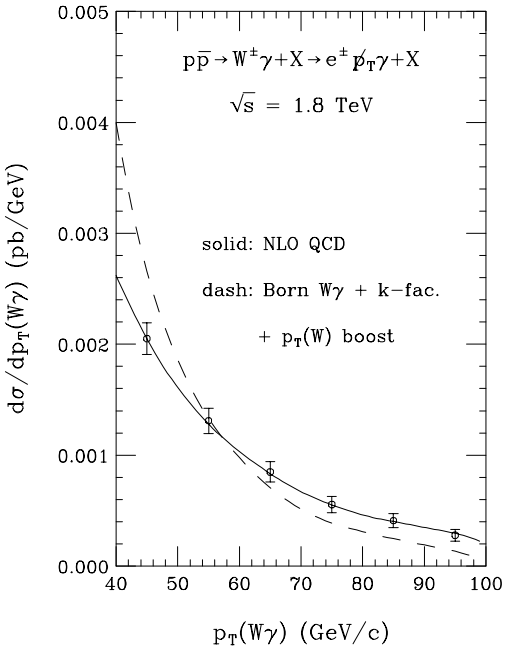

Figure 4.25: $W\gamma$ transverse momentum distribution at the Tevatron in the perturbative region. The solid curve shows the distribution predicted by QCD at $\mathcal{O}(\alpha_s)$. The dashed line displays the distribution one would expect if the shape of the W and $W\gamma$ transverse momentum would be identical. The error bars indicate the statistical uncertainties expected for an integrated luminosity of 10 fb^{-1}.

4.8 Triple Gauge Boson Production

The very large integrated luminosities expected in future Tevatron runs offer also the possibility to search for triple vector boson production and thus to probe the quartic boson self-interactions ($WW\gamma\gamma$, $WWZZ$ *etc.*). The triple vector boson production processes can be classified according to the number of photons in the final state:

$$p\bar{p} \to \gamma\gamma\gamma, \tag{4.56}$$

$$p\bar{p} \to W^{\pm}\gamma\gamma,\ Z\gamma\gamma, \tag{4.57}$$

$$p\bar{p} \to W^{+}W^{-}\gamma,\ W^{\pm}Z\gamma,\ ZZ\gamma, \tag{4.58}$$

$$p\bar{p} \to W^{+}W^{-}W^{\pm},\ W^{+}W^{-}Z,\ W^{\pm}ZZ,\ ZZZ. \tag{4.59}$$

We will not consider the pure QED process $p\bar{p} \to \gamma\gamma\gamma$ here. Since top quarks decay almost exclusively into Wb, the $W^{+}W^{-}V$, $V = W^{\pm}$, γ, Z channels also receive contributions from $t\bar{t}V$ production. For a top quark mass of 175 GeV/c^2, the $t\bar{t}V$ and $W^{+}W^{-}V$ production cross sections are very similar at the Tevatron. The b-quarks produced in top quark decays frequently lead to one or two hadronic jets. The jet activity of WWV events may therefore be used to separate the WWV and $t\bar{t}V$ processes. Higgs boson exchange contributes to the processes listed in Eq. (4.59) and enhances the cross section by up to a factor 6.

Table 4.7: Triple gauge boson production cross sections at the Tevatron ($\sqrt{s} = 2$ TeV) for $M_{top} = 175$ GeV/c^2 and $M_H = 100$ GeV/c^2. The branching ratios of the leptonic W and Z decays with $\ell = e, \mu$ are included in the cross section listed.

channel	cross section (fb)
$W^{\pm}\gamma\gamma \to \ell^{\pm}\nu\gamma\gamma$, $p_T(\gamma) > 10$ GeV, $\lvert\eta(\gamma)\rvert < 2.5$	4.6
$Z\gamma\gamma \to \ell^+\ell^-\gamma\gamma$, $p_T(\gamma) > 10$ GeV, $\lvert\eta(\gamma)\rvert < 2.5$	3.2
$W^+W^-\gamma \to \ell_1^+\nu_1\ell_2^-\bar{\nu}_2\gamma$, $p_T(\gamma) > 10$ GeV, $\lvert\eta(\gamma)\rvert < 2.5$ $t\bar{t}\gamma \to W^+W^-\gamma \to \ell_1^+\nu_1\ell_2^-\bar{\nu}_2\gamma$, $p_T(\gamma) > 10$ GeV, $\lvert\eta(\gamma)\rvert < 2.5$	2.0 1.7
$W^{\pm}Z\gamma \to \ell_1^{\pm}\nu_1\ell_2^+\ell_2^-\gamma$, $p_T(\gamma) > 10$ GeV, $\lvert\eta(\gamma)\rvert < 2.5$	0.12
$ZZ\gamma \to \ell^+\ell^-\bar{\nu}\nu\gamma$, $p_T(\gamma) > 10$ GeV, $\lvert\eta(\gamma)\rvert < 2.5$	0.18
$ZZ\gamma \to \ell_1^+\ell_1^-\ell_2^+\ell_2^-\gamma$, $p_T(\gamma) > 10$ GeV, $\lvert\eta(\gamma)\rvert < 2.5$	0.03
$W^+W^-W^{\pm} \to \ell_1^+\nu_1\ell_2^-\nu_2\ell_3^{\pm}\nu_3$ $t\bar{t}W^{\pm} \to W^+W^-W^{\pm} \to \ell_1^+\nu_1\ell_2^-\nu_2\ell_3^{\pm}\nu_3$	0.06 0.05
$W^+W^-Z \to \ell_1^+\nu_1\ell_2^-\nu_2\ell_3^+\ell_3^-$ $t\bar{t}Z \to W^+W^-Z \to \ell_1^+\nu_1\ell_2^-\nu_2\ell_3^+\ell_3^-$	0.02 0.01
$W^{\pm}ZZ \to \ell_1^{\pm}\nu_1\ell_2^+\ell_2^-\ell_3^+\ell_3^-$	$1.1 \cdot 10^{-3}$
$ZZZ \to \ell_1^+\ell_1^-\ell_2^+\ell_2^-\bar{\nu}\nu$	$1.3 \cdot 10^{-3}$
$ZZZ \to \ell_1^+\ell_1^-\ell_2^+\ell_2^-\ell_3^+\ell_3^-$	$1.5 \cdot 10^{-4}$

The cross sections for the triple gauge boson production processes at the Tevatron are listed in Table 4.7 [5]. For an integrated luminosity of 10 fb^{-1}, a sufficient number of $W\gamma\gamma$, $Z\gamma\gamma$ and $WW\gamma$ events should be observed to extract information on the quartic gauge boson couplings. For all other processes one expects at most a few candidate events, unless the quartic couplings substantially deviate from the SM prediction.

4.9 Conclusions

With very large integrated luminosities at the Tevatron, the electroweak sector sector of the SM can be probed in great detail. From our partly preliminary studies we arrive at the following conclusions:

- With 10 fb^{-1} it should be possible to measure the mass of the W boson with a precision of at least 30 MeV/c^2. An uncertainty of 20 MeV/c^2 may well be within reach. This

is about a factor of 2 better than what one expects for LEP II. With a precision of 20 MeV/c^2 (30 MeV/c^2) for the W mass, and 2 GeV/c^2 for the top quark mass, the Higgs Boson mass can be predicted with an uncertainty of about 40% (50%). Comparison with the results of a direct search at the Tevatron and LHC may constitute the ultimate test of the SM.

- The W width can be measured with an uncertainty of about 15 MeV. This is an improvement of almost one order of magnitude of the current uncertainty. At LEP II , $_W$ can only be measured with a precision of a few hundred MeV.

- The W charge asymmetry will be a very powerful tool in constraining the parton distribution functions. In many processes the error in the parton distribution functions currently constitutes a major source of uncertainty. The forward backward asymmetry, A_{FB} in Z boson decays provides a useful cross check on the Higgs boson mass extracted from the W mass measurement.

- With an integrated luminosity of 10 fb^{-1}, limits on the branching ratios of rare W decays of $\mathcal{O}(10^{-5})$ to $\mathcal{O}(10^{-7})$ can be obtained. W decays into two pseudoscalar mesons offer an opportunity to probe meson decay form factors at a very high momentum transfer where these form factors have not been tested so far.

- The Tevatron offers a unique opportunity to search for CP violation in W boson production and decay since it collides protons and antiprotons, *ie.* the initial state is a CP eigenstate. The extremely large number of W boson events expected at a superluminous Tevatron will make it possible to search for small CP-violating contributions to W boson production, at the level of $\mathcal{O}(10^{-3} - 10^{-4})$.

- With 10 fb^{-1}, the WWV and $Z\gamma V$, $V = \gamma, Z$, vertices can be determined with a precision of $\mathcal{O}(10\%)$ and $\mathcal{O}(10^{-2} - 10^{-3})$, respectively, at the Tevatron. The expected accuracy for the WWV couplings is comparable or better than that of LEP II. However, since the methods used to extract limits on anomalous couplings at the two colliders are different, data from the Tevatron and LEP II yield complementary information. Tevatron experiments will be able to place limits on the $Z\gamma V$ couplings which are up to a factor 100 better than those which can be achieved at LEP II. At the LHC, with 100 fb^{-1}, it will be possible to place limits on anomalous WWV and $Z\gamma V$ couplings which are a factor 3 to 100 better than those one can expect for the Tevatron with 10 fb^{-1}.

- The Tevatron offers a unique chance to search for the SM "radiation zero" in $W\gamma$ production, which provides an additional powerful test of the gauge theory nature of the SM. At the LHC, due to the large qg luminosity, QCD corrections obscure the dip in the photon lepton rapidity difference distribution which is caused by the radiation zero. This is not the case at Tevatron energies. Currently, the experimental results are statistically limited. With integrated luminosities of 2 fb^{-1} or more, it should be possible to conclusively establish the existence of the radiation zero.

- A superluminous Tevatron will make it possible to obtain direct information on the quartic vector boson couplings. For an integrated luminosity of 10 fb^{-1}, a sufficient

number of $W\gamma\gamma$, $Z\gamma\gamma$ and $WW\gamma$ events should be observed to extract information on the quartic gauge boson couplings.

Acknowledgements

We would like to thank W. Bardeen, G. Burdman, E. Eichten, K. Einsweiler, W. Giele, C. Hill and P. Tipton for stimulating discussions.

Bibliography

[1] P. Renton, OUNP-95-20 (preprint, October 1995), to appear in the Proceedings of the International Symposium on Lepton Photon Interactions, Beijing, August 1995.

[2] D. Schaile, CERN-PPE/94-162 (preprint, October 1994), in Proceedings of the *"27th International Conference on High Energy Physics"*, Glasgow, Scotland, July 1994, Vol. I, p. 27; The LEP Collaborations, CERN-PPE/94-187 (preprint, November 1994).

[3] G. Jackson, Recycler Ring Conceptual Design Study, FERMILAB-TM-1936 (July 1995).

[4] S. Dawson and G. Valencia, Phys. Rev. **D52**, 2717 (1995).

[5] T. Han and R. Sobey, UCD-95-22 (preprint, July 1995).

[6] S. Godfrey, Proceedings of the *"International Symposium of Vector Boson Self Interactions"*, Los Angeles, CA, February 1995, p. 209.

[7] F. Abe *et al.* (CDF Collaboration), Phys. Rev. Lett. **75**, 11 (1995) and Phys. Rev. **D52**, 4784 (1995).

[8] U. Baur and D. Zeppenfeld, Phys. Rev. Lett. **75**, 1002 (1995).

[9] V. Khoze and W.J. Stirling, Phys. Lett. **B356**, 373 (1995); V. Khoze and T. Sjostrand, DTP/95/68 (preprint, August 1995).

[10] C. Balázs, J. Qiu and C.P. Yuan, Phys. Lett. **B355**, 548 (1995).

[11] M.H. Reno, Phys. Rev. **D49**, 4326 (1994).

[12] W. Carithers, TEV2000 workshop note (October 1994).

[13] A. Peryshkin, Proceedings of the Workshop on Physics at Current Accelerators and the Supercollider, Argonne, June 1993, p. 295.

[14] M. Austern and R. Cahn, LBL-33780, April 1993; H.S. Chen and G.J. Zhou, Phys. Lett. **B331**, 441 (1994); W.J. Stirling, DTP/95/24 (preprint, February 1995).

[15] P. Perez, DAPNIA/SPP 95-21 (preprint, October 1995), to appear in the Proceedings of the International Europhysics Conference on High Energy Physics, Brussels, Belgium, July 27 – August 2, 1995.

[16] D. Gingrich *et al.* (ATLAS Collaboration), ATLAS Letter of Intent, CERN-LHCC-92-4 (October 1992); W. W. Armstrong *et al.* (ATLAS Collaboration), ATLAS Technical Design Report, CERN-LHCC-94-43 (December 1994).

[17] M. Della Negra *et al.* (CMS Collaboration), CMS Letter of Intent, CERN-LHCC-92-3 (October 1992); G. L. Bayatian *et al.* (CMS Collaboration), CMS Technical Design Report, CERN-LHCC-94-38 (December 1994).

[18] K. Einsweiler, private communication.

[19] F. Halzen, B. Kniehl, and M.L. Stong, Z. Phys. **C58**, 119 (1993); F. Halzen and B. Kniehl, Nucl. Phys. **B353**, 567 (1990).

[20] F. Merritt, H. Montgomery, A. Sirlin and M. Swartz, *"Precision Tests of Electroweak Physics"*, in *"Particle Physics – Perspectives and Opportunities, Report of the DPF Committee on Long Term Planning"*, eds. R.D. Peccei *et al.*, p. 19.

[21] H. Burkhardt and B. Pietrzyk, Phys. Lett. **B356**, 398 (1995); S. Eidelmann and F. Jegerlehner, Z. Phys. **C67**, 585 (1995); R.B.Nevzorov, A.V. Novikov and M.I. Vysotsky, JETP Lett. **60**, 399 (1994); A.D. Martin and D. Zeppenfeld, Phys. Lett. **B345**, 558 (1995); M. Swartz, SLAC-PUB-95-7001 (preprint, September 1995).

[22] F. Abe *et al.* (CDF Collaboration), Phys. Rev. Lett. **74**, 341 (1995).

[23] F. Abe *et al.* (CDF Collaboration), Phys. Rev. Lett. **73**, 220 (1994) and Phys. Rev. **D52**, 2624 (1995); S. Abachi *et al.* (DØ Collaboration), Phys. Rev. Lett. **75**, 1456 (1995).

[24] J. Rosner, M. Worah and T. Takeuchi, Phys. Rev. **D49**, 1363 (1994).

[25] M. Swartz, SLAC-PUB-5258 (June 1990).

[26] F. Nang (DØ Collaboration), Proceedings of the *"DPF94 Conference"*, Albuquerque, NM, August 1994, pp. 1644; W. Giele, E.W.N. Glover and D. Kosower, Phys. Rev. **D52**, 1486 (1995); S.D. Ellis and D.E. Soper, Phys. Rev. Lett. **74**, 5182 (1995).

[27] E. Kovacs (CDF Collaboration), Proceedings of the *"DPF94 Conference"*, Albuquerque, NM, August 1994, p. 1653; W. Giele, E.W.N. Glover and D. Kosower, Phys. Lett. **B339**, 181 (1994).

[28] A.D. Martin, R.G. Roberts and W.J. Stirling, Mod. Phys. Lett. **A4**, 1135 (1989); E.L. Berger *et al.*, Phys. Rev. **D40**, 83 (1989).

[29] F. Abe *et al.* (CDF Collaboration), Phys. Rev. Lett. **74**, 850 (1995).

[30] H.L. Lai *et al.*, (CTEQ Collaboration), Phys. Rev. **D51**, 4763 (1995); A.D. Martin, R.G. Roberts and W.J. Stirling, Phys Rev. **D50**, 6734 (1994).

[31] J.L. Rosner, Phys. Lett. **B221**, 85 (1989).

[32] F. Abe *et al.* (CDF Collaboration), Phys. Rev. Lett. **67**, 1502 (1991).

[33] P. Fisher, U. Becker and P. Kirkby, Phys. Lett. **B356**, 404 (1995).

[34] M. Schmelling, CERN-PPE/95-129 (preprint, August 1995), to appear in the Proceedings of the *"XV International Conference on Physics in Collision"*, Cracow, Poland, June, 1995; P. Langacker and N. Polonsky, Phys. Rev. **D52**, 3081 (1995).

[35] W. Giele, E.W.N. Glover and J. Yu, FERMILAB-Pub-95/127-T (preprint, July 1995).

[36] C. Balazs and C.P. Yuan, in preparation.

[37] A.D. Martin, R.G. Roberts and W.J. Stirling, Phys. Lett. **B356**, 89 (1995); CTEQ Collaboration, in preparation.

[38] P. Arnold and M.H. Reno, Nucl. Phys. **B319**, 37 (1989); (E) **B330**, 284 (1990); P. Arnold, R.K. Ellis and M.H. Reno, Phys. Rev. **D40**, 912 (1989).

[39] F. Abe *et al.* (CDF Collaboration), Phys. Rev. Lett. **67**, 2938 (1991); S. Abachi *et al.* (DØ Collaboration), FERMILAB-Conf-95/259-E (preprint, August 1995), contributed paper to the Europhysics Conference on High Energy Physics, Brussels, Belgium, July 27 – August 2, 1995.

[40] F. Abe *et al.* (CDF Collaboration), FERMILAB-Pub-95/301-E (preprint, September 1995), submitted to Phys. Rev. Lett.

[41] W. Bernreuther *et al.*, in *"Z Physics at LEP I"*, CERN 89-08, 1989 (Yellow Report), Vol. 2, p. 1.

[42] F. Abe *et al.* (CDF Collaboration), Phys. Rev. Lett. **69**, 2160 (1992); S. Kopp, FERMILAB-Pub-95/264-E (preprint, August 1995), to appear in Int. J. Mod. Phys. **A**; F. Abe, *et al.* (CDF Collaboration), to be submitted (Oct. 1995) to Phys. Rev. Lett. See also J. Alitti, *et al.* (UA2 Collaboration), Phys. Lett. **B277**, 203 (1992).

[43] C. Albajar *et al.* (UA1 Collaboration), Phys. Lett **B241**, 283 (1990); J. Alitti *et al.* (UA2 Collaboration), Phys. Lett **B277**, 203 (1992).

[44] L. Arnellos, W.J. Marciano and Z. Parsa, Nucl. Phys. **B196**, 378 (1982).

[45] G.P. Lepage and S.J. Brodsky, Phys. Lett. **B87**, 359 (1979); A. Duncan and A. Mueller, Phys. Rev. **D21**, 1636 (1980).

[46] J. Richman and P. Burchat, UCSB-HEP-95-08, to appear in Rev. Mod. Phys.

[47] E. Eichten and C. Quigg, Phys. Rev. **D49**, 5845 (1994).

[48] L. Montanet *et al.* (Particle Data Group), Phys. Rev. **D50**, 1173 (1994).

[49] G. Burdman, private communication.

[50] R. Barbieri, A. Georges and P. Le Doussal, Z. Phys. **C32**, 437 (1986).

[51] A. Brandenburg, J. Ma, R. Munch, and O. Nachtmann, Z. Phys. **C51**, 225 (1991).

[52] A. Brandenburg, J. Ma, and O. Nachtmann, Z. Phys. **C55**, 115 (1992).

[53] P. Chiappetta and M. Le Bellac, Z. Phys. **C32**, 521 (1986).

[54] K. Hagiwara, K. Hikasa, R. D. Peccei, D. Zeppenfeld, Nucl. Phys. **B282**, 253 (1987); K. Gaemers and G. Gounaris, Z. Phys. **C1**, 259 (1979).

[55] H. Aronson, Phys. Rev. **186**, 1434 (1969); K. J. Kim and Y.-S. Tsai, Phys. Rev. **D7**, 3710 (1973).

[56] U. Baur and D. Zeppenfeld, Phys. Lett. **B201**, 383 (1988).

[57] F. Abe *et al.* (CDF Collaboration), Phys. Rev. Lett. **74**, 1936 (1995).

[58] S. Abachi *et al.* (DØ Collaboration), Phys. Rev. Lett. **75**, 1034 (1995).

[59] D. Benjamin, FERMILAB-Conf-95/241-E (June 1995), to appear in the Proceedings of the *"10th Topical Workshop on Proton Antiproton Collider Physics"*, Fermilab, May 1995.

[60] F. Abe *et al.* (CDF Collaboration), Phys. Rev. Lett. **74**, 1941 (1995).

[61] S. Abachi *et al.* (DØ Collaboration), Phys. Rev. Lett. **75**, 1028 (1995).

[62] F. Abe *et al.* (CDF Collaboration), Phys. Rev. Lett. **75**, 1018 (1995).

[63] S. Abachi *et al.* (DØ Collaboration), Phys. Rev. Lett. **75**, 1024 (1995).

[64] S. Abachi *et al.* (DØ Collaboration), FERMILAB-Conf-95/250-E (July 1995), contributed paper to the Europhysics Conference on High Energy Physics, Brussels, 27 July – 2 August 1995.

[65] M. Acciarri *et al.* (L3 Collaboration), Phys. Lett. **B346**, 190 (1995).

[66] U. Baur and E. L. Berger, Phys. Rev. **D47**, 4889 (1993).

[67] H. Aihara *et al.*, Summary of the Working Subgroup on Anomalous Gauge Boson Interactions of the DPF Long Range Planning Study, FERMILAB-Pub-95/031, March 1995, preprint, to appear in *"Electroweak Symmetry Breaking and New Physics at the TeV Scale"*, eds. T. Barklow, S. Dawson, H. Haber and J. Siegrist.

[68] J. Ohnemus, Phys. Rev. **D44**, 1403 (1991); Phys. Rev. **D44**, 3477 (1991); Phys. Rev. **D50**, 1931 (1994); J. Ohnemus and J. Owens, Phys. Rev. **D43**, 3626 (1991); S. Frixione, Nucl. Phys. **B410**, 280 (1993); S. Frixione, P. Nason, and S. Ridolfi, Nucl. Phys. **B383**, 3 (1992).

[69] U. Baur, J. Ohnemus, and T. Han, Phys. Rev. **D51**, 3381 (1995).

[70] K. Hagiwara, J. Woodside, and D. Zeppenfeld, Phys. Rev. **D41**, 2113 (1990).

[71] F. A. Berends *et al.*, Nucl. Phys. **B357**, 32 (1991).

[72] K. Hagiwara, S. Ishihara, R. Szalapski, and D. Zeppenfeld, Phys. Lett. **B283**, 353 (1992), and Phys. Rev. **D48**, 2182 (1993).

[73] U. Baur, J. Ohnemus, and T. Han, UCD-95-21 (preprint, July 1995), to appear in Phys. Rev. **D**.

[74] R. W. Brown *et al.*, Phys. Rev. **D20**, 1164 (1979); K. O. Mikaelian *et al.*, Phys. Rev. Lett. **43**, 746 (1979).

[75] S. J. Brodsky and R. W. Brown, Phys. Rev. Lett. **49**, 966 (1982); R. W. Brown *et al.*, Phys. Rev. **D28**, 624 (1983); R. W. Brown and K. L. Kowalski, Phys. Rev. **D29**, 2100 (1984).

[76] U. Baur, S. Errede, and G. Landsberg, Phys. Rev. **D50**, 1917 (1994).

[77] C. Bilchak, R. Brown, and J. Stroughair, Phys. Rev. **D29**, 375 (1984).

[78] U. Baur, T. Han, and J. Ohnemus, Phys. Rev. **D48**, 5140 (1993).

[79] U. Baur, S. Errede, and J. Ohnemus, Phys. Rev. **D48**, 4103 (1993).

[80] C. Albajar *et al.* (UA1 Collaboration), Z. Phys. **C44**, 15 (1989); J. Alitti *et al.* (UA2 Collaboration), Z. Phys. **47**, 523 (1990); F. Abe *et al.* (CDF Collaboration); Phys. Lett. **66**, 2951 (1991); Phys. Lett. **67**, 2938 (1991); S. Abachi *et al.* (DØ Collaboration), FERMILAB-Conf-95/259-E (August 1995), contributed paper to the International Europhysics Conference on High Energy Physics, Brussels, Belgium, 27 July – 2 August, 1995.

[81] G. Ladinsky and C.P. Yuan, Phys. Rev. **D50**, 4239 (1994).

[82] U. Baur and E. L. Berger, Phys. Rev. **D41**, 1476 (1990).

[83] F. Abe *et al.* (CDF Collaboration); Phys. Lett. **66**, 2951 (1991).

[84] P. Arnold and R. Kauffman, Nucl. Phys. **B349**, 381 (1991).

Chapter 5

Light Higgs Physics at the Tevatron

5.1 Introduction

One of the primary goals of present and future colliders is to discover the mechanism responsible for the spontaneous symmetry breaking of the $SU(2)_L \times U(1)_Y$ electroweak interaction. The simplest model for this mechanism is the standard Higgs model, based on a doublet of fundamental scalar fields. This model predicts the existence of a new particle, the Higgs boson, of unknown mass, but with fixed couplings to other particles. The search for the Higgs boson represents a benchmark in our search for the mechanism of electroweak symmetry breaking.

The current lower bound on the Higgs mass is 64.5 GeV from LEP. In the near future, LEP II will extend the search to higher masses via $e^+e^- \to ZH$. The reach in Higgs mass depends on the machine energy, and is roughly $m_H < \sqrt{s} - M_Z - (5-10)$ GeV. The current plan is for LEP II to achieve $\sqrt{s} = 184$ GeV in 1996, which would cover up to $m_H = 85$ GeV. In 1999, the energy will be further increased to $\sqrt{s} = 192$ GeV, which will allow coverage up to $m_H \approx 95$ GeV.

Much higher Higgs masses will be explored by the CERN Large Hadron Collider (LHC), beginning in 2004 at $\sqrt{s} = 10$ TeV and increasing to $\sqrt{s} = 14$ TeV in 2008. For example, the process $gg \to H \to ZZ \to \ell^+\ell^-\ell^+\ell^-$ will cover from $m_H \approx 130 - 700$ GeV at full energy and luminosity [1, 2].

Ironically, the light intermediate-mass region, $m_H \approx 80 - 130$ GeV, which is the favored region for a SUSY Higgs boson, is the most difficult at the LHC. The CMS detector intends to cover this region with the rare decay $H \to \gamma\gamma$ [1]. The ATLAS detector covers down to $m_H \approx 110$ GeV with this mode, and requires 500 fb^{-1} to cover down to $m_H \approx 80$ GeV [2].

The dominant decay mode of the Higgs boson in this mass range is $H \to b\bar{b}$; the branching ratio is about 80%. There does not exist any established method to detect the Higgs in this decay mode at the LHC (see the section on the LHC for more details). It has been suggested that the process $q\bar{q} \to WH$, followed by $H \to b\bar{b}$ and leptonic decay of the W boson, could be used at the Tevatron to discover the light intermediate-mass Higgs boson [3, 4, 5]. This is discussed in the next section. This signal may be more difficult to detect at the LHC due to the very large top-quark background.

The most useful subleading decay mode of the Higgs boson in the light intermediate-mass range is $H \to \tau^+\tau^-$, with a branching ratio of about 8% [9]. It has been suggested that the process $q\bar{q} \to (W,Z)H$, followed by $H \to \tau^+\tau^-$ and $W,Z \to jj$ (j denotes a jet) could be used at the Tevatron for Higgs masses above the Z mass, roughly $m_H > 110$ GeV [4]. This is discussed in the third section. This process is hopeless at the LHC due to the enormous $(Z \to \tau^+\tau^-)jj$ background.

Precision electroweak data weakly favor a light Higgs boson, with the best fit from LEP and SLC data centered on $m_H \approx 100$ GeV. It is vital that we not leave the intermediate-mass Higgs window open, and the Tevatron can potentially play a crucial role in closing this window.

The standard Higgs model has a number of unappealing features, such as the *ad hoc* introduction of fundamental scalar fields with special interactions, and difficulties with naturally producing electroweak symmetry breaking at the weak scale rather than some much higher energy scale. A supersymmetric model ameliorates many of these problems. The minimal supersymmetric standard model requires two Higgs doublets, yielding a spectrum of Higgs bosons: two neutral scalars, h and H; a neutral pseudoscalar, A; and a charged pair, $H^\pm$. There is an upper bound on the mass of the lightest scalar, h, which depends on the top quark and top squark masses. For $m_t = 175$ GeV and $m_{\tilde{t}} < 1$ TeV, this bound is $m_h < 125$ GeV. The couplings of this Higgs boson to ordinary particles are usually very close to those of the standard Higgs boson. However, the coupling to bottom quarks (and τ leptons) is sometimes enhanced, which suppresses the rare decay to two photons. Thus there is a region of SUSY parameter space in which the h is invisible at the LHC. In fact, throughout most of this region, none of the SUSY Higgs particles are visible. Thus the $h \to b\bar{b}$ and $h \to \tau^+\tau^-$ modes at the Tevatron could be crucial for exploring the Higgs sector of the minimal SUSY model.

5.2 $q\bar{q} \to WH$ with $H \to b\bar{b}$

5.2.1 Introduction and Selection Cuts

The associated production of a Higgs boson and a W or Z boson, with the Higgs decaying to $b\bar{b}$ and the W or Z decaying leptonically, is a possible way to detect the Higgs in the mass range 60-130 GeV. As an example, the total Standard Model cross section for WH (Higgs mass 80 GeV) at $\sqrt{s} = 2\,TeV$ is $\approx 500fb$, and coupled with the 2/9 branching ratio of the W into electrons or muons, means that with small backgrounds one could consider such searches with integrated luminosities of less than $1fb^{-1}$. The question then becomes: What are the backgrounds? The Higgs decays give rise to 2 jets, thus we will start with the basic W+2 jet backgrounds. This will lead to the issue of b tagging, and the physics backgrounds that include a W and one or more b quarks. After considering the signal and all the backgrounds, we will observe the importance of dijet mass resolution, which appears to be the "make or break" issue in finding the Higgs in the W+H mode. We will compare the prospects for the same measurements at the LHC. We will also find that observing a Higgs with mass of 100-130 GeV is more complicated than 60-100 GeV. The 100-130 GeV Higgs search depends

critically on statistics and uncertain (at present) top backgrounds. We will discuss in some detail how much luminosity is needed to reduce the statistical *and* systematic uncertainties to an acceptable level to find the 100-130 GeV Higgs.

The default cuts in this note are those in ref [3], and are briefly summarized as follows: a) both b jets $p_t > 15\ GeV$ and $|y| < 2.0$, b) typical W cuts on leptons + missing E_t, and c) no extra jets with $p_t > 30\ GeV$ (or two extra jets above 15 GeV) and no extra leptons with $p_t > 20\ GeV$ to reduce top backgrounds. Jets were clustered with the CDF cone algorithm, with a 0.7 cone-size. By default we will make the b jet energy corrections CDF uses in the top search for vertex-tagged jets.

5.2.2 $W + 2$ Jet Backgrounds to WH, b tagging

A light, SM Higgs will decay to $b\bar{b}$ 82% of the time, $\tau\bar{\tau}$ 9%, $c\bar{c}$ 8%, and $s\bar{s}$ 1%. Without further information, each decay mode gives rise to two jets. We thus begin with the backgrounds from a leptonic W decay, and two jets. We will measure the rate of this directly from present CDF data, then multiply the rate by a factor 1.3 to convert to $\sqrt{s} = 2$ TeV. Figure 5.1 shows this measurement, along with the expected distribution from an 80 GeV Higgs, produced in association with a W. All of the Higgs distributions in this note will be generated with PYTHIA + CDF's best calorimeter simulation, and the number of events normalized with the calculated NLO cross sections. This figure shows the W+2 jet backgrounds are a 1000 times larger than the expected signal, thus we will need significant additional handles. Since b tagging is now well established, and the $b\bar{b}$ decay mode is largest, it is natural to investigate b tagging first.

Tagging b quarks using displaced vertices and semi-leptonic decays is now well established. Tagging efficiencies on the other hand are often confusing. The most common number quoted is the efficiency for tagging at least one b quark in a $t\bar{t}$ event. This number depends on many different factors and is irrelevant for almost anything else. The number one wants for any other physics is how often a single b jet with a given energy will be tagged, if that jet is inside the relevant detector. Then the problem can be broken down into two parts, the fiducial acceptance for a certain jet from a certain process, and how often that jet is tagged. For the WH process in Run II and beyond it is even simpler. Both b jets have $|y| < 2.0$ a large fraction of the time, and the present upgrades of CDF/D0 are expected to have b tagging capabilities within this region. Thus the problem reduces to the tagging efficiency versus b jet energy, and this is shown in figure 5.2 for the present CDF detector if the b jet is in the fiducial region of the SVX. The efficiency at high energies is above 50%, and falls off at lower energies due to the necessary cuts on track p_t. The present probability for a non-heavy-flavor jet faking a b tag is $\approx 0.5\%$. The 50% efficiency and 0.5% fake rate are only estimates of course for Run II, but some factors such as improved silicon or pixel detectors will make these better, and some factors such as multiple interactions will make them worse. And these estimates do not include soft lepton tagging of b quarks. We will use 50%/0.5% as our best estimate at this time.

Once we have an estimate of b tagging potential, the issue is whether to use single or double b tagging. With single b tagging, the signal efficiency is 50%, and S/B improvement is 100, with double tagging the signal efficiency is 25%, and S/B improvement 10000. Figure 5.3

shows the resulting signal and background distributions for the two cases, only considering the W+2 jet fake backgrounds. We conclude that the W+2 jet backgrounds are too large to use single b tagging, and double tagging with the present algorithm is certainly sufficient, but it appears there is room for a "loose" double tag method that would improve the signal efficiency. We will not pursue this further, and will use double b tagging with the 50%/0.5% estimates mentioned earlier. Other physics backgrounds that include two b quarks are not reduced by b tagging, and these are considered next.

5.2.3 Backgrounds to WH containing heavy quarks

There are six other notable backgrounds to the WH process, each containing two heavy quarks already. They are the $Wb\bar{b}$ process, the WZ process with $Z \rightarrow b\bar{b}$, $t\bar{t}$, $W^* \rightarrow tb$ (offshell W), W-gluon fusion (t+q+b final state), and $Wc\bar{c}$ with the charm faking a b quark. We will state briefly what we have used to estimate each of these backgrounds.

The largest background to the WH process is $Wb\bar{b}$ production, and for this we use the matrix element calculation of Mangano, interfaced with the HERWIG shower monte carlo and the CDF calorimeter simulation. Figure 5.4 shows four kinematic distributions of this background, compared to the WH signal. This calculation is already being checked with W+tagged jet data, the background for the top quark. The backgrounds to the top search are mostly W+heavy quark production, thus the agreement with data in the W+1 jet and W+2 jet bins, where the top contribution is small, is a test already of the Mangano calculation. In addition, fits to $c\tau$ in these bins are being used to separate the $W + b\bar{b}$ and $W + c\bar{c}$ contributions. For the $W + c\bar{c}$ contribution to the Higgs, we have simply scaled down $W + b\bar{b}$ by 1/10, due to the calculated equal production cross section(by two groups), and the tagging efficiency which is 1/3 of the b tagging efficiency..

The WZ process, with $Z \rightarrow b\bar{b}$, is estimated with PYTHIA + CDF calorimeter simulation, then the cross section is normalized to the calculated NLO cross section of Ohnemus. As the process is initiated by $q\bar{q}$, these cross sections should be reliable. In addition, this background has the feature that with a few fb^{-1} of data, one can use the clean all-leptonic decay channels to normalize the $b\bar{b}$ decay mode. Figure 5.5 shows four kinematic distributions of this background, compared to the WH signal.

We have used the HERWIG $t\bar{t}$ generator + CDF calorimeter simulation, with a 6200fb total cross section to model this background. As with $W + b\bar{b}$ and WZ, with a few fb^{-1} of data we should have enough $t\bar{t}$ events to understand them well. One complication from this background are "dilepton" events where both Ws decay leptonically, and one of the leptons is not detected. This part of the $t\bar{t}$ background is very detector and analysis specific, thus is hard to estimate. Since the $t\bar{t}$ backgrounds are small at the Tevatron, we can safely ignore this contribution at this time. The same is true of τ+jet backgrounds. Figure 5.6 shows four kinematic distributions of this background, compared to the WH signal.

We have used the PYTHIA W^* generator + CDF calorimeter simulation, with a total cross section of 594fb, to model this background. Figure 5.7 shows four kinematic distributions of this background, compared to the WH signal. And finally we used HERWIG + simulation to model the W-gluon fusion(tqb) background with a total cross section of 2360fb. Figure 5.8 shows four kinematic distributions of this background, compared to the WH sig-

nal. These two backgrounds are small at the Tevatron at lower masses, but nevertheless are significant for Higgs masses 100-130 GeV. They are an experimental challenge in their own right, as they mix with each other, and with the much larger $t\bar{t}$ events.

Figure 5.9 summarizes all the backgrounds to the WH process. One can see that $W + b\bar{b}$ dominates at low masses, with the top backgrounds becoming significant for masses above 100 GeV. In table 5.2.8 we have compared our results for each background, in the different signal regions, with the reference [3] results. Overall they are very close for the important backgrounds, while there are remaining discrepancies with the small top backgrounds. The increase in the $W + b\bar{b}$ backgrounds at the fully simulated jet level, compared to the parton level used in reference [3], we believe is due to lower energy b partons fluctuating to higher energy due to detector effects.

5.2.4 Signal+Background Distributions

We have two choices to make before showing signal+background distributions, 1) optimized or non-optimized cuts, and 2) optimized or non-optimized jet resolutions. Reference [7] describes fairly sophisticated cuts at the parton level which give a x4 better S/B ratio than the cuts in reference [3] which we are using. The optimized cuts come from the $b\bar{b}$ angles, the center-of-mass scattering angles, and the total invariant mass of the event. We have investigated some of these optimized cuts very briefly, and do see improvements in S/B. But one complication with trying to use optimized cuts is that they will certainly be mass dependent, and different for the Tevatron and LHC which we compare later. Thus without further investigation we will assume as a default that we can maintain a x2 improvement in S/B at the full simulation level, then show later the effect of removing this improvement completely in a worst case scenario. Likewise for jet resolutions, we will pick a resolution as a default that is better than we currently observe from the simulation, but which is reasonable to assume can be achieved with more study. We will give the details of the jet resolutions we are using in the next section.

Figure 5.10 shows the signal+background distributions for Higgs masses 60,80,100,120 GeV for 1 fb^{-1} of data, with our "nominal" jet resolutions and the x2 improvement in S/B. The solid lines are the signal+background, while the dashed line is the sum of all backgrounds. Clearly this is not enough data to see anything. With 5 fb^{-1} of data, one can see the signal begin to emerge at lower masses in figure 5.11. With 10 fb^{-1} of data, figure 5.12 shows the signals for masses below 120 GeV have become more pronounced, while the 120 GeV Higgs is still not clearly seen. The excess at 60 GeV is more than 9 standard deviations above background, 80 GeV is more than 7 sigma, and 100 GeV is 4.9 sigma. These numbers are all without systematic uncertainties, of course, but in this mass range the dominant backgrounds will be $W + b\bar{b}$ and WZ, which should be well-understood by this time. Figure 5.13 is a blowup of the higher mass plots. There is a small excess at 120 GeV, but with only a small number of events and uncertain single top backgrounds this will be more difficult. In a later section we will discuss how much luminosity will be needed to find a 120 GeV Higgs, and whether it is possible Z+H signals can be used to supplement the high mass search.

We now present three variations of the plot for 10 fb^{-1}, in order to illustrate the sen-

sitivity to jet resolutions and optimized cuts. Figure 5.14 is the same plot, except using the present jet resolutions the simulation is giving. The clear peaks in the previous plot are now smeared out. As mentioned earlier, we feel with more study the resolution can be improved to the level of our choice of "nominal" resolution, this is discussed in a later section. If one uses the jet resolution used in reference [3], which is more optimistic than our "nominal", one gets sharper peaks as displayed in figure 5.15. In fact the 120 GeV Higgs starts to become noticeable, albeit still low statistics. Finally, we display the same plots with the best jet resolution, but with the x2 improvement in cuts removed. This is shown in figure 5.16, and corresponds to repeating the reference [3] study but with a full simulation of all the backgrounds, while keeping the signal mass resolution constant. Clearly the effect of optimized cuts is also very important in the Higgs search.

5.2.5 Comparison with LHC

We will make a simple extrapolation of the Tevatron studies to estimate the capability of the LHC to make the WH measurements. We will simply repeat the Tevatron analysis, but increase the number of events by the ratio of cross sections as given by HERWIG or PYTHIA, 14 TeV/2 TeV. This is optimistic in favor of the LHC for 2 reasons, the signal efficiency due to the extra jet cut is reduced at the LHC since there is more initial state radiation. This was checked with PYTHIA and the reduction is not that large, from 92% efficiency at the Tevatron to 72% at the LHC. The second reason this is optimistic is that the details of the $t\bar{t}$ backgrounds become important at the LHC, for example the ignored dilepton top events may be a significant background at the LHC. Nevertheless, it is very instructive to simply repeat the same analysis, with the same monte carlo data, with different total cross sections. The cross section ratios used are: 1) WH 60 GeV = 7.0, WH 80 GeV = 7.68, WH 100 GeV = 8.53, WH 120 GeV = 9.54, 2) WZ = 9.2, 3) $W + b\bar{b}$ and $W + c\bar{c}$ = 6.24, 4) $t\bar{t}$ = 104, 5) W^* = 12, 6) tqb = 85, 7) W+2 jet = 13. Figure 5.17 shows all the backgrounds to the WH process at the LHC. Compared to the Tevatron, it is clear the top quark backgrounds become important at much lower masses, since the cross section ratios for those backgrounds are so large. Figure 5.18 shows the signal and background distributions for the LHC. A 60 GeV Higgs clearly stands out, since the main background there is still $W + b\bar{b}$, but 80-100 GeV masses appear more difficult to observe at the LHC than at the Tevatron due to the increased top backgrounds.

5.2.6 Dijet Mass Resolutions

As mentioned previously, the issue of jet energy resolution, or more accurately dijet mass resolution, is crucial to finding the Higgs in Run II. We have used three different mass resolutions, now we specify what those are: 1) The "best" resolution, used in reference [3], is $0.8/\sqrt{M}+0.03$, with the two terms added in quadrature. This gives a 7.5 GeV resolution at 80 GeV. 2) The "nominal" resolution, $1.0/\sqrt{M}+0.03$, with the two terms added linearly. This gives an 11.3 GeV resolution at 80 GeV. 3) The "worst" resolution, which is from the full simulation results without optimization, gives a resolution of 15.5 GeV at 80 GeV.

To investigate the source of the increase in resolution with the full simulation, we gen-

erated a sample of single W events, with the W decaying to 2 jets. When matching the daughter quark direction to the measured jet direction, there is a large peak near zero in delta-R, but also a well-known long tail expected from hard gluon radiation. If we separate the events into two classes, delta-R>0.2 and delta-R<0.2, we get two very different W mass distributions, the small delta-R peaked at 80 GeV with an 11 GeV RMS, while large delta-R peaked at 60 GeV and very broad. The combined distribution has an RMS of 15.5 GeV, shown in figure 5.19. The events with large delta-R have been checked and an extra jet does appear in the detector most of the time. Thus one large component of the dijet mass resolution is from physics, and does not depend on the detector. Clearly an intelligent algorithm needs to be developed to include these extra jets, whether with the cone algorithm or the Kt algorithm. Additional improvements in dijet mass resolution are possible by using charge tracks, shower maximum detectors for photons, etc. It clearly is crucial for this physics to improve the dijet mass resolution in all ways possible, whether by physics effects or detector effects.

One other concern is that we will optimize our jet resolutions, then lose it all due to multiple interactions. To investigate this we generated the 80 GeV signal events with 5 additional interactions (6 total), and 8 additional interactions (9 total). Figure 5.20 shows the mass resolution for the 6 interaction case, the mean has shifted but the width has not significantly increased. The same was true of the 9 interaction case. This is with a cone radius 0.7, with smaller cones one will be less sensitive, with larger cones or perhaps a Kt algorithm we will be more sensitive to pileup. And the extra interactions may harm any algorithm we devise to merge in soft extra jets. But with the basic algorithm used in this note, additional interactions do not seem to be a problem in mass resolution.

5.2.7 Masses above 100 GeV

It has been shown that the Higgs masses above 100 GeV are more difficult to observe than the lower masses. This is mostly due to the smaller cross sections, but also due to the top backgrounds that only contribute at larger masses. Here we will discuss briefly what it might take to observe a 120 GeV Higgs. This will include how much data it would take, using only the WH mode, as well as the possibility of using the Z+H mode, which do not have top backgrounds.

In figure 5.13 there is a closeup of the 120 GeV Higgs with 10 fb^{-1}. If one takes an objective mass range such as the Willenbrock range, without looking at the data fluctuations, then there is a 3.3σ statistical excess in this plot from 102-141 GeV. Namely 27 events on a background of 65. If one simply scales this up to get a 5σ excess, one needs $\approx 25 fb^{-1}$ of data. Then there are systematics. Of the 65 background events 19 are from top backgrounds. Thus assuming the other backgrounds are known well, one would have to have a total systematic on the combined top backgrounds of $\approx 25\%$ to get a 5σ excess. There will certainly be measurements of W^* and tqb production with 10 fb^{-1} or less, but not only will the cross sections need to measured independently, but how often they pass the tight Higgs analysis cuts needs to be estimated. We believe it likely that this can be done accurately with 25 fb^{-1}, but probably not with only 10 fb^{-1}. Thus from both the statistics and systematics of the analysis, it seems 25 fb^{-1} is necessary to measure a 120 GeV Higgs in the WH channel

alone.

If one is only trying to find the Higgs, rather than measuring the WH coupling alone, then perhaps Z+H modes could supplement the 120 GeV Higgs search and make it possible with only 5-10 fb^{-1}. The events with a Z decay to electrons and muons only add about 15% to the WH cross section, so this is not much help. The $Z \to \nu\bar{\nu} + H \to \tau\bar{\tau}$ mode has been investigated by D0 and does not look promising. The $Z \to \nu\bar{\nu} + H \to b\bar{b}$ mode offers another possibility. We have generated this mode with Pythia, and find the signal can be triggered on with 85% efficiency in CDF with the missing-Et trigger of 35 GeV. The question then becomes the backgrounds, which would be a useful study to pursue in detail in the future.

5.2.8 Conclusions for $q\bar{q} \to WH$ with $H \to b\bar{b}$

We have investigated the potential to observe the Higgs particle in the production mode $W + H \to l\nu + b\bar{b}$ at the Tevatron. We find that with 25 fb^{-1} this process will enable the observation of a Higgs boson up to $m_H \sim 120$ GeV/c^2.

With modest improvements to jet energy resolutions, a 60-100 GeV Higgs is observable with just 5-10 fb^{-1}. Physics effects appear to play an important role in the dijet mass resolutions, thus studies of jet clustering may be more important than detector resolutions. Discovering a 100-130 GeV Higgs in this mode alone, with only 5-10 fb^{-1}, will be more difficult because of low statistics and somewhat uncertain single top backgrounds, and argues for more luminosity. For any mass range, the significance of the observation can be strengthened through use of the Z+H production modes, and also using the $H \to \tau^+\tau^-$ channel discussed in Section 5.3 following.

We have also evaluated the potential of the LHC to make the same measurement, and find that for Higgs masses less than 70 GeV/c^2, the LHC measurement is easier than the Tevatron due to better statistics, but for masses greater than 70 GeV/c^2, the LHC measurement is much more difficult due to larger top backgrounds.

Some more general conclusions about Light Higgs detection at the Tevatron are given in Section 5.5.

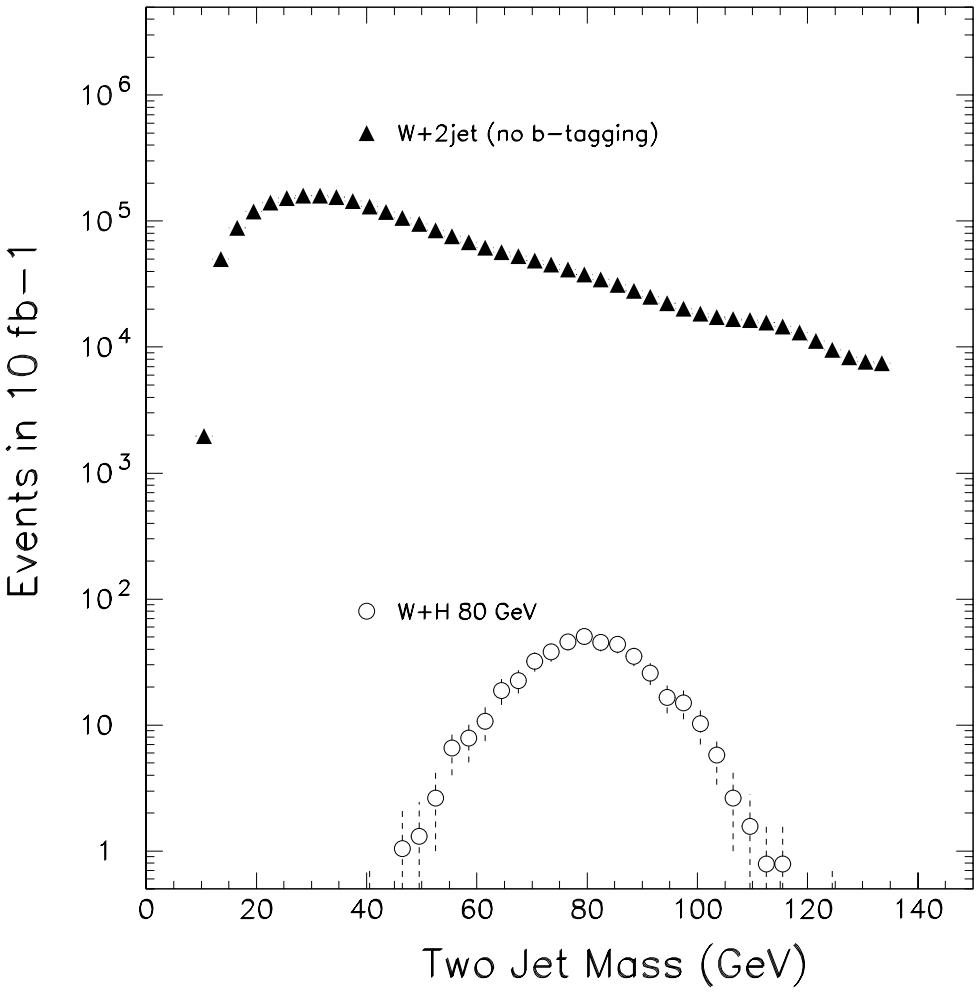

Figure 5.1: The W+2 jet mass distribution measured with CDF data and the expected W+H signal, all before b tagging is applied.

Process	Total σ (fb)	$\sigma \times$BR (fb)	Ref. [3] # Partons in 10 fb^{-1}	This Study # Partons in 10 fb^{-1}	This Study # Jets in 10 fb^{-1}
WH (60 GeV)	1260	230	221	250	166
WZ	3192	110	0	7	7
$W + bb$	50607	11246	300	322	564
$t\bar{t}$	6200	1837	8	21	5
W^*	594	132	30	10	9
tqb	2366	526	11	5	15
WH (80 GeV)	575	105	138	120	98
WZ	above	above	83	69	69
$W + bb$	"	"	194	216	270
$t\bar{t}$	"	"	8	33	4
W^*	"	"	44	22	29
tqb	"	"	16	12	12
WH (100 GeV)	289	53	75	60	52
WZ	above	above	102	104	77
$W + bb$	"	"	125	113	134
$t\bar{t}$	"	"	11	30	5
W^*	"	"	55	28	21
tqb	"	"	13	17	12
WH (120 GeV)	155	28	38	33	27
WZ	above	above	8	0	16
$W + b\bar{b}$	"	"	86	92	77
$t\bar{t}$	"	"	13	38	9
W^*	"	"	58	27	17
tqb	"	"	11	27	11

Table 5.1: Comparison of Stange et al. results and this study's results. The Stange et al. results have been renormalized to a 50% b-tagging efficiency. The bins for all of the signal and background numbers are the same as the Stange paper: 1) 60 GeV Higgs, 48-72 GeV; 2) 80 GeV Higgs, 66-96 GeV; 3) 100 GeV Higgs, 84-117 GeV; 4) 120 GeV Higgs, 102-141 GeV.

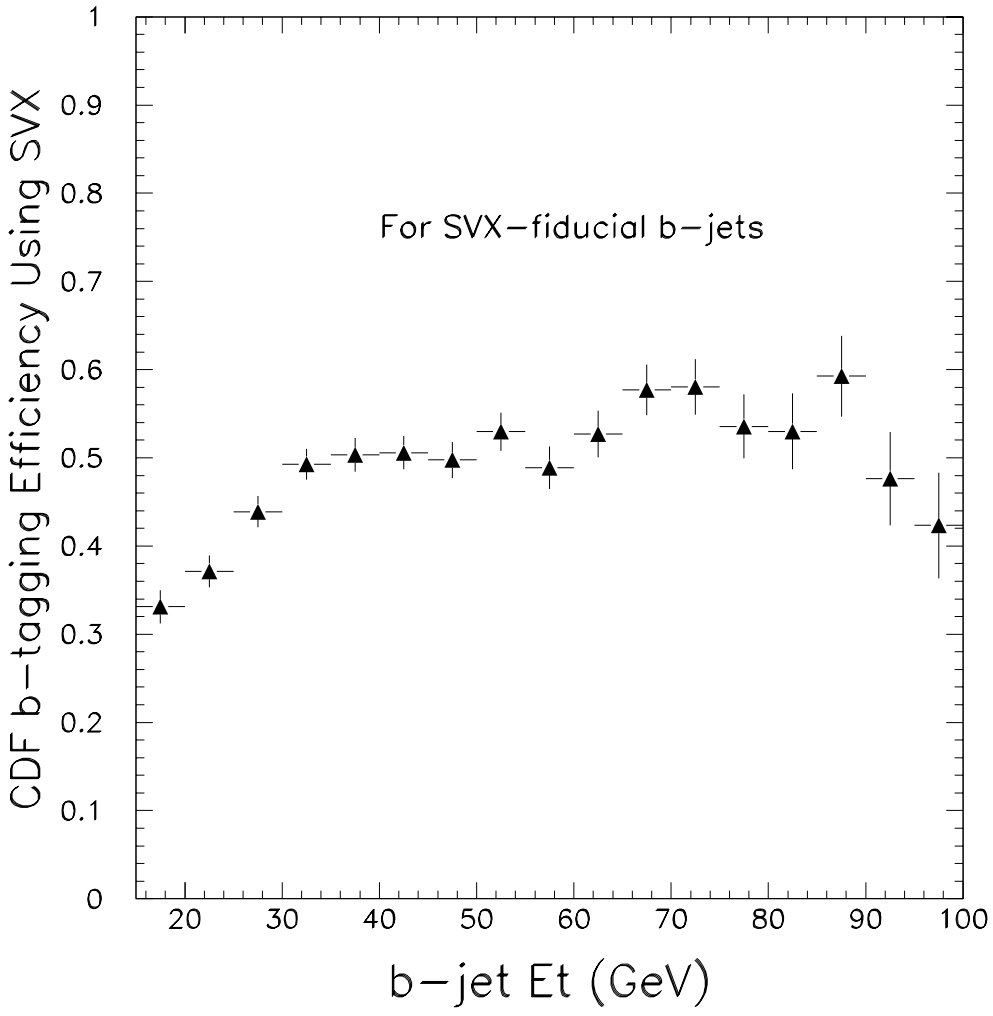

Figure 5.2: The present CDF SVX b tagging efficiency if the b jet centroid is inside the SVX. This represents a reasonable guess for what the b tagging efficiency for the WH process in Tevatron Run II and beyond will be.

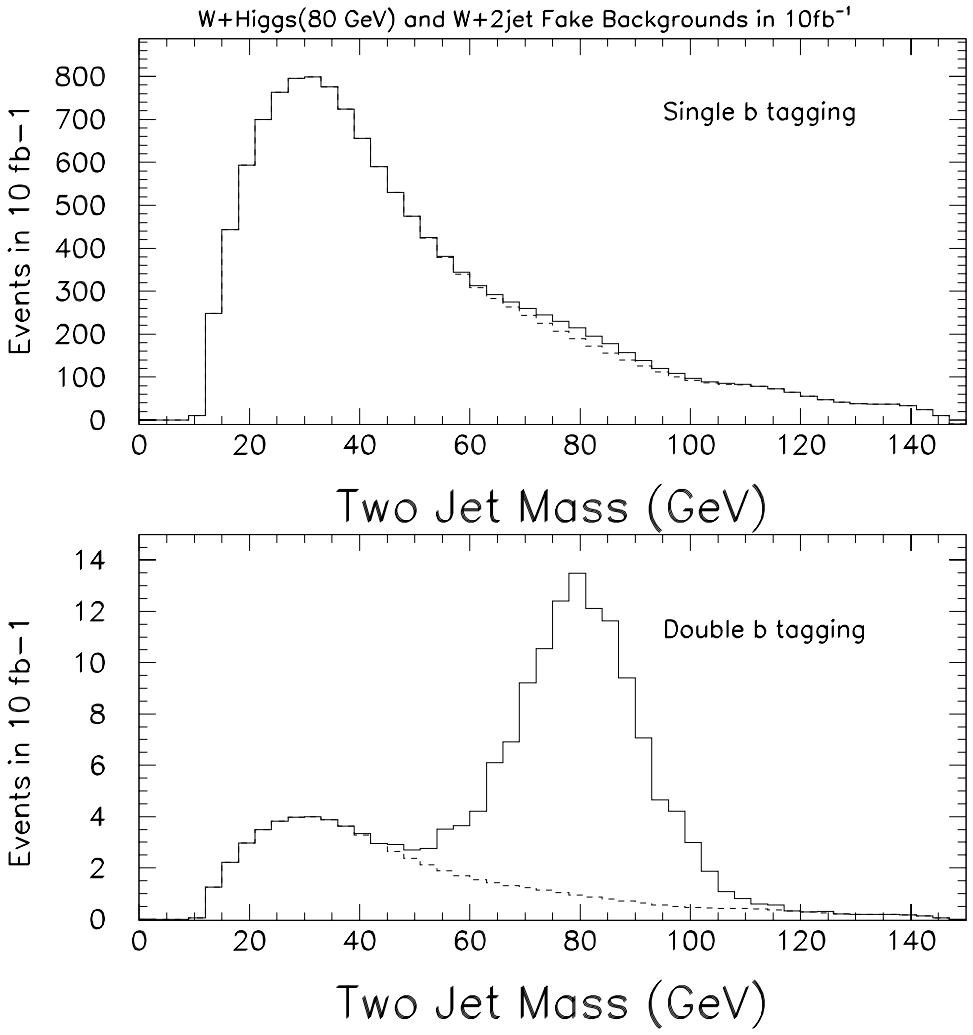

Figure 5.3: The signal+background and background only distributions for single and double b tagging. The background in this case only includes the W+2 jet backgrounds with fake b tag(s).

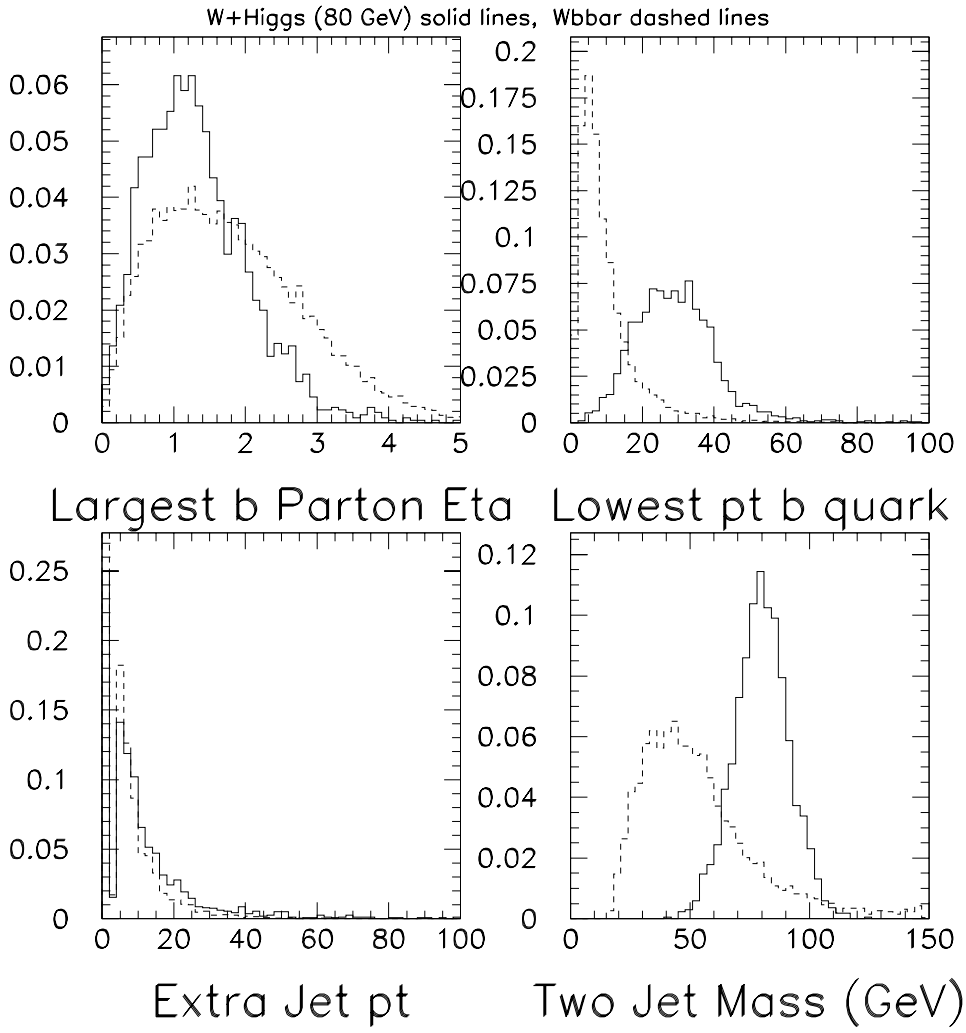

Figure 5.4: Various kinematic properties of the W+Higgs signal (solid) and the $W + b\bar{b}$ backgrounds (dashed). Shown are the largest b parton η, the smallest b parton p_t, the third jet p_t distribution, and the $b\bar{b}$ invariant mass distribution.

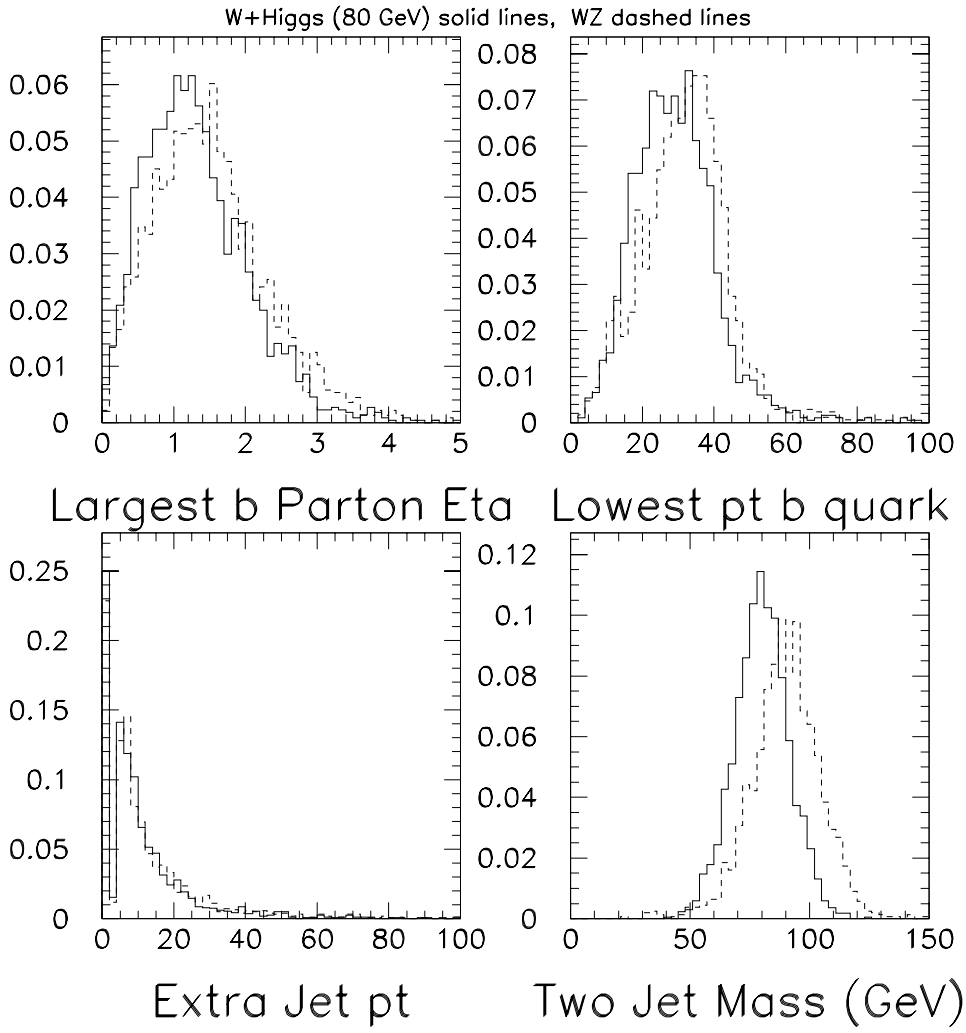

Figure 5.5: Various kinematic properties of the W+Higgs signal (solid) and the WZ backgrounds (dashed). Shown are the largest b parton η, the smallest b parton p_t, the third jet p_t distribution, and the $b\bar{b}$ invariant mass distribution.

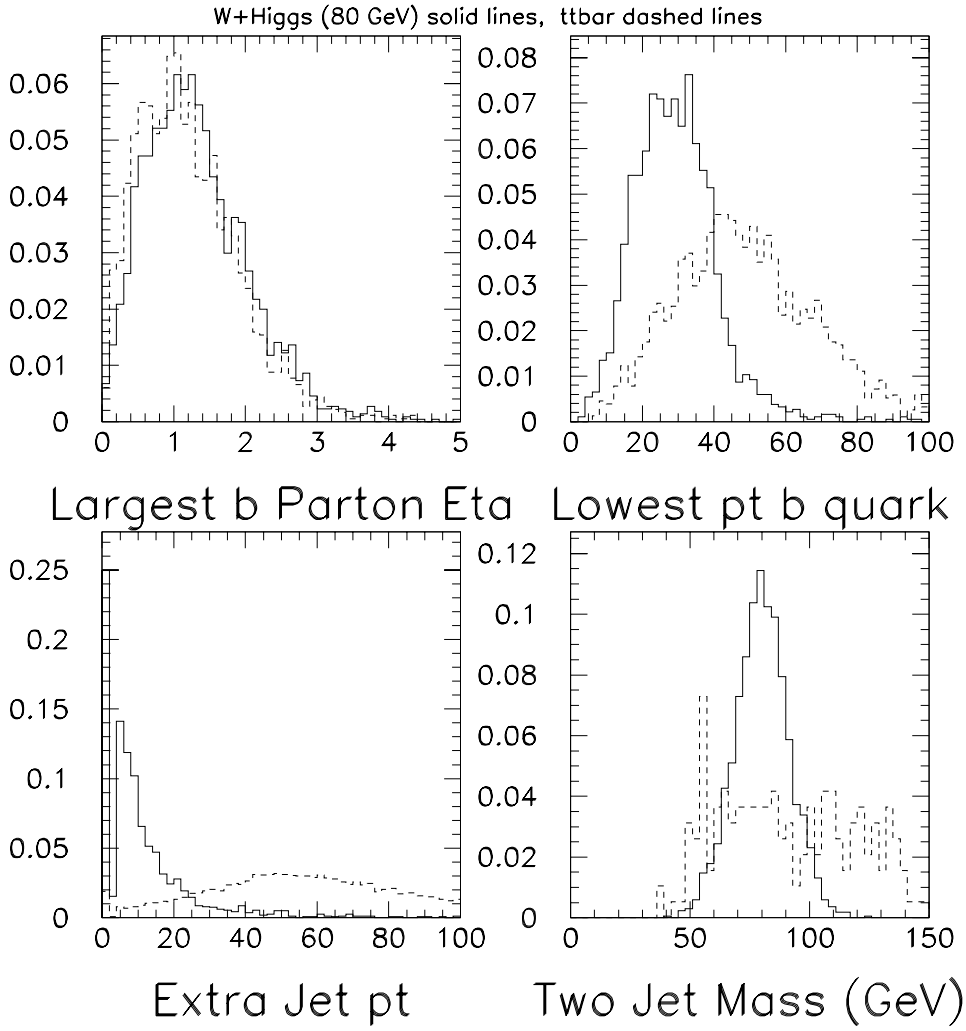

Figure 5.6: Various kinematic properties of the W+Higgs signal (solid) and the $t\bar{t}$ backgrounds (dashed). Shown are the largest b parton η, the smallest b parton p_t, the third jet p_t distribution, and the $b\bar{b}$ invariant mass distribution.

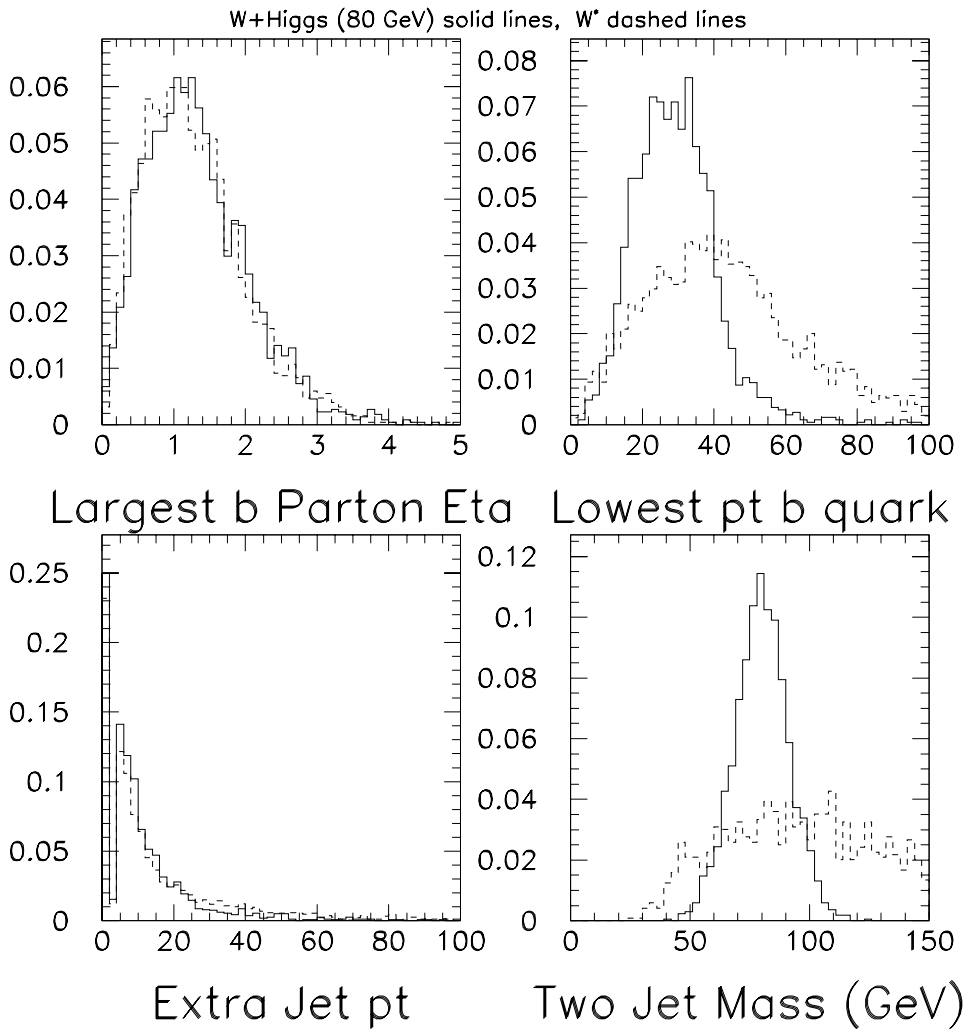

Figure 5.7: Various kinematic properties of the W+Higgs signal (solid) and the W^* backgrounds (dashed). Shown are the largest b parton η, the smallest b parton p_t, the third jet p_t distribution, and the $b\bar{b}$ invariant mass distribution.

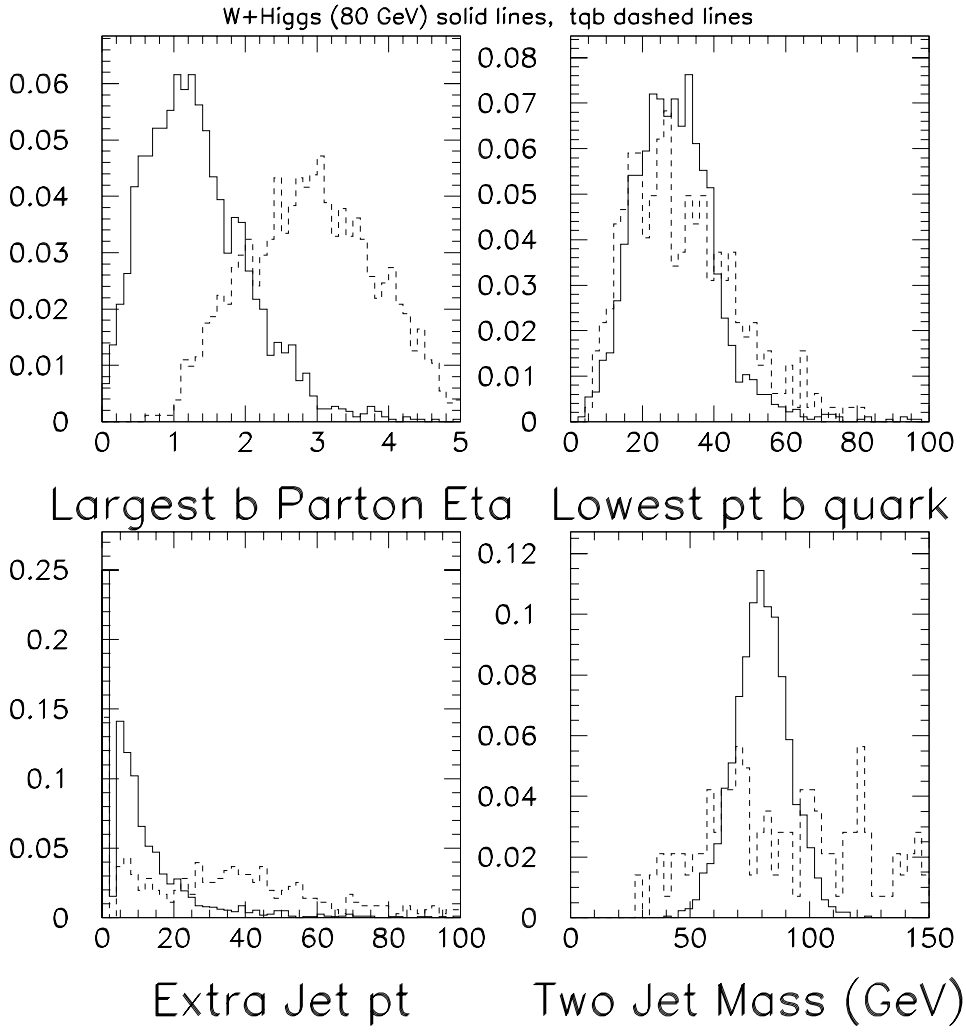

Figure 5.8: Various kinematic properties of the W+Higgs signal (solid) and the tqb backgrounds (dashed). Shown are the largest b parton η, the smallest b parton p_t, the third jet p_t distribution, and the $b\bar{b}$ invariant mass distribution.

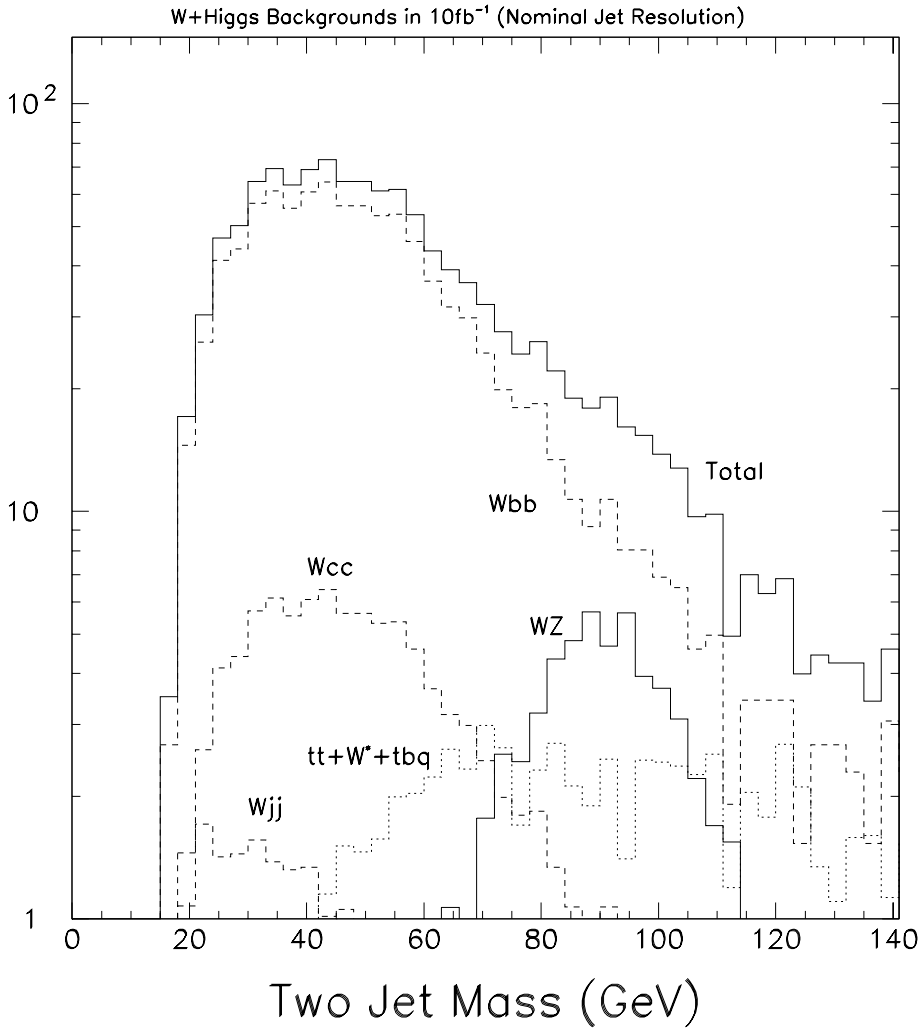

Figure 5.9: The 2 jet mass distributions for the backgrounds to the WH process. Double b-tagging is assumed for each.

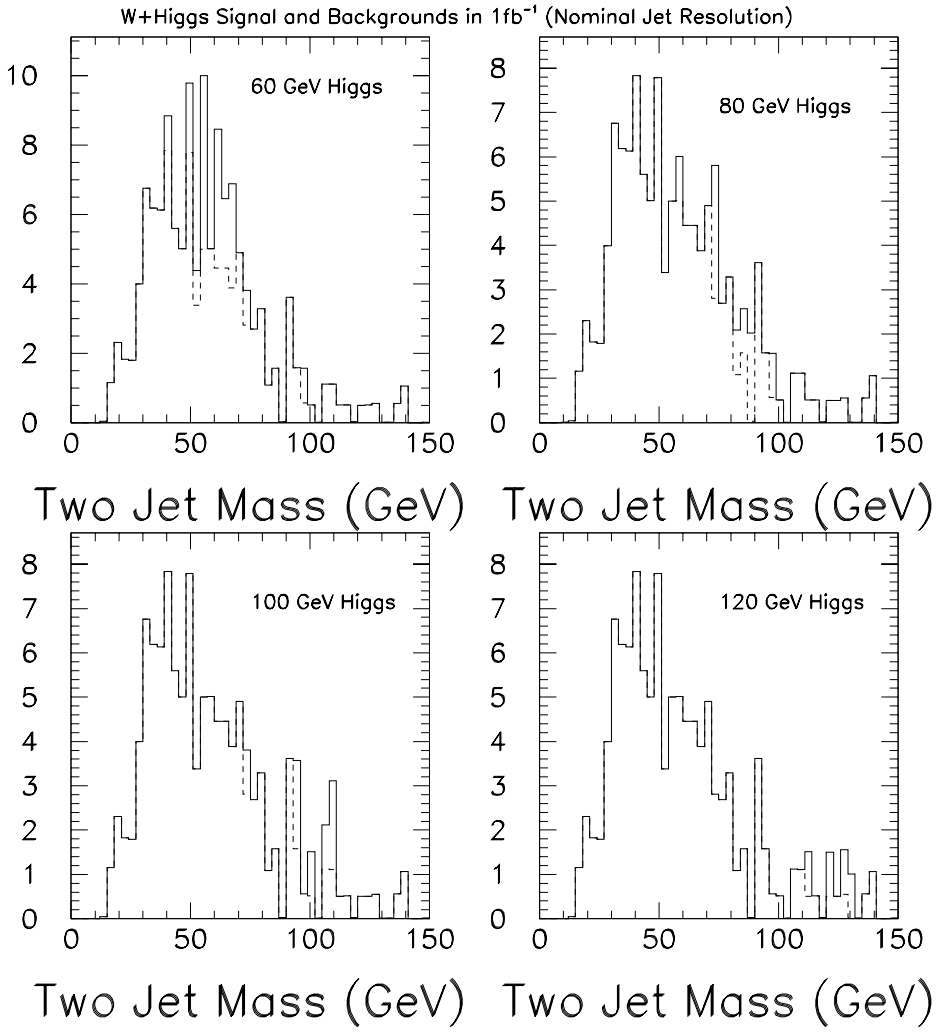

Figure 5.10: The signal+background mass distributions for the WH process with 1 fb^{-1} of data at 2 TeV. The solid line is signal+background, the dashed line the sum of all backgrounds.

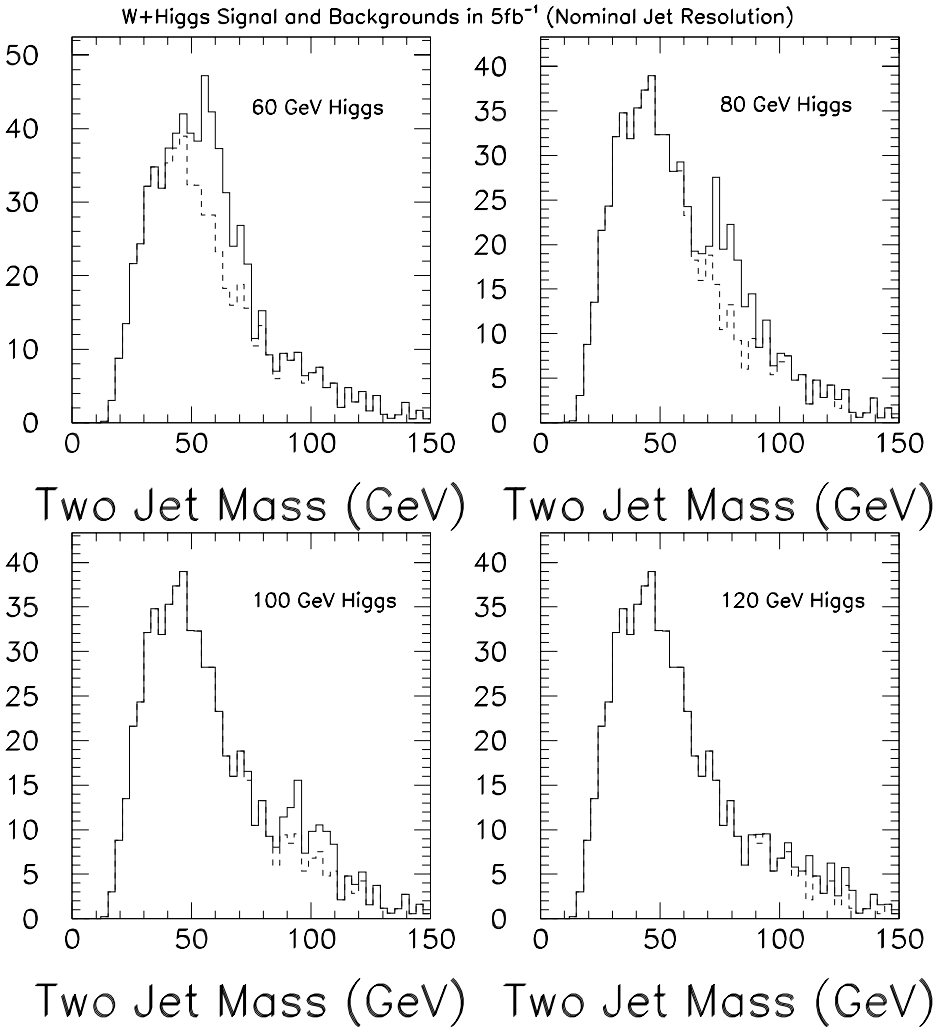

Figure 5.11: The signal+background mass distributions for the WH process with 5 fb^{-1} of data at 2 TeV. The solid line is signal+background, the dashed line the sum of all backgrounds.

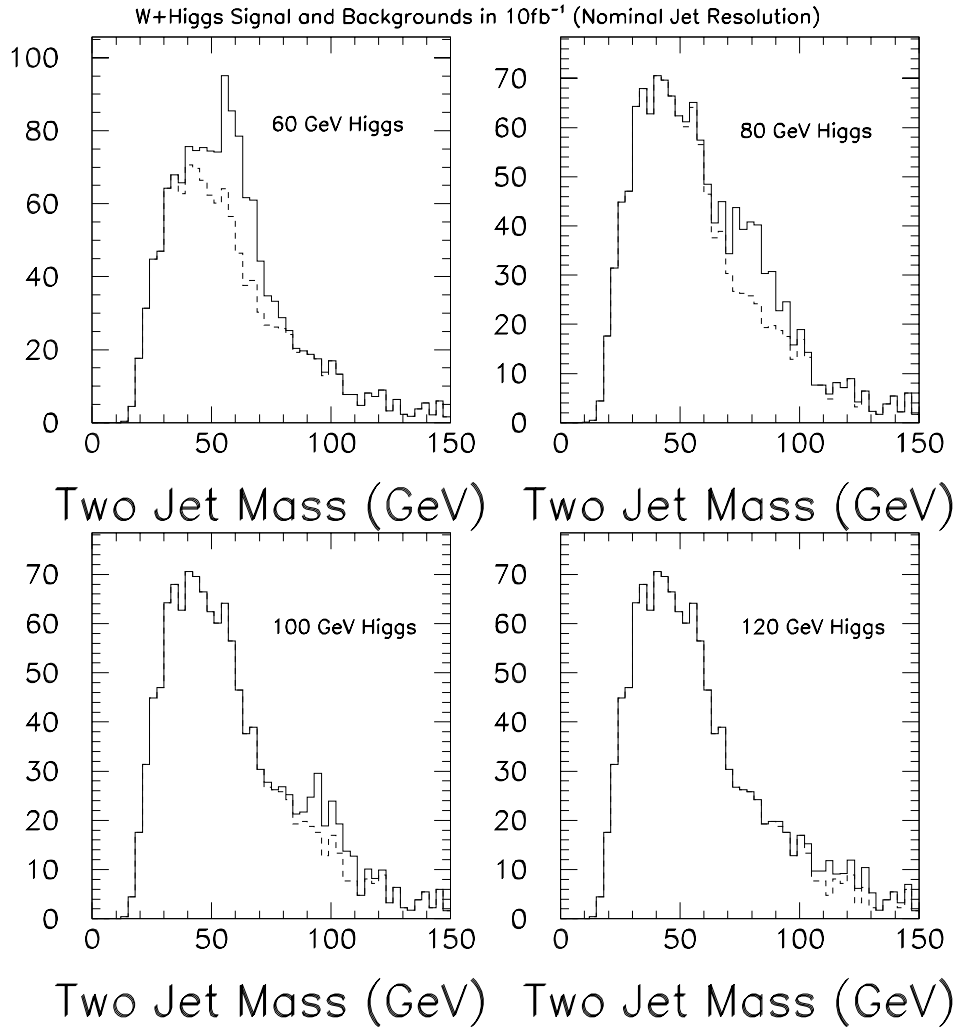

Figure 5.12: The signal+background mass distributions for the WH process with 10 fb^{-1} of data at 2 TeV. The solid line is signal+background, the dashed line the sum of all backgrounds.

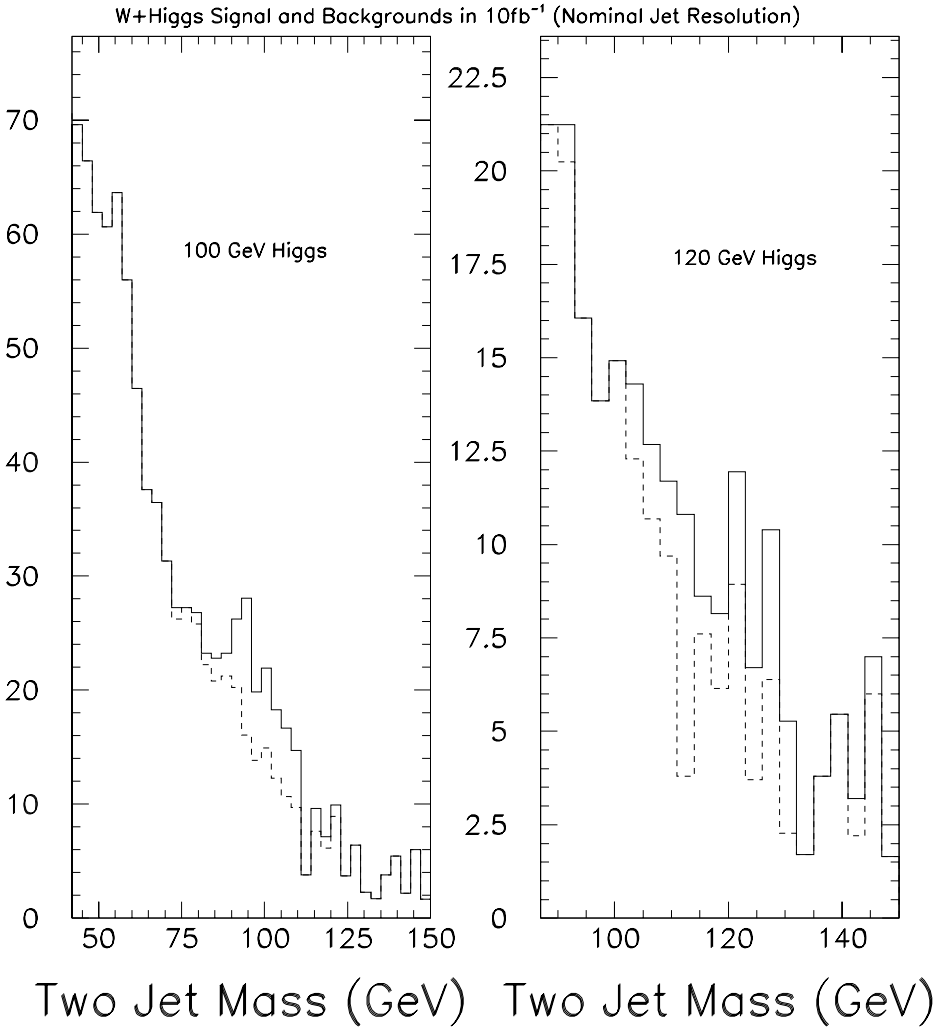

Figure 5.13: Same as the last figure but only the highest two masses.

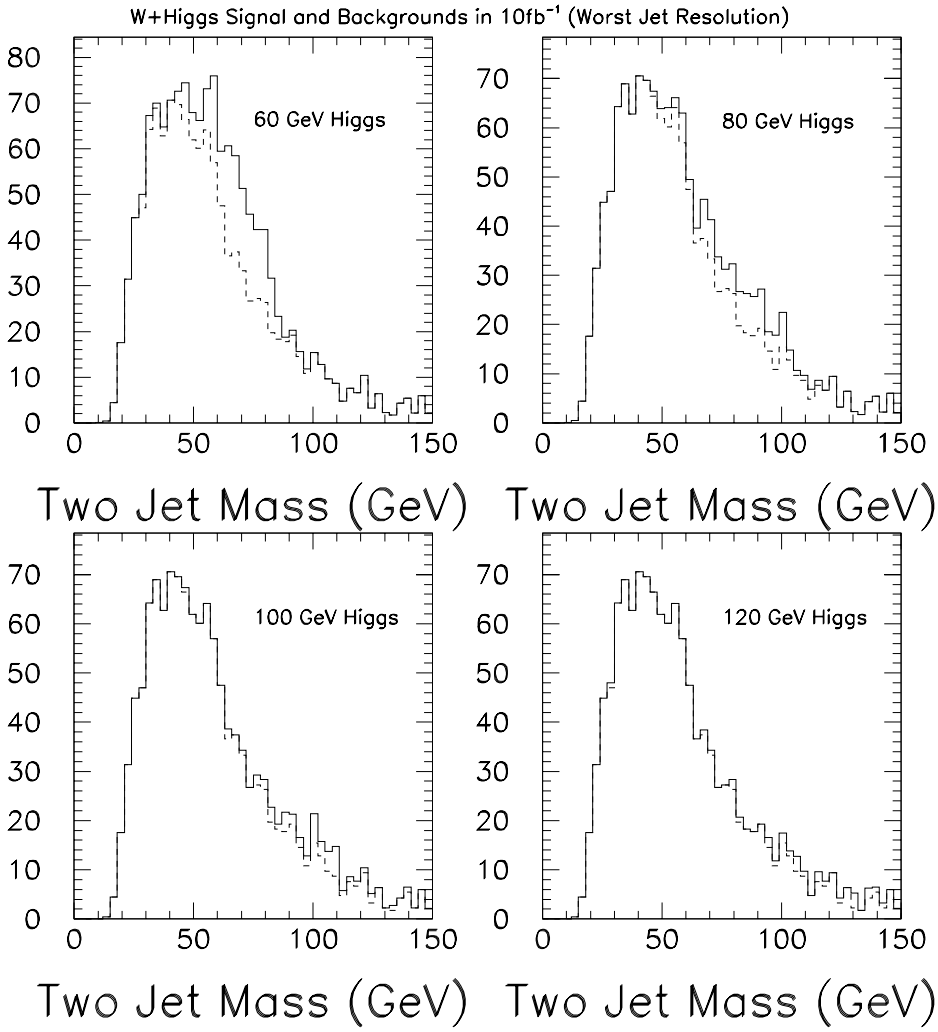

Figure 5.14: The signal+background mass distributions for 10 fb^{-1} of data, but with a worse jet resolution compared to the nominal.

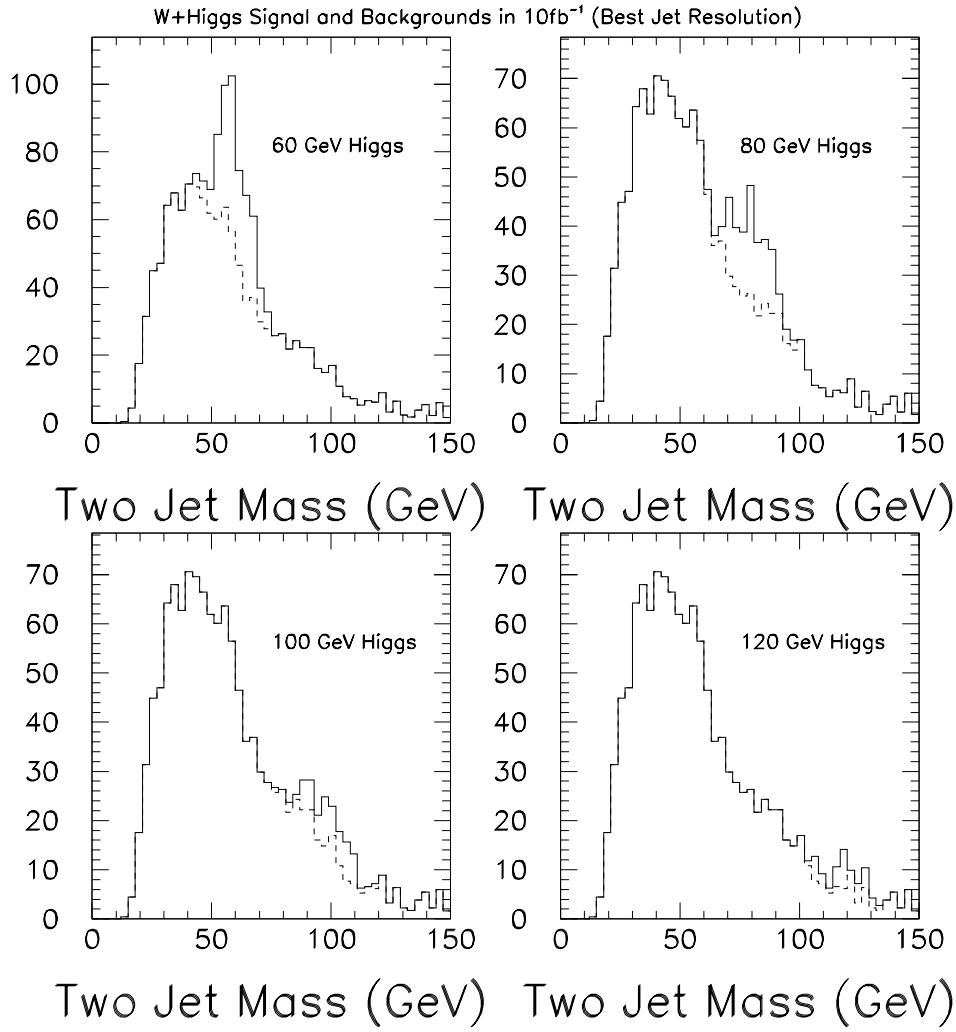

Figure 5.15: The signal+background mass distributions for 10 fb^{-1} of data, but with a better jet resolution compared to the nominal.

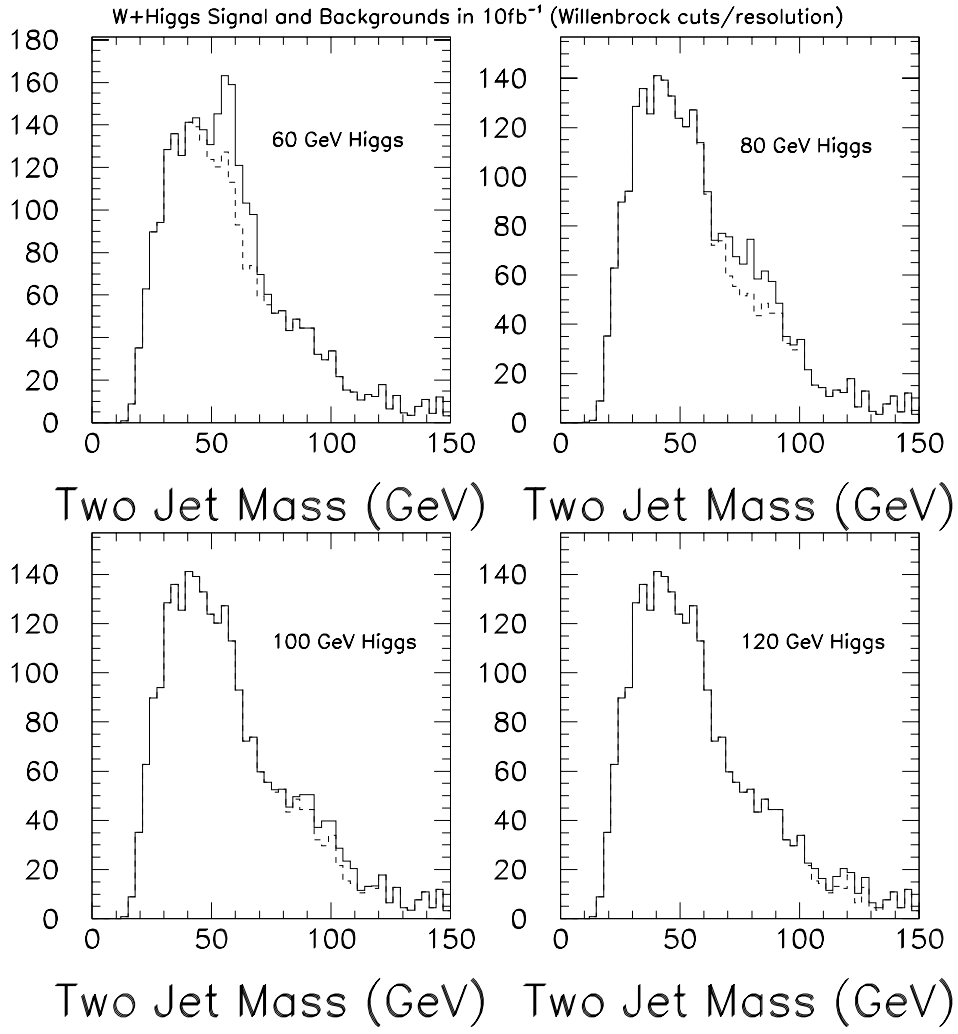

Figure 5.16: The signal+background mass distributions for 10 fb^{-1} of data, using the better jet resolution of the previous plot but removing the effect of optimized cuts.

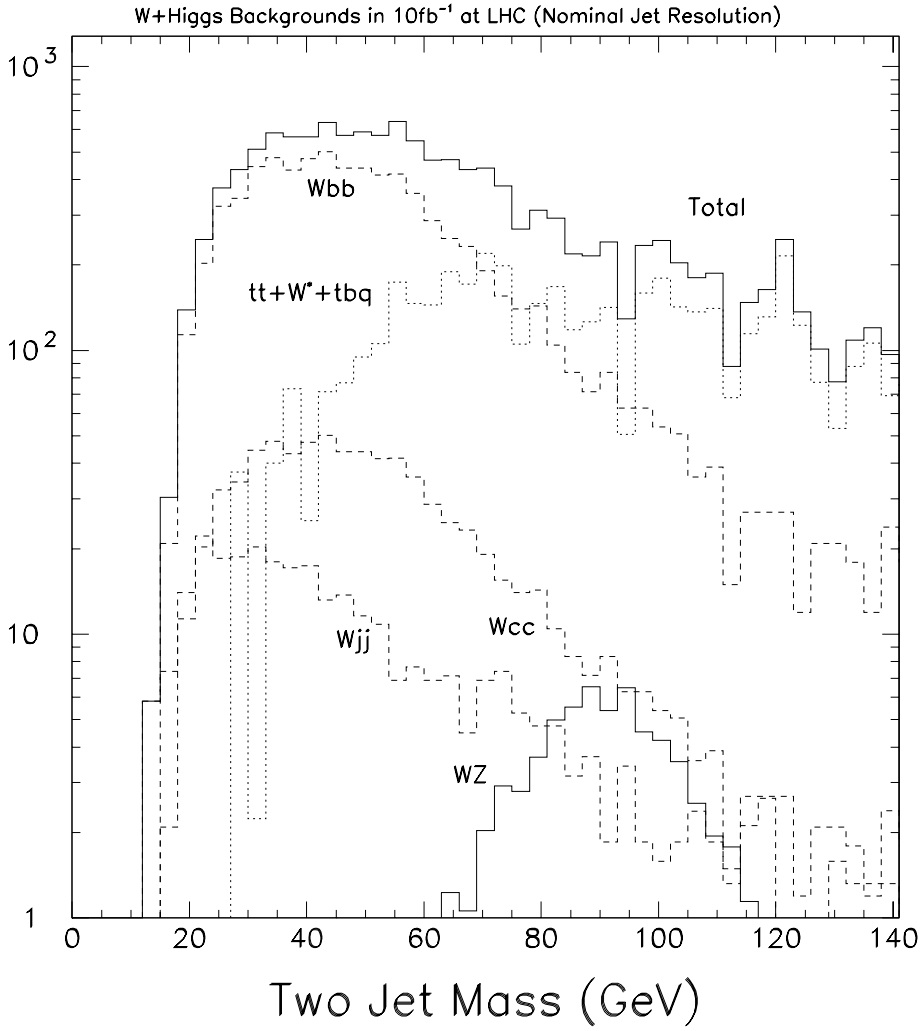

Figure 5.17: The background mass distributions for the WH process with 10 fb^{-1} of data in pp collisions at 14 TeV.

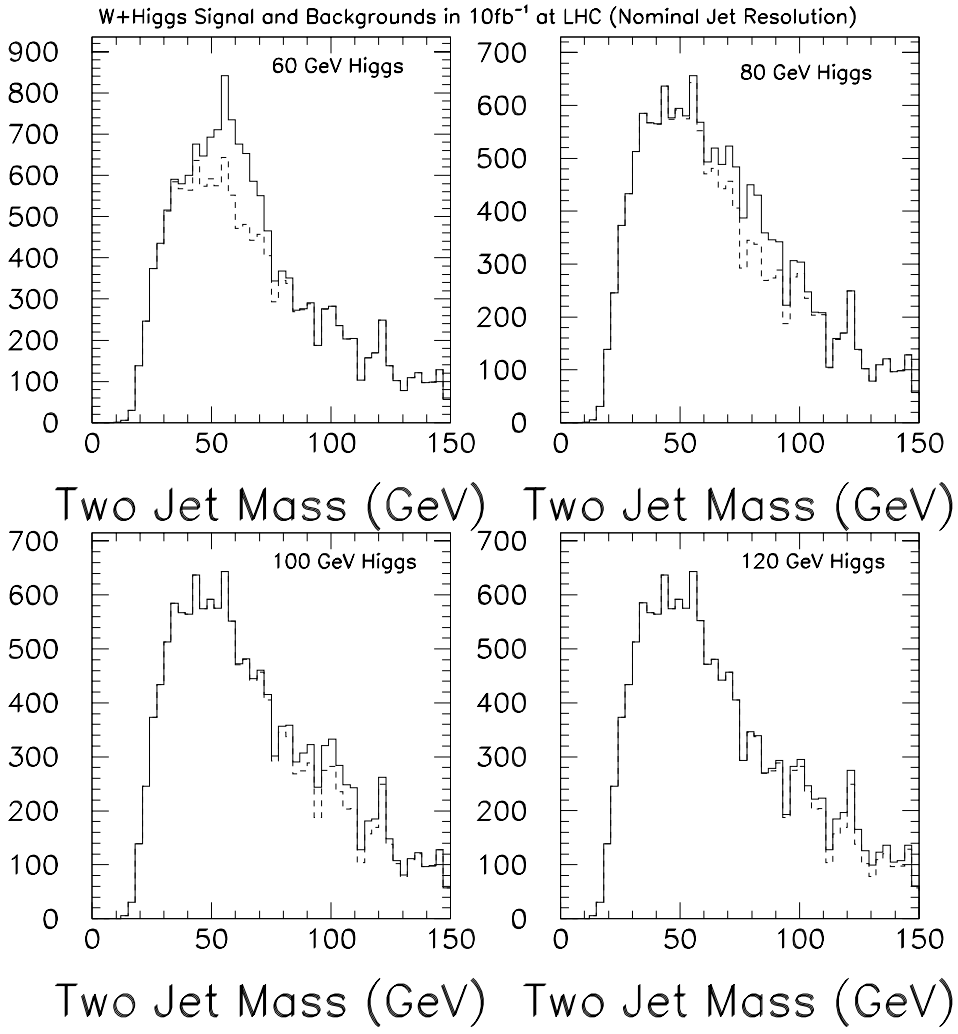

Figure 5.18: The signal+background mass distributions for the WH process with 10 fb^{-1} of data in pp collisions at 14 TeV. The solid line is signal+background, the dashed line the sum of all backgrounds.

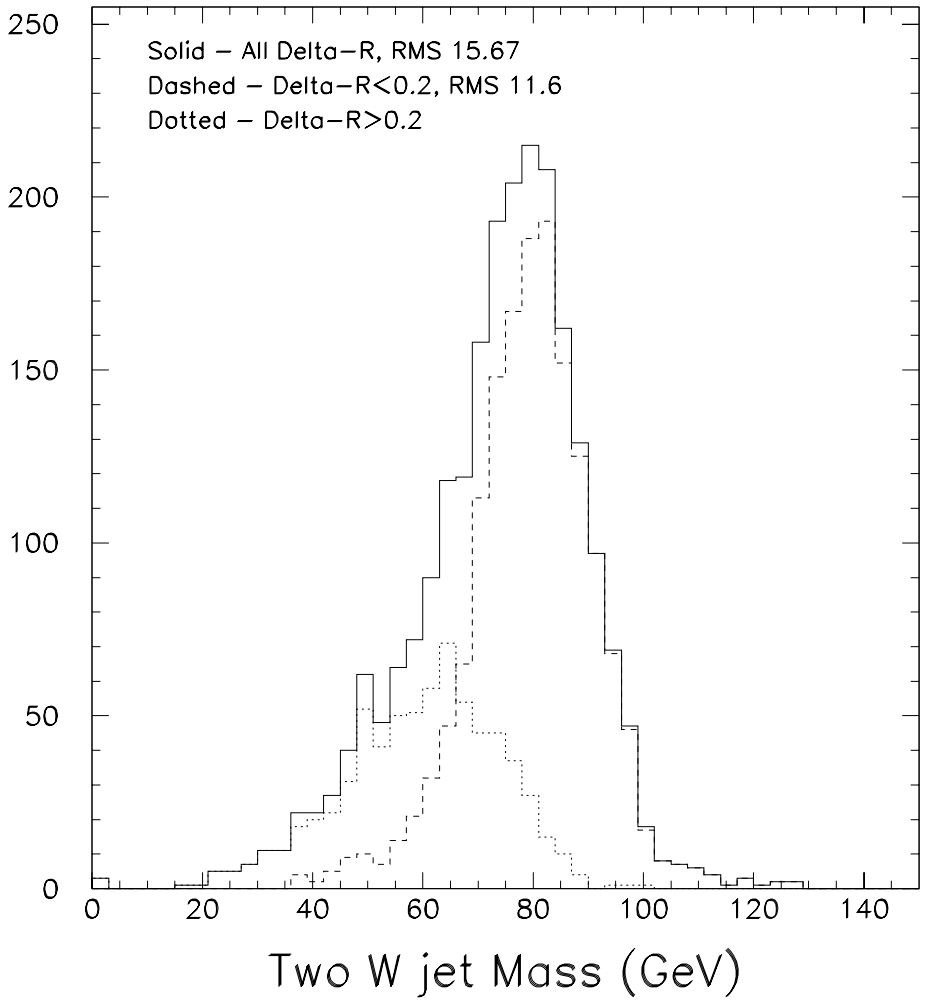

Figure 5.19: The 2 jet mass distribution from a W decay. The solid distribution is for all events, the dashed is for those events when the match between parton and jet is less than 0.2, the dotted is when the match is greater than 0.2.

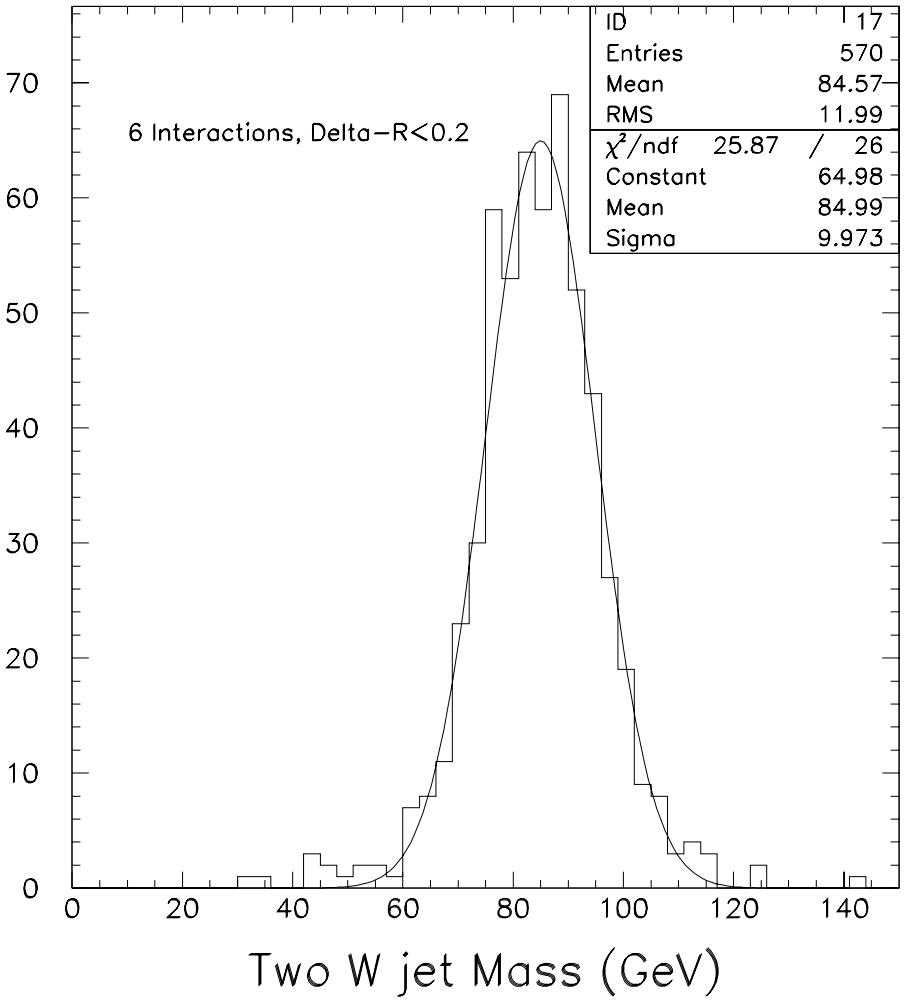

Figure 5.20: The 2 jet mass distribution from a W decay with six interactions.

5.3 $q\bar{q} \rightarrow (W, Z)H$ with $H \rightarrow \tau^+\tau^-$

The motivation for this work was derived from a paper by S. Mrenna and G. Kane [4], which suggests that all (W,Z)H channels should be combined, and that the $H \rightarrow \tau^+\tau^-$ channel adds to the $W + H \rightarrow \ l + \nu + b + \bar{b}$ channels to give good statistical significance for Higgs masses up to 130 GeV/c^2 in a data set over 10 fb^{-1}.

5.3.1 Signal Process

The Higgs is produced in association with an intermediate vector boson in the processes

$$p\overline{p} \rightarrow W + H \quad \text{and} \quad p\overline{p} \rightarrow Z + H. \tag{5.1}$$

Since not all decay products of the τs are reconstructed we cannot directly reconstruct the Higgs. We follow the technique suggested in reference [4] and reconstruct the $\tau\tau$ mass from the direction of the τs and the transverse momentum of the $\tau\tau$ system, $\vec{p}_T(\tau\tau)$. Let $\hat{\imath}$ and $\hat{\jmath}$ be unit vectors in the plane transverse to the beam in direction of the τs. If they are linearly independent we can solve the equation

$$\vec{p}_T(\tau\tau) = p_T(\tau_1)\hat{\imath} + p_T(\tau_2)\hat{\jmath} \tag{5.2}$$

for the transverse momenta $p_T(\tau_1)$ and $p_T(\tau_2)$ of the τs. Using the known mass and directions of the τs we can then compute the $\tau\tau$ mass.

We shall only use 1-prong τ decays and approximate the direction of the τs by the direction of their charged daughter particle. In order to be able to reconstruct the p_T of the $\tau\tau$ system we select events in which the vector boson decays hadronically, so that we can attribute any transverse momentum imbalance to the neutrinos from the τ decays. We infer the p_T of the $\tau\tau$ system from the measured transverse momentum of the system that recoils against the Higgs, which is given by the sum of the momenta of all detected particles excluding the decay products of the τs.

5.3.2 Background Processes

The dominant background process is

$$p\overline{p} \rightarrow Z(\rightarrow \tau^+\tau^-) + jj. \tag{5.3}$$

Other sources of events with $\tau\tau$ pairs are

$$p\overline{p} \ \rightarrow \ W/Z(\rightarrow jj) + Z(\rightarrow \tau^+\tau^-), \tag{5.4}$$

$$p\overline{p} \ \rightarrow \ t(\rightarrow \tau^+\nu b)\overline{t}(\rightarrow \tau^-\overline{\nu}\overline{b}). \tag{5.5}$$

These are much smaller than the dominant process and we shall neglect them. We did not consider backgrounds due to fake τs, such as

$$p\overline{p} \rightarrow W(\rightarrow \tau\nu) + j(\rightarrow \text{ fake } \tau) + jj. \tag{5.6}$$

5.3.3 Detector Requirements

The detector must be capable of measuring transverse momentum balance ($\not{p}_T$) with excellent resolution. We assume that the detector can identify jets with $|\eta| < 3$ and measure their energy E with a resolution of $\sigma_E = 0.8\sqrt{E} \oplus 0.03E$.

We shall in the following assume that we can identify 1-prong τ decays with 100 % efficiency if the charged daughter particle is within $|\eta| < 3$ and has $p_T > 5$ GeV. This is obviously not realistic, but the quoted yields can easily be scaled by the τ detection efficiency for a given detector.

This requires a hermetic and uniform calorimeter with good energy resolution and a good tracking system that extends into the forward regions. A vertex detector might be of use in detecting the τ decay vertex.

5.3.4 Signal and Background Yields

To enhance the signal process against the dominant Z background we make the following cuts:

- transverse momentum of $\tau^+\tau^-$ pair $p_T(\tau\tau) > 20$ GeV,
- two jets with $p_T > 15$ GeV and $60 < m(jj) < 110$ GeV,
- $\not{p}_T > 40$ GeV,
- $p_T > 5$ GeV for charged particles from τ decays,
- opening angle between τs $|\Delta\phi(\tau\tau) - \pi| > 0.6$.

We use PYTHIA to simulate the signal and background processes but estimate the rejection power of the jet cuts for the Z background from data taken by DØ. The following table lists event yields for $m_H = 120$ GeV and 100 fb^{-1}. The column σB gives the production cross section times all branching ratios, including the branching ratios of the τs to 1-prong final states. We use $B(H \to \tau\tau) = 8\%$ [9]. The next column gives the total number of events expected after all selection cuts and the last column lists the number of events expected with $105 < m(\tau\tau) < 129$ GeV.

process	total σ	σB	yield after cuts	$m(\tau\tau)$ cut
$H + W/Z$	230 fb	9.4 fb	157	107
$Z + jj$	6.5 nb	180 pb	8030	940

5.3.5 $\tau\tau$ Mass Resolution

The $\tau\tau$ mass resolution is crucial in distinguishing a Higgs signal from the Z background. We studied the effect of various detector resolutions on the $\tau\tau$ mass resolution. Figure 5.21

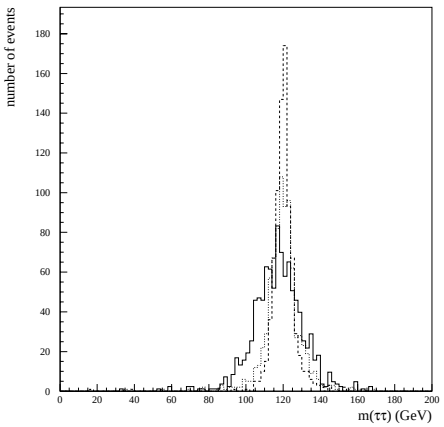

Figure 5.21: Reconstructed $\tau\tau$ mass distribution for $m_H = 120$ GeV with different resolution effects

shows the reconstructed $\tau\tau$ mass distribution for $m_H = 120$ GeV. The true $\tau\tau$ mass distribution is a delta function at 120 GeV. The dashed histogram shows the effect of approximating the τ directions by the directions of their charged daughter particles. The dotted histogram includes in addition a gaussian smearing of the x and y components of the $\not{p}_T$ vector independently by 3 GeV. This is representative of the $\not{p}_T$ resolution observed by DØ for minimum bias events, due to particles lost down the beam pipe and the calorimeter resolution. The solid histogram finally also includes the effect of the jet energy resolution in the calorimeter.

The $\tau\tau$ mass distributions can be fit well with two gaussians of different widths but equal mean. Figure 5.22 shows this for $Z \to \tau\tau$ decays (solid points) and $H \to \tau\tau$ decays (open points). The mass resolution is about 10 GeV with substantial nongaussian tails. For a 120 GeV Higgs $\approx$68% of the events have $105 < m(\tau\tau) < 129$ GeV and $\approx$95% of the events have $89 < m(\tau\tau) < 145$ GeV.

5.3.6 Significance of Signal

Figure 5.23 and Figure 5.24 show the $H \to \tau\tau$ signal for $m_H = 120$ GeV superimposed on the $Z \to \tau\tau$ background for a data sample of 100 fb^{-1}. The dashed line shows the Higgs signal, the solid line shows background only and the data points show signal+background. The error bars indicate the expected statistical fluctuations for 100 fb^{-1}. The event yield within $\pm 1\sigma$ of m_H suggests that we should expect a signal with about 3.5 standard deviations significance. However, to achieve this significance exact *a priori* knowledge of the Z background is required.

This result differs somewhat from reference [4]. The difference is largely due to different assumptions about the $\not{p}_T$ resolution. This study assumes the resolution achieved in existing detectors while reference [4] assumed an improved resolution in the upgraded detectors.

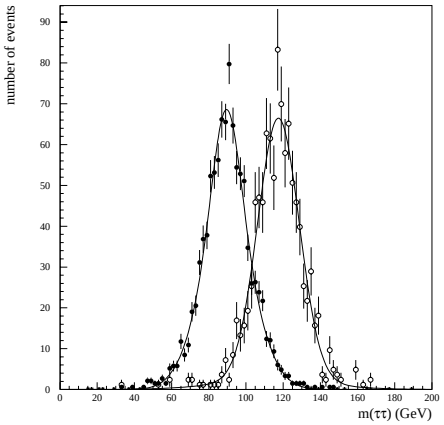

Figure 5.22: Reconstructed $\tau\tau$ mass distribution for $m_H = 120$ GeV and $Z \to \tau\tau$ decays

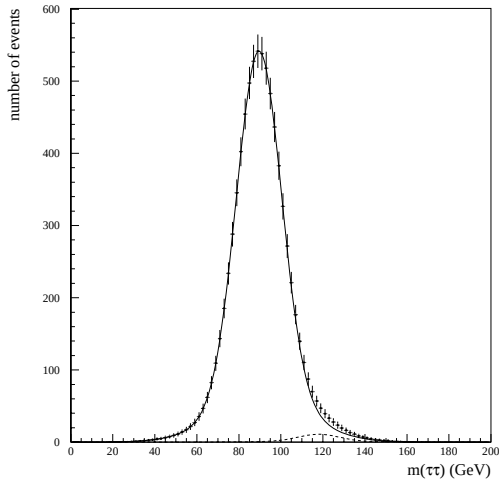

Figure 5.23: Expected $Z \to \tau\tau$ background and $H \to \tau\tau$ signal.

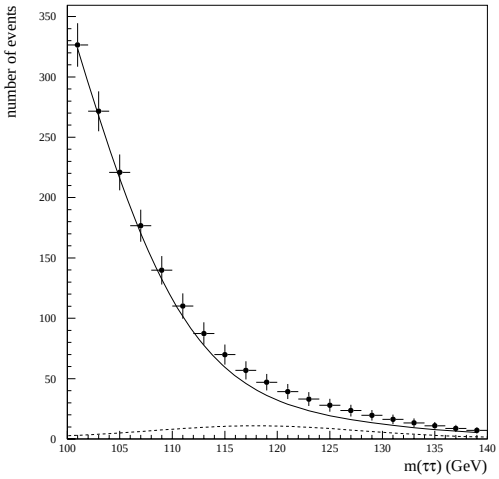

Figure 5.24: Enlarged region of previous figure.

5.3.7 Conclusions on $H \to \tau\tau$ Mode

It seems doubtful that we can establish the existence of the Higgs boson in this channel alone against the $Z \to \tau\tau$ background. However this channel may be combined with results from the $H \to b\bar{b}$ channel to confirm a signal and to increase its statistical significance. It will also constrain the $H \to \tau\tau$ branching ratio relative to $H \to b\bar{b}$ which should be consistent with that expected for Higgs decay.

5.4 Other Accelerators

5.4.1 LEPII

As described in the Introduction, the reach in Higgs mass of LEP II depends on the machine energy, roughly $m_H < \sqrt{s} - M_Z - (5-10)$ GeV. The current plan is for $\sqrt{s} = 184$ GeV, which covers up to $m_H < 85$ GeV, and in 1998 the energy will be increased to 192 GeV, which covers up to $m_H \approx 95$ GeV.

It is technically possible to increase the energy to $\sqrt{s} = 205$ GeV by nearly doubling the number of superconducting cavities over the current plan. This would cover up to $m_H < 105$ GeV. It is conceivable that an energy as high as $\sqrt{s} = 240$ GeV could be attained with yet more superconducting cavities and a cryogenics upgrade. This would cover up to $m_H < 140$ GeV, and would thus cover the entire light intermediate-mass Higgs region. There is no consideration of either of these energies at present, since they are incompatible with the approved LHC construction.

5.4.2 LHC

As described in the introduction, the light intermediate-mass Higgs region is difficult at the LHC. The main hope is the rare decay mode $H \to \gamma\gamma$. The dominant decay mode $H \to b\bar{b}$ may be accessible via $q\bar{q} \to WH$ [3, 4, 6, 7] (the same process as at the Tevatron) and $gg \to t\bar{t}H$ [8]. The ATLAS Collaboration has investigated both of these processes [2]. Their results are encouraging, but neither of these modes can be considered as established at the LHC at this time. Both suffer from enormous top-quark backgrounds, which are much less problematic at the Tevatron.

5.4.3 NLC

Higgs discovery is straightforward at a higher-energy e^+e^- collider, such as the NLC, via $e^+e^- \to ZH$, the same as at LEP II. The reach in Higgs mass is limited only by machine energy, roughly $m_H < \sqrt{s} - M_Z - 10$ GeV. To cover the light intermediate-mass region, $m_H = 80 - 130$ GeV, requires a machine of energy $\sqrt{s} > 230$ GeV. This energy could potentially be attained at LEP II, as described above.

5.5 Conclusions

The mass of the Higgs boson is a free parameter in the standard model of electroweak symmetry breaking. We must therefore be prepared to cover the range of masses from 65 GeV up to about 1 TeV. Precision electroweak experiments suggest that the Higgs-boson mass may lie at the lower end of this range. Furthermore, in the minimal supersymmetric Higgs model, the lightest Higgs boson is less massive than about 125 GeV. Thus there are good reasons to be concerned with the "intermediate mass" region, 65 GeV $< m_H <$ 130 GeV.

We have found promising sensitivity for the discovery of an intermediate-mass Higgs boson at the Tevatron via the process $q\bar{q} \to WH$, with $H \to b\bar{b}$. We tentatively conclude that a Higgs mass of 80 GeV can be reached with about 5 fb^{-1}, a mass of 100 GeV with about 10 fb^{-1}, and a mass of 120 GeV with about 25 fb^{-1}. These results are very encouraging, and suggest that the Tevatron could play a significant role in the quest for an intermediate-mass Higgs boson.

Our analysis makes use of three plausible assumptions, for which there is some support, but which have yet to be established, and represent important areas in need of further research. The first is that the signal-to-background ratio can be improved, by about a factor of two, by a judicious choice of cuts (suggested in Ref. [7]), without a significant loss in signal rate. The second is that the $b\bar{b}$ invariant-mass resolution can be substantially improved with respect to its present value. Our study indicates that it is important to develop an algorithm to merge gluons radiated from the b quarks back into the reconstructed $b\bar{b}$ invariant mass. The third is that the top-quark backgrounds, which become significant for masses above 100 GeV, are indeed manageable. The issues involved in the last two assumptions are, in fact, an extension of the top-quark physics program.

Some other pertinent considerations are as follows:

- The WH with $H \to b\bar{b}$ process also has some potential at the LHC. However, we have found that the top-quark backgrounds are relatively much more severe at the LHC, and as a result this process has more promise at the Tevatron.

- The process $q\bar{q} \to ZH$, with $H \to b\bar{b}$ and $Z \to \nu\bar{\nu}$, has not been studied, but has significant potential as a Higgs discovery mode, comparable to that of the WH process. Along with the other issues mentioned above, this is one of the most important areas in need of further research.

- The process $q\bar{q} \to (W,Z)H$, with $H \to \tau^+\tau^-$ and $(W,Z) \to jj$, is difficult at the Tevatron due to the large $(Z \to \tau^+\tau^-)jj$ background, but it may provide confirmation of a signal in the $H \to b\bar{b}$ decay channel. This process is hopeless at the LHC since the background is relatively worse than at the Tevatron.

- If the Higgs boson is discovered at LEP II ($m_H < 95$ GeV), it is potentially accessible at the Tevatron with less than 10 fb^{-1} of integrated luminosity. The Tevatron process, WH, involves the coupling of the Higgs to the W boson, and is therefore complementary to the LEP II process, ZH, which involves the coupling of the Higgs to the Z boson. The ratio of these couplings differs in multi-Higgs models with higher-dimensional

Higgs representations (such as Higgs triplets), so it is a test of the Higgs-doublet structure of the standard model.

- If no Higgs boson is detected at LEP II ($m_H > 95$ GeV), it will be left to future colliders to discover or rule out the Higgs boson. The only established discovery mode for the intermediate-mass Higgs boson at the LHC is the difficult $H \to \gamma\gamma$ mode, which is particularly challenging for $m_H < 100$ GeV. Furthermore, this mode can become invisible for the lightest supersymmetric Higgs boson, which can have enhanced coupling to b quarks. Thus the $H \to b\bar{b}$ decay mode at the Tevatron could be crucial to ensuring that both the standard Higgs boson and the lightest supersymmetric Higgs boson do not escape the gaze of future hadron colliders.

- The intermediate-mass Higgs boson is easily accessible to a very high-energy linear e^+e^- collider of sufficient energy and luminosity via ZH production. As mentioned above, this is complementary to the WH process at the Tevatron.

Our study thus far has been encouraging. Although further study is needed, the opportunity to detect an intermediate-mass Higgs boson at the Tevatron appears promising.

Bibliography

[1] CMS Technical Proposal, CERN/LHCC/94-38, LHCC/P1 (1994).

[2] ATLAS Technical Proposal, CERN/LHCC/94-43, LHCC/P2 (1994).

[3] A. Stange, W. Marciano, and S. Willenbrock, Phys. Rev. D **49**, 1354 (1994); D **50**, 4491 1994 .

[4] S. Mrenna and G. Kane, CALT-68-1938 (1994).

[5] A. Belyaev, E. Boos, and L. Dudko, Mod. Phys. Lett. **A10**, 25 (1995).

[6] D. Froidevaux and E. Richter-Was, Z. Phys. C **67**, 213 (1995).

[7] P. Agrawal, D. Bowser-Chao, and K. Chung, Phys. Rev. D **51**, 6114 (1995).

[8] J. Dai, J. Gunion, and R. Vega, Phys. Rev. Lett. **71**, 2699 (1993).

[9] E. Gross, B. Kniehl, G. Wolf, Z. Phys. C 63, 417 (1994) and erratum Z. Phys. C 66, 321 (1995).

Chapter 6

Supersymmetric Physics

6.1 Introduction

The recent observation of the top quark by the CDF and DØ Collaborations [1, 2] provides the last quark in the Standard Model (SM). Future experiments at the highest energy accelerators should plan to search for signs of physics beyond the Standard Model as well as continue testing the Standard Model. A very well motivated candidate for physics beyond the Standard Model is supersymmetry (SUSY).

Supersymmetry [3] is needed to connect the Standard Model with an ultimate perturbative unification of the fundamental interactions. Recent measurements of the gauge couplings at LEP [4] show that the Standard Model, when extrapolated to very high energies, fails to provide such unification, whereas a supersymmetrized Standard Model works very well [5]. SUSY also solves the fine tuning problem associated with the Higgs mass and provides a natural candidate for cold dark matter. Thus, a direct search for SUSY phenomena at high energy particle accelerators is crucially important. Recent indirect indications provide optimism that superpartners may be accessible at Fermilab.

Previous studies [6] have examined the potential of various planned or proposed accelerators for the discovery of supersymmetry. All of these studies assume one interaction per beam crossing. In this report, we specifically examine the SUSY discovery potential at an upgraded Tevatron. Multiple interaction effects are taken into account. Experimental issues specific to the Tevatron are also discussed.

We first describe briefly phenomenological arguments for the existence of SUSY particles in the mass range between 100 GeV/c^2 and a few TeV/c^2. We show that a large fraction of the predicted mass range is accessible at the Tevatron through the search for the lower mass particles in the model. The capabilities for discovering SUSY particles at a luminosity-upgraded Tevatron (TeV33) are summarized for 2 fb^{-1}, 10 fb^{-1} and 100 fb^{-1}.

6.2 Motivations for SUSY

The Standard Model has been enormously successful in explaining a wide variety of physics. Its principles appear to be valid over a remarkable range, from cosmological phenomena in the very early universe, to all microscopic phenomena up to the electroweak energy of about 100 GeV. At present, aside from a few two or three standard deviation effects, the Standard Model is in agreement with all current experimental data. In spite of this, there are a number of "structural" defects in the Standard Model, related mainly to the Higgs phenomenon. The Standard Model gives no explanation for the breaking of $SU(2) \times U(1)$, but merely accommodates it by giving the square of the Higgs mass (m_H^2) an unphysical negative value. Further, the Higgs boson, being a spin zero particle, possesses a quadratic self mass divergence. It leads to large quantum corrections ($\mathcal{O}(M_X^2/M_W^2)$) if one assumed the Standard Model held up from the electroweak scale M_W to ultra-high energy scale M_X (*e.g.*, the GUT or Planck scales). This correction requires major fine tuning to specify parameters of the theory to 23 decimal places.

Supersymmetry can protect the electroweak scale from the large corrections in the Higgs sector [3]. SUSY treats Bose and Fermi degrees of freedom on an equal footing. For every Bose helicity state, there is a corresponding Fermi state. The Bose and Fermi states make equal and opposite contributions to the Higgs self energy, thus canceling the quadratic divergence. SUSY is likely the only symmetry that can solve this problem. Further, when combined with supergravity grand unification [7], the Higgs mechanism can be derived since the breaking of supersymmetry at the GUT scale leads to electroweak breaking at the Z scale. Currently, no other theory possesses a working natural explanation of the Higgs mechanism. In the Standard Model the Higgs mechanism is assumed. To maintain supersymmetry, however, one must assume the existence of the SUSY partners of the Standard Model particles (*i.e.*, the squarks, sleptons, gluino, etc.), 32 new particles as listed in Table 6.1. To prevent the fine tuning problem from re-arising, their masses must lie in the general range of

$$M_{SUSY} \simeq 100 \text{ GeV/c}^2 \text{ to } 1 \text{ TeV/c}^2.$$

Since the current CDF/DØ sensitivity for gluinos and squarks is about 170 GeV/c^2, one sees that the lack of present evidence for these particles is not surprising, but that they should be within reach of the next round of accelerator experiments.

The first (indirect) experimental indication for the existence of the new SUSY particles was shown with the 1990 precision LEP measurements of the Standard Model couplings, α_1, α_2, and α_3 [5]. When extrapolated to higher energies by the renormalization group equations, these three running couplings within the Standard Model with one Higgs doublet do not meet at a point. On the other hand, in the supersymmetrized Standard Model the couplings do meet at a GUT scale M_G of about 10^{16} GeV/c^2 within the experimental uncertainties. This requires that:

- the SUSY mass spectrum is consistent with the range between about 100 GeV/c^2 to a few TeV/c^2, just as was required to resolve the fine tuning problem;
- there exists two (and only two) Higgs doublets.

Table 6.1: List of supersymmetric partners and Higgs bosons. Here, $\tilde{t}_i, \tilde{b}_i$, and $\tilde{\tau}_i$ $(i = 1, 2)$ are mixtures of the corresponding left- and right- chiral scalar fields, charginos are mixtures of charged higgsino and wino, and neutralinos are mixtures of two neutral higgsinos, bino and the neutral wino.

Particle Name	Spin	Physical States
squarks	0	$\tilde{d}_L$, $\tilde{u}_L$, $\tilde{s}_L$, $\tilde{c}_L$, $\tilde{b}_1$, $\tilde{t}_1$, $\tilde{d}_R$, $\tilde{u}_R$, $\tilde{s}_R$, $\tilde{c}_R$, $\tilde{b}_2$, $\tilde{t}_2$
sleptons	0	$\tilde{e}_L$, $\tilde{\nu}_{eL}$, $\tilde{\mu}_L$, $\tilde{\nu}_{\mu L}$, $\tilde{\tau}_1$, $\tilde{\nu}_{\tau L}$, $\tilde{e}_R$, $\tilde{\mu}_R$, $\tilde{\tau}_2$
charginos	$\frac{1}{2}$	$\tilde{\chi}_1^{\pm}$, $\tilde{\chi}_2^{\pm}$
neutralinos	$\frac{1}{2}$	$\tilde{\chi}_1^0$, $\tilde{\chi}_2^0$, $\tilde{\chi}_3^0$, $\tilde{\chi}_4^0$
gluino	$\frac{1}{2}$	$\tilde{g}$
Higgs bosons	0	h, H, A, $H^{\pm}$

The supersymmetrized Standard Model with two Higgs doublets plus grand unification is thus consistent with the low energy LEP measurements.

With two Higgs doublets, there are five physical Higgs states (3 neutral and 2 charged Higgs bosons): h, H^0, A^0, $H^{\pm}$. Supersymmetry predicts one of them to be a relatively light Higgs boson. The lightest Higgs boson (h) should be lighter than the Z^0 at tree level. However, a large top-quark Yukawa coupling induces a correction to the prediction at the one-loop level. The upper bound is pushed up to

$$M_h \simeq 130 \text{ GeV/c}^2.$$

This limit is beyond the reach of LEP-II, but may be possible to detect via the $h \to b\bar{b}$ mode (see "Light Higgs Physics" chapter) at TeV33.

The above description of supersymmetry has been refined over the past four years with improved data and more accurate theory, and has withstood the test of time. One has the outline of a minimal model to describe physics beyond the Standard Model and yet be consistent with all the LEP data supporting the Standard Model: *a supersymmetrized Standard Model with two Higgs doublets, with this spectrum holding up to M_G.*

The minimal model does not predict the many new mass parameters associated with the new supersymmetric particles. However, in the minimal supergravity models, all SUSY effects are determined by only 4 additional parameters and one sign. These may be taken to be the following: m_0 (a common scalar mass - related to squark masses), $m_{1/2}$ (a common gaugino mass - related to gluino mass), A_0 (a common trilinear interaction amongst the scalars), $\tan\beta = \langle H_2 \rangle / \langle H_1 \rangle$ (H_2 gives mass to up-quarks and H_1 to down-quarks and leptons), and the sign of μ (the Higgsino mixing parameter). The universality of m_0 automatically suppresses unwanted flavor changing neutral currents [1] (FCNC). Further, and most important, this makes *supersymmetry the most highly predictive proposal of physics beyond the Standard Model.*

[1] Non-universal models can be constructed, but they cannot deviate greatly from the universal ones in the FCNC channels. The existence of the superparticles below 1 TeV generally leads to large FCNC, especially in K^0-$\bar{K}^0$ oscillations. To avoid this requires the squark masses to be highly degenerate.

Models with R-parity conservation yield a natural candidate ($\tilde{\chi}_1^0$), the lightest neutralino, for the cold dark matter that astronomers now believe constitute the majority of matter in our galaxy and the universe. Remarkably, the relic abundance of these neutralinos left over from the Big Bang, is consistent with the amount required by cosmological theory of the inflationary scenario[8] over a wide range of the SUSY parameters.

If the representations used to break the GUT group are not too large, the low energy predictions are mostly independent of the GUT physics. Thus the theory does not need any commitment to a specific (and little understood) GUT dynamics.

The above discussion describes a supersymmetric theory that is relatively model independent, is highly theoretically motivated, calculationally straight forward, and depends on only a few parameters to describe a large amount of phenomena. The relatively few parameters in the theory, makes the theory highly predictive, and one may further limit the parameter space by the existing bounds on the SUSY parameters from LEP and the Tevatron, and most recently from the CLEO measurement of the $b \to s + \gamma$ decay. The recent measurement of the top mass by CDF and DØ also aids in restricting the parameter space (since the top is apparently quite close to its Landau pole value), and an accurate value of M_{top}, which might be expected from a Tevatron upgrade, would significantly help in making more precise SUSY particle predictions, within the assumed framework.

6.3 The SUSY Particle Spectrum

There are a minimum of 32 new particles in the SUSY+Higgs sector. In the most general model, these masses and their couplings are arbitrary parameters not constrained by the model. The large number of arbitrary parameters in the general SUSY model make experimental predictions difficult and unattractive. Even assuming a GUT hypothesis (SUSY-GUT), the number of arbitrary parameters remain large. As mentioned before, much progress has been made recently in developing a minimal model with few parameters. The models we studied in this report are mostly these minimal supergravity models (MSGM or Constrained MSSM in some literature) with only 4 arbitrary parameters and an arbitrary sign.

The supersymmetric partners to the particles in the Standard Model and the five Higgs states in the MSSM are shown in Table 6.1. Note that the charginos ($\tilde{\chi}_1^{\pm}$, $\tilde{\chi}_2^{\pm}$) are mixtures of charged higgsino and wino states. In the literature, they are sometimes labelled as $\tilde{W}_1$ and $\tilde{W}_2$. Similar nomenclature is also used for the neutralino states.

Requiring unification of the coupling constants at the GUT scale ("the GUT hypothesis") leads to the following relationships at any scale:

$$\begin{aligned} M_{\tilde{W}} &= \frac{\alpha_2}{\alpha_3} M_{\tilde{g}} \\ M_{\tilde{B}} &= \frac{5\alpha_1}{3\alpha_2} M_{\tilde{W}} \end{aligned}$$

Confirmation of these mass-relations, would provide crucial insight into unification.

The current limits on the masses of SUSY particles are summarized in Table 6.2. Some of these limits are model specific. Note that all the current experimental limits on SUSY states

Table 6.2: Current mass limits on supersymmetric partners (some are model dependent).

Sparticle	Mass Limit	Comments
$\tilde{g}$	173 GeV/c^2	DØ & CDF
$\tilde{q}$	229 GeV/c^2	DØ & CDF ($M_{\tilde{q}} = M_{\tilde{g}}$)
$\tilde{t}_1$	100 GeV/c^2	DØ ($\tilde{t}_1 \rightarrow c\tilde{\chi}_1^0$)
	48 GeV/c^2	LEP140 (purely right stop and $M_{\tilde{\chi}_1^0} = 30$ GeV/c^2)
$\tilde{\chi}_1^\pm$	65 GeV/c^2	LEP140 (higgsino-like $\tilde{\chi}_1^\pm$ and $M_{\tilde{\chi}_1^\pm} - M_{\tilde{\chi}_1^0} > 10$ GeV/c^2)
$\tilde{\chi}_2^0$	69 GeV/c^2	LEP140 (higgsino-like $\tilde{\chi}_2^0$ and $M_{\tilde{\chi}_2^0} - M_{\tilde{\chi}_1^0} > 10$ GeV/c^2)
$\tilde{\chi}_1^0$	20 GeV/c^2	LEP
$\tilde{\ell}$	45 GeV/c^2	LEP
$\tilde{e}$	53 GeV/c^2	LEP140 (gaugino-like $\tilde{\chi}_1^0$ and $M_{\tilde{\chi}_1^0} < 35$ GeV/c^2)
$\tilde{\nu}$	43 GeV/c^2	LEP
h	60 GeV/c^2	LEP

are below the expected mass spectrum of weak scale MSSM. Therefore, it is not surprising that none of the SUSY particles have been found yet. A luminosity upgraded Tevatron or new accelerators are needed to explore the mass regime where weak scale MSSM is expected.

At hadron colliders, sparticles can be produced via the following lowest order reactions:

- $q\bar{q},\ gg,\ qg \rightarrow \tilde{g}\tilde{g},\ \tilde{g}\tilde{q},\ \tilde{q}\tilde{q}$ (strong production)
- $q\bar{q},\ qg \rightarrow \tilde{g}\tilde{\chi}_i^0,\ \tilde{g}\tilde{\chi}_i^\pm,\ \tilde{q}\tilde{\chi}_i^0,\ \tilde{q}\tilde{\chi}_i^\pm$ (associated production)
- $q\bar{q} \rightarrow \tilde{\chi}_i^\pm\tilde{\chi}_j^\mp,\ \tilde{\chi}_i^\pm\tilde{\chi}_j^0,\ \tilde{\chi}_i^0\tilde{\chi}_j^0$ ($\tilde{\chi}$ pair production)
- $q\bar{q} \rightarrow \tilde{\ell}\tilde{\nu},\ \tilde{\ell}\tilde{\ell},\ \tilde{\nu}\tilde{\nu}$ (slepton pair production)

Figure 6.1 shows the cross section for sparticle pair production as a function of the gluino mass assuming a mass relation in SUSY-GUTs. Once produced, sparticles rapidly decay to other sparticles initiating a cascade which ends with the LSP ($\tilde{\chi}_1^0$).

The Higgs bosons of the MSSM can be produced via direct s-channel subprocesses:

- $q\bar{q},\ gg \rightarrow h,\ H,\ A,\ H^\pm H^\mp$,

They can also be produced in association with other heavy quarks and vector bosons, and in some cases, via vector boson fusion.

6.4 "SUSY Physics" Search Strategies at TeV33

Historically, collider experiments have concentrated on the search for squarks and gluinos. At the maximum center of mass energy of 2 TeV, Figure 6.1 shows that the squark/gluino

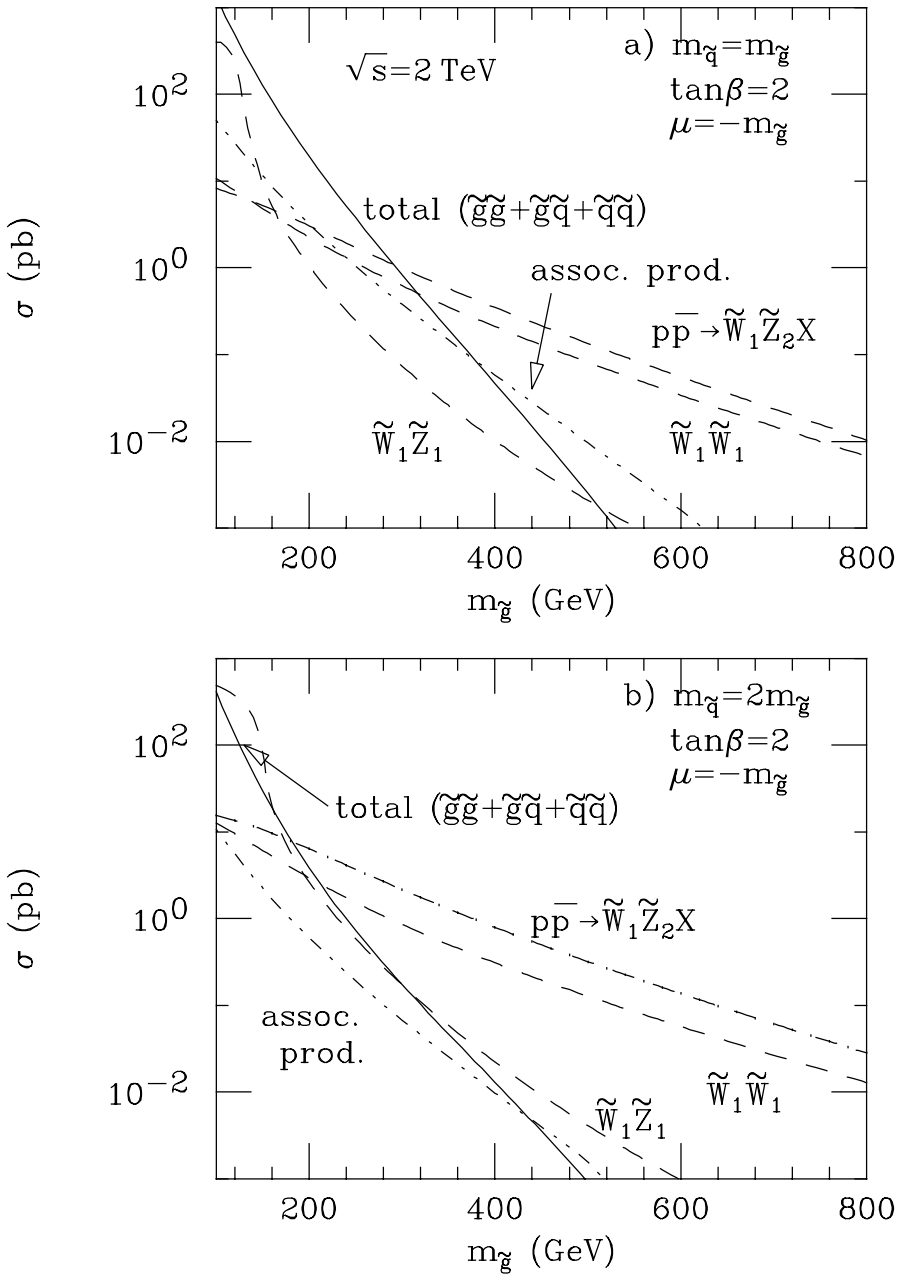

Figure 6.1: Cross section for sparticle pair-production as a function of the gluino mass for two specific parameter sets [6]; (a) $\tan\beta = 2$, $\mu = -M_{\tilde{g}}$, $M_{\tilde{q}} = M_{\tilde{g}}$, (b) $\tan\beta = 2$, $\mu = -M_{\tilde{g}}$, $M_{\tilde{q}} = 2\ M_{\tilde{g}}$.

Table 6.3: Search for Supersymmetric Partners (LSP = $\tilde{\chi}_1^0$)

Production	Key Decay Mode	Signature
$\tilde{g}\tilde{g}$, $\tilde{g}\tilde{q}$, $\tilde{q}\tilde{q}$	$e.g., \tilde{g} \to qq\tilde{\chi}_1^0$, $\tilde{q} \to qqq\tilde{\chi}_1^0$ $(M_{\tilde{q}} > M_{\tilde{g}})$	$\not\!\!E_T$ + multijets
$\tilde{\chi}_1^\pm\tilde{\chi}_2^0$	$\tilde{\chi}_1^\pm \to \tilde{\chi}_1^0\ell\nu$, $\tilde{\chi}_2^0 \to \tilde{\chi}_1^0\ell\ell$,	Trilepton + $\not\!\!E_T$
	$\tilde{\chi}_1^\pm \to \tilde{\chi}_1^0 qq$, $\tilde{\chi}_2^0 \to \tilde{\chi}_1^0\ell\ell$,	Dilepton + $\not\!\!E_T$ + jets
$\tilde{t}_1\tilde{t}_1$	$\tilde{t}_1 \to \tilde{\chi}_1^0 c$	$\not\!\!E_T$ + 2 acollinear jets
	$\tilde{t}_1 \to \tilde{\chi}_1^\pm b$, $\tilde{\chi}_1^\pm \to \tilde{\chi}_1^0\ell^\pm\nu$, $\tilde{\chi}_1^\mp \to \tilde{\chi}_1^0 qq$	Single lepton + $\not\!\!E_T$ + b's
	$\tilde{t}_1 \to \tilde{\chi}_1^\pm b$, $\tilde{\chi}_1^\pm \to \tilde{\chi}_1^0\ell^\pm\nu$, $\tilde{\chi}_1^\mp \to \tilde{\chi}_1^0\ell^\mp\nu$	Dilepton + $\not\!\!E_T$ + b's
$W/Z + h$	$h \to b\bar{b}, \tau\bar{\tau}$	2 b's or 2 τ's

production cross section drops rapidly with higher gluino masses. The searches become kinematically limited. However, the lightest chargino and the second lightest neutralino are one-third to one-fourth as massive as the squark and gluinos. Their production cross sections become dominant for high gluino masses, thereby greatly enhancing the possibility of discovering supersymmetry at the Tevatron with large integrated luminosities.

Table 6.3 shows some of the channels which may be used to search for SUSY at the Tevatron. Clearly, we must maintain good parton identification capabilities with the Tevatron detectors in order to take full advantage of the high luminosities: good identification of leptons (e and μ), $\not\!\!E_T$ (ν and LSP), b-jets, and light quark/gluon jets.

Multiple interactions will be one of the major challenges faced at high luminosities. We will discuss some of the effects of multiple interactions on parton identification (specifically on lepton isolation, missing E_T resolution and b-tagging) in the next section. We will also explore the potential for SUSY discovery for specific channels in a high luminosity environment.

6.5 Physics Reaches at TeV33

6.5.1 Search for the Lightest Chargino using Trilepton Events

One of the most promising channels for the discovery of SUSY at a hadron collider is the trilepton final state [9] arising from chargino-neutralino ($\tilde{\chi}_1^\pm\tilde{\chi}_2^0$) pair production with subsequent leptonic decays ($\tilde{\chi}_1^\pm \to \ell\nu\tilde{\chi}_1^0$ and $\tilde{\chi}_2^0 \to \ell\bar{\ell}\tilde{\chi}_1^0$) in the framework of the Minimal Supersymmetric Standard Model.

Trilepton analysis at $\sqrt{s}$ = 1.8 TeV and 100 pb^{-1}

The current CDF and DØ analyses use inclusive electron and muon trigger samples at $p_T^{trig} \sim 10$ GeV/c when $\mathcal{L} < 1 \times 10^{31}$ cm^{-2}·sec^{-1}, and/or a lower p_T ($e.g., p_{T1}^{trig} > 8$ GeV/c, $p_{T2}^{trig} > 3$ GeV/c) dilepton trigger sample at higher luminosity, $\mathcal{L} > 1 \times 10^{31}$ cm^{-2}·sec^{-1}. The signal event must contain three isolated leptons. After some additional requirements, both

CDF and DØ found zero event candidates in Run 1A data. This is completely consistent with CDF/DØ estimate of the backgrounds (Drell-Yan, Z, $b\bar{b}$, $t\bar{t}$ and diboson). The current CDF and DØ limits[2] (from Run 1A) of the chargino mass are comparable to the LEP result [10].

The DØ analysis requires a cut on $\not\!\!E_T$ (> 10 GeV), while the CDF analysis does not require any $\not\!\!E_T$ cut. These analyses are optimized for a low mass chargino search at the level of 20 pb^{-1}. With 100 pb^{-1}, we need to reduce some backgrounds (Drell-Yan, Z and $b\bar{b}$) substantially by using a $\not\!\!E_T$ cut. With $\not\!\!E_T > 15$ GeV, the total background will be $\sigma_{BG} \sim$ 4 fb, while a large fraction of signal events will be accepted (*e.g.*, about 80% for 70-GeV/c^2 $\tilde{\chi}_1^{\pm}$). With this higher $\not\!\!E_T$ cut, the total number of background events is expected to be less than one at 100 pb^{-1}. The 95% confidence level (C.L.) upper limit curve at 100 pb^{-1} is extrapolated from the current Run 1A results. We find that chargino masses up to 70 GeV/c^2 can be probed with 100 pb^{-1}. Since this limit is model specific, we extract the maximum reach from Fig. 1 of Ref. [11] and find the reach could be as large as 90 GeV/c^2 in some region of parameter space, requiring 5 signal events for zero background.

Trilepton analysis at $\sqrt{s} = 2$ TeV and 2-100 fb^{-1}

The chargino search using the trilepton channel at a luminosity upgraded Tevatron (M.I. and TeV33) is studied by three groups [11, 12, 13]. Table 6.4 summarizes their analyses. Both Refs. [12] and [13] assumed a large acceptance for the leptons (e and μ), while coverage similar to the current CDF detector is assumed in Ref.[11].

The analyses in Refs. [11] and [13] are optimized for the search without $\not\!\!E_T$ cut. The main differences between the two analyses are (a) the geometric coverage of the leptons, (b) the transverse mass cut, and (c) DY/Z background estimate.

The acceptance for the signal and background events in Ref. [13] is typically larger by a factor of 2-3 than that in Ref. [11] due to the different geometric coverage for leptons assumed. The transverse mass cut efficiently reduces $t\bar{t}$ and WZ backgrounds. Cut 3 ($M_{\ell\ell} <$ 20 GeV/c^2 for any dilepton) reduces $t\bar{t}$ events (with $b \to \ell + X$). Table 6.5 summarizes the comparison of $t\bar{t}$, WZ and ZZ backgrounds. There are no obvious disagreements between two analyses if the lepton coverage is taken into account.

The main concern in Ref. [11] is the fake probability that dilepton events (DY and Z) are identified as trilepton events by picking up an additional lepton (real or misidentified lepton) because of the low lepton p_T. They assume 10^{-4} per event which is somewhat better than the current CDF and DØ analyses. Reference [13] assumes that it will be smaller with their analysis cuts. Their Cut 3 is optimized to achieve this. Another way to reduce the background is to apply a $\not\!\!E_T$ cut. We have revised the analysis in Ref. [11] by requiring $\not\!\!E_T >$ 20 GeV. The background cross section for DY/Z + X is expected to be ~0.1 fb (from 2.19 fb), while about 80% of 120-GeV/c^2 chargino events are accepted. The total background becomes ~0.5 fb which is the same level as in Ref. [13]. Taking into account the difference in the geometric coverage and details of the selection cuts, there are no obvious disagreements for the estimate of the total background. We should achieve a total background estimate

[2]The limits are model-dependent. The CDF result, for example, was obtained by assuming that $M_{\tilde{\ell}}$ and $M_{\tilde{\nu}}$ are given by RGE equations and that $M_{\tilde{q}} = 1.2 \times M_{\tilde{g}}$. Therefore, there are large regions of parameter space where the current CDF and DØ data do not have sensitivity.

Table 6.4: Comparison of three trilepton analyses

Monte Carlo Generator → Cuts:	Ref. [11] ISAJET [14]	Ref. [13] PYTHIA [15]	Ref. [12] ISAJET [14]
(1) Kine/Geom			
$p_T(\ell_1)$	>10 GeV/c	>10 GeV/c	>20 GeV/c
$p_T(\ell_2)$	> 4 GeV/c (5 GeV/c for e)	> 5 GeV/c	>15 GeV/c
$p_T(\ell_3)$	> 4 GeV/c (5 GeV/c for e)	> 5 GeV/c	>10 GeV/c
$\|\eta(e)\|$	<2.4 (1.1 for e_1)	<2.5	<2.5
$\|\eta(\mu)\|$	<1.1 (0.6 for μ_1)	<2.5	<2.5
ISO($\Delta R = 0.4$)	<2 GeV	<2 GeV	$< E_T(\ell)/4$
(2) Z veto	75-105 GeV/c^2	76-106 GeV/c^2	81-101 GeV/c^2
(3) Other $M_{\ell\ell}$ veto	9-11 GeV/c^2 (Υ)	<20 GeV/c^2	N/A
	2.9-3.1 GeV/c^2 (J/ψ)	(ee, $\mu\mu$, and $e\mu$)	
(4) $\Delta\phi_{\ell_1\ell_2}$	$< 170°$	$< 143°$	N/A
(5) $M_T(\ell_1 \not\!\!E_T)$	N/A	<70 GeV/c^2	N/A
(6) $\not\!\!E_T$	N/A	N/A	>25 GeV
(7) $N_{jet}(E_T$ >15 GeV)	N/A	N/A	0
Background [fb]			
$t\bar{t}$	0.19	0.06	0.005
WZ *etc.*	0.21	0.38	0.2
ZZ *etc.*	0.04	0.09	N/A
DY/Z + X	2.19	0.14	N/A
Total BG	2.63	0.67	0.21

Table 6.5: Comparison of backgrounds (in fb) in two trilepton analyses. There is no obvious disagreement if one takes into account the difference of the $\eta(\ell)$ coverage.

Cuts	Ref. [11]	Ref. [13]
$t\bar{t}$	0.19	0.33 (Cuts 1-2)
WZ *etc.*	0.21	0.85 (Cuts 1-4)
ZZ *etc.*	0.04	0.12 (Cuts 1-4)

less than 1 fb with any of the 3 sets of cuts.

Figure 6.2 is taken from Ref. [13] as a representative plot. The cross section times branching fraction times detection efficiency is plotted as a function of the $\tilde{\chi}_1^{\pm}$ mass. Typical DØ or CDF detection efficiencies have been applied. Each point in the plot represents the prediction from a specific MSSM model (that is, from a specific choice of the MSSM parameters). We find that the minimum $\sigma \cdot BR \cdot \epsilon_{tot}$ for integrated luminosities of 2 fb^{-1}, 10 fb^{-1} and 100 fb^{-1} are 3.0 fb, 1.3 fb and 0.4 fb, respectively, by requiring the number of signal events for a 5σ significance above background. The maximum $\tilde{\chi}_1^{\pm}$ masses we can probe are 210 GeV/c^2, 235 GeV/c^2, and 265 GeV/c^2. Note that for a few models, $\tilde{\chi}_1^{\pm}$ might escape detection with much lower masses.

For 10 fb^{-1} and 100 fb^{-1} integrated luminosities (at TeV33), we have to consider the effect of multiple interactions in lepton selection. Based on our preliminary calculations, we expect that the trilepton signal and background efficiencies will be additionally reduced by $f_S = 72\%$ and $f_{BG} = 75\%$ with respect to the MC studies performed without multiple interactions. Thus, the significance will be modified by the factor D, given by

$$D = \frac{f_S}{\sqrt{f_{BG}}}.$$

The modified significance can be applied to Fig. 6.2. We find that the modified $\sigma \cdot BR \cdot \epsilon_{tot}$ for 10 fb^{-1} and 100 fb^{-1} are 1.6 fb and 0.48 fb, respectively. The corresponding maximum $\tilde{\chi}_1^{\pm}$ masses we can probe are 230 GeV/c^2 and 255 GeV/c^2. Thus we expect the mass limits are decreased by about 10 GeV/c^2. It should be noted that for certain ranges of parameters, charginos as light as the current LEP bound will be undetectable in this channel. Therefore, it will not be possible to infer an absolute model independent lower mass limit on the charginos if no signal is seen at the Tevatron. However, Fig. 6.2 shows that at these high luminosities, a majority of the low mass MSSM models can be reached at the Tevatron.

The analysis in Ref. [12] was optimized for high mass charginos where $\not\!\!E_T$ and lepton p_T are substantially larger. Thus, the fake lepton problem is negligible. The dominant background is WZ events. The total background is smaller than that in Ref. [13]. However, the signal acceptance is also smaller, so that both analyses have similar sensitivities. Figure 6.3(a) from Ref. [12] shows $\tilde{\chi}_1^{\pm}$ reach in the $m_{1/2}$-m_0 plane when $A_0 = 0$, $\tan\beta = 2$ and $\mu > 0$. The maximum chargino masses accessible are 180 GeV/c^2, 210 GeV/c^2 and 260 GeV/c^2 for integrated luminosities of 2 fb^{-1}, 10 fb^{-1} and 100 fb^{-1}, respectively (see Fig. 6.3(b)). A similar figure for $\mu < 0$ can be found in Ref. [12]. The maximum chargino masses accessible in this case are 170 GeV/c^2, 230 GeV/c^2 and 280 GeV/c^2 for integrated luminosities of 2 fb^{-1}, 10 fb^{-1} and 100 fb^{-1}, respectively. Once again, if we take into account the effect due to multiple interactions, we expect the mass limits are decreased by about 10 GeV/c^2. The corresponding maximum $\tilde{\chi}_1^{\pm}$ masses we can probe are 220 GeV/c^2 and 270 GeV/c^2 for integrated luminosities of 10 fb^{-1} and 100 fb^{-1}, respectively.

Figures 6.3(c) and (d) show the analysis results for $\tilde{\chi}_1^{\pm}\tilde{\chi}_1^{\mp} \to (\ell^{\pm}\nu\tilde{\chi}_1^0)(\ell^{\mp}\nu\tilde{\chi}_1^0) \to$ dilepton + $\not\!\!E_T$ and $\tilde{\chi}_1^{\pm}\tilde{\chi}_2^0 \to (q\bar{q}\tilde{\chi}_1^0)(\ell^{\pm}\ell^{\mp}\tilde{\chi}_1^0) \to$ dilepton + $\not\!\!E_T$ + jets. Though the discovery reach in these channels is mostly a subset of the region probed via trilepton events, they could provide an important independent confirmation of supersymmetry if it is discovered in the trilepton channel. In the $m_0 > 400$ GeV/c^2 region and for $\mu > 0$, the dilepton reach is actually

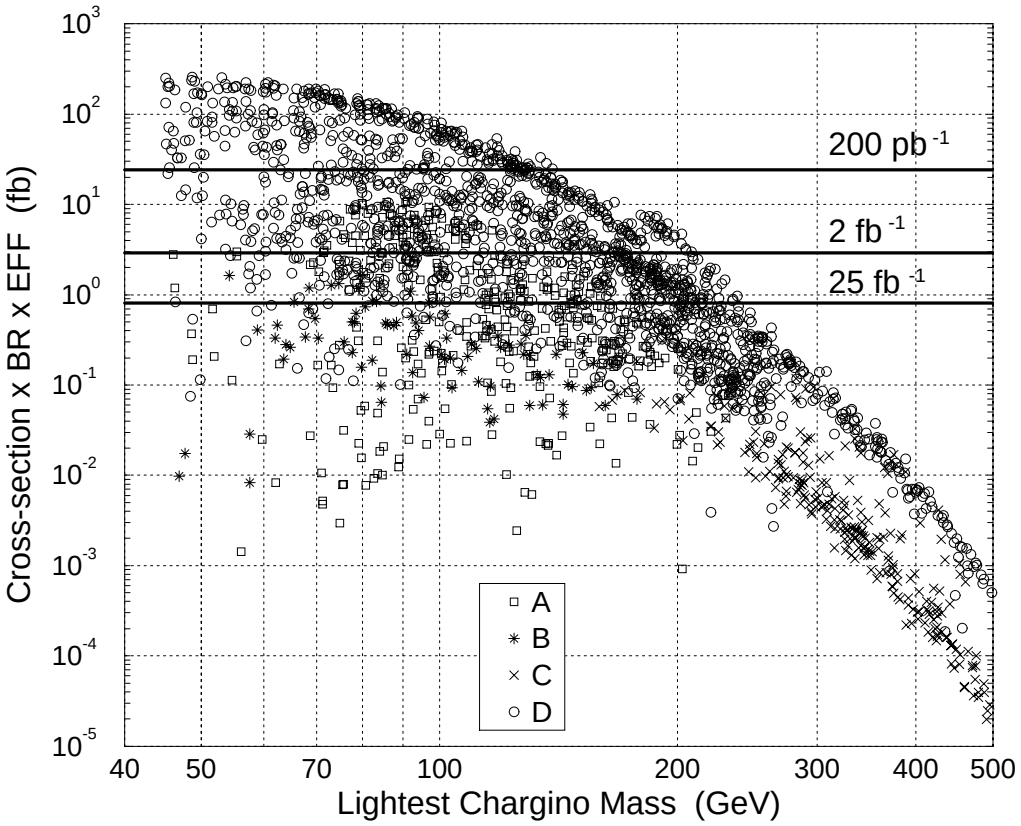

Figure 6.2: Total supersymmetric trilepton signal ($\sigma \times BR \times$ EFF) after cuts versus the lightest chargino mass in minimal supergravity models [13]. The branching ratio (BR) is defined as the fraction of $\tilde{\chi}_1^{\pm}\tilde{\chi}_2^0$ events that decay to 3 leptons. The efficiency (EFF) is defined as the fraction of 3 lepton events that pass the cuts. The 5σ significances for integrated luminosities 200 pb^{-1}, 2 fb^{-1}, and 25 fb^{-1} are shown by the dark horizontal lines at 25 fb, 3.0 fb, and 0.82 fb, respectively. The different symbols refer to solutions that the second lightest neutralino ($\tilde{\chi}_2^0$) has (A) a neutral "invisible" branching ratio $> 90\%$, (B) a large destructive interference in 3-body leptonic decays, (C) a branching ratio to Higgs $> 50\%$, or (D) all other solutions.

better than the trilepton reach at high luminosities. Once supersymmetry is discovered, the dilepton + $\not\!\!E_T$ + jets channel can also be used to determine parameters of supersymmetric models by looking at the dilepton invariant mass which is bounded by $M_{\tilde{\chi}_2^0} - M_{\tilde{\chi}_1^0}$.

It should be noted that we have assumed an upgraded detector for Main Injector and TeV33 scenarios. The upgraded coverage for leptons is assumed to be $|\eta| < 2.5$. If one performed the analysis with a current CDF-like detector [11] with $\sigma_{BG} = 0.5$ fb, the reach for chargino mass would be ~150 GeV/c^2 at 2 fb^{-1}. This is about 30% lower than the 210 GeV/c^2 in Ref. [13].

In summary, a majority of the SUSY parameter space accessible in the trilepton mode can be reached at the Tevatron with high luminosities. Chargino masses up to 270 GeV/c^2 can be probed with 100 fb^{-1} of data. As shown in Figure 6.3(c), this range is equivalent to the search for 500-600 GeV/c^2 gluinos.

6.5.2 Search for Gluinos using Missing E_T + Multijet Events

We explore the potential for the traditional gluino and squark search in multi-jet events with large $\not\!\!E_T$. In the Run-1A analysis, both CDF and DØ found $\sigma_{BG} \sim 2$ pb and set the 95% C.L. limit on the gluino mass of 220-229 GeV/c^2 if $M_{\tilde{q}} = M_{\tilde{g}}$. The asymptotic limit is $M_{\tilde{g}} >$ 170 GeV/c^2, independent of squark mass. Both limits are determined for a specific choice of SUSY parameters.

$\not\!\!E_T$ + multijet analysis at $\sqrt{s} = 1.8$ TeV and 100 pb^{-1}

For 100 pb^{-1}, we need to reduce the background substantially. CDF used cuts of $\not\!\!E_T >$ 60 GeV and $N_{jet}(E_T > 15 \text{ GeV}) \geq 3$ in the Run-1A analysis. For this study, we revised the CDF analysis with cuts of $\not\!\!E_T > 80$ GeV and $N_{jet}(E_T > 20 \text{ GeV}) \geq 4$. The other cuts on lepton veto, fake $\not\!\!E_T$ due to mismeasured jets etc. remain the same. With the new cuts, our expectation of the background cross section is

$$\sigma_{BG} \;=\; 0.16 \text{ pb.}$$

The 1.64σ significance above background for 100 pb^{-1} is 0.07 pb (or 7 events). Therefore, we find the 95% C.L. limit on the gluino mass of 270 GeV/c^2 if $M_{\tilde{q}} \sim M_{\tilde{g}}$, for a specific choice of supersymmetry model.

$\not\!\!E_T$ + multijets analysis at $\sqrt{s} = 2$ TeV and 2-100 fb^{-1}

Table 6.6 shows a comparison of two analyses [16, 13]. The analysis in Ref. [16] (similar to the DØ analysis), estimates the background to be $\sigma_{BG} = 1.2$ pb. This is consistent with the current DØ (and CDF) result of 2 pb. The dominant background sources are $t\bar{t}$, W and Z events. These backgrounds will be reduced by requiring

$$E_T(j_1) + E_T(j_2) + \not\!\!E_T \;>\; 300 \text{ GeV,}$$

as suggested by Ref. [13]. The total background is then expected to be

$$\sigma_{BG} \;=\; 40 \text{ fb.}$$

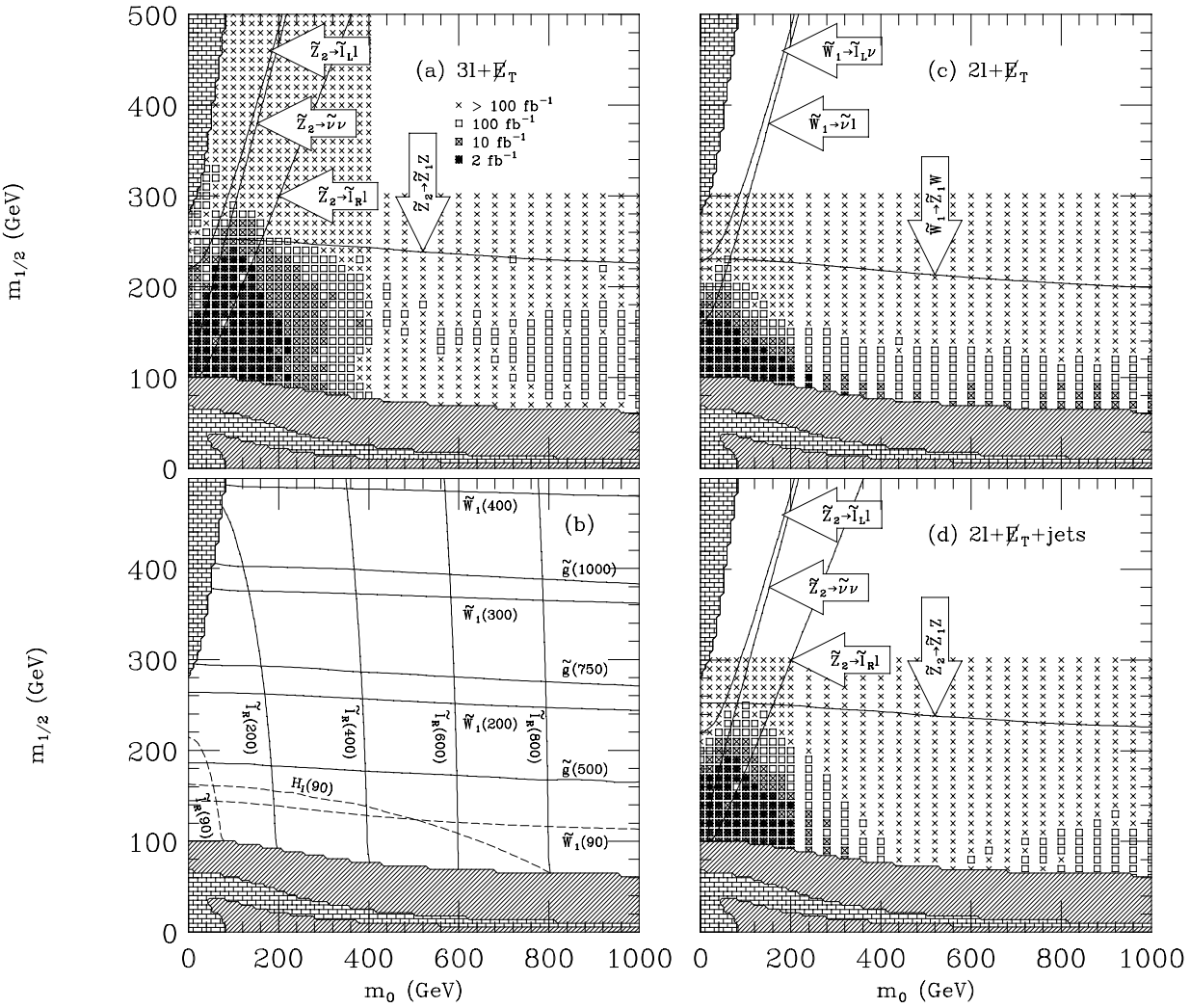

Figure 6.3: (a) Regions of the $m_{1/2}$ versus m_0 plane (with $A_0 = 0$, $\tan\beta = 2$, $\mu > 0$) where trilepton events should be detectable for integrated luminosities of 2 fb^{-1}, 10 fb^{-1} and 100 fb^{-1} in minimal supergravity models. The bricked region is excluded by theoretical constraints, while the gray shaded region is excluded by experiment [12]. (b) Contours for $M_{\tilde{g}}$, $M_{\tilde{\chi}_1^\pm}$, and $M_{\tilde{\ell}_R}$ for comparison with (a). (c) Regions of parameter space that can be probed in the opposite dilepton + $\not\!\!E_T$ events from $\tilde{\chi}_1^\pm\tilde{\chi}_1^\mp$ pair-production. (d) Regions of parameter space that can be probed in the opposite dilepton + jets events from $\tilde{\chi}_1^\pm\tilde{\chi}_2^0$ pair-production followed by decays to $\tilde{\chi}_1^\pm \to \tilde{\chi}_1^0 q\bar{q}$ and $\tilde{\chi}_2^0 \to \tilde{\chi}_1^0\ell^+\ell^-$.

Table 6.6: Comparison of two different $\not\!\!E_T$ + multijet analyses

Monte carlo generator → Cuts	Ref. [16] ISAJET [14]	Ref. [13] PYTHIA [15]
(1) $\not\!\!E_T$	>75 GeV	>75 GeV
(2) $\Delta\phi(j\not\!\!E_T)$	$> 30°$	$> 25.6°$
(3) $p_T(\ell)$ for the lepton veto	>15 GeV/c	>15 GeV/c
(4) $N_{jet}(E_T > 15$ GeV)	≥ 4	N/A
(5) S_T (Transverse Sphericity)	N/A	>0.2
(6) $E_T(j_1) + E_T(j_2) + \not\!\!E_T$	N/A	>300 GeV
Background [fb]		
$t\bar{t}$	145	24
W	710	11
Z	320	5
WW	0.4	N/A
ZZ	0.04	N/A
Total BG	1175	40

For TeV33 ($\int \mathcal{L}dt \geq 10$ fb^{-1}), there are two possible factors that may degrade the reach:

- $\not\!\!E_T$ – the $\not\!\!E_T$ resolution may be degraded in the high luminosity environment. We use a fairly high cut on $\not\!\!E_T$ (75 GeV), compared to 20 GeV in the trilepton analysis. We estimated an additional r.m.s. spread of 6 GeV in $\not\!\!E_T$ resolution due to events with an average of 10 multiple interactions. This led to a small effect for the signal events with $\not\!\!E_T > 20$ GeV. The effect on a 75 GeV cut is therefore assumed to be negligible. The effect on the QCD background is also assumed to be small.

- Jet identification – extra jets may be expected from additional events overlapped with the signal events. Currently, we are studying the probability of observing the jets ($E_T > 15$ GeV) from 9 additional events using Run 1 data. We assume this to be a small effect for this report.

We, therefore summarize the studies for $\not\!\!E_T$ + multijets channel without considering any degradation due to the multiple interactions.

Figure 6.4 shows $\sigma \times$ EFF versus $M_{\tilde{g}}$ for a variety of SUSY models. The maximum possible reach (5σ significance above the background) in the gluino mass is ~390 GeV/c^2 for 2 fb^{-1}. For luminosities of 10 fb^{-1} and 100 fb^{-1}, the maximum reach[3] is ≥400 GeV/c^2. Note that the reach in this direct search is considerably lower than the trilepton search for equivalent luminosities.

[3]The production cross section is falling steeply, so we only quote a minimum value for the maximum reach.

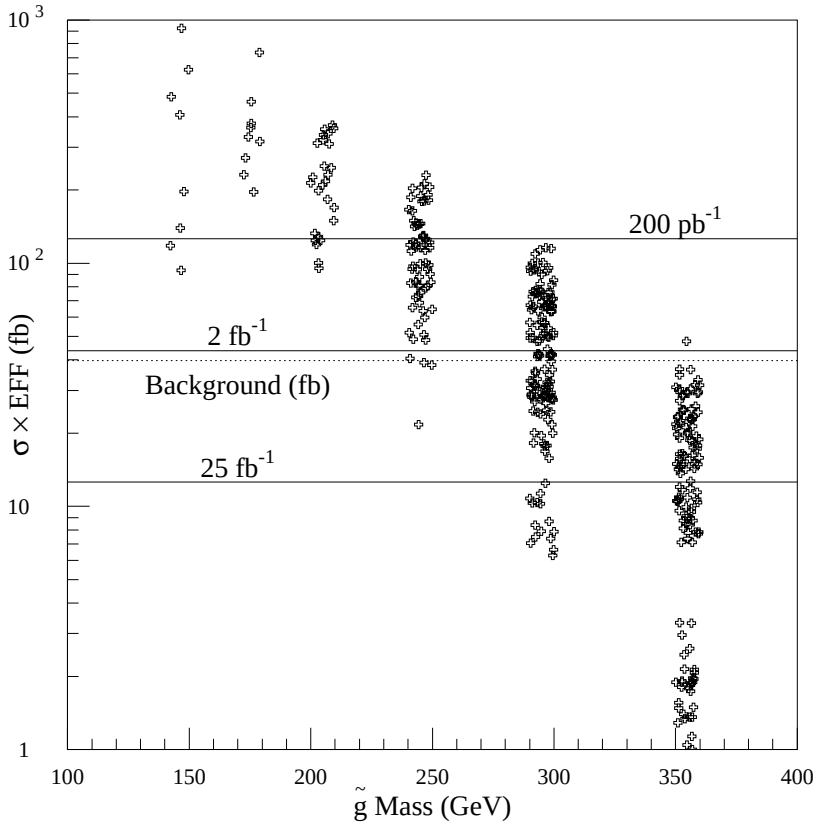

Figure 6.4: Gluino search in minimal supergravity models (or CMSSM): The $\sigma \times$ EFF is plotted for $\not{E}_T$ + jets signal versus the gluino mass [13]. The dotted line represents the background cross section of 40 fb. Three solid lines indicate the 10σ significance of the signal events above the background for integrated luminosities of 200 pb^{-1}, 2 fb^{-1} and 25 fb^{-1}.

Table 6.7: Cross section for $\tilde{t}_1\tilde{t}_1$ pair-production at 2 TeV, calculated with ISAJET (V7.06) and CTEQ2L parton distribution functions.

Mass (GeV/c^2)	σ (pb)
80	42
100	14
130	3.6
150	1.7

6.5.3 Light Top Squark Search

In the "$\not\!\!E_T$ " strategy outlined above, we assumed that all the squarks are mass degenerate. Given the high value for the top mass recently reported by DØ and CDF, Yukawa interactions should drive the stop ($\tilde{t}_1$) mass to a value much lower than the other squarks. There are three alternate decay modes possible for the light stop if it is lighter than the Standard Model top quark: (1) the two-body decay into a chargino ($\tilde{\chi}_1^{\pm}$) plus a b quark if the chargino is lighter than the stop; or (2) the three body decays to (s)lepton, (s)neutrino plus a b quark if the sleptons and sneutrinos are light enough; or (3) the two body decay into a neutralino ($\tilde{\chi}_1^0$) plus a c quark. Only possibilities (1) and (3) would be detectable at the Tevatron. The search strategies for a light stop are outlined in Refs. [17, 13].

Typical $\tilde{t}_1\tilde{t}_1$ Cross-sections

The cross section for stop production calculated using CTEQ2L parton distribution functions is given in Table 6.7. The $\tilde{t}_1\tilde{t}_1$ events are generated with ISAJET (Version 7.06) and simulated using a CDF parameterized detector simulation [18]. This has the advantage of providing realistic lepton identification efficiencies, as well as jet and $\not\!\!E_T$ resolution. The stop cross section depends only on the stop mass, but the decay kinematics depend on the mass of the chargino and the LSP.

Single-lepton Channel

If we look for one chargino in the event to decay leptonically, the large background from W + multijets can be reduced to an acceptable level by identifying one jet as coming from a b quark by a secondary vertex tag.

The event selection criteria similar to Ref. [17] are:

- At least one lepton ($ISO < 4$ GeV) with $E_T > 12$ GeV and $|\eta| < 1$;
- $2 \leq N_{jet} \leq 4$ with $E_T > 15$ GeV in $|\eta| < 2$;
- $\not\!\!E_T > 25$ GeV;
- $M_T(\ell\not\!\!E_T) < 45$ GeV;

Table 6.8: Observed $\tilde{t}_1\tilde{t}_1$ cross section via single-lepton (e or μ) events as a function of stop mass. We assume the branching ratio of $\tilde{\chi}_1^{\pm} \to \ell^{\pm}\nu\tilde{\chi}_1^0$ to be 11% for electron or muon channels. The b-tagging (per b jet) efficiency is taken to be a **conservative** number of ϵ_b = 20% being independent of $E_T(b)$ above 15 GeV.

Mass (GeV/c^2)	ϵ_{sel} (%)	ϵ_{tag} (%)	σ_{obs} (fb)
80	11	21	430
100	13	26	210
130	19	28	84
150	19	29	41

- At least one b-tagged jet in $|\eta(b)| < 2.4$;
- $|z_{vertex}| < 50$ cm.

The b-tagging (per b jet) efficiency is taken to be a **conservative** number of $\epsilon_b = 20\%$ being independent of $E_T(b)$ above 15 GeV.

The efficiency for these cuts together with the observed cross section as a function of stop mass is tabulated in Table 6.8. For simplicity, we assume the chargino mass to be 60 GeV/c^2, the LSP mass to be 30 GeV/c^2, and the branching ratio of $\tilde{\chi}_1^{\pm} \to \ell^{\pm}\nu\tilde{\chi}_1^0$ to be 11% for electron or muon channels. The selection includes a lepton geometric and identification efficiency of about 60%. The inclusion of leptons with rapidity out to 2 will increase the efficiency by only about 15% for a stop mass of 100 GeV/c^2. The efficiency falls off for high stop mass due to the transverse mass cut. It should be noted that both analyses in Refs. [17, 13] use $\epsilon_b = 30\%$.

We expect a signal to background ratio of $\approx$1 at $M_{\tilde{t}_1}$ = 110-120 GeV/c^2 [17, 13]. With an integrated luminosity of 2 fb^{-1}, it should be possible to probe a top squark up to 130 GeV/c^2 (5σ) for $M_{\tilde{\chi}_1^{\pm}} \sim 2M_{\tilde{\chi}_1^0} \sim 60$ GeV/c^2. If the b-tagging (per b jet) efficiency is ϵ_b = 50% (independent of $E_T(b)$ above 15 GeV), the observed $\tilde{t}_1\tilde{t}_1$ cross section via single-lepton (e or μ) events increases by a factor of 2 and the limit of about 150 GeV/c^2 is found.

Since this limit is model specific, we extract the maximum reach from more general analysis ($\epsilon_b = 30\%$ being independent of $E_T(b)$ above 15 GeV) in Ref. [13] and finds the 5σ mass limits of 150, 175 and 210 GeV/c^2 for 2, 10 and 100 fb^{-1}.

Di-lepton Channel

If we require both charginos to decay leptonically, we expect the background to be significantly reduced at the price of the additional leptonic branching fraction (here taken to be 11%). The event selection requires two identified electrons with a geometric and identification efficiency of about a 40% per event. The selection criteria similar to Ref. [17] are as follows:

- At least one lepton with $E_T > 8$ GeV and $|\eta| < 1$;
- The second lepton with $E_T > 5$ GeV and $|\eta| < 2.4$;

Table 6.9: Observed $\tilde{t}_1\tilde{t}_1$ cross section via di-lepton (ee, $e\mu$, $\mu\mu$) events as a function of stop mass. We assume the branching ratio of $\tilde{\chi}_1^{\pm} \to \ell^{\pm}\nu\tilde{\chi}_1^0$ to be 11% for electron or muon channels.

Mass (GeV/c^2)	ϵ_{sel} (%)	σ_{obs} (fb)
80	9	190
100	11	74
130	12	22
150	12	9.5

- $N_{jet} \geq 1$ with $E_T > 15$ GeV;
- $20^\circ < \phi_{\ell\ell} < 160^\circ$, where $\phi_{\ell\ell}$ is the opening angle between the lepton momenta in the plane transverse to the beam;
- $B\ (= p_T(\ell_1) + p_T(\ell_2) + \not\!\!E_T\ ) < 100$ GeV.

We separate the stop from standard model top events by defining a variable B [17] as the scalar sum of the lepton momenta and the missing transverse energy. The results including both electrons and muons are summarized in Table 6.9. In this study, we assume the chargino mass to be 60 GeV/c^2, the LSP mass to be 30 GeV/c^2. The cut on B parameter reduces the efficiency as the stop mass approaches that of the top quark. The observable cross section is reduced relative to the single lepton channel mostly due to the fact that the tagging efficiency is 2-3 times the branching fraction. However, this signal is expected to be cleaner than the single lepton decay mode. The signal to background ratio is expected to be $\approx$1 at $M_{\tilde{t}_1}$ = 130-150 GeV/c^2 [17, 13]. In an integrated luminosity of 2 fb^{-1}, it should be possible to explore a top squark mass up to $\sim$130 GeV/c^2 (5σ).

Since this limit is model specific, we extract the maximum reach from more general analysis ($\epsilon_b = 30\%$ being independent of $E_T(b)$ above 15 GeV) in Ref. [13] and finds the 5σ mass limits of 150, 170 and 200 GeV/c^2 for 2, 10 and 100 fb^{-1}.

$\not\!\!E_T$ + 2 acollinear jets

A recent analysis of Run 1a data by DØ [19] shows that for the case $\tilde{t}_1 \to \tilde{\chi}_1^0 c$, the Tevatron more than doubles the mass region excluded by LEP, as shown in Fig. 6.5. For this search, the signal is $\not\!\!E_T$ plus two acollinear jets. No significant signal is observed above background. The main cuts used are:

- $\not\!\!E_T\ > 40$ GeV
- $E_t(j_2) > 30$ GeV
- $\not\!\!E_T$ not back to back with jets
- no leptons (e or μ) in the event with $P_t > 10$ GeV/c

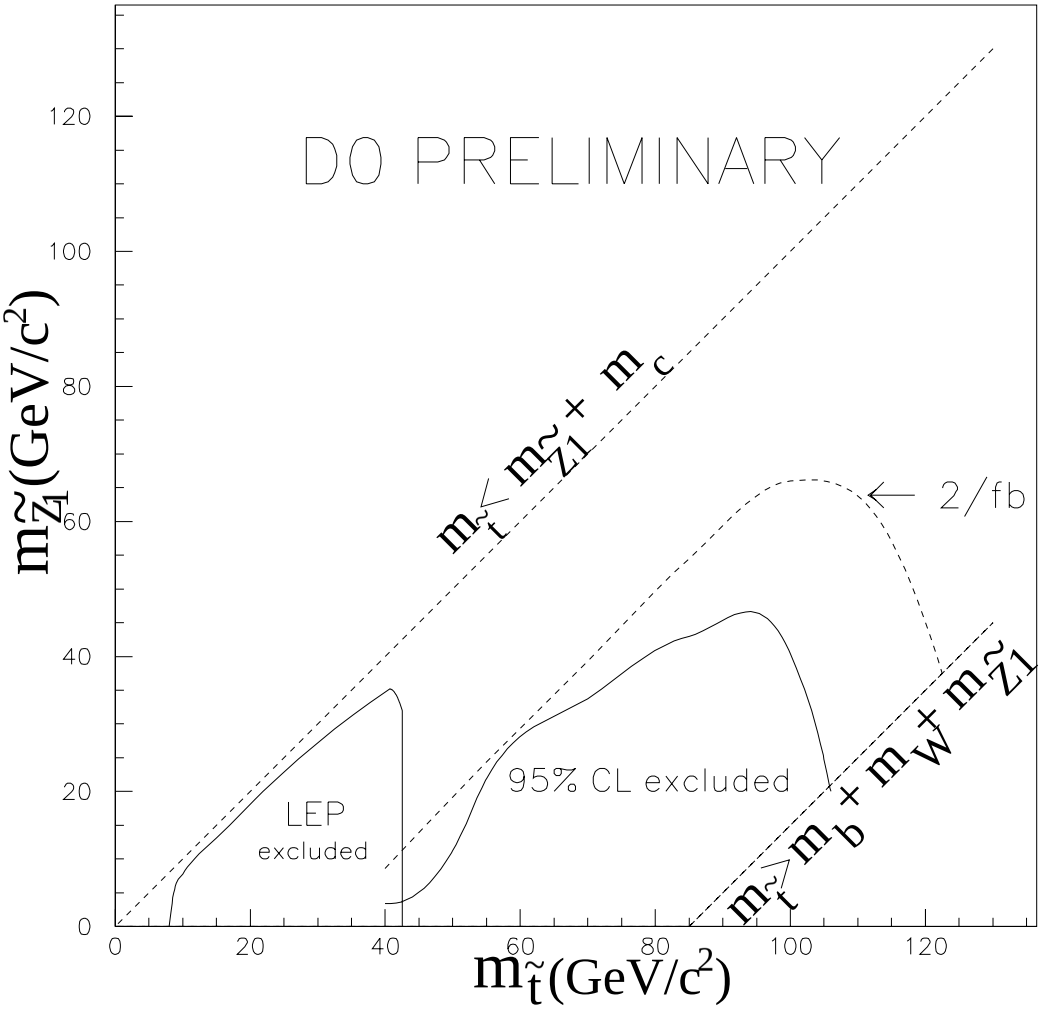

Figure 6.5: Current 95% CL DØ limit for the signal $\tilde{t}_1 \rightarrow \tilde{\chi}_1^0 c$ (solid line), and estimated future reach with the same cuts for an integrated luminosity of 2 fb^{-1} (dashed line).

The above analysis is repeated for an integrated luminosity of 2 fb^{-1} with the same event selection procedure as the original analysis. Assuming no additional signal events are found, the region to be excluded is shown in Fig. 6.5. This technique can be used for top squark masses as high as 150 GeV/c^2. However, the analysis is not able to improve the reach for integrated luminosities of 10 and 100 fb^{-1}, because the backgrounds are dominant. Additional reach may be obtained by reoptimizing the event selection for higher mass objects (*e.g.*, higher $\not\!\!E_T$ cut). If the top squark exists at masses below the top quark, and the $\tilde{t}_1 \rightarrow \tilde{\chi}_1^0 c$ signal is kinematically favored, it will most likely be discovered at TeV33.

6.5.4 Summary

The Standard Model (SM) of particle physics is in remarkably excellent agreement with existing data. In spite of this fact, there are strong theoretical arguments to suggest that the SM will break down in the TeV domain. Thus high energy physics is currently in the unique position of having a theory that works at a level of high precision, but must in fact be modified at an energy scale not far above existing accelerators. There are of course many reasons for building a new high energy accelerator. However, in view of the present status of high energy physics, a primary purpose must be to discover new physics.

Any model of new physics must face the difficult task of accommodating the high precision tests of the SM, and yet significantly modifying it at an energy scale not much beyond the Z boson. Further, the solution that supersymmetry (SUSY) gives to the hierarchy problem requires that there be a large array of new SUSY particles lying approximately between 100 GeV and 1 TeV. In spite of this, supersymmetry succeeds in perturbing the successes of the SM negligibly due to the fact that it implies the rapid decoupling of these particles from the SM particles. Further, experimental searches for the SUSY particles have examined only a very small part of the expected mass range of 100 GeV - 1 TeV, and so it is not surprising that the new SUSY particles have not yet been discovered. It is thus of importance for new accelerators to try to increase the mass reach if supersymmetry is to be tested.

The SUSY model the TeV33 SUSY group analysed was based on the particle spectrum of the MSSM (a SUSY partner for each SM particle with two Higgs doublets) combined with grand unification (based on supergravity) and R parity. (Supergravity is the gauge theory of global supersymmetry (MSSM) just as Yang-Mills theory is the gauge theory of global (constant) phase invariance.) This model is the most attractive from both the theoretical and experimental considerations. The supergravity induced interactions allow one to deduce the soft breaking of supersymmetry at the GUT scale (which only can be done by hand for the low energy MSSM), and from this one obtains an explanation of the origin of electroweak symmetry breaking at the Z scale by radiative effects. In addition, low energy predictions are almost all independent of the grand unification group, and hence of the unknown GUT physics. Several experimental successes have led to the acceptance of the model. It predicted the existence of grand unification more than a decade before the precision LEP data allowed its verification. Further, unification occurs if SUSY masses are precisely in the range needed to resolve the gauge hierarchy problem mentioned above. The model is also consistent with the low energy SM tests, as well as current bounds on proton decay. Finally, we mention that the condition of R parity invariance leads to a stable lightest supersymmetric particle (LSP)

Table 6.10: Preliminary results on the maximum mass reach for SUSY particles at TeV33. The reach is defined such that the number of signal events is either 5 events or a 5σ significance above background. The effect due to multiple interactions is considered only for 10 fb^{-1} and 100 fb^{-1}. The $(*)$ indicates the 95% C.L. limit with specific model in CDF or DØ analysis. The gluino mass limit for 100 pb^{-1} is extrapolated from the current CDF/DØ analysis for their particular SUSY model and with $M_{\tilde{q}} = M_{\tilde{g}}$.

Sparticle	Tevatron 20 pb^{-1}	Tevatron 100 pb^{-1}	Main Injector 2 fb^{-1}	TeV33 10/100 fb^{-1}
$\tilde{\chi}_1^{\pm}$	47 GeV/c^2(*)	70 GeV/c^2(*)	210 GeV/c^2	230/270 GeV/c^2
$\tilde{g}$	229 GeV/c^2(*)	270 GeV/c^2(*)	390 GeV/c^2	$\sim$400/>400 GeV/c^2
$\tilde{t}_1(\rightarrow \tilde{\chi}_1^{\pm} b)$	n/a	n/a	150 GeV/c^2	175/210 GeV/c^2
$\tilde{t}_1(\rightarrow \tilde{\chi}_1^0 c)$	100 GeV/c^2(*)	n/a	150 GeV/c^2(*)	n/a

which gives the right amount of dark matter over a large fraction of the parameter space. (This prediction is non-trivial as the relic dark matter density depends on such disparate quantities as the electroweak coupling constant, the LSP mass, the gravitational constant and the Hubble constant.)

If one adds additional light Higgs doublets to the particle spectrum, agreement with grand unification (or proton decay bounds) is lost, while a Higgs singlet would generally destabilize the gauge hierarchy. While the assumption of four generations (though not more) is still consistent with grand unification, it would ruin the prediction of M_b/M_τ for groups such as SU(5) or SO(10). Thus, the chosen model is fairly constrained, and it is therefore worthwhile to use it as the prototype for accelerator tests.

The SUSY mass limits at Tevatron, Main Injector and TeV33 are summarized in Table 6.10. This table shows the strong possibility of discovering SUSY at the Tevatron over a large region of parameter space. The theory predicts the existence of a light chargino ($\tilde{\chi}_1^{\pm}$) and two light neutralinos ($\tilde{\chi}_{1,2}^0$). These are generally lighter than the gluino and hence most accessible to observation at TeV33. We also have significant potential for dicovering the top squark, especially if the top proves to be heavy.

The SUSY mass limits at TeV33 (25 fb^{-1}) are also compared to the limits expected at LEP-II and NLC in Table 6.11. While LEP-II can find or exclude the light chargino ($\tilde{\chi}_1^{\pm}$) and light top-squark ($\tilde{t}_1$) masses up to nearly its kinematical limit ($\sqrt{s}/2$), searches at TeV33 improve a reach 2-3 times that of LEP-II. If LEP-II found a 90-GeV chargino, we should study 270-360 GeV gluino at TeV33. A preliminary study on determination of gluino mass shows the 300-GeV gluino mass could be measured within about 20 GeV [21]. TeV33 is also competitive to NLC in the gluino/squark searches. Thus, the SUSY searches at TeV33 is complementary to those at LEP-II and NLC. It should be noted that the light Higgs (h) search is also an important concomitant search, since SUSY predicts it to be lighter than 130 GeV/c^2.

The CERN Large Hadron Collider (LHC) will be a machine capable of a thorough search

Table 6.11: Summary of SUSY mass limits (5σ) at various colliders. "Exhaustive limit" means the least mass limit. Searches at LHC are not shown here. However, the limits are largely improved, *e.g.*, 1300-2000 TeV/c^2 for gluino depending on the choice of the parameter space.

Collider	LEP-II [6]	TeV33		NLC [6]
$\sqrt{s}$	190 GeV	2 TeV		500 GeV
$\int \mathcal{L}dt$	500 pb^{-1}	25 fb^{-1}		20 fb^{-1}
	Max. limit	Exhaustive limit	Max. limit	Max. limit
$\tilde{\chi}_1^{\pm}$	90 GeV	65 GeV [20]	250 GeV	248 GeV
$\tilde{g}/\tilde{q}$	85 GeV (100 pb^{-1})	300 GeV	over 400 GeV	$\sim$250 GeV
$\tilde{t}_1$ ($\rightarrow c\chi_1^0$)	83 GeV	48 GeV [20]	120 GeV (2 fb^{-1})	$\sim$250 GeV
$\tilde{t}_1$ ($\rightarrow b\chi_1^{\pm}$)	N/A	100 GeV	180 GeV	$\sim$250 GeV

for SUSY particles below the TeV scale [6]. If Fermilab can deliver an integrated luminosity of order 20-25 fb^{-1} (not 100 fb^{-1}) with reasonably upgraded CDF and DØ detectors before the LHC turns on, we can have the first physics result within $\sim$1 year after LHC turns on. If the gluino (chargino) is $\leq$ 400 (250) GeV, TeV33 (25 fb^{-1}) still has a chance to discover the SUSY particles during the LHC era.

In conclusion, the Tevatron may not be able to exclude SUSY theories if the searches prove inconclusive. However, TeV33 provides an excellent opportunity for the discovery of SUSY, as shown in this report.

Bibliography

[1] CDF Collaboration, Phys. Rev. Lett. **74**, 2626 (1995).

[2] D $\emptyset$ Collaboration, Phys. Rev. Lett. **74**, 2632 (1995).

[3] For reviews, see H.P. Nilles, Phys. Rep. **110**, 1 (1984); H.E. Haber and G.L. Kane, Phys. Rep. **117**, 75 (1985).

[4] LEP Collaborations, Phys. Lett., B **276**, 247 (1992).

[5] J. Ellis, S. Kelley, and D.V. Nanopoulos, Phys. Lett. B **249**, 441 (1990); U. Amaldi, W. de Boer, and H. Furstenau, Phys. Lett. B **260**, 447 (1991); P. Langacker and M.-X. Luo, Phys. Rev. D **44**, 817 (1991).

[6] For a recent review, H. Baer *et al.*, "Low Energy Supersymmetry Phenomenology," (DPF report) hep-ph/9503479, FSU-HEP-950401, LBL-37016, UH-511-822-95 (1995).

[7] For recent review, see R. Arnowitt and P. Nath, Proceedings of VIIth J.A. Swieca Summer School (World Scientific, Singapore, 1994).

[8] R. Arnowitt and P. Nath, Phys. Lett. **B299**, 58 (1993); **B303**, 403 (1993);CTP-TAMU-14/95-NUB-TH-3121/95; J. Lopez, D. Nanopoulos and K. Yuan, Phys. Rev. D **48**, 2766 (1993); G. Kane, C. Kolda, L .Roszkowski and J. Wells, Phys. Rev. D **49**, 6173 (1994); H. Baer and M. Brhlick, Phys. Rev. D **53**, 597 (1996).

[9] P. Nath and R. Arnowitt, Mod. Phys. Lett. **A2**, 331 (1987); R. Barbieri, F. Caravaglios, M. Frigeni and M. Mangano, Nucl. Phys. B **367**, 28 (1991); H. Baer and X. Tata, Phys. Rev. D **47**, 2739 (1992); J.L. Lopez, D.V. Nanopoulos, X. Wang and A. Zichichi, Phys. Rev. D **48**, 2062 (1993); H. Baer, C. Kao, and X. Tata, Phys. Rev. D **48**, 5175 (1993).

[10] ALEPH Collaboration, Phys. Lett. B **244**, 541 (1990) and Phys. Rep. **216C**, 253 (1992); DELPHI Collaboration, Phys. Lett. B **247**, 157 (1990); L3 Collaboration, Phys. Lett. B **233**, 530 (1989) and Phys. Rep. **236**, 1 (1993); OPAL Collaboration, Phys. Lett. B **240**, 261 (1990) and Phys. Lett. **B248**, 211 (1990). For review, see G. Giacomelli and P. Giacomelli, Riv. Nuovo Cim. **16**, 1 (1993).

[11] T. Kamon, J.L. Lopez, P. McIntyre, and J.T. White, Phys. Rev. D **50**, 5676 (1994).

[12] H. Baer, C.-H. Chen, C. Kao, and X. Tata, Phys. Rev. D **52**, 1565 (1995).

[13] S. Mrenna, G.L. Kane, G.D. Kribs, and J.D. Wells, Phys. Rev. D **53**, 1168 (1996).

[14] H. Baer, F.E. Paige, S.D. Protopopescu and X. Tata, "Simulating Supersymmetry with ISAJET 7.0/ISASUSY 1.0," *Proceedings of Workshop on Physics at Current Accelerators and the Supercollider*, eds. J. Hewett, A. White and D. Zeppenfeld (Argonne National Laboratory, 1993); F.E. Paige and S.D. Protopopescu, "ISAJET 7.0 : A Monte Carlo Event Generator for pp and $p\,\bar{p}$ Reactions," Brookhaven National Laboratory Report No. BNL-38774 (1986), (unpublished).

[15] S. Mrenna, "Simulating Supersymmetry with PYTHIA and JETSET," Report No. CIT 68-1987 (in preparation).

[16] H. Baer, C. Kao, and X. Tata, Phys. Rev. D **51**, 2180 (1995).

[17] H. Baer, J. Sender, and X. Tata, Phys. Rev. D **50**, 4517 (1994).

[18] M. Gold and T.L. Thomas, "Progress Report on Top Squark Search at the Fermilab Tevatron Collider," (unpublished) (1995).

[19] S. Abachi, et al, (D $\emptyset$ Collaboration), Phys. Rev. Lett. **76**, 2222, (1996).

[20] See, for example, "Search for Supersymmetric Particles in e^+e^- Collisions at Center-Of-Mass Energies of 130 and 136 GeV," CERN-PPE/96-10 (1996), submitted to Physics Letters B.

[21] S. Mrenna, private communication.

Chapter 7

Prospects for Exotic Physics at the Tevatron

7.1 Introduction

7.1.1 TeV2000 Exotics Group

This note is the first summary report of the TeV2000 Exotics Working Group, given the charge of examining the future prospects for non-SUSY exotic physics at the Tevatron. The group originated from the separate CDF and D0 efforts toward an expression of interest for Run III physics, which were united by the TeV2000 workshop at Ann Arbor in October 1994 organized by Dan Amidei and Chip Brock. Because we are a small group, we have only touched on a small fraction of the possible exotic physics we can explore at the Tevatron, and we welcome others into this collaborative CDF and D0 effort. We need as many people as possible to help us build the case for running the Tevatron with the highest luminosities and energies we can obtain. To join in this effort please send electronic mail to RHARRIS@FNALD.FNAL.GOV.

7.1.2 Motivation

Although the Standard Model is able to account for all known phenomena, it tells us nothing about the masses and mixing angles of quarks and leptons, the nature of the higgs mechanism and the value of the coupling constants. This proliferation of arbitrary parameters suggests the presence of new physics beyond the standard model. For convenience, we group the ideas for new physics into three categories. First, *extended gauge theories* which embed all or part of the standard model symmetry ($SU(3)_C \times SU(2)_L \times U(1)_Y$) within larger symmetry groups. For example grand unified theories based on the groups E_6, $SO(10)$, $SU(5)$, $SU(2)_L \times SU(2)_R$, or $SU(3)_L \times SU(3)_R$ which predict new gauge bosons (W' and Z'), leptoquarks, E_6 diquarks, axigluons, or topcolor gauge bosons. Second, *compositeness*, including models of composite quarks, leptons or higgs bosons. For example quark compositeness producing contact interactions and excited fermions, or technicolor in which the higgs boson is a composite technipion. Third, *miscellaneous phenomena*, which for now only

includes massive stable particles, but we hope to study a fourth generation quark b' and also unbiased searches for mass resonances without a theoretical model.

7.1.3 Technique

Here we present the capabilities of the Tevatron collider to find or exclude models of new physics. For models with a new particle we measure our sensitivity in terms of *mass reach* for the new particle, and for compositeness scales we similarly define an energy reach. For simplicity we will define mass reach as the largest excluded mass at 95% CL, and where possible we also present discovery reach numbers which represent the observation of significant deviations ($\sim 5\sigma$ effects). Defining mass reach in terms of exclusions allows easy comparison with prior searches where these limits are almost always stated. Mass reach is presented as a function of integrated luminosity, and also as a function of CMS energy where possible.

Our estimates are based on either fast simulations or extrapolations from existing searches. Extrapolations are based on the simple principle that when background is present the cross section limit scale inversely with the square root of the luminosity and when background is not present they scale inversely with the luminosity. We assume that current CDF and D0 capabilities for detection of high P_T jets, photons, and isolated leptons will not be significantly reduced at higher luminosities or energies. This assumes that if CDF and D0 are given 100 fb^{-1} in run III, we will also have the time and money to make modest modifications to the dynamic range of electronics and trigger systems to handle very high P_T objects.

7.2 Extended Gauge Theories

7.2.1 New Gauge Bosons W' and Z'

Heavy W bosons, generically denoted as W', occur in the left-right symmetric model [1] of electroweak interactions $SU(2)_R \times SU(2)_L \times U(1)_Y$. This model reproduces the standard electroweak model and also contains new right-handed W and Z bosons: W_R and Z_{LR}. Heavy Z bosons, generically denoted as Z', also occur in any extension of the standard model that contains an extra U(1) after symmetry breaking. For example, in one model with E_6 as the grand unified gauge group [2] there exists a Z_ψ from the symmetry breaking $E_6 \rightarrow SO(10) \times U(1)_\psi$ and a Z_χ from the symmetry breaking $SO(10) \rightarrow SU(5) \times U(1)_\chi$. Finally the SU(5) symmetry breaks to recover the standard model: $SU(5) \rightarrow SU(3)_C \times SU(2)_L \times U(1)_Y$. In superstring inspired E_6 models there exists a Z_η which is the linear combination $Z_\eta = \sqrt{3/8}Z_\chi + \sqrt{5/8}Z_\psi$.

$W' \rightarrow l\nu$

Searches for $W' \rightarrow l\nu$ have been conducted by both CDF in the electron and muon channels [3, 4] and by D0 in the electron channel [5]. Here we extrapolate the CDF limit in the electron channel [6]. The search assumes the decay mode $W' \rightarrow WZ$ is suppressed, and that

ν' in the decay $W' \to e\nu'$ is light, stable and non-interacting. The extrapolation assumes the background in the search region remains zero events, as it was in the CDF and D0 searches. The 95% CL upper limit on the cross section times branching ratio then scales inversely with luminosity. The theoretical W' cross section is calculated assuming standard model couplings and using $MRSD-'$ parton distributions and a K-factor to account for higher order terms [7]. Comparing the cross section upper limit to the theoretical calculation gives the results in Table 7.1 for the 95% CL lower limit on the W' mass.

Run	IA	IB	II	III
$\int \mathcal{L}dt$ (fb^{-1})	0.02	0.1	2.0	100
95% CL Limit (TeV)	0.65	0.77	0.99	1.28

Table 7.1: Current and projected CDF 95% CL lower limits on the mass of a heavy charged gauge boson from the decays $W' \to e\nu$. The limits are shown in TeV as a function of the luminosity exposure $\int \mathcal{L}dt$ for a $p\bar{p}$ center of mass energy $\sqrt{s} = 1.8$ TeV.

$W' \to$ dijets

Here we extrapolate CDF searches for new particles in the dijet mass spectrum [8]. There are significant backgrounds in the search region so the 95% CL upper limit on the cross section times branching ratio scales inversely with the square root of the luminosity. The theoretical W' cross section is calculated assuming standard model couplings and using CTEQ2L parton distributions and a K-factor to account for higher order terms [7]. As in the leptonic search, this search assumes the decay mode $W' \to WZ$ suppressed. In Fig. 7.1 we compare the current and projected CDF upper limits on cross section times branching ratio to the theoretical calculation to give the results in Table 7.2 for the 95% CL excluded regions for the W' mass. These projected limits are compared with those for other phenomena decaying to dijets in Fig. 7.2.

Run	IA	IB	II	III
$\int \mathcal{L}dt$ (fb^{-1})	0.02	0.1	2.0	100
95% CL Lower Excluded (TeV)	–	0.33	0.20	0.20
95% CL Upper Excluded (TeV)	–	0.47	0.72	0.92

Table 7.2: Current and projected CDF 95% CL limits on the mass of a heavy charged gauge boson from the decays $W' \to$ dijets. The upper and lower excluded ranges are shown in TeV as a function of the luminosity exposure $\int \mathcal{L}dt$ for a $p\bar{p}$ center of mass energy $\sqrt{s} = 1.8$ TeV.

$Z' \to ll$

Searches for $Z' \to l\nu$ have been conducted by both CDF in the electron and muon channels [9, 10] and by D0 in the electron channel [11]. Here we extrapolate the CDF limit in the electron and muon channels. The extrapolation assumes the background in the search region remains practically zero events, as it was in the CDF and D0 searches. The 95% CL upper limit on the

cross section times branching ratio then scales inversely with luminosity. The theoretical Z' cross section is calculated assuming standard model couplings and using $MRSD-'$ parton distributions and a K-factor to account for higher order terms [7]. Comparing the cross section upper limit to the theoretical calculation gives the results in Table 7.3 for the 95% CL lower limit on the Z' mass.

Run	IA	IB	II	III
$\int \mathcal{L}dt$ (fb^{-1})	0.02	0.1	2.0	100
95% CL Limit (TeV) at $\sqrt{s} = 1.8$ TeV	0.55	0.68	0.9	1.2
95% CL Limit (TeV) at $\sqrt{s} = 2.0$ TeV	—	0.74	1.0	1.3

Table 7.3: Projected CDF 95% CL lower limits on the mass of a heavy neutral gauge boson from the decays $Z' \to ee, \mu\mu$. The limits are shown in TeV as a function of the luminosity exposure $\int \mathcal{L}dt$ for various $p\bar{p}$ center of mass energies.

$Z' \to$ dijets

Here we extrapolate CDF searches for new particles in the dijet mass spectrum [8]. There are significant backgrounds in the search region so the 95% CL upper limit on the cross section times branching ratio scales inversely with the square root of the luminosity. The theoretical Z' cross section is calculated assuming standard model couplings and using CTEQ2L parton distributions and a K-factor to account for higher order terms [7]. In Fig. 7.1 we compare the current and projected CDF upper limits on cross section times branching ratio to the theoretical calculation to give the results in Table 7.4 for the 95% CL excluded regions for the Z' mass. These projected limits are compared with those for other phenomena decaying to dijets in Fig. 7.2.

Run	IA	IB	II	III
$\int \mathcal{L}dt$ (fb^{-1})	0.02	0.1	2.0	100
95% CL Lower Excluded (TeV)	–	0.34	0.29	0.20
95% CL Upper Excluded (TeV)	–	0.46	0.72	0.94

Table 7.4: Current and projected CDF 95% CL lower limits on the mass of a heave charged gauge boson from the decays from the decays $W' \to$ dijets. The upper and lower excluded ranges are shown in TeV as a function of the luminosity exposure $\int \mathcal{L}dt$ for a $p\bar{p}$ center of mass energy $\sqrt{s} = 1.8$ TeV.

New Gauge Boson Summary

In Fig. 7.3 current and projected search results for new gauge bosons at Fermilab are compared with the maximum capabilities of LEP II and NLC for direct searches. Until LHC, Fermilab has no competition in direct searches for new gauge bosons. Fig. 7.3 shows that Run III has the potential to effectively double our current mass reach for new gauge bosons.

7.2.2 E_6 diquarks $\rightarrow$ dijets

Superstring theory in 10 dimensions, which holds the prospect of unifying all forces including gravity, is anomaly free if the gauge group is $E_8 \times E_8$. The compactification of the extra 6 dimensions can lead to E_6 as the grand unification group for the strong and electroweak interactions. The E_6 models in turn predict the existence of many kinds of new particles [22], including a color triplet scalar diquark $D(D^c)$ with charge $-1/3(+1/3)$ which couples to $\bar{u}\bar{d}(ud)$. Thus the discovery of a dijet mass resonance could indicate an E_6 diquark and be interpreted as evidence for a "theory of everything". Here we extrapolate CDF searches for new particles in the dijet mass spectrum [8]. There are significant backgrounds in the search region so the 95% CL upper limit on the cross section times branching ratio scales inversely with the square root of the luminosity. The theoretical E_6 diquark cross section is calculated assuming electromagnetic Yukawa couplings, mass degenerate diquarks D and D^c, and using CTEQ2L parton distributions. In Fig. 7.1 we compare the current and projected CDF upper limits on cross section times branching ratio to the theoretical calculation to give the results in Table 7.5 for the 95% CL excluded regions for the E_6 diquark mass. These projected limits are compared with those for other phenomena decaying to dijets in Fig. 7.2.

Run	IA	IB	II	III
$\int \mathcal{L}dt$ (fb^{-1})	0.02	0.1	2.0	100
95% CL Lower Excluded (TeV)	–	0.33	0.20	0.20
95% CL Upper Excluded (TeV)	–	0.46	0.57	0.78

Table 7.5: Projected CDF 95% CL limits on the mass of an E_6 diquark from decays to dijets. The upper and lower excluded ranges are shown in TeV as a function of the luminosity exposure $\int \mathcal{L}dt$ for a $p\bar{p}$ center of mass energy $\sqrt{s} = 1.8$ TeV.

7.2.3 Axigluons $\rightarrow$ dijets

Although there is now little doubt that strong interactions result from an SU(3) gauge symmetry, there remains the possibility that the unbroken color symmetry $SU(3)_C$ results from the breaking of the larger chiral color group $SU(3)_L \times SU(3)_R$ [12]. One unambiguous prediction of all chiral color models is the axigluon, a massive color-octet of axial vector gluons. Axigluons are produced and decay strongly from quark-antiquark interactions, giving very large cross section times branching ratio to dijets. There is a long history of searches for axilguons at UA1 [13] and CDF [14, 15]. Here we extrapolate CDF searches for new particles in the dijet mass spectrum [8]. There are significant backgrounds in the search region so the 95% CL upper limit on the cross section times branching ratio scales inversely with the square root of the luminosity. The theoretical axigluon cross section is calculated assuming decays to the six flavors of quarks in the standard model and using CTEQ2L parton distributions. In Fig. 7.1 we compare the current and projected CDF upper limits on cross section times branching ratio to the theoretical calculation to give the results in Table 7.6 for the 95% CL excluded regions for the axigluon mass. These projected limits are compared with those for other phenomena decaying to dijets in Fig. 7.2.

Run	IA	IB	II	III
$\int \mathcal{L}dt$ (fb^{-1})	0.02	0.1	2.0	100
95% CL Lower Limit (TeV)	0.87	1.0	1.16	$\sim$1.3

Table 7.6: Actual and projected CDF 95% CL lower limits on the mass of an axigluon from decays to dijets. The limits are shown in TeV as a function of the luminosity exposure $\int \mathcal{L}dt$ at $\sqrt{s} = 1.8$ TeV.

7.2.4 Topcolor

The large mass of the top quark suggests that the third generation may be special. Topcolor [16, 17, 18] assumes that the top mass is large mainly because of a dynamical $t\bar{t}$ condensate generated by a new strong dynamics coupling to the third generation. Here the $SU(3)_C$ of QCD is a low energy symmetry arising from the breaking of an $SU(3)_1$ coupling to the third generation and an $SU(3)_2$ coupling to the first two generations only. There are then massive color octet bosons, topgluons B, which couple largely to $b\bar{b}$ and $t\bar{t}$. An additional $U(1)$ symmetry is introduced [18] to keep the b quark light while the top quark is heavy; this leads to a new gauge boson, Z'_{TopC}, which again couples largely to $b\bar{b}$ and $t\bar{t}$. CDF has preliminary results on the search for topgluons B and Z'_{TopC} in the $b\bar{b}$ channel using b-tagged dijets [19] and we hope to extrapolate these limits soon. Searches are also underway in the $t\bar{t}$ mass distribution [20].

7.2.5 Leptoquarks

Leptoquarks, color triplet particles coupling to a lepton and quark, appear in many extensions of the standard model [21, 22]. In grand unified theories with E_6, $SO(10)$ or $SU(5)$ as the grand unified gauge group, quarks and leptons are in the same multiplet and there exist leptoquarks which connect them. In composite models some bound states of preons are leptoquarks. In technicolor some technipions are leptoquarks. Also, models with a horizontal symmetry connecting leptons and quarks contain leptoquarks.

Leptoquarks are generally assumed to link, through an unknown coupling strength, λ, quark and lepton multiplets of the same generation in order to prevent violation of bounds on rare decays of mesons and bounds on flavor changing neutral currents [21, 23]. First generation leptoquarks decay to first generation quarks and leptons, etc. Leptoquarks can be produced singly via λ or in pairs through α_s or λ. Some constraints on λ [24] restrict λ to be less than one for leptoquark masses less than 200 GeV/c^2. Ignoring leptoquark production through λ, Tevatron experiments have searched for pair production of scalar leptoquarks where the production cross section is independent of λ.

First Generation Leptoquarks

Searches for first generation scalar leptoquarks have been conducted by CDF [26] and D0 [27]. Searches for second generation scalar leptoquarks have also been conducted by CDF [28] and D0 [29]. We have made an attempt to estimate the mass reach for leptoquarks with the

proposed upgrades of the Tevatron center of mass energy or luminosity. Here we employ a simulation of leptoquark detection at D0 from which we estimate a 25% detection efficiency for leptoquarks with masses between 300 and 400 GeV/c^2. The efficiency will be a little less for lighter mass leptoquarks and a little more for heavier mass leptoquarks, but the 25% will be used for all masses. The calculation of the theoretical cross section was performed by taking the pair production sub-process cross section for supersymmetric squarks in the limit of a very heavy gluino and folding it with the CTEQ lowest order parton distribution functions. This was found to be consistent with ISAJET's cross section. Here, we again assumed that λ is small compared to α_s and is ignored. In Table 7.7 we present mass thresholds for a ten event discovery of a scalar leptoquark; for a three event observation, corresponding to a 95% CL upper limit, add roughly 0.05 TeV to the numbers listed except where the three event limit is indicated by the numbers in the parentheses. The 100 fb^{-1} mass numbers at the $\sqrt{s} = 2.0$ TeV and $\sqrt{s} = 3.5$ center of mass energies were extrapolated from the other numbers. The three event, 95% C.L., limit should not be significantly different for these two numbers.

$\int \mathcal{L}dt$ (fb^{-1})	0.1	1.0	10	100
Discovery Reach (TeV) at $\sqrt{s} = 2.0$ TeV	0.175	0.235	0.325	0.360
Discovery Reach (TeV) at $\sqrt{s} = 3.5$ TeV	0.250	0.356	0.438(0.460)	0.470
Discovery Reach (TeV) at $\sqrt{s} = 4.0$ TeV	0.278	0.380	0.452(0.470)	0.486(0.490)

Table 7.7: Projected D0 10 event discovery reach for a leptoquark. The masses are shown in TeV as a function of the luminosity exposure $\int \mathcal{L}dt$ for various $p\bar{p}$ center of mass energies.

In Fig. 7.4 these projected search results for leptoquarks at Fermilab are compared with the maximum capabilities of HERA, LEP II and NLC for direct searches. Until LHC, Fermilab has little competition in direct searches for scalar leptoquarks. In addition to scalar leptoquarks, the possibility of vector leptoquarks exist. Cross sections for the pair production of vector leptoquarks are in the process of being calculated [25]. The pair production cross section for vector leptoquarks appears to be much larger than that for scalar leptoquarks. Though verified cross sections are not yet available, mass reaches of about twice those for scalar leptoquarks may be possible.

In summary, for the 1994 - 1996 run in progress at the Tevatron ($\sqrt{s} = 1.8$ TeV), the expected reach in mass is about 200 GeV/c^2 for scalar leptoquarks and perhaps 400 GeV/c^2 for vector leptoquarks. The mass reach for the most aggressive upgrade of the Tevatron for scalar leptoquarks seems to top out at about 0.5 TeV and perhaps about 1 TeV for vector leptoquarks. These limits represent a significant amount of search space, and the potential for discovery is exciting.

Second Generation Leptoquarks

Searches for second generation scalar leptoquarks have been conducted by CDF [28] and D0 [29]. The mass reach for second generation leptoquarks is expected to be similar to first generation leptoquarks.

7.3 Compositeness

Perhaps the most historically compelling model of new physics is compositeness. If quarks and leptons are composite particles we expect four fermion contact interactions [30] to modify the quark and lepton production cross sections at high transverse momentum. If quarks are composite particles excited states [31] are expected and can be searched for in the quark plus gauge boson invariant mass spectrum. Finally, technicolor provides a dynamic mechanism for electroweak symmetry breaking based on composite higgs bosons. Models of walking technicolor have not been excluded and predict color octet technirhos which decay to dijets and color singlet technirhos which decay to W or Z plus dijets.

7.3.1 Contact Interactions

$\Lambda(qqqq)$

The four quark contact interaction has been extensively searched for at the CERN SPPS collider [32] and the Tevatron [33]. The usual method has been to search for either an excess of high P_T jets or a more isotropic jet angular distribution than the QCD prediction, the most stringent limits coming from the former. D0 is searching for contact interactions in the distribution of the scalar sum of event transverse energy. All other limits presented in this note scale roughly proportionally with the logarithm of the luminosity, so for a first pass we will assume the same for the compositeness scale. We fit the last 2 published CDF compositeness limits from the high P_T jet search to a straight line in the limit vs. log luminosity plane, and obtain the results presented in table 7.8. We caution the reader that this gives a higher projected limit than indicated by preliminary CDF data in Run 1A. This data is currently fit better by QCD + compositeness with $\Lambda = 1.5$ TeV, than by QCD alone [34].

Run	IA	IB	II	III
$\int \mathcal{L}dt$ (fb^{-1})	0.02	0.1	2.0	100
95% CL Limit (TeV) at $\sqrt{s} = 1.8$ TeV	1.6	1.8	2.2	2.8

Table 7.8: Projected CDF 95% CL lower limits on the compositeness scale for a four quark contact interaction $\Lambda(qqqq)$. The limits are shown in TeV as a function of the luminosity exposure $\int \mathcal{L}dt$.

$\Lambda(qqll)$

If quarks and leptons are both composite and share constituents, then effective contact interactions arise between them at low energies [30]. The quark-lepton contact interaction has been searched for at CDF in the dielectron [35] and dimuon [9] channels. The technique is to search for an excess of high mass dileptons compared to the Drell-Yan prediction. We define a mass above which there will be essentially no Drell-Yan background– $M(0.5)$, the mass above which 0.5 events are expected. We then calculate the integrated cross

section above this mass including a contact interaction. Figure 7.5 shows the effect of the compositeness interaction on the integrated cross section. We take as the 95% CL lower limit the size of this interaction that would give less then 3.2 events above this mass. Here, the lepton-quark compositeness scale ($\Lambda(qqll)$) corresponds to a left-left coupling with constructive interference with the dominant u-quark contribution to the cross section. The results are tabluated in table 7.9.

$\int \mathcal{L}dt$ fb^{-1}	σ_{DY} fb^{-1}	M(0.5) GeV	$\Lambda(qqll)$
1	0.5	660	5.1
2	0.25	712	5.4
5	0.1	780	6.1
100	0.005	980	7.4

Table 7.9: Projected CDF 95% CL lower limits on the compositeness scale for a lepton-quark contact interaction $\Lambda(qqll)$. The limits are shown in TeV as a function of the luminosity exposure $\int \mathcal{L}dt$.

7.3.2 Excited Quarks

Excited states of composite quarks, denoted q^*, have been searched for at UA2 [36], CDF [37, 8] and soon at D0 [38]. They are produced singly by quark gluon fusion and can decay to a common quark and any gauge boson (g, γ, W or Z) [31].

$q^* \rightarrow q\gamma, qW$

Here we extrapolate the CDF search [37] in the photon + jet and W + jet channels. There are almost no events in the mass region where the combined limit is set, and we assume this will remain the case so that the cross section limit will roughly scale inversely with luminosity. For the theoretical prediction we perform a lowest order calculation using CTEQ1L parton distributions and assume standard model couplings and mass degenerate diquarks u^* and d^*. In Fig. 7.6 we compare the current and projected CDF upper limits on cross section times branching ratio to the theoretical calculation to give the results in Table 7.10 for the 95% CL excluded regions for the excited quark mass.

Run	IA	IB	II	III
$\int \mathcal{L}dt$ (fb^{-1})	0.025	0.1	2.0	100
95% CL Limit (TeV) at $\sqrt{s}$ = 1.8 TeV	0.54	0.64	0.82	1.08
95% CL Limit (TeV) at $\sqrt{s}$ = 2.0 TeV	—	0.69	0.91	1.18
95% CL Limit (TeV) at $\sqrt{s}$ = 3.5 TeV	—	1.03	1.41	1.90

Table 7.10: Actual and projected CDF 95% CL lower limits on the mass of a excited quark from the decays $q^* \rightarrow\rightarrow q\gamma, qW$. The limits are shown in TeV as a function of the luminosity exposure $\int \mathcal{L}dt$ for various $p\bar{p}$ center of mass energies.

$q^* \to qg$

Here we extrapolate CDF searches for new particles in the dijet mass spectrum [8]. There are significant backgrounds in the search region so the 95% CL upper limit on the cross section times branching ratio scales inversely with the square root of the luminosity. The theoretical q^* cross section is calculated assuming standard model couplings, mass degenerate excited quarks u^* and d^*, and uses CTEQ2L parton distributions. In Fig. 7.1 we compare the current and projected CDF upper limits on cross section times branching ratio to the theoretical calculation to give the results in Table 7.11 for the 95% CL excluded regions for the q^* mass.

Run	IA	IB	II	III
$\int \mathcal{L}dt$ (fb^{-1})	0.02	0.1	2.0	100
95% CL limit (TeV)	0.56	0.71	0.82	1.02

Table 7.11: Current and projected CDF 95% CL lower limits on the mass of an excited quark from the decays $q^* \to$ dijets. The limits are shown in TeV as a function of the luminosity exposure $\int \mathcal{L}dt$ for a $p\bar{p}$ center of mass energy $\sqrt{s} = 1.8$ TeV.

Excited Quark Summary

In Fig. 7.7 current and projected search results for excited quarks at Fermilab are compared with the maximum capabilities of HERA and NLC for direct searches. Until LHC, Fermilab has no competition in direct searches for excited quarks. Fig. 7.7 shows that a luminosity upgrade for Run III has the potential to effectively double our current mass reach for excited quarks, and an energy upgrade for run III has the potential to triple it.

7.3.3 Technicolor

The origin of electroweak symmetry breaking is arguably the last remaining puzzle of the standard model. Symmetry breaking arising from a fundamental Higgs boson is admittedly ad hoc. Instead, technicolor assumes that pairs of fundamental techniquarks are bound into a composite scalar, a technipion, which generates a dynamical symmetry breaking. The mechanism is similar to the way cooper pairs of electrons generate a superconducting phase transition in the BCS theory of superconductivity.

Color Octet Technirho $\rho_T \to$ dijets

In a recent technicolor model [39, 40] there exists a color octet technirho (ρ_T) which couples to $q\bar{q}$ and gg via a virtual intermediate gluon ($\rho_T \to g \to q\bar{q}, gg$). Here we extrapolate CDF searches for new particles in the dijet mass spectrum [8]. There are significant backgrounds in the search region so the 95% CL upper limit on the cross section times branching ratio scales inversely with the square root of the luminosity. The theoretical cross section is calculated assuming the technirho decays only to dijets (assumes all technipions are too massive to be

decay products). We use CTEQ2L parton distributions. In Fig. 7.1 we compare the current and projected CDF upper limits on cross section times branching ratio to the theoretical calculation to give the results in Table 7.12 for the 95% CL excluded regions for the ρ_T mass. These projected limits are compared with those for other phenomena decaying to dijets in Fig. 7.2.

Run	IA	IB	II	III
$\int \mathcal{L}dt$ (fb^{-1})	0.02	0.1	2.0	100
95% CL Lower Excluded (TeV)	.32	0.26	0.20	0.20
95% CL Upper Excluded (TeV)	.48	0.54	0.77	0.96

Table 7.12: Current and projected CDF 95% CL limits on the mass of a color octet technirho from the decays $\rho_T \rightarrow$ dijets. The upper and lower excluded ranges are shown in TeV as a function of the luminosity exposure $\int \mathcal{L}dt$ for a $p\bar{p}$ center of mass energy $\sqrt{s} = 1.8$ TeV.

7.4 Miscellaneous Phenomena

7.4.1 Massive Stable Particles

Massive stable particles are possible features of several theories which go beyond the standard model including supersymmetry, mirror fermions, technicolor, and compositeness. CDF has conducted a search for heavy stable charged particles [41, 42] based upon their expected high transverse momenta, relatively low velocities, and muon-like penetration of matter.

The basic CDF result consisted of upper limits on the cross-section for the production of heavy stable particles as a function of their mass. To translate this into mass limits, one has to assume a theoretical cross-section appropriate to a particular theory. As an example we consider unit-charged fermionic particles which are pair-produced and belong to various color multiplets, ie. triplets, sextets, octets, and decuplets. Table 7.13 gives the expected lower mass limits as a function of integrated luminosity. It has been assumed that the cross-section limits scale inversely with the luminosity and that the relevant detector components remain as they are currently configured. In particular, a new time-of-flight system could improve these results significantly.

Run	IA	IB	II	III
$\int \mathcal{L}dt$ (fb^{-1})	0.02	0.1	2.0	100
color triplets	0.19	0.25	0.38	0.54
color sextets	0.26	0.32	0.45	0.60
color octets	0.26	0.33	0.45	0.60
color decuplets	0.33	0.39	0.52	0.66

Table 7.13: Projected CDF 95% CL lower limits on the mass of stable unit-charged particles at $\sqrt{s} = 1.8$ TeV. The limits are shown in TeV as a function of the luminosity exposure $\int \mathcal{L}dt$.

In Fig. 7.8 projected search results for massive stable particles at Fermilab are compared with the maximum capabilities of LEP II and NLC for direct searches. Until LHC, Fermilab has no competition in direct searches for these particles. Fig. 7.8 shows that Run III has the potential to effectively double our current mass reach.

7.5 Summary and Conclusions

We have investigated the exotics search potential of a superluminous Tevatron. The mass reach for many new particles at the Tevatron is summarized in figure 7.9. For excited quarks and leptoquarks we have also presented the search potential of an energy upgraded Ditevatron. In many channels the results are similar: a luminosity upgrade to 100 fb^{-1} will effectively double our current mass reach, and an energy upgrade to 4 TeV will effectively triple it. Although these results prefer an energy upgrade, they illustrate that a luminosity upgrade is the equivalent of exploring a completely new energy scale. Most new phenomena have no preferred mass scale, so doubling the mass reach with a superluminous tevatron provides an experiment with twice the discovery capability of all previous experiments in high energy physics. These prospects are quite exciting.

Bibliography

[1] For a review and original references see R. N. Mohapatra, *Unification and Supersymmetry* (Springer, New York, 1986).

[2] See F. del Aguila, M. Quiros, and F. Zwirner, Nucl. Phys. **B287**, 457 (1987) and references therein.

[3] (CDF Collaboration) F. Abe et al., Phys. Rev. Lett. **67**, 2609 (1991).

[4] (CDF Collaboration) F. Abe et al., Fermilab-PUB-94/268-E, submitted to Phys. Rev. Lett.

[5] (D0 Collaboration).

[6] (CDF Collaboration) S. Kopp and J. Wahl, CDF Note 2541, 1994.

[7] V. Barger and R. Phillips, *Collider Physics*, (Addison-Wesley, 1987), p.233 for Z' K-factor and p. 248 for W' K-factor.

[8] (CDF Collaboration) R. Harris, Fermilab-Conf-94/222-E, proceedings of the meeting of the Division of Particles and Fields, Albuquerque, New Mexico, August 2-6, 1994.

[9] (CDF Collaboration) F. Abe et al., Phys. Rev. Lett. **68**, 1462 (1992).

[10] (CDF Collaboration) F. Abe et al., Fermilab-PUB-94/198-E, submitted to Phys. Rev. Lett.

[11] (D0 Collaboration).

[12] P. Frampton and S. Glashow, Phys. Lett. **B190**, 157 (1987).

[13] (UA1 Collaboration), C. Albajar et al., Phys. Lett. **B209**, 127 (1988).

[14] (CDF Collaboration) F. Abe et al., Phys. Rev. **D41**, 1722 (1990).

[15] (CDF Collaboration) F. Abe et al., Phys. Rev. Lett. **71**, 2542 (1993).

[16] C. Hill and S. Parke, Phys. Rev. **D49**, 4454 (1994).

[17] C. Hill and X. Zang, Fermilab-PUB-94/231-T (1994).

[18] C. Hill, Fermilab-PUB-94/395-T (1994).

[19] (CDF Collab) J. Bao, J. Benlloch, and R. Harris, CDF Note 3024, or on the WWW see http://www-cdf.fnal.gov/physics/new/qcd/btag_dijet/btag_dijet.html

[20] (CDF Collab) Kirsten Tollefson, private communication.

[21] J. Hewett and S. Pakvasa, Phys. Rev. **D37**, 3165 (1988).

[22] J. Hewett and T. Rizzo, Phys. Rep. **C183**, 193 (1989).

[23] W. Buckmüller and D. Wyler, Phys. Lett. B *177*, 377 (1986).

[24] J. L. Hewett and T. G. Rizzo, Phys. Rev. D *36*, 3367 (1988).

[25] J. L. Hewett, T. G. Rizzo, S. Pakvasa, H. E. Harber, A. Pomarol, Proceedings of the Workshop on Physics at Current Accelerators and the Supercollider, Argon National Laboratory, June2-5, 1993, ANL-HEP-CP-93-52.

[26] (CDF Collaboration) F. Abe et al., Phys. Rev. **D48**, 3939 (1993).

[27] (D0 Collaboration) S. Abachi et al., Phys. Rev. Lett. **72**, 965 (1994).

[28] (CDF Collaboration) S. Park.

[29] (D0 Collaboration) D. Norman.

[30] E. Eichten, K. Lane, and M. Peskin, Phys. Rev. Lett. **50**, 811 (1983).

[31] U. Baur, I. Hinchliffe, and D. Zeppenfeld, Int. J. Mod. Phys. **A2**, 1285 (1987); U. Baur, M. Spira and P. Zerwas, Phys. Rev. **D37**, 1188 (1988).

[32] (UA2 Collaboration) J. A. Appel et al., Phys. Lett. **B160**, 349 (1985); (UA1 Collaboration) G. Arnison et al., Phys. Lett. **B172**, 461 (1986), Phys. Lett. **B177**, 244 (1986).

[33] (CDF Collaboration) F. Abe et al., Phys. Rev. Lett. **62**, 613 (1989), Phys. Rev. Lett. **62**, 3020 (1989), Phys. Rev. Lett. **68**, 1104 (1992), Phys. Rev. Lett. **69**, 2896 (1992).

[34] (CDF Collaboration) A. Bhatti, CDF Note 2457, Version 3.0.

[35] (CDF Collaboration) F. Abe et al., Phys. Rev. Lett. **67**, 2418 (1991).

[36] (UA2 Collaboration) J. Alitti et al., Nucl. Phys. **B400**, 3 (1993).

[37] (CDF Collaboration) F. Abe et al., Phys. Rev. Lett. **72**, 3004 (1994).

[38] (D0 Collaboration) Bob Madden, private communication.

[39] K. Lane and M. V. Ramana, Phys. Rev. **D44**, 2678 (1991).

[40] E. Eichten and K. Lane, Phys. Lett. **B327**, 129 (1994).

[41] (CDF Collaboration) F. Abe et al., Phys. Rev. Lett. **63**, 1447 (1989).

[42] (CDF Collaboration) F. Abe et al., Phys. Rev. **D46**, 1889 (1992).

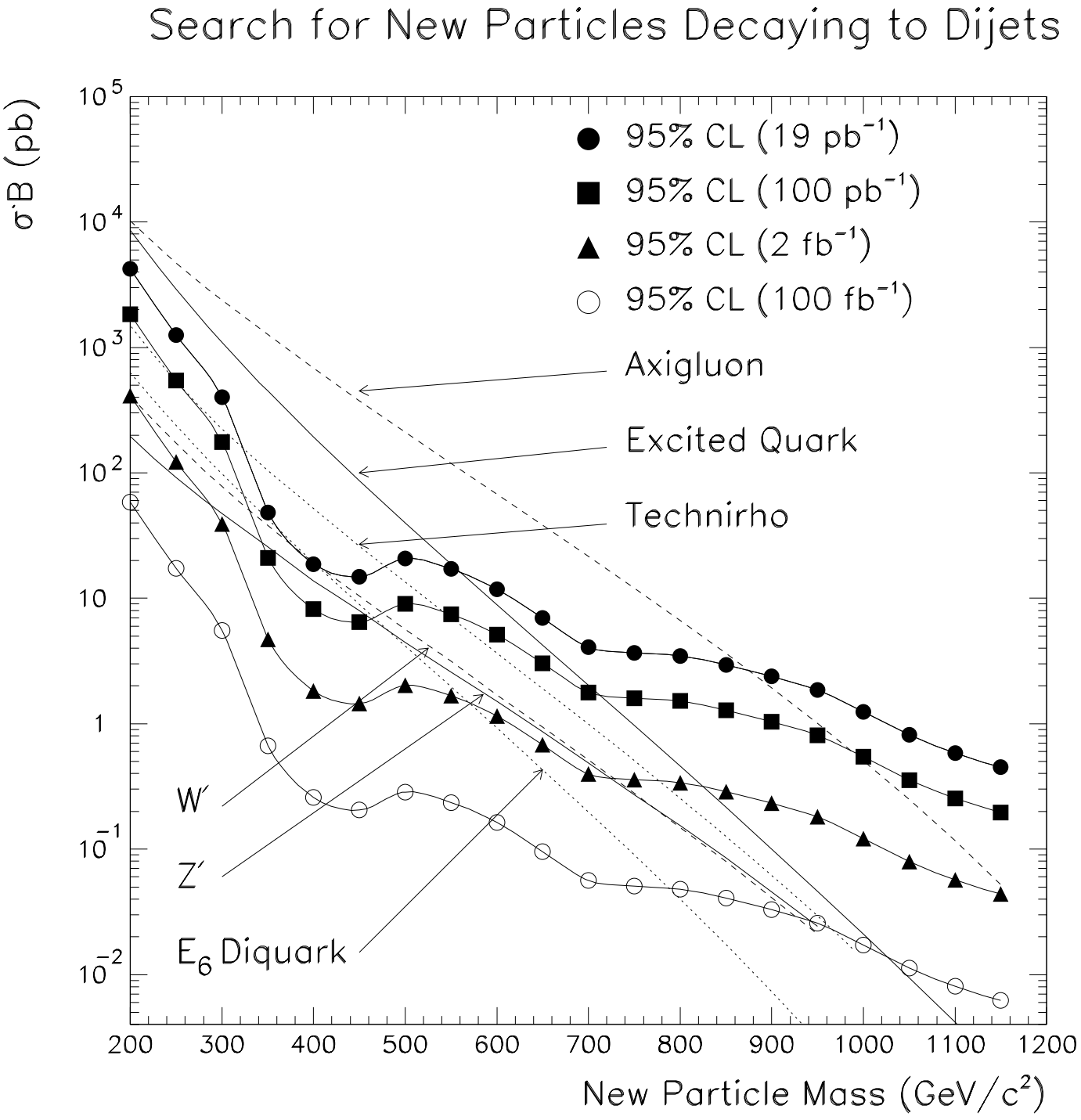

Figure 7.1: The 95% confidence level upper limit on the cross section times branching ratio for new particles decaying to dijets vs. new particle mass for an exposure of 19 pb^{-1} (closed circles) 100 pb^{-1} (squares) 2 fb^{-1} (triangles) and 100 fb^{-1} (open circles) is compared to the theoretical prediction for the cross section for axigluons, excited quarks, technirhos, new gauge bosons (W' and Z'), and E_6 diquarks.

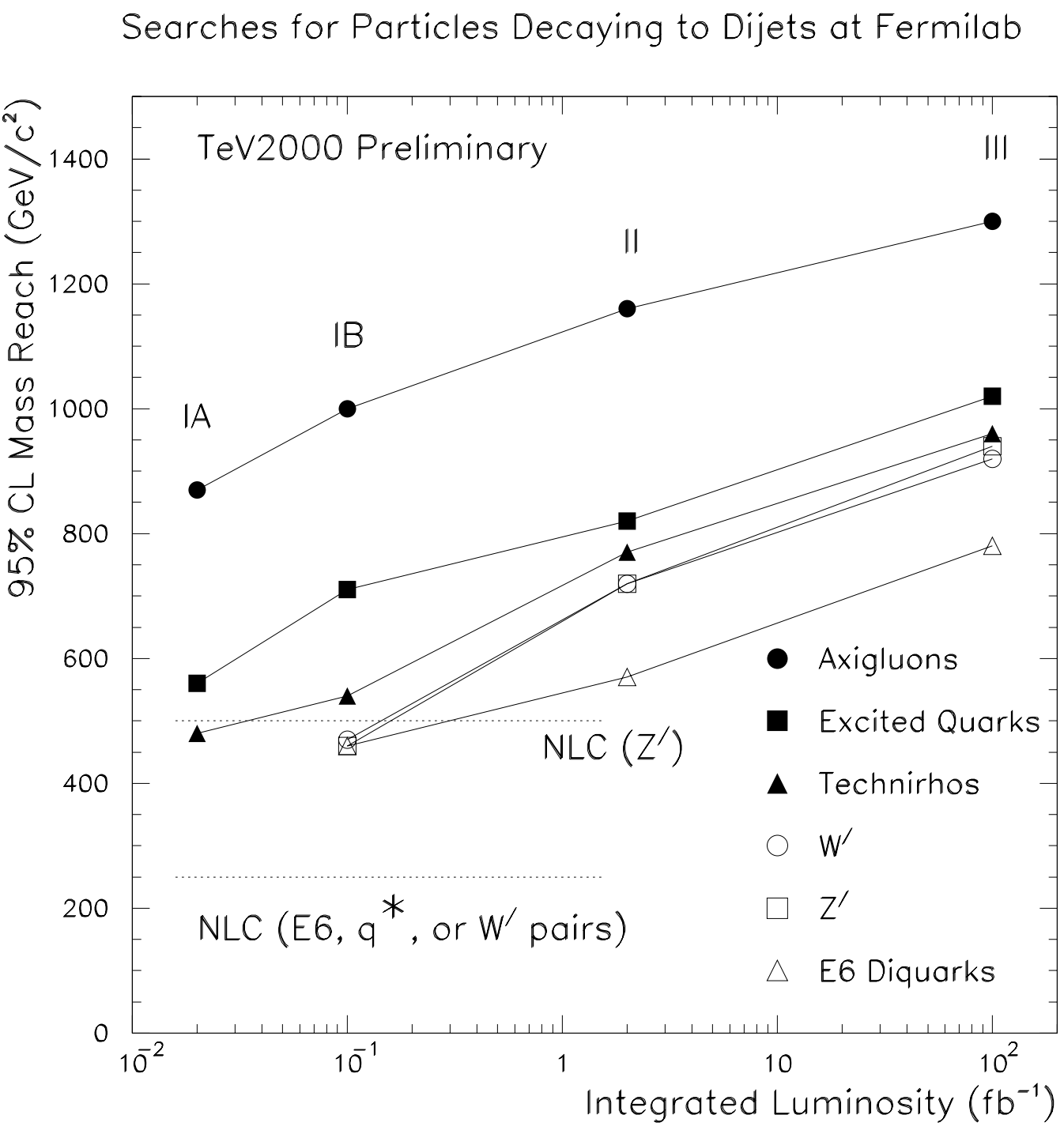

Figure 7.2: The mass reach for new particles decaying to dijets, defined as the 95% CL lower limit on the mass, is plotted vs. integrated luminosity at the Tevatron. The maximum mass reach of other accelerators is shown.

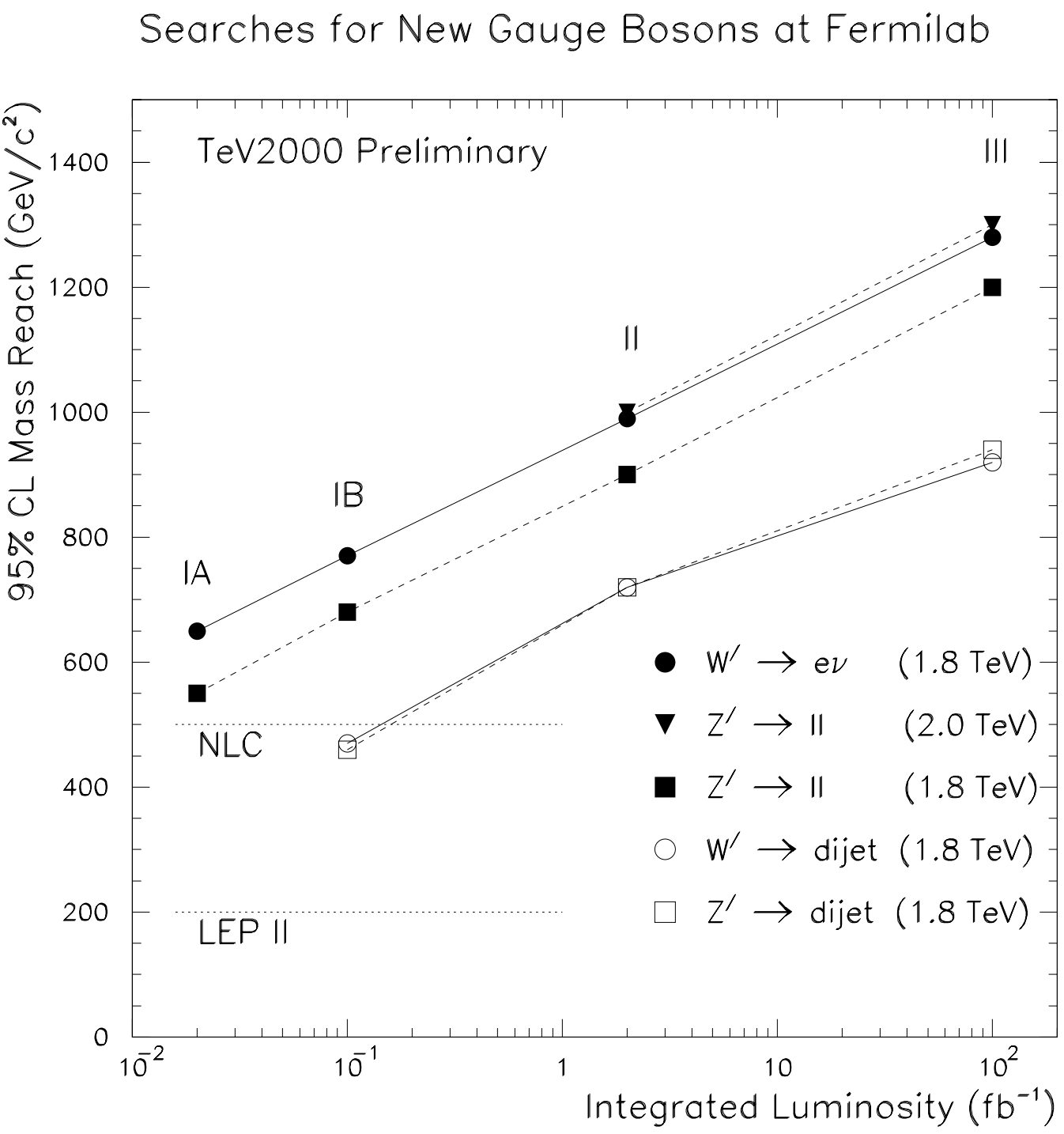

Figure 7.3: The mass reach for new gauge bosons, defined as the 95% CL lower limit on the mass, is plotted vs. integrated luminosity at the Tevatron. The maximum mass reach of other accelerators is shown.

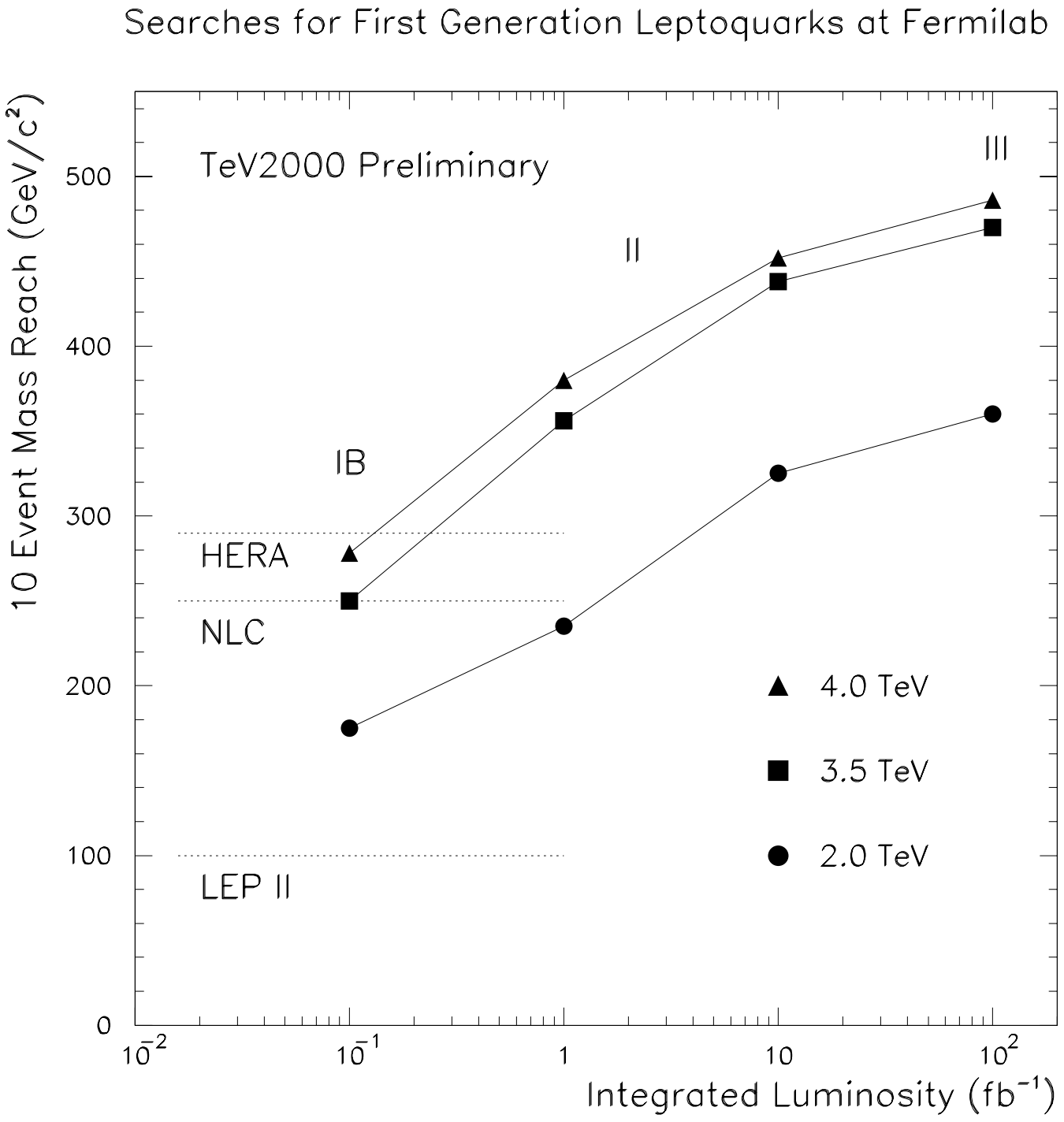

Figure 7.4: The mass reach for new particles decaying to dijets, defined as the mass at which 10 events can be observed, is plotted vs. integrated luminosity at the Tevatron. The maximum mass reach of other accelerators is shown.

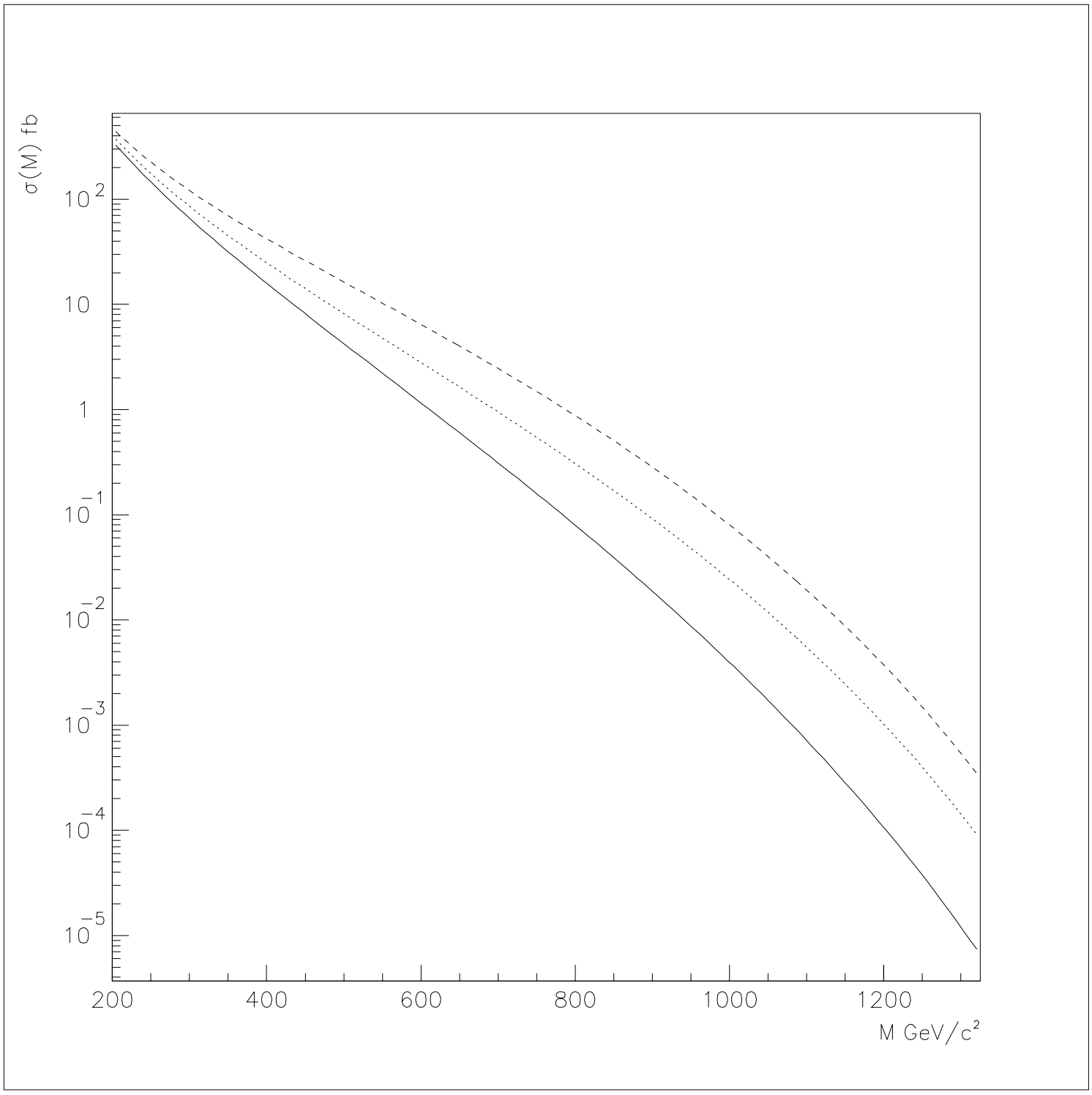

Figure 7.5: The standard model integrated Drell-Yan cross section for lepton pair production (solid line); integral cross section including a contact interaction $\Lambda(qqll) = 5$ TeV (dashed line); integral cross section including a contact interaction $\Lambda(qqll) = 7.5$ TeV (dotted line).

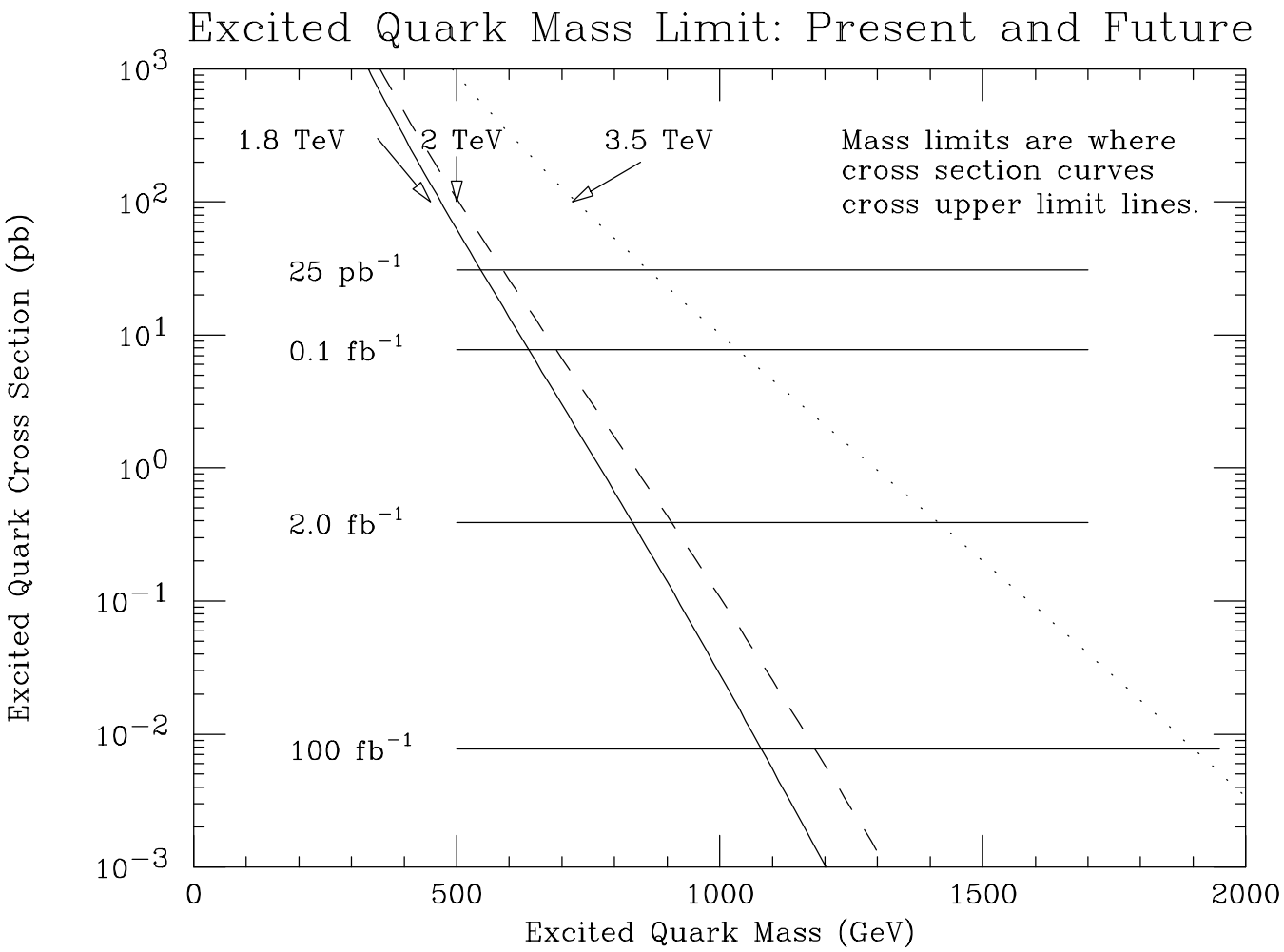

Figure 7.6: The 95% confidence level upper limit on the total cross section for excited quarks from searches in the $q\gamma$ and qW channel is shown by horizontal solid lines for exposures corresponding to the 1988-89 run + run 1A, run 1B, run II and run III. This limit is compared to the theoretical cross section for excited quarks at three CMS energies.

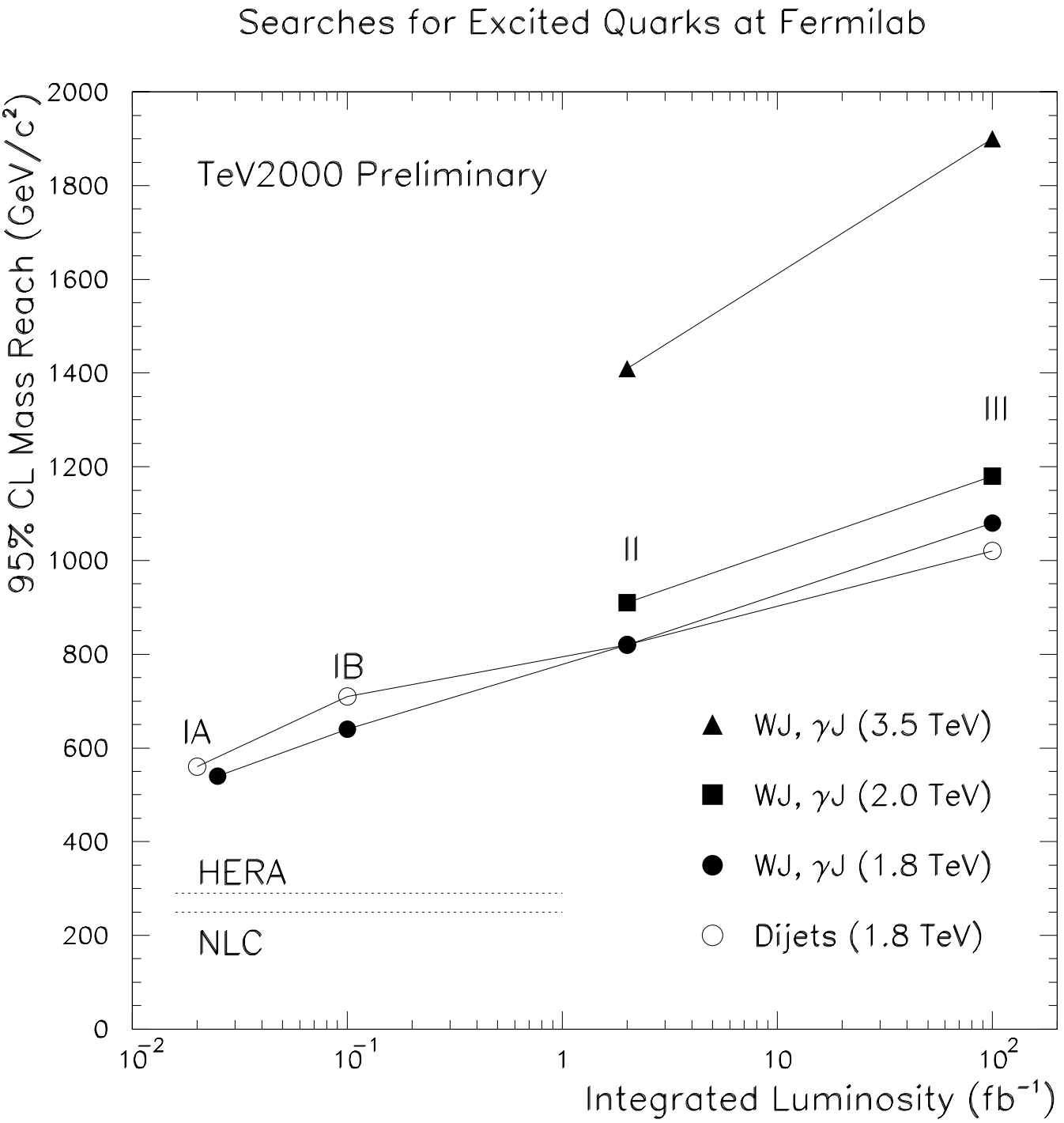

Figure 7.7: The mass reach for excited quarks, defined as the 95% CL lower limit on the mass, is plotted vs. integrated luminosity at the Tevatron. The maximum mass reach of other accelerators is shown.

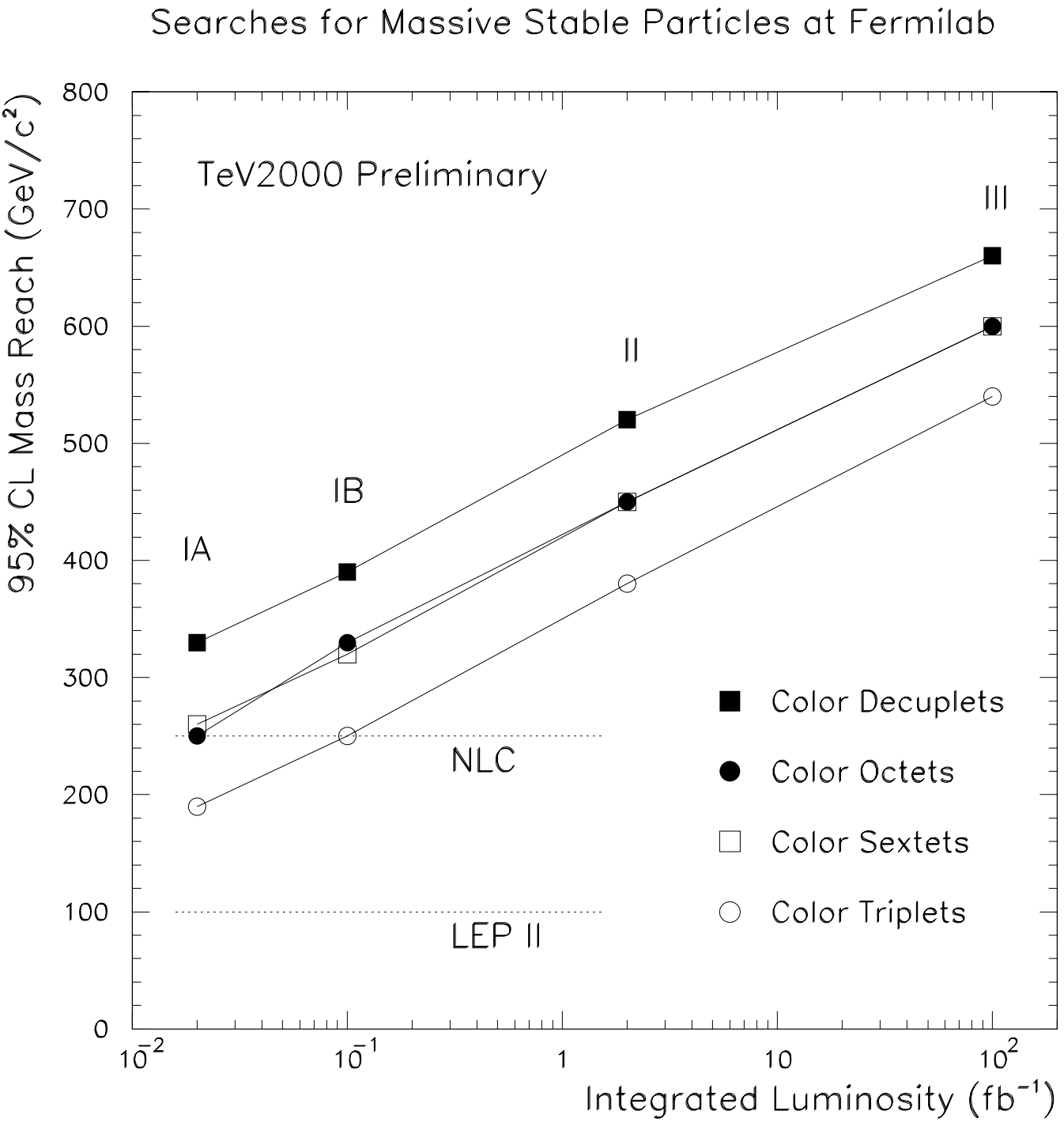

Figure 7.8: The mass reach for heavy stable particles, defined as the 95% CL lower limit on the mass, is plotted vs. integrated luminosity at the Tevatron. The maximum mass reach of other accelerators is shown.

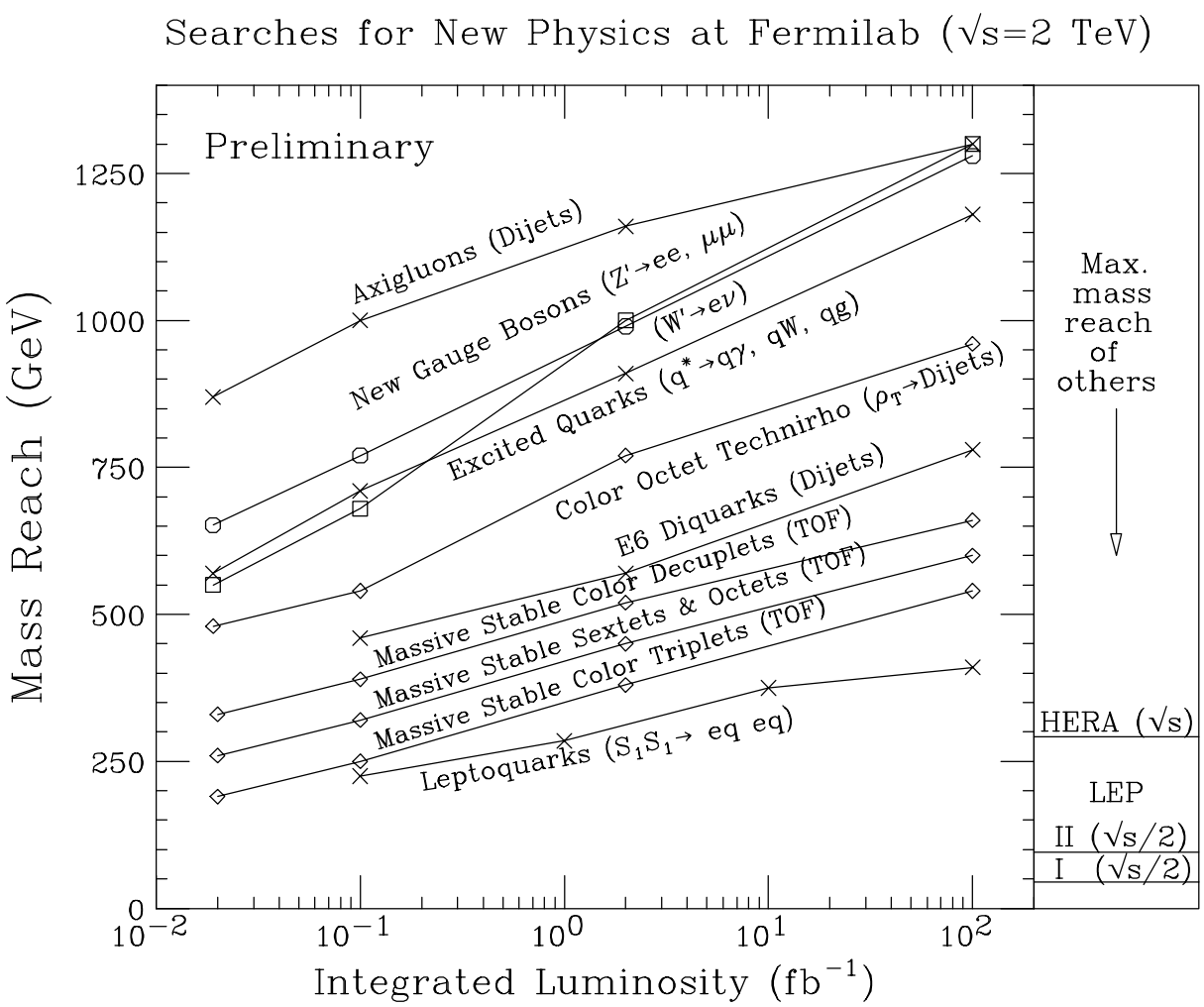

Figure 7.9: The mass reach, defined as the 95% CL lower limit on the mass, is plotted as a function of integrated luminosity at the Tevatron. The maximum mass reach of other accelerators is shown for selected processes.

Chapter 8

Physics with a Polarized Proton Beam at the Tevatron

8.1 Introduction

At the Tevatron Collider we would expect to have one polarized proton beam colliding with an unpolarized antiproton beam. Having one beam polarized longitudinally essentially restricts us to investigating parity violating phenomena, unless efforts are made to extract spin information from other particles in the final state[1, 2]. Similarly, having one beam polarized transversely often leaves us focusing on higher twist effects. Parity violation is manifest in the weak interactions, and much of the new physics being proposed, like supersymmetry, is replete with parity violating interactions. The chiral couplings of the weak bosons, combined with the different phenomenology found in the polarized parton densities for the up and down quarks, enhances our ability to understand how the proton spin is distributed among its constituents. Generally speaking, polarization should also find use in studying the couplings that govern particle interactions, provided there is no large loss in luminosity for the polarized proton beam as compared to the unpolarized case. For some cases where the signal events are invariant under parity and the corresponding background is parity violating, polarization may also provide a means to affect the background without ruining the signal.

In the following we consider the longitudinal and transverse polarization cases separately. The single-spin quantities of interest are the longitudinal asymmetry A_L and the transverse asymmetry A_N. Defining a particular cross section measured with the two different helicity states of the beam as σ_R (for the right-handed proton) and σ_L (for the left-handed proton), the longitudinal asymmetry is given by

$$A_L = \frac{\sigma_L - \sigma_R}{\sigma_L + \sigma_R}.$$

The transverse asymmetry is defined analogously,

$$A_N = \frac{\sigma_\uparrow - \sigma_\downarrow}{\sigma_\uparrow + \sigma_\downarrow},$$

where $\sigma_\uparrow$ and $\sigma_\downarrow$ correspond to cross sections for opposite directions of transverse spin for the beam. These asymmetries may also be discussed with regard to differential cross sections.

8.2 Longitudinal Polarization

8.2.1 Inclusive High P_T Processes

The production of jets, direct photons, Drell-Yan pairs, or in general any purely QED or QCD based process, is expected to result in $A_L = 0$ because the strong and electromagnetic interactions are parity conserving. This is a rather fundamental prediction of QED and QCD, so any large deviations observed from this behavior would be very hard to explain. (Small deviations at the percent level are expected since these final states can also be produced through intermediate W and Z bosons which harbor parity violating behavior.) This is especially true for production at large P_T, where large means $> 50 - 100$ GeV; this region is governed by perturbative QCD, and any deviations from $A_L = 0$ could not be attributed to non-perturbative effects which always result in uncertainties in QCD predictions at small P_T. For example, measuring the jet inclusive cross section ($\frac{d^2\sigma}{dP_T\,d\eta}$) in the P_T region 50 to 100 GeV could be done with limited luminosity, because the unpolarized cross sections in this region are between 1 and 100 nb/GeV for rapidities less than 3. This measurement by itself constitutes a very fundamental test of the theory of strong interactions. In addition to measuring the total inclusive cross section, more differential two jet cross sections can be measured: For example, one can measure the angular distribution $d\sigma/d\cos\theta^*$, where θ^* is the scattering angle in the center of mass; a more differential measurement, more sensitive to higher order QCD corrections, is the triple differential dijet cross section, $d^3\sigma/dE_T d\eta_1 d\eta_2$, where E_T is the transverse energy of the leading jet and η_1, η_2 are the rapidities of the two jets. This latter cross section covers a Bjorken x-range between 0.005 and 0.7. Both the CDF and DØ experiments are currently measuring this cross section to extract parton distributions, especially for gluons at low x.

Analogous to the above jet cross sections, the cross sections can be measured for direct photons. Another example is the inclusive b-quark production cross section. The b-quark cross section has now been measured by both CDF and DØ with different techniques, and the agreement between perturbative QCD predictions and the data has significantly improved. All these cross sections are being measured rather accurately at this moment by both experiments with a total integrated luminosity of about 15 pb^{-1}. The asymmetry in such cross sections could be measured to the same precision with a similar integrated luminosity; however, accumulating such statistics with Main Injector luminosities would only take a small fraction of the running time.

2.2 W and Z Boson Production.

From the production of W and Z bosons, nonzero asymmetries are expected because the weak interaction does not conserve parity. Here we concentrate on W boson production[5].

Measuring the cross section for inclusive W boson production in a polarized collider, especially for the W^+ and W^- bosons separately, provides a measurement of the polarized

quark distributions. Measuring the rapidity dependence of the lepton resulting from the decay of the produced $W^{\pm}$ bosons, which is currently called the charge asymmetry measurement, gives similar accurate information about the ratio of polarized u and d quark densities.

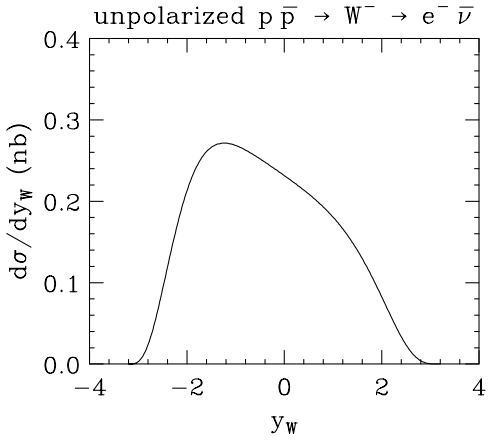

Fig. 1a. The rapidity distribution for the production of W^- bosons in unpolarized $p\bar{p}$ collisions at $\sqrt{s}$ =2 TeV.

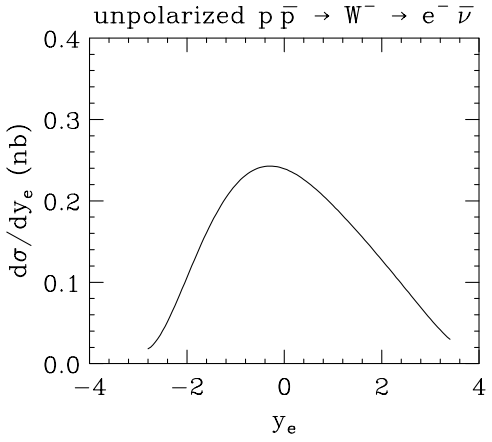

Fig. 1b. The rapidity distribution for the leptons obtained from the decays $W^- \rightarrow e^-\bar{\nu}$ from Fig. 1a.

In Figs. 1a and 1b the rapidity dependence for the unpolarized production of W^- bosons is presented both for the W^- boson and the lepton from the decay $W^- \rightarrow e^-\bar{\nu}$. The W^- boson (e^-) rapidity is symbolized by y_W (y_e). Figs. 2a and 2b show the differential cross sections in rapidity for W^- boson production using two different choices for the polarized parton densities of Nadolsky[3]. Present data still allow significant variation in fitting the polarized parton densities. In Figs. 3a and 3b a kinematic cut has been applied restriciting the transverse momentum of the lepton to be greater than 25 GeV; this constraint shifts the lepton asymmetry curve closer to that of the W boson and provides a better distinction

between the two different choices for the polarized parton densities. Asymmetries around 30% are clearly possible, providing a means for determining better fits and in particular distintuishing between various models that describe the polarized parton densities at large x[4]. The reduction in the event rate due to the cut is 69%, but keep in mind that this study has yet to be optimized. The overall W boson cross section varies with proton spin, but since the polarized parton distributions have a different x-dependence than the unpolarized ones, the P_T^W distribution and the jet multiplicity distributions change accordingly.

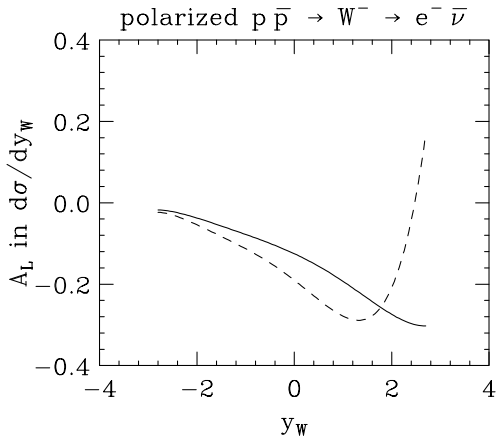

Fig. 2a. The longitudinal asymmetry A_L using the differential rapidity distribution for the W^- boson produced in polarized $p\bar{p}$ collisions at $\sqrt{s}$ =2 TeV. The solid (dashed) curve uses Set 1 (Set 2) distributions from [3].

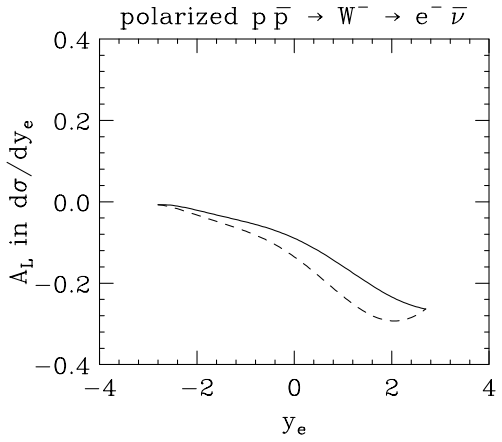

Fig. 2b. The longitudinal asymmetry A_L using the differential rapidity distribution for the lepton from $W^- \to e^-\bar{\nu}$ of Fig. 2a

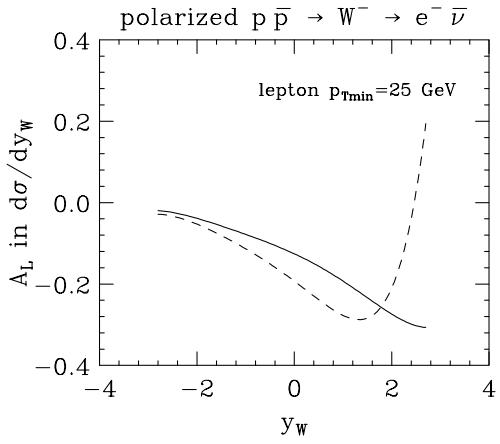

Fig. 3a. The longitudinal asymmetry A_L using the differential rapidity distribution for the W^- boson produced in polarized $p\bar{p}$ collisions at $\sqrt{s}$ =2 TeV. Here the lepton is constrained to have P_T >25 GeV. The solid (dashed) curve uses Set 1 (Set 2) distributions from [3].

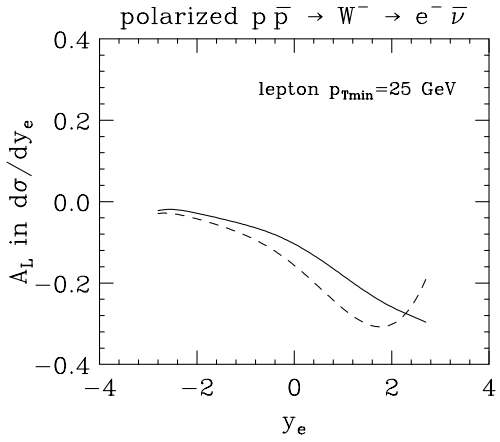

Fig. 3b. The longitudinal asymmetry A_L using the differential rapidity distribution for the lepton from $W^- \to e^-\bar{\nu}$ of Fig. 3a.

Much of the controversy regarding the polarized parton densities centers around how the proton spin is shared between the sea quarks and the gluons. Though only the proton beam is polarized, it should be possible to get a handle on the strange quark polarization by considering W+jet production via $g + s \to W^- + c$, where by tagging the charm quark with the associated W^- produced, one obtains a measure of the strange quark polarization.

With control over the beam polarization, it is possible to modify event rates. For one particular channel, $W + 2$ jets $\to e + \nu + 2$ jets, the change in cross section has been estimated[6] by using polarized parton distributions citeglenn,polpar. The following table shows the change in the cross section for W^+ and W^- bosons in going from an unpolarized beam to a right-handed or left-handed polarized beam. (The subscripts R and L used for protons and quarks in this chapter respectively denote right-handed and left-handed helicities

for those particles.)

W + 2 jet Production	
process	σ (pb)
without 2 jet mass cut:	
$p_R\bar{p} \to W^-\ 2j$	50.56±.58
$p_L\bar{p} \to W^-\ 2j$	41.36±.52
$p_L\bar{p} \to W^+\ 2j$	65.46±.78
$p_R\bar{p} \to W^+\ 2j$	26.84±.28
$p\bar{p} \to W^\pm\ 2j$	45.30±.50
with 2 jet mass cut (70-90 GeV):	
$p_R\bar{p} \to W^-\ 2j$	7.324±.070
$p_L\bar{p} \to W^-\ 2j$	5.910±.056
$p_L\bar{p} \to W^+\ 2j$	9.404±.092
$p_R\bar{p} \to W^+\ 2j$	3.874±.034
$p\bar{p} \to W^\pm\ 2j$	6.514±.060
with 2 jet mass cut	
and $\sqrt{\hat{s}} > 340$ GeV:	
$p_R\bar{p} \to W^-\ 2j$	0.348±.004
$p_L\bar{p} \to W^-\ 2j$	0.308±.004
$p_L\bar{p} \to W^+\ 2j$	0.520±.004
$p_R\bar{p} \to W^+\ 2j$	0.144±.004
$p\bar{p} \to W^\pm\ 2j$	0.358±.002

Table 1. QCD background cross-sections for $p\bar{p} \to W^\pm + 2$ jets at $\sqrt{s}$ =2 TeV, for various proton polarizations and kinematic cuts. The unpolarized cases were calculated separately using CTEQ2 parton distribution functions.

There is a significant change in the W^+ boson cross section expected. This in itself is an interesting measurement. Nonetheless, in most searches for new particles (*e.g.*, top quarks or SUSY partners) being used at the moment, W boson production is a serious background. Polarization makes it feasible to "control" the background to some level, which may help in determining its magnitude. One current example would be the reduction of the $W + 4$ jets background in top quark studies (see the next section).

Single helicity asymmetries also enter in the study of couplings, *e.g.*, the anomalous couplings involved in $W\gamma$ production[6], the contact interactions in direct photon or diboson production, or technicolor physics[8]. It is necessary, however, that the machine luminosity and the variation in event rates due to changes in beam polarization be large enough to make the helicity asymmetries observable.

2.3 Studying the $t\bar{t}$ Signal.

An important mode for studying $t\bar{t}$ events is where $t \to$ jets and $\bar{t} \to l^- +$ jets (or likewise $\bar{t} \to$ jets and $t \to l^+ +$ jets). The most serious background for studying the t and $\bar{t}$ quarks in this channel is due to $W + 4$ jets. Though there are differences, for the purpose of this discussion we pretend that the $W + 4$ jets rate is affected by the beam polarization in the same way that the $W + 2$ jets rate is shown to vary in Table 1.

Indeed, polarized beams create reduced backgrounds

(a)when we tag the l^+ from t decay using p_R or

(b)when we tag the l^- from $\bar{t}$ decay using p_L.

One reason to make this lepton identifcation would be to study separately the t and $\bar{t}$ quarks. Though the background in both cases looks better than the unpolarized situation when we identify lepton charge, case (a) provides a better background reduction of about 26.8/45.3=59%, given the kinematics and polarized parton densities used.

The dominant mode for top quark production at the Tevatron via $q + \bar{q} \to g \to t + \bar{t}$ is a purely QCD process and QCD is parity invariant. The QCD $gq\bar{q}$ vertex is vector-like and does conserve helicity for massless initial quarks. This means that the helicity of the initial quark must be opposite that of the initial antiquark; there are no annihilating $q_L\bar{q}_L$ or $q_R\bar{q}_R$ states, independent of p and $\bar{p}$ polarizations. So, the initial state $q_L\bar{q}_L + q_R\bar{q}_R$ contribution is zero, whether or not the beams are polarized.

Consequently, there should not be any reduction in the top quark event rate simply because the proton beam is polarized. One way to see this is that no matter what helicity quark we pull out of the polarized proton, the probability is 50% for finding the matching antiquark spin in the unpolarized antiproton. This is exacltly the same situation as with both beams unpolarized. Therefore, there is no reduction in signal.

One can also see this by examining the math. We'll just examine the up quark contributions for simplicity, but the other quark contributions enter the same way. We use the notation where $f^{(+)}$ is the parton density for getting a parton with spin aligned with that of the proton and where $f^{(-)}$ is the parton density for getting a parton with spin anti-aligned with that of the proton; the unpolarized density is $f = f^{(+)} + f^{(-)}$. The cross section for $u + \bar{u}$ annihilation when colliding a right-handed proton with an unpolarized antiproton is

$$\begin{aligned} d\sigma(p_R + \bar{p} \to X) &= f^{(+)}_{u/p} * f_{\bar{u}/\bar{p}} d\hat{\sigma}(u_R + \bar{u} \to X) + f^{(-)}_{u/p} * f_{\bar{u}/\bar{p}} d\hat{\sigma}(u_L + \bar{u} \to X) \\ d\sigma(p_R + \bar{p} \to X) &= (f^{(+)}_{u/p} + f^{(-)}_{u/p}) * f_{\bar{u}/\bar{p}} d\hat{\sigma}(u + \bar{u} \to X) \end{aligned}$$

where you should note in the last line that parity invariance of the QCD subprocess was invoked to equate the polarized parton subprocess with the unpolarized parton subprocess:

$$d\hat{\sigma}(u_R + \bar{u} \to X) = d\hat{\sigma}(u_L + \bar{u} \to X) = d\hat{\sigma}(u + \bar{u} \to X).$$

Substituting for the sum of the polarized densities,

$$d\sigma(p_R + \bar{p} \to X) = f_{u/p} * f_{\bar{u}/\bar{p}} d\hat{\sigma}(u + \bar{u} \to X),$$

which represents the unpolarized production rate.

The result is that there is no significant loss in the $q + \bar{q} \to t + \bar{t}$ signal with polarization on one proton beam, but we have been able to exert control over the background (see previous section).

As for the effect on the significance, it does depend a bit on perspective. Taking the significance for studying $t\bar{t}$ pairs at an unpolarized collider without lepton identification as the standard, we can examine the relative change in significance resulting from lepton identification and beam polarization.

Choice 1: No lepton identification and no polarization is our standard,

$$S/\sqrt{B} \propto (1)/\sqrt{1} = 1.$$

When applying lepton identification, let us focus on the case where $\bar{t} \to$ jets and $t \to l^+ +$jets). Note that both the signal and background event rates drop by a factor of $\frac{1}{2}$ since half of the time the decays go to l^+ and the other half of the time the decays go to l^-.

Choice 2: Lepton identification and no polarization changes the significance by

$$S/\sqrt{B} \propto (1/2)/\sqrt{1/2} = 0.71.$$

Proton polarization does not affect the signal, but from Table 1 the backgound gets reduced by about 40%.

Choice 3: Lepton identification with a polarized beam changes the significance by

$$S/\sqrt{B} \propto (1/2)/\sqrt{1/2 * 0.6} = 0.91.$$

Though the polarization does not affect the production of top quarks, the considerations on the decay with lepton identification make a difference. Indeed, it is difficult to get a factor of two drop in background from the single polarized proton beam, particularly in light of the incomplete beam polarization, spin distribution of parton densities, etc.; and yes, the square root in the denominator does not help. Nevertheless, if there is a desire to separately distinguish top quark decays from antitop quark decays with lepton identification, polarization is beneficial, albeit not with a big factor here (0.71 vs. 0.91).

There are also kinematic cuts that hit the background harder than the signal. The W emission will be guided by the single-beam polarization, while the top quark production is less affected. This requires a detailed study.

Continuing with this idea, it is apparent that polarizing the antiproton would be exceptional help. We want the case where the proton and antiproton have opposite helicities because with identical hadron polarizations, all $q\bar{q}$ annihilation is suppressed, including the signal. Again, let's look at $t \to bl^+\nu$ decays; a similar discussion applies to $\bar{t} \to \bar{b}l^-\bar{\nu}$ decays.

Now, with the proton and antiproton carrying the opposite helicity, we may control the background by making the proton right-handed and looking at $t \to bl^+\nu$ decays. Say, in an ideal kinematic limit (*e.g.*, the momentum fraction of the up quark from the proton is large so that the up quark helicity is predominatly right-handed[9]), few W+jet events could be produced where the W^+ is emitted off the up quarks from the proton; the W^+ would come from the left-handed sea u quarks in the antiproton (note the antiproton is left-handed in this example) combining with the right-handed $\bar{d}$ quarks of the proton, also a sea contribution.

With the background vanishing to a sea contribution (plus a spin suppressed valence contribution), what happens to the top quark rate? Well, the parton level cross section is

$$\begin{aligned} d\hat{\sigma}(u_R\bar{u}_L \to X) &= d\hat{\sigma}(u_L\bar{u}_R \to X) \qquad \text{(by QCD parity invariance)} \\ &= 2 * d\hat{\sigma}(u + \bar{u} \to X), \end{aligned}$$

that is, the top quark production rate has increased by about a factor of two compared to the unpolarized production rate. This is because by forcing the initial quarks into opposite helicity states, we don't have to average over all of the non-annihilating $u_R + \bar{u}_R$ and $u_L + \bar{u}_L$ states that dilute the production rate by 50%. Including the factor of 1/2 reduction for picking only the positive lepton decays, the signal event number does not change compared to the total unpolarized event number (assuming there isn't too much luminosity loss due to polarizing the beam).

This provides another choice,

Choice 4: Lepton identification with TWO polarized beams

$$S/\sqrt{B} \propto (1)/\sqrt{\text{small number}}.$$

Of course, reality won't give us the full factor of two for the signal, but with the signal rate relatively unchanged and the background dropping at a better rate than in the case where only the proton beam is polarized, we definitely have a better significance.

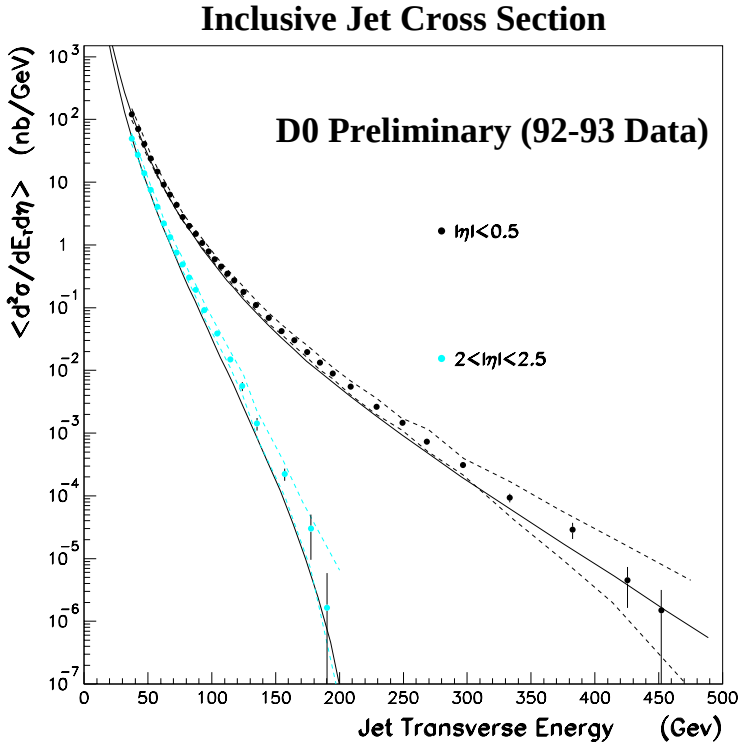

Fig. 4. Jet cross section plotted against transverse energy.

8.2.2 Asymmetries at One Loop

Though parity conservation yields $A_L = 0$ for single particle inclusive processes at the tree level, it is possible to get nonzero asymmetries by observing more than one particle in the final state. In particular, Pire and Ralston[?] and Carlitz and Willey[14] demonstrate nonzero asymmetries that appear at the one loop level in the production of dilepton pairs. These dileptons may be produced by a Drell-Yan mechanism or through decays *e.g.* of J/ψ.

The longitudinal asymmetry arises from the vector product $\mathbf{s} \cdot \mathbf{q}^+ \times \mathbf{q}^-$, which is odd under time reversal. ($\mathbf{s}$ is the pin vector, $\mathbf{q}^+$ is the μ^+ momentum and $\mathbf{q}^-$ is the μ^- momentum.) Consequently, imaginary parts of the one loop amplitude in the lepton pair production provide for the nonzero asymmetry. The parton level asymmetry corresponding to A_L is computed by Carlitz and Willey and found to $10 - 30\%$ for $\tau = -t/(\mathbf{q}^+ + \mathbf{q}^-)^2 < 10$. Ideally, by using on different kinematics, it should be possible to focus on subprocesses with either the quarks or gluons in the initial state. Through this asymmetry, it becomes possible to collect information on the helicity distributions.

These ideas can be applied to other processes also, like open heavy quark production, dijet production and γ+jet production.

8.2.3 Transverse Polarization

Measuring inclusive spin effects at the Tevatron Collider would provide a new probe of the strong interaction. One could explore the contribution of the valence quarks, sea quarks and gluons to the hadrons' spin. Since higher twists should not contribute at TeV energies, one could also test the prediction of perturbative QCD for a vanishing one-spin transverse asymmetry ($A_N = 0$) in high-P_T inclusive production. The study of the P_T dependence of one-spin asymmetries might reveal the transition from the nonperturbative phase of QCD ($A_N \neq 0$) to the perturbative part ($A_N = 0$). Measuring one-spin asymmetries in the process

$$p + \bar{p} \rightarrow \text{jet} + \text{anything}$$

seems especially interesting. The DØ and CDF detectors could easily measure, with high accuracy, the one-spin asymmetry in jet production at E_T of 100 to 200 GeV. The unpolarized data in Fig. 4 show that jets are easily measured in this E_T region. The prediction $A_N = 0$ could definitively be tested with high precision; this PQCD prediction should certainly be valid at $\sqrt{s}$ =2 TeV and E_T =100 GeV.

To be able to measure an asymmetry A_N in the case of transverse polarization (with only the proton beam polarized) one needs to define one more polarization direction in either the initial or final state. Since this is not possible in the initial state, the only possibility is the final state. For example, reconstructing τ-leptons in the final state might give a final state spin direction. Currently, this has not been achieved, but with the upgraded detectors this could be possible. Another possibility is to reconstruct the polarization of a jet by measuring the leading two charged particles in a jet. This has been suggested by J.Collins, S. F. Heppelmann, G.Ladinsky [10] and should in principle be possible in CDF and with the upgraded DØ detector. This is an area where a lot of work is needed to make this feasible.

In the case where no final state polarization direction is given, cross sections measured with and without transverse polarization should be identical. Deviations are possible only due to higher twist contributions and/or from imaginary parts of the contributing amplitudes. So, any measured deviations would be a direct sign of such contributions which are otherwise difficult to isolate.

8.3 Summary

Obviously, the fact that only the proton beam is polarized limits the physics capabilities of a potential collider program with polarized beams, especially in light of a possible polarization program at RHIC, where both beams would be polarized. The big advantage of a polarized collider program at Fermilab would be the detectors:

- Detectors are doing high P_T physics and will be upgraded to run at the higher luminosities. This is in contrast to the RHIC detectors which have to be adapted at a fairly large expense.

- Detectors have been used for an extensive amount of time and their systematics are very well understood.

A possible disadvantage of running in polarized mode at Fermilab is the reduction in luminosity by about a factor of six compared to unpolarized running. This is mainly limited by the output of the polarized source, which is currently 1.6 mA[11]. It is conceivable that this output could be increased in the next few years, but at this point it is not guaranteed.

The presently planned polarized collider program has proton polarization only; polarized antiprotons have been studied[12], but there is still no clear way to produce an intense highly polarized antiproton source suitable for the Tevatron. This is unfortunate since having the polarized antiproton beam would make a significant difference; polarizing the proton beam right-handed and the antiproton beam left-handed not only could have provided a strong suppression of the W^+ background to top pair production, but it also could have increased the $t\bar{t}$ signal rate. This would have provided a much cleaner environment for studying top quarks at the Tevatron.

We feel that at this time it is not possible to make a clear statement whether a polarized collider program, with proton polarization only, can be justified given that the cost of such a project is roughly estimated at \$25M. On the other hand, we feel that not all the physics potential of such a facility with the existing detectors has been fully explored. We plan to pursue this further.

Bibliography

[1] O.Nachtman, Nucl.Phys. **B127** (1977) 314.

[2] G.A. Ladinsky, Phys. Rev. **D46** (1992) 3789.

[3] P.M. Nadolsky, Institute for High Energy Physics (Protvino, Russia) preprint, Jan. 1994.

[4] P.M. Nadolsky, Institute for High Energy Physics (Protvino, Russia) preprint, Mar. 1995.

[5] Figures provided by D. Stump, Michigan State University.

[6] M. Wiest, et al., Michigan State University preprint, MSUHEP-50501, Apr. 1995.

[7] H.-Y.Cheng, S.-N. Lai, Phys. Rev. **D41** (1990) 91.

[8] C. Bourrely, et al., Phys. Rep. **177** (1989) 319.

[9] G.R. Farrar and D.R. Jackson, Phys. Rev. Lett. **35** (1975) 1416.

[10] J. C. Collins, S. F. Heppelmann, G. A. Ladinsky, Nucl.Phys. **B420** (1994) 565.

[11] SPIN Collaboration, *Acceleration of Polarized Protons to 120 GeV and to 1 TeV at Fermilab*, final report to the FNAL PAC, June 1995.

[12] *Proceedings of the 1985 Bodega Bay Workshop on Polarized Antiprotons*, eds. A.D. Krisch, A.M.T. Lin, O. Chamberlain, AIP Conf. Proc. **145** (AIP, New York 1986).

[13] B. Pire and J.P. Ralston, Phys. Rev. D28 (1983) 260.

[14] R.D. Carlitz and R.S. Willey, Phys. Rev. D45 (1992) 2323.

Chapter 9

Detector Requirements

9.1 Detector Systems

The physics signatures described above place rather well-defined requirements on the detector needed at an upgraded Tevatron. We feel that the requirements, though quite stringent, are all technically achievable. The recent discovery of the top quark at the Tevatron has re-emphasized the feasibility of lepton and jet identification, b-tagging, measurement of $\not\!\!E_T$ and reconstruction of a massive state from its decays into jets, in a hadron collider environment. These techniques will continue to be refined as more Tevatron collider data is accumulated, and this gives us confidence that the detector systems and analysis techniques required represent a reasonable extrapolation of the present state of the art.

9.1.1 Tracking and Vertex-tagging

A magnetic central tracking system is needed in order to measure and trigger on isolated high momentum charged tracks. This will form part of the electron and muon identification and will allow detection of one and three-prong hadronic tau decays.

We expect that the following generic detectors will be needed:

- Silicon vertex detector:
  - Innermost layer is a radiation-hard device;
  - 2-D readouts (some of them should be stereo layers);
  - Self-vertexing capability (with efficiency $\epsilon_{sv} > 99\%$);
  - At least 5 layers;
  - Coverage up to at least $|\eta| = 2$–2.5;
  - Be capable of identifying a displaced vertex from b-decay up to $|\eta| \leq 2$ with an efficiency of 50% and a mistag rate of $\leq 1\%$.
- Outer tracker (e.g. fibers, MSGC's, or straw tubes):

- Tracking efficiency $\epsilon_{track} > 99\%$ for single isolated tracks;
- 3-D tracking;
- Momentum resolution comparable to the current CDF CTC system;
- Tracking up to $|\eta| = 2$–2.5.

It is crucial for a number of analyses (top and light Higgs, for example) to understand whether the 50% b-tagging efficiency and $\leq$ 1% mistag rate are achievable at the high luminosities envisaged. A detailed Monte Carlo simulation of b-tagging at the upgraded Tevatron is not yet available, but we can make some preliminary observations based on experience with (and/or simulations of) four silicon vertex detector designs:

- The CDF SVX detector as currently operating in Run 1B.
- The DØ Silicon detector under construction for Run 2.
- The ATLAS and CMS silicon detector systems for LHC.

The present performance of the CDF SVX at $\mathcal{L} = 10^{31}\,\mathrm{cm}^{-2}\mathrm{s}^{-1}$ is a b-tagging efficiency, ϵ_b, of about 60% per jet (within the fiducial region), and a rejection, R, of about 200 against light quark jets. The DØ Silicon detector for Run 2 has been simulated to give $\epsilon_b = 0.5$ or 0.35 for $R = 50$ or 100 respectively, at $\mathcal{L} = 10^{32}\,\mathrm{cm}^{-2}\mathrm{s}^{-1}$. The CDF and DØ silicon detectors are broadly similar, with 4 or 5 layers of silicon arranged close to the beampipe (the DØ detector covers a larger range of rapidity). The LHC detectors both propose to use many more layers of silicon, covering a larger range of radius from the beam, and to employ finely segmented pixel detectors close to the beam to enhance the tagging capabilities in the high-ocupancy environment. The ATLAS simulations claim a performance of $\epsilon_b = 0.6$ for $R = 200$ at $\mathcal{L} = 10^{33}\,\mathrm{cm}^{-2}\mathrm{s}^{-1}$, and $\epsilon_b = 0.5$ for $R = 50$ at $\mathcal{L} = 10^{34}\,\mathrm{cm}^{-2}\mathrm{s}^{-1}$. The CMS design is somewhat more conservative, and its expected performance is $\epsilon_b = 0.5$ or 0.4 for $R = 50$ or 150 at $\mathcal{L} = 10^{33}\,\mathrm{cm}^{-2}\mathrm{s}^{-1}$.

As described earlier, the present performance of the CDF SVX is adequate for the Higgs search in the $b\overline{b}$ channel — the challenge is to maintain this performance at much higher luminosity. The LHC designs have chosen to add more silicon layers and to use pixel detectors in order to increase redundancy and reduce occupancy; their performance is also quite adequate for the Higgs search (though at greater cost). An evolution in a similar direction may be expected for the detector(s) at an upgraded Tevatron. We are confident that the necessary b-tagging performance can be obtained, though the design and optimization of the detector will require detailed studies beyond the scope of this report.

9.1.2 Calorimetry

Electromagnetic calorimetry is required for the identification and measurement of isolated electrons (from $W \rightarrow e$ decays) and of soft electrons as b-tagging technique. Ultra-precise energy resolution is not called for (typical EM resolutions of $\sim 15\%/\sqrt{E}$ should be sufficient). The EM calorimeter must cover the pseudorapidity range up to $|\eta| \leq 2.5$ in order to have

adequate Higgs acceptance. The EM calorimeter should provide an isolated electron trigger; in principle one could also attempt to trigger on soft electron b-tags but this has not been assumed in the trigger rate estimates.

Electron and photon identification will be degraded by the extra energy from minimum bias pileup events, which will make isolation cuts less efficient. As described earlier, the supersymmetry study group for this workshop have found that an electron efficiency of 90% may still be obtained in the presence of nine pileup events with a cut of $E_T \leq 4\,\mathrm{GeV}$ in a cone of $R = 0.4$.

The EM calorimeter must be backed with a hadronic section capable of identification and measurement of jets and measurement of missing transverse energy. Again, ultra-precise energy resolution is not called for (typical hadronic resolutions of $\sim 70\%/\sqrt{E}$ should be sufficient) but emphasis should be placed on the performance of the calorimeter for jet-jet invariant mass reconstruction. Studies for the LHC suggest that transverse segmentation of $\Delta\eta \times \Delta\phi \sim 0.1 \times 0.1$ is desirable in order to reconstruct boosted $W \to jj$ decays but that segmentation finer than this is not called for. The hadron calorimeter should cover at least the range up to $|\eta| \sim 3.5$ in order to be efficient for jets up to $|\eta| = 2.5$ and in order to provide a good measurement of $\not\!\!E_T$. The hadronic calorimeter must be capable of triggering on jets and on $\not\!\!E_T$.

Pileup will also degrade the $\not\!\!E_T$ resolution. The supersymmetry study group have found that ten minimum bias pileup events give an average contribution to $\not\!\!E_T$ of about 10 GeV but do not yield any extra events with $\not\!\!E_T \geq 20\,\mathrm{GeV}$.

9.1.3 Muon Detection

A muon detector is required for the identification and measurement of isolated muons (from $W \to \mu$ decays) and of soft muons as a b-tagging technique. The muon system must cover the pseudorapidity range up to $|\eta| \leq 2.5$ in order to have adequate Higgs acceptance. The detector should provide an isolated muon trigger at moderate momenta ($p_T \geq 15 - 20$ GeV/c); one could also attempt to trigger on soft muon b-tags but this has not been assumed in the trigger rate estimates. The most precise measurement of muon momentum will most likely come from the central tracker, so the muon system should concentrate on tagging and triggering fuctions.

It will be noted that these requirements specify a rather general-purpose detector well suited to electroweak and top studies and also capable of some interesting b-physics if sufficient bandwidth is available.

In addition to the physics requirements, the detector systems must operate and be triggerable in the high-rate, high-radiation environment of the upgraded Tevatron collider.

9.2 Lepton Isolation at High Luminosity

Many of the physics topics of interest at the upgraded Tevatron will rely on isolated, high-p_T leptons as a tag for signal events. Examples are W and Z production, top, and mutilepton

signatures for supersymmetry.

Isolation is defined as the sum of all transverse energy, excluding the energy of the lepton, in a cone of radius $\Delta R = 0.4$ surrounding the lepton:

$$\text{ISO} \quad = \quad \sum_{\Delta R<0.4} E_T - E_T(\ell)$$

Here $\Delta R = \sqrt{(\Delta\eta)^2 + (\Delta\phi)^2}$. The leptons from W/Z, top and supersymmetry events are expected to be quite well separated from hadronic activity in the event. In contrast, leptons from heavy flavors (b/c quarks) are expected to be non-isolated. Thus, a requirement of small isolation is a powerful tool to reduce backgrounds due to Standard Model jet processes.

The effectiveness of a cut on lepton isolation depends on the level of isotropic energy flow (the underlying event). In Tevatron Run 1A, $\sim \mathcal{O}(1)$ interactions were produced during each bunch crossing. At the large luminosities expected at an upgraded Tevatron (TeV33), as many as $\sim$10 interactions can occur coincident with the physics event of interest. Although these additional interactions are almost always minimum bias events, they create an elevated level of isotropic energy deposition in the calorimeters.

In order to simulate multiple interactions, calorimeter energy is summed in random cones of radius $\Delta R = 0.4$. A random direction in $\eta - \phi$ space is then generated, with the cone centered in the pseudo-rapidity region $|\eta| < 1.0$ (this is approximately the η range of the CDF central calorimeter). We also generate Poisson-distributed random numbers $\mathrm{N_{cones}}$, with mean μ_{P}. Using one random cone per minimum bias event, the $\mathrm{E_T}$ in $\mathrm{N_{cones}}$ + 1 random cones was then added, simulating the effect of adding a Poisson averaged μ_{P} additional interactions to the primary physics event of interest.

For this study, a sample of minimum bias (MB) events ($< \mathcal{L} > = 3.6 \times 10^{30}$ cm^{-2}sec^{-1}) from the CDF Run 1A data was used. Minimum bias events at CDF are collected via a special trigger line, which periodically accepts any event that merely exhibits a beam-beam counter coincidence - no additional trigger requirements are imposed.

Table 9.1 lists the preliminary results of this study. The high efficiency obtained for 0 additional MB (cone) events (*i.e.*, $\sim$Tevatron Run 1A conditions) is in agreement with previous studies. When 9 additional MB (cone) events are present, the efficiency drops by 9% for ISO $<$ 4 GeV, or 46% for ISO $<$ 2 GeV.

The results shown in the table are conservative estimates since the average number of interactions in one MB trigger is greater than one. Table 9.2 shows the distribution of number of interactions after removing 0-interaction events from a Poisson distribution. Therefore, one MB trigger in the sample will contain 1.34 interactions on average. In order to simulate 9 additional MB events, we should add 6.7 random cones from MB trigger data. The inefficiencies for ISO $<$ 2, 3 and 4 GeV are 68%, 86%, and 94% respectively for 6.7 random cones.

For the CDF supersymmetry to trileptons analysis in Run 1A, a cut of ISO $<$ 2 GeV was used, yielding

$$\epsilon_\ell(\text{Run 1A}) \quad = \quad 96\%,$$

(obtained from the Z sample). This should be compared to ϵ_ℓ(ISO$<$2 GeV) for $\mu_{\mathrm{P}} = 1$ in Table 9.1: 97%. The 2-GeV cut is optimized to provide the best signal/background ratio

Table 9.1: Efficiencies of isolation cuts for a single lepton. A minimum bias data sample (Tape CCE788) was used.

# additional cones (μ_P)	ϵ_ℓ [%]		
	ISO<2.0 GeV	ISO<3.0 GeV	ISO<4.0 GeV
0	99.2 ± 1.0	99.9 ± 1.0	100. ± 1.0
1	97.3 ± 1.3	99.4 ± 1.4	99.8 ± 1.4
3	90.6 ± 1.8	97.2 ± 1.9	98.9 ± 1.9
6	72.3 ± 2.2	88.8 ± 2.4	95.5 ± 2.5
9	54.3 ± 2.2	78.6 ± 2.7	90.6 ± 2.9

Table 9.2: Fraction of number of interactions after removing N(int) = 0 at $\mathcal{L} = 3.6 \times 10^{30}$ $cm^{-2}sec^{-1}$).

	N(int)			
	1	2	3	4
Fraction	72%	23%	4%	1%

for single interaction luminosities. Naively, we expect the same rejection power of the b-decay lepton with a 3-GeV cut. Detailed MC study is under way. Therefore, for TeV33, we expect a single electron efficiency of 86% with no loss of background rejection. The resultant trilepton efficiency of 64% will be acceptable.

9.3 Missing E_T at High Luminosity

A study of the effect of pile-up of minimum bias events on the $\not\!\!E_T$ was done using a simulation of the D$\emptyset$ detector. This study was only concerned with the effects of pile-up on the calorimeter measurement; it was assumed that the hard scatter vertex was found correctly by the tracking. The effect of the vertex position resolution is likely to be the dominant effect in the $\not\!\!E_T$ resolution, but due to the lack of any model for an upgraded tracker (realistic or not), it is not possible to study this effect at this time. One should also note that in the present study no serious attempt to model upgrade calorimeter electronics or accelerator parameters was made. Instead a model of the current D$\emptyset$ experiment and accelerator was implemented. The simulation program used for this study also takes into account the effects of ten minimum bias events in the previous and post buckets.

As a benchmark for a physics process with a $\not\!\!E_T$ signal, a sample of $\tilde{\chi}_1^\pm \tilde{\chi}_2^0 \to eee + X$ (supersymmetry) events was used as the hard scattering event. The events were generated using ISAJET [14] with the following parameter cards:

Figure 9.1: Missing E_T distribution for $\tilde{\chi}_1^{\pm}\tilde{\chi}_2^0 \to eee + X$ events with a full D$\emptyset$ detector simulation: (a) no pile-up and (b) 10 MB events.

MSSM1 $M_{\tilde{g}} = 265$, $M_{\tilde{q}} = 1000$, $M_{\tilde{l}_R} = 200$, $M_{\tilde{l}_L} = 200$, $M_{\tilde{\nu}} = 1000$;

MSSM2 $M_{\tilde{t}_L} = 1000$, $M_{\tilde{t}_R} = 1000$, $A_t = -100$, $M_{\tilde{b}_R} = 1000$, $A_b = 1000$;

MSSM3 $\tan\beta = 2.0$, $\mu = -500$, $M_A = 500$.

Ten random minimum bias, Monte Carlo generated, events were added to each chargino-neutralino event in addition to the measured calorimeter uranium and electronic noise on a cell by cell basis. These combined events were then reconstructed with a standard version of the D$\emptyset$ reconstruction program. The correct vertex was always found.

The calculated $\not\!\!E_T$ before and after the addition of pile-up for a sample of 100 events is shown in Fig. 9.1. As can be seen, the addition of the ten minimum bias events makes little difference to the calorimetric measurement of $\not\!\!E_T$. Less than 0.5 GeV change in the average $\not\!\!E_T$ and slightly more than 1 GeV increase in the spread of the $\not\!\!E_T$ is observed. We also find

$$\epsilon_{\not\!\!E_T}\ (\text{pile-up}) \quad = \quad \epsilon_{\not\!\!E_T}\ (\text{no pile-up}) \quad (\not\!\!E_T > 20\ \text{GeV}).$$

Figure 9.1 represents the effect of adding the $\not\!\!E_T$ from a random set of minimum bias events vectorially to the $\not\!\!E_T$ of a signal event. As a cross-check, if the signal event is subtracted, then one finds that the average $\not\!\!E_T$ from the minimum bias is about 10 GeV with a spread of about 6 GeV. These numbers closely matched results derived from a study of adding ten minimum bias events together using a toy calorimeter model.

In conclusion, it appears that from the standpoint of the calorimetric measurement of $\not\!\!E_T$, pile-up should not be a problem in degrading the $\not\!\!E_T$ measurement. One should also note that the signal sample used in this study has a relatively flat $\not\!\!E_T$ distribution. The effect of adding ten minimum bias events to a background sample with a steeply falling $\not\!\!E_T$ spectrum is likely to be different. The effect on signal efficiency for a given $\not\!\!E_T$ cut will probably be less than the effect on the rejection power of the $\not\!\!E_T$ cut on some backgrounds.

9.4 Trigger and Data Acquisition

In order to obtain some semi-realistic estimates of trigger rates at an upgraded Tevatron detector, we have assumed a three-level trigger system. The first level is assumed to be analogue hardware (e.g. a calorimeter tower above threshold); the second level programmable digital hardware (e.g. isolation or track-matching using a DSP chip); and the third level a software trigger running on general purpose cpu's with access to full event information.

The following primitives should be available to the trigger:

- **Isolated Electrons** based on the EM calorimeter up to $|\eta| \leq 2.5$. In principle one could also attempt to trigger on soft electron b-tags but this has not been assumed in the rate estimates.

- **Isolated Muons** using the muon system up to $|\eta| \leq 2.5$. Again, soft muon b-tags could also be added to the trigger but this has not been assumed in the rate estimates.
- **Charged Tracks**. An isolated high momentum charged track trigger will be needed to trigger on one and three-prong hadronic tau decays.
- **Jets** based on EM+hadronic calorimeter up to $|\eta| \leq 2.5$. At trigger level 2 or 3 a jet-jet invariant mass requirement could be used but this has not been assumed in the rate estimates.
- **Missing** E_T based on the sum of towers in the EM+hadronic calorimeters. At trigger levels 2 or 3 this estimate can be refined by inclusion of muons, use of fitted vertex z-position, etc.
- **Displaced Vertex**. A silicon vertex tracking trigger capable of a displaced vertex b-tag up to $|\eta| \leq 2$ at trigger level 2 or 3 may be useful but has not been assumed in the rate estimates.

9.4.1 Available Bandwidth

A survey of current and proposed experiments gives the following trigger bandwidths at each level. The last line of the table shows the rates that we have assumed as limits on what is feasible; they are consistent with being audacious but technically achievable on the timescale of an upgraded Tevatron.

Experiment	*L1* $\rightarrow$ *L2* (kHz)	*L2* $\rightarrow$ *L3* (KHz)	*L3* $\rightarrow$ *host* (Hz)
DØ (Run 1b)	0.25	0.25	4
DØ (Run 2)	10	1	10
DØ (Run 3 EOI)	50	5	200
CDF (Run 1b)	?	?	100?
CDF (Run 2)	?	?	?
CDF (Run 3 EOI)	?	1	?
SDC	10–100	0.1–1	100
GEM	10–100	0.3–3	100
ATLAS	few $\times$10	few $\times$10?	few$\times$100
CMS	few $\times$10	few $\times$10?	< 100
Assumed	50 kHz	10–20 kHz	100–200 Hz

9.4.2 A Toy Trigger Menu

Rates have been estimated for an illustrative mix of triggers:

- *top*: single and dilepton top triggers based on the current DØ menu.
- $W/Z \rightarrow e, \mu$: unprescaled single lepton plus $\not\!\!E_T$ trigger for W's and uprescaled dilepton trigger for Z's.

- $\not\!\!E_T$ +jets: for supersymmetry and $ZH \to \nu\nu b\bar{b}$. The $\not\!\!E_T$ threshold would be about 40 GeV for a pure $\not\!\!E_T$ trigger, and could be lowered to about 25 GeV if two jets were also required.

- $(W/Z)H \to qq\tau\tau$: charged track tau trigger for Higgs.

The rate estimates use measured (Run 1b) DØ calorimeter trigger cross sections, estimates for DØ charged track and muon trigger cross sections for Run 2, and measured rejection factors at level 2 and 3. The rates include allowance for the overlap between the electron and muon triggers for top, W/Z and $\tau \to \ell\nu\bar{\nu}$.

Mode	$L1 \to L2$	$L2 \to L3$	$L3 \to host$
Top	7.2 kHz	4.0 kHz	50 Hz
$W/Z \to \ell$	8.0 kHz	3.4 kHz	28 Hz
met + jets	1.3 kHz	1.3 kHz	30 Hz
$(W/Z)H \to q\bar{q}\tau^+\tau^-$	15 kHz	5.8 kHz	37 Hz
Total	23.5 kHz	11.1 kHz	145 Hz
(Limit)	50 kHz	5–10 kHz	100–200 Hz

The immediate conclusion is that the situation does not look too bad. The rates at all levels are consistent with the limits assumed. Some more rejection at level 2 may be desirable, but there are a number of tools available that have not been assumed to be used so far — triggering for top on soft lepton tags or displaced vertex b-tags at level 2 or 3, for example.

Two points must be emphasized. Firstly this is, of course, only a very first look at trigger rates. Many factors such as multiple interactions at higher luminosity may dramatically increase the rates over what is quoted here. Secondly the bandwidths listed, while achievable, represent a large increase over the capabilities of the present DØ and CDF data acquisition systems and will be expensive and technically challenging to implement.

9.5 Offline Processing

If the rate of events out of Level 3 is 200 Hz, this cannot be spooled to tape (unless the event size is tiny or a large number of drives is used). It is more reasonable to imagine a 'near-line' processing farm where the reconstruction is performed in quasi-real-time. The present DØ and CDF reconstruction programs requires of the order of 15–20 seconds per event on a $\sim$ 30 MIPS machine, i.e. 500 MIPS-sec. If we assume the same reconstruction time per event then a reconstruction facility of 10^5 MIPS will be required to keep pace with the events being written. This could be thought of as a farm of two hundred workstations, each with 500 MIPS of cpu(s), which is quite conceivable on the timescale required.

Chapter 10

Afterword

D. Amidei and R. Brock

In the past year, a convincing case has emerged for an extended evolution of the Fermilab collider. Why did we go through this exercise when there are other opportunities in the world for future accelerators?

Two recent and familiar examples of surprises in High Energy Physics illustrate a feature of research which deserves protection when future plans are considered. These surprises, which dominate much active work in our field, are the long lifetime of B hadrons and the extremely large mass of the top quark. The efforts which eventually led to these understandings didn't come from strategic leaps, but rather from the accumulation of experimental results and techniques over time. No accelerators were proposed, planned, or constructed to make these discoveries. Instead, hints and leads, accompanied by new detector technologies, were followed over many years to eventual discovery and understanding. This is an "evolutionary path" to scientific progress. The continued importance of results from CESR (the Cornell Electron Synchrotron Ring) is one of the excellent examples of the success of the evolutionary approach in facility planning, and reminds us that continued investment and the establishment of *depth* with promising platforms ensures progress.

Particularly applicable to our concerns in the 1990's are the following four points regarding the evolutionary path for High Energy Physics:

1. The bottom quark and top quark stories referred to above represent the usual path toward scientific breakthrough. "Throwing long" is a strategy which has a place as a component of a broad, stable physics program. However, it cannot dominate a program in difficult times.

2. As much as anything in science can come with a guarantee, success and surprise seem repeatedly to be the eventual outcomes of the evolutionary approach in high energy physics.

3. This sort of success doesn't happen accidentally. Rather, the guarantee is underwritten by the mounting of topical experiments which attract the brightest scientists, coupled

with the means to do those experiments in a timely way. We call this **Following the Physics**, as decidedly distinct from "waiting for the physics".

4. The Fermilab program outlined here is a paradigm example of Evolutionary Physics at its best and it is feasible now.

Like other sciences, in High Energy Physics there are periodic and sometimes dramatic advances in understanding. What's perhaps unique about our field is that these changes occur primarily through massive efforts, each requiring many years and large sums of money. This means that an historical perspective is necessary to see incremental progress. If we pause and view the present from the standpoint of 10 to 15 years ago, our current understanding of elementary particle physics would have looked unpredictably unfamiliar. Sensible planning would take into account that such unpredictability is a part of doing well planned scientific experiments and therefore would build in our ability to make a similar statement about a new physics landscape 15 years from now. We need to prepare and defend a plan which combines the proper mix of sensible short term extrapolation, far–future opportunities, and faith in scientific unpredictability which is borne of a broad perspective. This report forms the beginning of such a plan by describing a set of significant experiments all within the context of a feasible collider program. That 100 physicists began this exercise and that 70% of them are authors of the individual detailed chapters is evidence of the excitement of the science and the commitment of the Tevatron community.

If resources are limited, and there is no expectation that this will not be the case for years, we should pay attention to the hints which exist and **Follow the Physics**. While the precise locations of surprises can't be predicted, we are fortunate that the various general areas are woven together in an increasingly correlated tapestry. The general threads are:

- **Top and Electroweak physics, combining direct measurements and indirect constraints from many different experiments.**
  If the Standard Model is correct, the generation of mass is related to at least two important length scales: the mass of the W and Z, of $\approx$ 100 GeV/c^2. and the vacuum expectation value of $\approx$ 246 GeV/c^2. That the top quark mass is nearly twice the former, and not far from the latter is probably a hint about the top quark which should not be ignored. Many measurements are possible to probe these scales.

- **Symmetry Breaking**
  Inherent within the Standard Model are explicit predictions, but also a set of underlying assumptions regarding the symmetry breaking mechanism. One of these predictions is the existence of a Higgs boson of indeterminate mass, playing the role of the quasiparticle of a possible phase transition. Other related but different schemes, also encompass Standard Model predictions but are more general. Supersymmetry is a leading example of such an extension. A component of any electroweak "prospecting" will include emphasis on these anticipated themes.

- **Generational Mixing among quarks and among leptons.**
  Among the oddest of field–theoretic consequences is the apparent quantum mechanical mixing of fundamental fermions of grossly differing mass scales which seems to be operative only in

the quark sector. Why? The opportunities for studying this phenomenon in the bottom system and perhaps the top system have been well–documented. Further, the astrophysical motivations for continued investigation of this phenomenon in the lepton sector are similarly well–documented.

- **CP violation in the strange, bottom, and top(?) systems.**
  Large–scale CP violation in the bottom system is expected as in the strange system. What about their $I_3 = 1/2$ partners, charm and top? While probably related to fermion mixing, this question stands alone as an experimental question, independent of models.

- **Spectroscopy and Rare Decays in the strange, charm, bottom, and top systems.**
  From the strange and charm to the bottom and now top systems, the "onia" of baryonic and mesonic spectroscopies and rare decays are always of interest. The study of the bottom sector will be with us for decades. With the top quark, we have the first quark which will not hadronize, but remains bare...it will not likely form hadronic matter, like a lepton. This second top quark hint may provide important clues to new physics.

- **Hadronic Structure in both high and low $p_{\rm T}$ regimes.**
  We tend to become excited about the extremes of the electroweak world. Could this be, in part, related to our familiarity with a perturbative and straightforward diagrammatic language? Experimentally accessible but much less well–understood, is the passage from the perturbative regime into the actual binding regimes. The structure of hadrons and the many–body aspects of gluon and low–x physics may become clearer with continued focus. Of course, the high p_T extreme is always of great interest, with higher statistical precision leading to probes of higher mass scales.

- **The Zoo**
  This is the part of elementary particle physics which is always revolutionary, and inherently unpredictable. The unusual seems to happen on a periodic basis, albeit at a timescale which is long. Because of that, we become complacent and tend toward a self–assured posture that we know what to expect. But reflection over the past 40 years of this field reminds one of the "who ordered *that*...!" aspects of digging deeper. The muon, partons and scaling, weak neutral currents, CP violation, the tau, the strange quark, the huge top quark mass, and the bottom quark lifetime were all largely unanticipated. They were brought to prominence and shown to be true only by experimental skill and theoretical imagination.

This is a list of broad themes, but it does surround what most would acknowledge to be the important general areas of elementary particle research. As befitting for the National High Energy Physics Laboratory:

the Fermilab complex is guaranteed to impact each of these areas.

From the collider to the fixed target area to the neutrino oscillation program, this facility offers significant short term gains and long term promise. Fermilab will allow us to weave a tight pattern in the physics tapestry presented above by following the physics as it develops within a vigorous and comprehensive program. That this evolutionary path is *completely*

within the scope and control of the U. S. program is crucial to the maintenance of the flexibity and autonomy which is befitting our history and traditional commitment to this field.

We have outlined here a program of research specifically for the Tevatron collider at Fermilab. It is rich in guaranteed physics (top, IVB), surprising in its reach to the next level (SUSY, Higgs, exotics), fertile in the different configurations which are feasible, stimulating to continued R&D in accelerator and detector technologies, and stable as a platform for the far future of high energy physics (ultra–high energy pp, or $p\bar{p}$, an e^+e^- linear collider, or a μ–collider). Much work still remains to be done, but we hope that those who have not considered the evolutionary opportunities at the Fermilab complex will begin to look deeper with us. We urge our colleagues, the Fermilab management, the Department of Energy, the National Science Foundation, and members of Congress to take seriously a Physics Program for the United States which builds on the significant investment of millions of dollars and thousands of physicist–years to continue to **Follow the Physics**.